



Publicly Accessible Penn Dissertations


1-1-2015

Nanofibrous Disc-Like Angle Ply Structure for Total Disc Replacement in a Small Animal Model

John Thomas Martin

University of Pennsylvania, johnma@mail.med.upenn.edu

Follow this and additional works at: <http://repository.upenn.edu/edissertations>

 Part of the [Biomedical Commons](#), [Mechanical Engineering Commons](#), and the [Medicine and Health Sciences Commons](#)

Recommended Citation

Martin, John Thomas, "Nanofibrous Disc-Like Angle Ply Structure for Total Disc Replacement in a Small Animal Model" (2015). *Publicly Accessible Penn Dissertations*. 1882.
<http://repository.upenn.edu/edissertations/1882>

This paper is posted at ScholarlyCommons. <http://repository.upenn.edu/edissertations/1882>
For more information, please contact libraryrepository@pobox.upenn.edu.

Nanofibrous Disc-Like Angle Ply Structure for Total Disc Replacement in a Small Animal Model

Abstract

Low back pain affects 85% of the population and carries a socioeconomic price tag of \$100 billion USD per year. Lumbar intervertebral disc disease is strongly implicated as a causative factor in back pain, as degeneration, which is ubiquitous in the population, leads to loss of normal spine function. For these reasons, our lab has developed disc-like angle ply structures (DAPS) for total disc replacement. These cell-seeded replacements are designed to match the natural hierarchical structure and function of the native disc and correct spinal kinematics after end-stage disc disease.

In this dissertation, I describe the development of a rat caudal spine (tail) model of total disc replacement as a platform to evaluate DAPS in vivo; an external fixation system that immobilized caudal vertebrae at the site of implantation was required for DAPS retention and a radiopaque scaffold was developed to confirm intervertebral DAPS positioning. A detailed analysis of the DAPS in vitro growth trajectory was performed to select the optimum pre-culture duration before implantation. Cell-seeded DAPS were subsequently implanted in the rat tail and evaluated by histological, mechanical, and MRI analyses. DAPS successfully restored the mechanical properties of the native motion segment in compression, providing the first evidence of the efficacy of engineered disc replacements. Adaptations of the implant to the in vivo environment were identified; there was a reduction in glycosaminoglycan after implantation, structural modifications to the NP material, and no evidence of vertebral integration. In tackling the first of these issues, a pre-culture strategy that primed DAPS for the in vivo environment was developed; using a rat subcutaneous model, implant phenotype was best conserved post-implantation using a pre-culture strategy with a transient high dose of TGF- β 3. Future work will address maintenance of NP structure, vertebral integration and scaling up to human sizes.

In my work, the most promising finding was that DAPS replicated compressive motion segment mechanical properties after implantation supporting the idea that engineered biological disc replacement is a possibility for clinical treatment of advanced disc disease.

Degree Type

Dissertation

Degree Name

Doctor of Philosophy (PhD)

Graduate Group

Mechanical Engineering & Applied Mechanics

First Advisor

Robert L. Mauck

Keywords

Intervertebral disc, Surgical model, Tissue engineering

Subject Categories

Biomedical | Mechanical Engineering | Medicine and Health Sciences

NANOFIBROUS DISC-LIKE ANGLE PLY STRUCTURES FOR TOTAL DISC
REPLACEMENT IN A SMALL ANIMAL MODEL

John T. Martin

A DISSERTATION

in

Mechanical Engineering and Applied Mechanics

Presented to the Faculties of the University of Pennsylvania

in

Partial Fulfillment of the Requirements for the

Degree of Doctor of Philosophy

2015

Supervisor of Dissertation

Graduate Group Chairperson

Robert L. Mauck, Ph.D.
Associate Professor of Orthopaedic
Surgery and Bioengineering, University
of Pennsylvania

Prashant K. Purohit, Ph.D.
Associate Professor of Mechanical
Engineering and Applied Mechanics,
University of Pennsylvania

Dissertation Committee

Beth A. Winkelstein, Ph.D. (Chair)
Professor of Bioengineering, University
of Pennsylvania

Dawn M. Elliott, Ph.D.
Professor and Chair of Biomedical
Engineering, University of Delaware

Harvey E. Smith, M.D.
Assistant Professor of Orthopaedic
Surgery and Neurosurgery, University of
Pennsylvania

Helen H. Lu, Ph.D.
Professor of Biomedical Engineering,
Columbia University

ACKNOWLEDGEMENTS

This dissertation is the representative of my own work and the contributions many people who have supported me (before and after I started Penn) including family, colleagues, and mentors.

After I received my undergrad degree at The College of New Jersey, I entered the Master's program at University of Colorado with only a long-term vacation in mind. There I met Ginger Ferguson who served as my thesis advisor. She welcomed me into her office and laid out some project ideas, and served as an anchor for me in a place where I was a stranger. She is a good scientist and a better person, and she encouraged me to pursue a career in research after the MS program. Colorado was too far from my family, so I could not stay long, and Ginger told me that when I returned to the East Coast, I should seek out an exceptional lab and stay in bioengineering research. I owe Ginger a debt of gratitude for the warm welcome, the encouragement to stay in research, and her continued mentorship.

After Colorado, I applied for a research staff position in Dawn Elliott's lab at Penn. Dawn was an exceptional mentor – she is smart, a great writer, and an excellent communicator. She trusted me; despite being a novice in research, she gave me free reign in the lab and we did great work together. I learned a lot from her. When I gave Dawn a draft of my first abstract on our mouse needle puncture injury model, she rewrote 90% of it. She asked me, “Why do you think needle puncture injury is a good model of disc degeneration?” I had no idea, but realized that I needed to get a better handle on how my work fit into the literature. Despite that I came from a small undergraduate school and

that my grades were average, Dawn took a chance on me and supported my entrance into the PhD program. But, I was a PhD student in her lab only for a short time; Dawn left Penn to start the biomedical engineering program at University of Delaware, and I stayed behind. I put so much into my work with her that, when she announced her plans to move, I took it really hard. Looking back now I wish I was more professional. Despite this, she financially supported me throughout my time at Penn and has stayed active in the work that I present in this dissertation, regularly travelling from Delaware to attend research meetings. I really enjoyed my time in Dawn's lab, she's fun (especially at happy hour), I always looked forward to our meetings, and she is a good scientist (ie "The Great Dawn Elliott", as an international researcher once dubbed her).

Rob took me on as a PhD student when Dawn transitioned to Delaware. I remember that Rob and I had a meeting right after Dawn announced she was leaving; I was really pissed about the move and Rob sensed that; out of a combination of compassion and genuine interest in working with me, he agreed to have me join the lab. Rob is a skilled mentor; he has helped me identify my own weaknesses and has helped me improve, not just superficial or technical shortcomings, but also long-ingrained personality traits that hurt me as a scientist (which speaks to his personability as much as his insight). I have been impressed everyday by his abilities as scientist, specifically, his ability to quickly see, interpret, and pull meaningful conclusions from a dataset, and his ability to generate ideas, not just the next incremental steps in a project, but long-term, ambitious strategic goals through creative problem solving. As the head of our lab, he has built a team through tireless mentoring that is motivated by a central focus on improving patient care through functional tissue engineering. This focus is not trivial; our

lab is diverse in terms of individual personalities and cultural backgrounds. Rob promotes an environment that is supportive, challenging, intellectually stimulating for all involved, and consequently, very productive. He has fostered a lab culture that is equal parts “fun” and “enthusiasm for science” and this is directly a result of his own personality, as he is by all accounts a good person and an enthusiastic and capable leader. In terms of fun, I thank Rob for the MANY beers he has bought for me, and look forward to doing the same for him. It has been a privilege to be a part of this lab.

One person has followed me from Elliott Lab to Mauck Lab, my good friend and mentor Lachlan Smith. I met Lachlan at Dawn’s lab happy hour at New Deck and the first thing I noticed was how soft-spoken he was. New Deck had a power outage and was running an extremely loud generator outside the bar to keep business going. Our group was fortunate to sit right next to the generator, and even if he used a megaphone, I would not have heard Lachlan at his usual low volume. I say this now, because you would never know this if you saw him present. He is an excellent public speaker; his presentations are organized, thorough, aesthetically appealing, and most importantly, directed specifically to the target audience. I have tried to imitate him with my own presentations. In addition, Lachlan is a dynamic scientist; over the past seven years, his research has grown from matrix characterization to disc mechanics to tissue culture to genetic diseases to growth plate biology to genetic sequencing. It has been very impressive to witness his maturation and a reminder to myself that a successful researcher cannot be stagnant. I remember once when I finished up some motion segment mechanical testing for Lachlan’s MPS project, we shared the results with Dawn, and we were all very excited by the significant changes that we saw between diseased and healthy animals. Lachlan had the idea that the

source of the deficiency was incomplete ossification of the vertebral endplates, and he was excited to do more indentation testing to show that the endplates were truly softer with disease. I was young and inexperienced and thought to myself, “You want to do more work??” Lachlan has an incredible work ethic and I am lucky to have him as an example. Through many dinners at Devil’s alley, craft beers, Game of Thrones episodes, and bad Netflix and Philly Film Fest movies, I have learned as much from Lachlan as anyone else and thank him for the good conversation.

Harvey Smith, our surgical collaborator from HUP, joined the spine team in about 2013, spending two years with me as I finished my PhD work. Harvey stands out from his surgical colleagues for two reasons. First, he has a rare level of interest in pursuing research as surgeon-scientist. Orthopaedic surgery is very demanding, yet Harvey finds a way to contribute real time and effort to research. He directly contributed to my work by performing ~50 rat surgeries, often showing up early in the morning after a long night in the human OR. He even takes a pay cut to spend this extra time in the lab (which in surgeon \$\$ is a lot!). Second, he is a deep thinker. One key difference between surgery and science is pace; surgeons have to make lightning fast decisions when things go wrong; scientists encounter a problem and then sit back and think, have a coffee, maybe a beer, sleep on it, talk to their colleague, sleep on it again, and make a decision. For Harvey to possess both those traits speaks to his intelligence and adaptability. Likewise, he brings a desire for technical rigor that is uncommon among clinicians, something I can appreciate as an engineer; he excelled as an undergraduate physics student at Harvard (and is even published in an astrophysics journal). I benefitted directly from his technical background as he guided my work with his expertise on T2 mapping, which generated

crucial data in determining DAPS fate after implantation. I look up to Harvey for his unmatched work ethic; when it comes to planning a huge day of surgery, his simple motto is: “gotta do it”. I also look up to him for his fashion sense; he buys only the finest suits from Manhattan; he even has his initials embroidered on his shirt sleeves.

Three of my lab colleagues contributed significantly to this dissertation, so much so that their names should also be on the cover.

First, Andrew Milby did a one year rotation in the lab during his residency in orthopaedic surgery. He started at a time when I was really struggling to get the rat model off the ground; there were many problems: vascular issues, implant stability, analysis methods. Working together, Andrew and I increased the amount of surgeries we could perform and eliminated all surgical methods that were not viable. Having Andrew on this project was paramount to the success of the rat model; he brought dedication, focus, and patience and, together, we developed a surgical strategy that worked for ~200 surgeries. He liked to say that he ensured “six sigma” quality control for each rat. In addition, Andrew developed a DAPS rolling technique that greatly reduced the time for DAPS fabrication, enabling many of the later in vitro studies. Andrew is an excellent surgeon and a good friend, and while I do not know where we will be in the future, I hope to collaborate with him.

Dong Hwa Kim (DHK) has been my partner in crime over the course of this project. Our backgrounds are opposite. She came from a materials/cells/tissue culture lab, whereas I had a tissue mechanics/animal models experience; our skillsets complimented each other well and we enjoyed a mutually beneficial collaboration. DHK taught me tissue culture and various assays, and made all the NP constructs for these studies. In

return, I helped her with mechanical testing and implanted her own engineered discs. She has been very dedicated to helping me; the most memorable moment is from the day her second daughter, Andrea, was born. That day, DHK was performing immunostaining for me, and she stayed in the lab until 4:30 pm to finish, at which point she called Sujin, her husband, to bring her to the hospital. DHK had a healthy baby girl by 6:30 pm, only two hours later (!). She later confirmed that she was in labor most of the day. It goes without saying that she is an amazing person and scientist.

Sarah Gullbrand joined the lab towards the end of my tenure and was immediately integrated into our spine team. She filled a void that Andrew left, as there were no other junior lab members besides myself that were primarily focused on spine, bringing enthusiasm for disc research and a fresh perspective to lab meetings. With her previous MRI experience, she quickly developed MRI protocols for scanning DAPS and rat tail motion segments and the data she ultimately generated was critical to understanding DAPS behavior in vivo. She is a little loopy from spending so much time near large magnets; Sarah scanned hundreds of DAPS samples over the ~2 years we worked together. I thank her for her (selfless) hard work and collegiality.

My girlfriend/colleague Katie Reuther was senior to me as a graduate student and is a much better researcher. She is an incredible teammate and defined the Soslowky lab culture for much of her tenure, and she is a master organizer (see our shared Google calendar) that creates and perfectly performs massively complex study designs. She leaves no room for error in her own work. Comparatively, I have the attention span of a gnat and have glaring errors that I constantly have to make up for. Academically, Katie is peerless and set an example for me that I had no chance in imitating. That said, she was

incredibly supportive throughout my time at Penn. As a fellow graduate student, she could relate to the number of hours I worked and the erratic schedule I kept. She always listened to my latest DAPS updates, while both encouraging and complimenting me, and she made me realize that it is important to celebrate every milestone along the way. We had a lot of fun together and I look forward to more with my best collaborator.

Finally, my parents have sacrificed time, money, comfort, happiness, freedom, and more to put me in this position. My mom is a nurse and my dad is a gearhead, and as they have educated me on their own interests, I chose a career path in bioengineering that combines aspects of their careers. There is an interesting chapter in *Outliers* by Malcolm Gladwell that discusses two boys with nearly equal mental capacity, one with a supportive family and one whose parents are absent. As he describes the coming of age and ultimate failures of the smart boy with a negligent family, Gladwell makes the case that a person will only be successful if they are surrounded by a support group. I am not an unusually smart person, but I am smart enough, and I was given every advantage by my parents growing up. Some examples: my mom read to me at night when I was still *in utero*, my mom read her nursing case studies to me when I was barely old enough to understand them, my parents moved our family to NJ for better schools, they financed my undergraduate education, they bought me the car that I used to travel to Colorado to start graduate school, they picked up my wash while I was writing my proposal and returned it the next day along with a week's worth of food, not to mention that my dad has chauffeured me around for the last 10 years. At Penn, I have been supported in recent years by a number of people, and while I am incredibly grateful to those who were a part

of my time here, they had no chance in replicating to the selflessness, love, and dedication my parents have demonstrated to me every day for the last three decades.

ABSTRACT

NANOFIBROUS DISC-LIKE ANGLE PLY STRUCTURES FOR TOTAL DISC REPLACEMENT IN A SMALL ANIMAL MODEL

John T. Martin

Robert L. Mauck, Ph.D.

Low back pain affects 85% of the population and carries a socioeconomic price tag of \$100 billion USD per year. Lumbar intervertebral disc disease is strongly implicated as a causative factor in back pain, as degeneration, which is ubiquitous in the population, leads to loss of normal spine function. For these reasons, our lab has developed disc-like angle ply structures (DAPS) for total disc replacement. These cell-seeded replacements are designed to match the natural hierarchical structure and function of the native disc and correct spinal kinematics after end-stage disc disease.

In this dissertation, I describe the development of a rat caudal spine (tail) model of total disc replacement as a platform to evaluate DAPS *in vivo*; an external fixation system that immobilized caudal vertebrae at the site of implantation was required for DAPS retention and a radiopaque scaffold was developed to confirm intervertebral DAPS positioning. A detailed analysis of the DAPS *in vitro* growth trajectory was performed to select the optimum pre-culture duration before implantation. Cell-seeded DAPS were subsequently implanted in the rat tail and evaluated by histological, mechanical, and MRI analyses. DAPS successfully restored the mechanical properties of the native motion

segment in compression, providing the first evidence of the efficacy of engineered disc replacements. Adaptations of the implant to the in vivo environment were identified; there was a reduction in glycosaminoglycan after implantation, structural modifications to the NP material, and no evidence of vertebral integration. In tackling the first of these issues, a pre-culture strategy that primed DAPS for the in vivo environment was developed; using a rat subcutaneous model, implant phenotype was best conserved post-implantation using a pre-culture strategy with a transient high dose of TGF- β 3. Future work will address maintenance of NP structure, vertebral integration and scaling up to human sizes.

In my work, the most promising finding was that DAPS replicated compressive motion segment mechanical properties after implantation supporting the idea that engineered biological disc replacement is a possibility for clinical treatment of advanced disc disease.

TABLE OF CONTENTS

ACKNOWLEDGEMENTS II

ABSTRACT..... X

LIST OF TABLES XVI

LIST OF ILLUSTRATIONS..... XVII

CHAPTER 1 - INTRODUCTION..... 1

1.1 Motivation: Low Back Pain.....1

1.2 Intervertebral Disc Anatomy.....2

1.3 Intervertebral Disc Mechanical Function7

1.4 Intervertebral Disc Degeneration.....9

1.5 Surgical Strategies for Treating Symptomatic Disc Disease13

1.6 Overview of Disc Regeneration Strategies14

1.7 Native Tissue Benchmarks for Successful Regeneration16

1.8 In Vitro Culture Systems for Developing Regenerative Therapies.....18

1.9 In Vivo Models for Disc Research.....38

1.10 Acellular Biomaterials as an Alternative to Traditional Tissue Engineering46

1.11 Current Challenges for Regenerative Therapies49

1.12 Conclusion of Introduction.....50

CHAPTER 2 – PREVIOUS WORK 52

2.1 Engineered Intervertebral Discs52

2.2 Trajectory Based Tissue Engineering – Implantation at Peak Maturation State vs. Maturation Rate.....	58
2.3 Summary	60
CHAPTER 3 – EXECUTIVE SUMMARY	61
CHAPTER 4 - TRANSLATION OF AN ENGINEERED NANOFIBROUS DISC-LIKE ANGLE PLY STRUCTURE (DAPS) FOR INTERVERTEBRAL DISC REPLACEMENT IN A SMALL ANIMAL MODEL	65
4.i Preface.....	65
4.1 Introduction	66
4.2 Methods	68
4.3 Results	77
4.4 Discussion	84
4.5 Conclusion.....	87
CHAPTER 5 - A RADIOPAQUE ELECTROSPUN SCAFFOLD FOR ENGINEERING FIBROUS MUSCULOSKELETAL TISSUES: SCAFFOLD CHARACTERIZATION AND IN VIVO APPLICATIONS.....	88
5.i Preface.....	88
5.1 Introduction	88
5.2 Methods	91
5.3 Results	99
5.4 Discussion.....	108
5.5 Conclusions	112
CHAPTER 6 - INTERMEDIATE AND LONG-TERM OUTCOMES OF AN ACELLULAR DISC-LIKE ANGLE PLY STRUCTURE (DAPS) FOR INTERVERTEBRAL DISC REPLACEMENT IN A SMALL ANIMAL MODEL	114
6.i. Preface.....	114
6.1. Introduction	114

6.2. Methods	116
6.3 Results	121
6.4 Discussion.....	130
6.5 Conclusion.....	133
CHAPTER 7 - IN VITRO GROWTH TRAJECTORY AND IN VIVO FUNCTION OF CELL-BASED DISC-LIKE ANGLE PLY STRUCTURES (DAPS) FOR TOTAL DISC ARTHROPLASTY.....	135
7.i Preface.....	135
7.1 Introduction	135
7.2 Materials and Methods	138
7.3 Results	144
7.4 Discussion.....	159
7.5 Conclusion.....	164
CHAPTER 8 - OPTIMIZATION OF IN VITRO PRE-CULTURE TO MAXIMIZE IN VIVO PERFORMANCE OF A CELL-SEEDED DISC-LIKE ANGLE PLY STRUCTURE (DAPS) FOR TOTAL DISC REPLACEMENT.....	166
8.i Preface.....	166
8.1 Introduction	166
8.2 Methods.....	169
8.3 Results	176
8.4. Discussion	187
8.5. Conclusion.....	191
CHAPTER 9 – SUMMARY, FUTURE DIRECTIONS AND CONCLUSIONS....	193
9.1 Summary	193
9.2 Future Directions.....	194
9.3 Conclusions	199

APPENDIX I – DEVELOPMENT OF A QUANTITATIVE MRI ANALYSIS PROTOCOL: POPULATION AVERAGE T2 MRI MAPS REVEAL QUANTITATIVE REGIONAL TRANSFORMATIONS IN THE DEGENERATING RABBIT INTERVERTEBRAL DISC THAT VARY BY LUMBAR LEVEL	201
I.i Preface	201
I.1 Introduction.....	201
I.2 Methods	204
I.3 Results.....	215
I.4 Discussion	224
I.5 Conclusion	228
APPENDIX II – DEVELOPMENT OF A PRECISION MECHANICAL TESTING PROTOCOL: NEEDLE PUNCTURE INJURY CAUSES ACUTE AND LONG- TERM MECHANICAL DEFICIENCY IN A MOUSE MODEL OF INTERVERTEBRAL DISC DEGENERATION.....	229
II.i Preface.....	229
II.1 Introduction	229
II.2 Methods.....	231
II.3 Results	240
II.4 Discussion.....	247
II.5 Conclusion.....	250
BIBLIOGRAPHY	252

LIST OF TABLES

Table 1-1 Relevant Native Tissue Benchmarks for Regeneration or Replacement

Table 5-1 Composition of Solutions Used to Produce Electrospun Scaffolds

Table 6-1 sDAPS and Control Group Sample Sizes

Table 8-1 Scoring System For Determining Best Pre-culture Condition

Table I-1 Modified Gaussian functions used for NP T2 curve and surface fits

Table I-2 Coefficient of Determination (R^2) for 4 modified Gaussian distribution functions fit to NP T2 Maps

LIST OF ILLUSTRATIONS

Chapter 1 – Introduction

Figure 1-1 Intervertebral disc anatomy

Figure 1-2 Annulus fibrosus structure

Figure 1-3 In vitro model systems

Figure 1-4 Three dimensional culture systems: material selection, fabrication, and examples

Figure 1-5 Composite engineered discs

Figure 1-6 Isolation of a bovine caudal disc for organ culture

Figure 1-7 External device for simulated loading in rat model

Figure 1-8 Needle puncture injury in the rat tail

Figure 1-9 In vivo models of total disc replacement

Figure 1-10 Acellular biomaterials for regenerative medicine

Chapter 2 – Previous Work

Figure 2-1 Hyaluronic acid (HA) hydrogels for NP regeneration

Figure 2-2 Electrospun scaffolds for AF tissue engineering

Figure 2-3 Fabrication of DAPS, an engineered composite disc

Figure 2-3 Trajectory-based tissue engineering

Chapter 4 – Translation of an Engineered Nanofibrous Disc-like Angle Ply Structure (DAPS) for Intervertebral Disc Replacement in a Small Animal Model

Figure 4-1 Fabrication of disc-like angle ply structures (DAPS) that replicate the intervertebral disc lamellar patterning

Figure 4-2 DAPS implantation into the rat caudal spine and analysis of disc height

Figure 4-3 External fixation to stabilize the caudal spine and improve DAPS retention

Figure 4-4 DHI and bony anatomy for DAPS implantations with or without external fixation

Figure 4-5 Histological appearance of DAPS in the rat caudal spine

Figure 4-6 Cell infiltration into PCL-only DAPS in vivo

Figure 4-7 Sacrificial DAPS (sDAPS) improve cell colonization in vitro and in vivo

**Chapter 5 – A Radiopaque Electrospun Scaffold for Engineering Fibrous
Musculoskeletal Tissues: Scaffold Characterization and In Vivo Applications**

Figure 5-1 Electrospun radiopaque scaffold

Figure 5-2 Radiopaque engineered discs in a rat model of total disc replacement

Figure 5-3 Structure, linear attenuation coefficient, and tensile modulus of radiopaque scaffolds

Figure 5-4 MSC viability and osteogenic potential on radiopaque scaffolds

Figure 5-5 Visualization of radiopaque scaffold implanted into the bovine meniscus

Figure 5-6 High radiopacity rDAPS in vivo

Figure 5-7 Multilayer rDAPS in vivo

Chapter 6 – Intermediate and long-term outcomes of an acellular disc-like angle ply structure (DAPS) for intervertebral disc replacement in a small animal model

Figure 6-1 Study design: evaluation of acellular engineered discs

Figure 6-2 Mechanical properties and gross appearance at 4 weeks

Figure 6-3 Three-dimensional μ CT reconstructions at 2, 4 and 12 weeks

Figure 6-4 – Alcian blue and picosirius red stained histological sections at 2, 4, and 12 weeks

Figure 6-5 – Immunostaining of types I and II collagen at 12 weeks

Chapter 7 - In Vitro Growth Trajectory and In Vivo Function of Cell-Based Disc-like Angle Ply Structures (DAPS) for Total Disc Arthroplasty

Figure 7-1 Study 1: In Vitro growth trajectory of cell-seeded DAPS: design and results

Figure 7-2 Geometry and Creep Model Parameters of Cultured DAPS

Figure 7-3 Study 2: In vivo implantation of immature, rapidly growing DAPS

Figure 7-4 Study 2 (cont.): Compositional analysis of implanted DAPS

Figure 7-5 Study 3: In vivo implantation of fully matured DAPS

Chapter 8 - Optimization of in vitro pre-culture to maximize in vivo performance of a cell-seeded disc-like angle ply structure (DAPS) for total disc replacement

Figure 8-1 Study design: Optimization of pre-culture strategies

Figure 8-2 – Picrosirius red (collagen) and Alcian blue (proteoglycan) staining

Figure 8-3 Detailed MTT (metabolic activity) results

Figure 8-4 Summary of MTT (metabolic activity) results

Figure 8-5 Detailed T2 MRI (composition) results

Figure 8-6 Summary of T2 MRI (composition) results

Chapter 9 – Summary and Future Directions

Figure 9-1 Combination Compression-Torsion Bioreactor

Appendix I – Development of a Quantitative MRI Analysis Protocol: Population Average T2 MRI Maps Reveal Quantitative Regional Transformations in the Degenerating Rabbit Intervertebral Disc that Vary by Lumbar Level

Figure I-1 Radiographic analysis of response to injury

Figure I-2 MRI analysis of response to injury

Figure I-3 Gaussian distribution functions for NP auto-segmentation

Figure I-4 Geometry analysis for MR

Figure I-5 Population average T2 maps and T2 quantification by disc region

Figure I-6 Disc geometry pre- and post-injury

Figure I-7 T2 difference as a function of level

Figure I-8 Effects of puncture by level and baseline differences

Appendix II – Development of a Precision Mechanical Testing Protocol: Needle Puncture Injury Causes Acute and Long-Term Mechanical Deficiency in a Mouse Model of Intervertebral Disc Degeneration

Figure II-1 μ CT analysis of disc

Figure II-2 Mechanical testing and optical displacement tracking setup

Figure II-3 Optical displacement vs. machine reported displacement

Figure II-5 Disc height, GAG content, and collagen content at week 8

Figure II-6 Histological results at week 8

Figure II-7 Elastic mechanical parameters before and 8 weeks after puncture injury

Figure II-8 Viscoelastic mechanical response before and 8 weeks after puncture injury

CHAPTER 1 - Introduction

1.1 Motivation: Low Back Pain

The etiology of low back pain is poorly understood, however its societal impact is well studied and remarkable. 70-85% of the population will experience a bout of back pain at one point in their life [5]. It is the second most common reason for visits to a primary care physician, behind the common cold [112], and is the second most common reason for surgery, behind coronary bypass procedures [193]. Chronic low back pain affects over 50% of the population aged 65 or younger, and prevalence increases with age [5], resulting in more than \$100 billion in medical costs and lost wages in the United States [112], approximately 1% of our gross domestic product [4]. Unfortunately, chronic low back pain is on the rise, increasing from 4% of the population to 10% of the population over the span of 14 years from 1992-2006 [69].

There are many risk factors for reported back pain; these are derived not only from physical sources, like musculoskeletal disease, but also from environmental, psychological and socioeconomic phenomena. Some are self-evident; previous musculoskeletal trauma is a risk factor for back pain, either directly related to the back or related to another joint where symptoms propagate through the kinetic chain and affect the back. There is a strong genetic component; the best evidence of which is derived from a study of Finnish twins, where twins had similar MRI findings despite discordant occupational histories [17]. Psychosocial factors, like anxiety/depression and Workers' compensation/job dissatisfaction, as well as self-induced comorbidities, like smoking, obesity, and type II diabetes, are all inextricably linked to reports of chronic pain.

There is an additional and important factor related to low back pain that will be the focus of this dissertation. Lumbar intervertebral disc degeneration, which is ubiquitous in the population, has been implicated as a causative factor in low back pain, as deficiency in disc function is closely tied to the degeneration of its components [89, 146, 189]. Disc pathology can result in back pain and also chronic radicular pain when the loss of disc height or the instability of the intervertebral joint cause compression of the adjacent neural structures. The disc itself may also be a direct source source of pain, termed discogenic pain, as the ingrowth of nociceptors can result from disc injury or degeneration [60]. Restoration of disc health and function may be necessary for long-term relief from chronic low back and radicular pain.

1.2 Intervertebral Disc Anatomy

The human spine is a major structural component of the skeleton, providing a flexible connection between the lower and upper halves of the body and shielding the spinal cord from external forces. Flexibility can be mainly credited to the spinal column's heterogeneous structure, predominantly made up of five vertebral bodies (L1, L2, L3, L4, L5) and five intervertebral discs (L1-L2, L2-L3, L3-L4, L4-L5 and L5-S1) organized as repeating vertebral body – intervertebral disc – vertebral body elements (referred to as motion segments). The intervertebral disc is a composite fibrocartilaginous tissue. It provides the spine with flexibility while maintaining the even distribution of joint forces from one vertebral body to the next. The disc has three major components, an inner gelatinous core, the nucleus pulposus (NP), a highly organized outer fibrocartilage, the

annulus fibrosus (AF), and a porous boundary between inferior and superior vertebral bodies, the cartilaginous endplate (CEP) [Fig. 1-1].

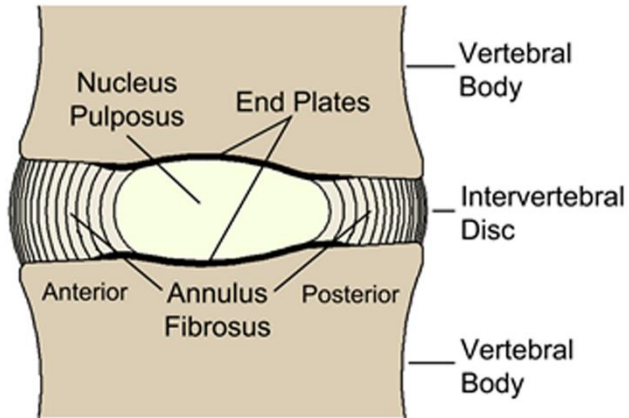


Figure 1-1 Intervertebral disc anatomy The disc lies between adjacent vertebral bodies and is composed of a gelatinous nucleus pulposus core, surrounded by an organized fibrocartilage, the annulus fibrosus. The nucleus is bounded superiorly and inferiorly by cartilaginous endplates. [223]

The NP is an anisotropic distribution of type II collagen fibrils encased in a matrix of hydrophilic proteoglycans at the core of the disc. It makes up approximately 30% of the disc by volume [188]. Type II collagen is a common extracellular matrix protein found throughout the body in hyaline cartilage. In the NP, it forms a loose meshwork of fibrils and while its function is not well understood, it is thought to provide a substrate for proteoglycan and cell accumulation [238]. Proteoglycans are complex high molecular weight biomolecules that consist of a backbone core protein connected to glycosaminoglycan (GAG) side chains that form a structure similar to a pipe brush. GAGs are highly negatively charged molecules and, as the pipe brush structure allows for a large reactive surface area, the GAG sidechains of a proteoglycan attract a significant amount of water molecules into the NP. As a result, the NP of the average adult human is approximately 70% water [97]. The most prevalent proteoglycan in the NP is aggrecan, which binds to the GAGs chondroitin sulfate and keratan sulfate. In addition, there are two major cell phenotypes within the NP, notochordal-like cells and chondrocyte-like cells. They are classified by their morphology; notochordal-like cells have similar appearance to cells that derive from the embryonic notochord, the precursor to the spinal column, and chondrocyte-like cells are similar to the typical chondrocyte found in other forms of cartilage. These cells both function similarly, maintaining and renewing the disc extracellular matrix, however, notochordal-like cells are believed to be more metabolically active [44]. With maturation, a gradual transition in NP cellularity occurs as notochordal cells disappear and are replaced by chondrocyte-like cells. In addition,

decreases in cell number and viability in adult NP compared to juvenile NP has been observed [97]. The disappearance of the notochordal-like cell population, occurring in the first 10 years of life, has therefore been linked to disc degeneration.

The NP is surrounded by a highly organized fibrocartilaginous structure, the AF [Fig. 1-2].

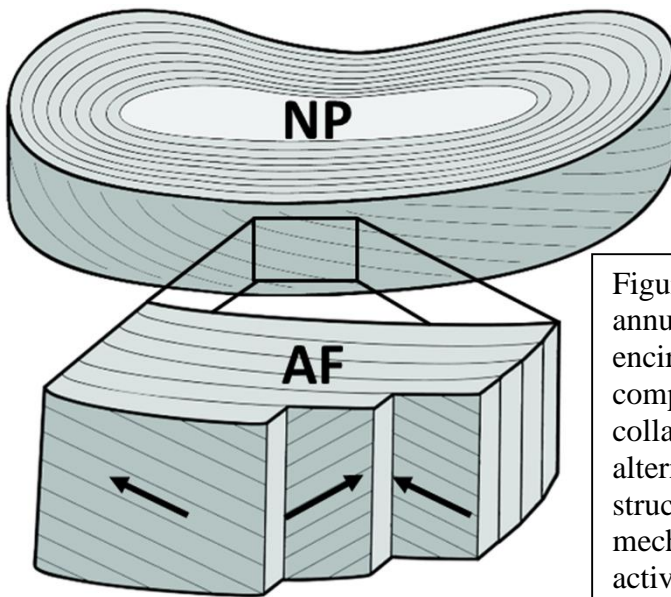


Figure 1-2 Annulus fibrosus structure The annulus fibrosus is a fibrocartilage that encircles the nucleus pulposus and is composed of multiple layers of aligned collagen fibers; apposed layers have alternating fiber alignment. This hierarchical structure supports multidirectional mechanical loads during routine daily activities.

There is no distinct boundary between the NP and the AF. From NP to AF, there is a gradual transition from type II collagen rich NP tissue to type I collagen rich AF tissue. The AF is organized into distinct concentric sheets of type I collagen fibers called lamellae which interdigitate with the inferior and superior vertebral bodies, enclosing the NP. The collagen fibers within each lamella are parallel and from lamella to lamella alternate $\pm 30^\circ$ to the transverse axis. The number and thickness of lamellae is individual and spinal location dependent. Specifically, in the adult human lumbar spine there are between 15 and 25 lamellae [206] that range in thickness from 200 to 400 μm [97]. Type I collagen is a major structural protein, thus, the arrangement of lamellae and intralammellar fibers provides a significant amount of functional versatility, allowing the disc to resist mechanical forces in tensile, compressive, torsional, and bending orientations. In addition to type I collagen, the lamellae also include proteoglycans and water, although to a lesser extent than the NP, and elastin, a protein that provides structural support at low loads. The primary cells of the AF are spindle shaped and fibroblast-like. They align themselves along collagen fibrils and maintain the disc extracellular matrix.

Finally, the NP and AF are constrained inferiorly and superiorly end by the CEPs, porous boundaries between vertebral bodies. The CEPs are thin permeable cartilaginous membranes, about 1 mm thick [97] located above and below the NP at the adjacent vertebral bodies. A network of vertebral blood vessels are embedded within the CEP, which function as the main source of nutrition delivery and waste removal for the NP.

1.3 Intervertebral Disc Mechanical Function

The functional properties of the disc are derived from its structural and material properties. In vivo the disc is primarily loaded in compression or in a combination of compressive and torsional or bending loads. In pure compression, the mechanical response of the disc as a structure is governed by the balancing of applied external forces with internal hydrostatic pressure. The NP is primarily composed of water and is therefore characterized as nearly incompressible [173]. As the disc is compressed, the NP hydrostatically pressurizes and expands radially. In turn, the AF is compressed radially and consequently experiences a circumferential hoop stress. Collagen fibers of the AF lamellae then reorient circumferentially, and as a result of the alternating fiber angles, are restricted by an interlamellar shear force [175].

The load response of the disc is both nonlinear and viscoelastic. At low loads, the collagen fiber network exhibits a nonlinear response, which is attributed to recruitment and realignment of the crimped collagen orientation. When all fibers are engaged, the response is approximately linear. Thus the stress/strain behavior is divided into two distinct regions, a low load/low stiffness “toe” region, and a high load/high stiffness “linear” region. During compression, water is expelled from the disc. Since the internal constituents have changed, the disc is unable to recapitulate its original stress/strain response as it is unloading. This phenomenon is known as hysteresis and is common to any biphasic material. As the disc transitions from tension to compression or compression to tension, there is a region of joint laxity known as the neutral zone. The disc primarily

functions during routine activities within the neutral zone, and thus this behavior, which can be characterized by low stiffness as collagen fibers are crimped and not engaged, is very important.

The disc demonstrates a viscoelastic response to compressive forces. This mechanical behavior is both time and history-dependent and can be characterized by both creep and stress relaxation behaviors. The creep response is governed by the movement of water out of the disc. Water is thought to leave in two phases. First, the path of least resistance is through the CEP, and therefore the short term creep response is governed by the permeability of the CEP. Once the pressure differential is balanced across the CEPs, fluid is pushed through the AF and out of the disc. The equilibrium creep response is therefore governed by the permeability of the AF [187].

There is a complex mechanical relationship between the NP and AF in other loading modes as well. For example, in torsion, the NP provides little resistance in comparison to the AF. Therefore, the torsional response is primarily driven by AF fiber tension. Since the AF has nonlinear behavior caused by the uncrimping of fibers as previously described, the torsional response of the disc is also nonlinear. During a consecutive sequence of counter clockwise and clockwise rotation, there is a region of joint laxity similar to what is experienced during cyclic tension/compression. This region is described as the torsional neutral zone, is characterized by low stiffness, and is the primary region in which the disc functions physiologically. In bending, one region of the disc is compressed, while the contralateral region is extended, and both the AF and NP are strained. The bending response is similarly nonlinear with regions of low and high stiffness. The axial component of the AF fiber direction is important in bending, as it

supports fiber tension on the extended side of the AF during bending events. The NP pressurizes during bending loads as well and previous reports have demonstrated that intradiscal pressures, or pressures generated in the NP, are highest during simulated occupation tasks involving bending from the waist and lifting heavy objects [242], suggesting that the disc materials are at a high risk for failure during bending.

Furthermore, complex loading events, where compression, bending, and torsional forces are superimposed, are known to be a risk for disc failure and herniation of the NP [39].

1.4 Intervertebral Disc Degeneration

1.4-1 Prevalence of degeneration

The lumbar intervertebral discs naturally degenerate even in the healthiest individuals; there is a strong correlation between MRI findings of disc degeneration and age [162]. Thus, disc degeneration is ubiquitous in the population; by age 40, 50% of all lumbar discs will be mildly degenerate while 40% while show signs of advanced degeneration [162]. This is true of both males and females, with the incidence rate slightly higher in males. Axial spinal loads and disc size increase when proceeding caudally along the lumbar spine, and as these are both certainly risk factors for degeneration, the incidence of degeneration does not correlate to caudal lumbar position. In fact, the discs with the highest risk for degeneration are the L3-L4 and L4-L5 discs, not the L5-S1 disc as one might expect [162]. This may be due to the specific orientations of the discs, as spinal curvature may affect the distribution of mechanical forces at the lowest lumbar level.

1.4-2 Clinical diagnosis of degeneration

Clinical diagnosis of degeneration usually occurs after and individual reports back pain and is primarily done through a combination of medical history examination, physical evaluation and radiography, and is eventually confirmed by magnetic resonance imaging (MRI). MRI allows for the quantitative, non-invasive assessment of soft tissues like the disc and, consequently, can be used to identify pathological changes in the disc. In the healthy disc, signal intensity on T2-weighted MR images is highest in the central, hydrated NP and dissipates radially with transition to the fibrocartilaginous AF [196]. With degeneration, there is a characteristic loss of NP signal intensity and consequently the NP and AF become indistinguishable [196]. These abnormalities are routinely assessed by visual inspection of MR images or by qualitative evaluations on an integer scale, like the Pfirrmann grading framework [196]. In addition, clinicians routinely evaluate candidates for surgery using MRI to identify disc abnormalities in the presence of radicular and/or low back pain. Disc-related surgery however is never performed for MRI indication of disc degeneration, as the correlation between back pain and degeneration is not perfect, and disc surgery is rarely performed for back pain alone, as the pathogenesis of back pain is complicated by a number of local substructures that are difficult to diagnose, including the disc, facet joints, spinal cord, spinal nerves, and surrounding muscles and other connective tissues.

1.4-3 Pathogenesis of degeneration

While the complete pathogenesis of disc degeneration is unknown, the hostile nature of the cellular environment has been implicated as an aggravating factor. The disc supports relatively large passive forces (body weight) and stabilizes the torso during dynamic movements, requiring abdominal muscle contraction and increasing spinal loads

[156]. In addition, the disc is almost completely avascular, as a sparsity of blood vessels is located at the periphery of the AF. Thus, any of the NPs nutritional needs are met by passive diffusion through the CEPs. The combination of large forces and avascularity provides for an extremely hostile environment for functioning disc cells. Consequently, the number and activity level of disc cells is quite low in comparison to other tissues [80].

Disc degeneration is characterized by several biological changes occurring in the NP, AF, and CEPs. The hallmark of degeneration is proteoglycan loss and the collapse of the intervertebral disc space. In addition to proteoglycan loss, other cellular and compositional changes occur. Specifically, number of viable NP cells is reduced, with the remaining forming clusters [206]. These cells display an increased expression of type I collagen mRNA and a decreased expression of Aggrecan and type II collagen mRNA, denoting a shift to a fibrocartilaginous phenotype. In addition, NP cells begin expressing an increased quantity of extracellular matrix catabolic factors and a decreased quantity of anabolic factors, coinciding with an increase in the prevalence in pro-inflammatory cytokines. Consequently, there is a shift in the internal disc biochemical constituents. With loss of pressure in the NP, the AF becomes disorganized, transitioning from radially bulged, to serpentine, to radially infolded. Also, the presence of annular defects like tears and delaminations increases, and AF cells increase their expression of catabolic matrix factors [75]. Changes in the CEP include calcification and complete disruption, which are both linked to degeneration. As a result of the altered mechanical loading, vertebral osteophytes form adjacent to the disc space.

1.4-4 Mechanical consequences of degeneration

Degenerative changes in the composition and structure of the disc have significant damaging effects on disc properties. While some studies have shown that human lumbar disc mechanics change as a result of degeneration, the number of studies to draw conclusions from is limited. This is due to the scarcity of non-degenerate tissue (to use as experimental controls) and a wide range of inter-subject variability. However, it has definitively been shown that both the proteoglycan content and disc height decrease, densely compacting the remaining tissue. In addition, there is an increased prevalence of type I collagen throughout the disc. These compositional and structural changes in the disc are important in understanding the resulting mechanical changes, at both the tissue and motion segment level. At the tissue level the loss of proteoglycan content results in a decreased swelling pressure in both the AF [100] and NP [107]. Hydraulic permeability also changes from an anisotropic distribution to an isotropic distribution in the AF [248] and decreases in the NP [107]. In addition, the biphasic compressive modulus of the AF increases [100] while that of the NP decreases [107]. The tensile modulus of the AF increases, while the Poisson's ratio, failure load, and strain energy density decrease [2]. At the motion segment level tissue compaction and proteoglycan loss result in decreased NP osmotic pressure; consequently there is an increased response to creep loads with degeneration [187]. This is supported by an increase in joint laxity displayed in flexion/extension, rotation, and bending [163]. Increases in axial strains in compression, and compression combined with flexion or extension have also been described. In addition, the disc loses its ability to transfer compressive forces through the hydrostatic NP pressure/annular tension mechanism during degeneration. The AF begins to bear

compressive loads as axial AF compressive strains are increased, and radial strains transition compressive to tensile [189].

1.5 Surgical Strategies for Treating Symptomatic Disc Disease

Regenerative strategies for treating disc degeneration must be compared to clinical techniques to evaluate their ability to improve clinical outcomes; a description of clinical techniques is thus a necessary part of the discussion of disc regeneration. The primary indications for clinical intervention related to spine disease are local or radicular pain and/or neurological dysfunction. Thus, current surgical strategies to treat disc disease aimed primarily at alleviating pain and reducing neurological deficits.

The current gold-standard surgical treatment for treating symptomatic degenerative disc disease is spinal fusion. This technique alleviates pain by expanding the disc height to decompress neural structures and by solidifying the disc space with a combination of vertebral hardware and intervertebral spacers. In the US, approximately 400,000 spinal fusion surgeries are performed per year, a rate that has consistently increased over the past 10 years in comparison to other standard musculoskeletal surgeries [200]. Many spinal fusion cases have unfavorable clinical outcomes however (approximately 20%) [184], and revision surgeries are required for a number of reasons, including mechanical complications related to fusion, post-operative stenosis and spondylosis, and the degeneration of adjacent discs [201]. Pseudoarthrosis, for example, is a common mechanical complication that accounts for the majority of revisions [201], as it occurs in approximately 0-15% of cervical fusion cases [215] and 5-10% of lumbar fusion cases [37, 144], and is a known cause of recurrent pain. Another complication

related to spinal fusion is adjacent segment degeneration, which may be caused by the artificial segment rigidity following fusion and altered loads in adjacent discs. There have been many reports of adjacent disc disease following fusion in the literature, though the incidence rates and epidemiology are still points of debate [85].

Total disc prostheses, like the Synthes Pro-Disc, are available as an alternative to fusion and are intended to preserve near-physiological spine kinematics, thus mitigating adjacent segment disease. These procedures involve decompressing the disc space, removing the native tissue, and inserting the prosthetic into the intervertebral space. While total knee and hip replacements have gained widespread acceptance as gold-standard treatments for knee and hip diseases, total disc arthroplasty has not. There are a number of reasons for this. In comparison to fusion, arthroplasty is a more complicated surgery and requires special training from the device manufacturer. In addition, fusion has been relatively successful, and controlled trials have not demonstrated any clinical benefit of arthroplasty in comparison [235]. Some complications of total disc arthroplasty include implant subsidence and migration, the degeneration of adjacent structures, the generation of wear particles and periprosthetic tissue inflammation [198].

1.6 Overview of Disc Regeneration Strategies

Spinal fusion and total disc arthroplasty have seen much success in recent years through the improvement of instrumentation and the rise of minimally invasive surgery. Inherently these techniques, however, do not restore normal spine function because; in both cases, the disc is removed and the original structure and mechanical functions of the spine are not replicated. Consequently, while they may initially relieve pain, they are

subject to these post-operative complications. Disc degeneration presents clinically as a spectrum that ranges from non-degenerate to mildly degenerate to severely degenerate, with the level of tissue degradation correlating to the age of the individual [162]. Thus new regeneration techniques aim to rescue the disc from either early or late stage degeneration, rather than remove it, and promise to improve upon current standards by restoring the intervertebral joint to a healthy and natural state. Early in the degenerative process, interventions with cell, gene, or pharmaceutical therapies may maintain disc function by reducing inflammation and preventing further matrix degradation [93, 152, 243]. A more substantial approach will likely be necessary for the treatment of end-stage disc disease, due to depletion of the endogenous cell population and irreversible deterioration of tissue structure. In such circumstances, a composite (or whole disc) approach would be required, where the entirety of disc structure and function is replicated. Two general strategies have emerged to treat at different points along the spectrum of intervertebral disc disease.

1) Injectable therapeutics. For early stage degeneration where the intrinsic ability of the tissue to repair itself is still intact but must be bolstered, the injection of therapeutics into the native disc may slow or reverse degeneration. These techniques are aimed at directly improving the quality of the NP, the disc region that displays degenerative changes earliest. Research efforts on injectable therapeutics are based either on the injection of cells that have the ability engraft into the host tissue, proliferate, and deposit new extracellular matrix to replenish the diseased tissue, or, the injection of growth factors that can modify the behavior of the resident cell population so that they develop a phenotype more conducive to anabolism.

2) Total or partial disc replacement. For end-stage degeneration when the native tissue likely has little capacity for regeneration, the removal of the native diseased AF and/or NP tissues and their replacement with an engineered substitute may restore healthy joint structure and function. Efforts to replace the native disc structure through the development of viable engineered tissues leverage the growing knowledge base on cell, biomaterial, and cell-material interactions. The ultimate goal of my work will be to develop an engineered intervertebral disc that functionally replaces the native disc.

1.7 Native Tissue Benchmarks for Successful Regeneration

A number of criteria must be met for validating the efficacy of the therapeutic modalities proposed above at achieving tissue regeneration. To define a set of criteria, non-diseased native tissue provides a number of compositional, structural, and functional benchmarks. Strict recapitulation of every native tissue characteristic may not be necessary for disc regeneration. Thus, we propose a set of relevant properties for “successful” disc regeneration which have been summarized from the literature and are listed here in Table 1-1. The parameters presented are specific to non-degenerate human tissue, and in addition, as the primary function of the disc is mechanical, emphasis is placed on mechanical properties, which are reported as measured from bone-disc-bone motion segments with facet joints removed.

Table 1-1. Relevant Native Tissue Benchmarks for Regeneration or Replacement

Compositional and Cellular	
<i>AF GAG</i>	10% dry weight OAF, 40% dry weight IAF [8]
<i>AF Collagen</i>	65-70% dry weight [190]
<i>AF Cell #</i>	9000 cells/mm ³ [190]
<i>NP GAG</i>	50% dry weight [8]
<i>NP Collagen</i>	15-20% dry weight [190]
<i>NP Cell #</i>	4000 cells/mm ³ [190]
<i>AF Water Content</i>	60-70% [190]
<i>NP Water Content</i>	80% [190]
Structural and Geometric	
<i>Disc Height</i>	11 mm [20, 188]
<i>Disc Width</i>	56 mm (lateral), 37 mm (AP) [188]
<i>NP %Volume</i>	30% [188]
<i>Lamellar Count</i>	15-25 [140]
<i>Lamellar Thickness</i>	200-400 um [102]
<i>Lamellar Fiber Angle</i>	alternating, 30-40 degrees [97]
Functional	
<i>Motion Segment Compressive Stiffness</i>	1700 N/mm [20]
<i>Motion Segment Bending Stiffness</i>	3-5 N-mm/degree [48]
<i>Motion Segment Creep Strain</i>	5% (Load = 750 N, 1 h) [20], 30% (Load =1000 N, 4h) [187]
<i>Motion Segment Creep Recovery Time</i>	8 h (Load = 2000N, 1 h) [187]
<i>Motion Segment Cyclic Loading Strain</i>	15% (1500 N, 10,000 cycles) [214]
<i>VB/AF Interface Stiffness or Failure Load</i>	2.85 MPa (unpublished internal data)
<i>AF Permeability</i>	0.25 (x10 ⁻¹⁵ m ⁴ /N-s) [23]
<i>NP Permeability</i>	0.90 (x10 ⁻¹⁵ m ⁴ /N-s) [107]

1.8 In Vitro Culture Systems for Developing Regenerative Therapies

In order to test if cells, growth factors, and biomaterials can function in a regenerative capacity, numerous in vitro model systems have been developed to mimic specific features of the intervertebral disc microenvironment. This applies to studying basic physiologic processes, injectable therapeutics and engineered tissue replacements. In vitro model systems generally include a cell source with regenerative potential, a material substrate on which the cells are cultured, and a set of external variables that can be controlled to replicate the disc microenvironment. The following section will introduce these three topics and provide examples from ongoing research in the field to present the current state of the art in this area.

1.8-1 Cell Sources

In the field of regenerative medicine, there are a wide variety of cell sources available for therapeutic use. In general, these can be categorized by their differentiation potential, that is, by their ability to assume phenotypic features similar to cells from different tissue types when provided with the appropriate environmental cues.

1.8-2 Pluripotent Cell Sources

Pluripotent stem cells can differentiate into all cell types and form all tissues derived from the three germ layers. Embryonic stem cells (ESCs), for example, are considered pluripotent and there has been some effort to use these as an injectable therapeutic for disc regeneration [11]. ESCs require special handling, however, as their phenotype is difficult to direct and maintain. In addition, clinical use of ESCs requires allogeneic cells and so their use incorporates limitations such as the potential for immune

rejection and infection. Likewise, the supply of such cells is currently limited and there are well-known ethical issues related to obtaining fetal cells.

As an alternative to ESCs, fully differentiated cells, such as skin fibroblasts, can be induced into pluripotency by introducing a series of reprogramming genes through viral transduction and other mechanisms [12]. These are aptly named induced pluripotent stem cells or iPSCs. Similar to ESCs, iPSCs require a fibroblast feeder layer and a number of chemical factors to first maintain the cells in an undifferentiated state and then to induce differentiation. In contrast to ESCs, however, there is an unlimited supply of donor cells from adult skin tissue. This is a promising, though new, line of research for the regeneration of the intervertebral disc [13, 14] as well as other musculoskeletal tissues [15, 16]. One drawback of iPSCs is that their preparation is time-consuming, requiring months to generate, differentiate, expand and direct towards skeletal lineages [17], which may limit their use as an autogenous source. To overcome this, researchers in Japan, Europe and the US are developing iPSC banks with fully differentiated cell lines for on-demand access.

1.8-3 Multipotent Cell Sources

There are a number of multipotent stem cell sources under investigation for disc regeneration. In general, multipotent cells have limited differentiation potential compared to pluripotent cells, but have more clinical relevance as they can be harvested from adults. For applications in orthopaedics, there are multipotent sources with the ability to adopt phenotypes of a number of musculoskeletal tissues [18, 19], including cartilage and fibrocartilage, like the NP and AF. Mesenchymal stem cells (MSCs), for example, are a popular source because they can be isolated from a number of locations, most commonly

bone marrow, adipose tissue, and synovium, and can generate tissues with compositional and functional properties similar to native cartilage [20-22]. There is a growing body of work on MSCs for disc regeneration that ranges from in vitro experiments to animal models to clinical trials [23]. A minor surgical procedure is required in most cases for retrieving MSCs from the donor, and so donor site morbidity remains an issue. Likewise, it is not clear that every MSC has the same potential, and so methods to sort and use optimized sub-populations of MSCs is an area of considerable interest.

1.8-4 Notochordal Cells

Another source of cells relevant to regeneration are those that reside within the disc at early development stages that are notochordal in origin. During development, the NP forms from the embryonic notochord [24], and cells that retain a notochordal-like appearance make up a portion of the NP cellular composition early in life. The disappearance of these cells, potentially due to either differentiation into less metabolically active chondrocyte-like cells or apoptosis, may be associated with the onset of degenerative change at older ages. It has been hypothesized that notochordal cells play an important role in healthy disc homeostasis and may have regenerative properties. Currently, there is significant research interest in notochordal cells for disc regeneration [25-34], either through direct injection into a degenerate disc, or for use in co-culture with another cell source like MSCs or degenerate NP cells. While studying the function of notochordal cells will likely elucidate mechanisms for regenerative therapies, a reliable source of notochordal cells, one that can be harvested and expanded for injection or tissue engineering, has yet to be identified.

1.8-5 Fully Differentiated Cell Sources

Fully differentiated or unipotent cells from a number of tissues lack stemness, but still have potential for regeneration. It has been well demonstrated that AF and NP cells can be isolated and cultured in vitro, and that these cells can produce tissue whose composition largely mirrors that of the native extracellular matrix; gene expression data suggests that AF cells maintain a fibrochondrogenic phenotype, with high levels of types I and II collagen mRNA; the NP phenotype is more chondrogenic and, similarly to articular chondrocytes, NP cells express type II collagen, the chondrogenic transcription factor SOX9, and aggrecan [35, 36]. NP cells also express unique factors that likely reflect their notochordal origin and the unique microenvironmental niche in which they must survive and function [37]. Potential sources for therapeutic AF and NP cells are from discarded disc tissue, such as degenerate tissue removed prior to spinal fusion for spondylolisthesis/disc disease. However, there exist technical hurdles related to this cell source given that degenerate tissue yields cells with an altered phenotype characterized by decreased proteoglycan production, senescence, catabolism, and a number of inflammatory markers [38-41]. These cells may be rescued from their degenerate state prior to their injection into the disc space, for example, by co-culture with a healthy cell population [42, 43].

Other terminally differentiated cells can be sourced from cartilage at various anatomical locations; these cells have demonstrated potential for musculoskeletal regeneration. Articular chondrocytes from non-load-bearing regions of the knee have been widely used (and are clinically available) for cartilage restoration procedures such as autologous chondrocyte implantation [44, 45]. While these cells have robust chondrogenic potential, their isolation is associated with local tissue damage. Nasal [46]

and auricular [47] chondrocytes have demonstrated potential for in vitro chondrogenesis, and local donor site morbidity related to the isolation of these cells may be preferable when compared to articular chondrocytes, as they are not in an environment which has potential for joint level communication of inflammatory signals, as is the case for a synovial joint. Additionally, allogeneic articular chondrocytes have recently become commercially available. As these cells are prepared from juvenile (deceased) donors, this is a source of highly active chondrocytes that has shown some clinical success in treating articular cartilage defects [48]; these cells may likewise have potential for disc regeneration applications.

1.8-6 Culture Systems

The physical environment in which cells are cultured has a significant influence on experimental outcomes; cells read cues from their material substrates to regulate phenotype and metabolic activity [49, 50]. The standard material platforms for disc cell culture fit into one of three categories: cells cultured in a thin layer on plastic dishes (monolayer culture), cells aggregated as pellets, encapsulated in hydrogels, or seeded onto fibrous scaffolds (three-dimensional culture), and live disc explants removed from animals or human cadavers and cultured in the lab (organ culture) [Fig. 1-3].

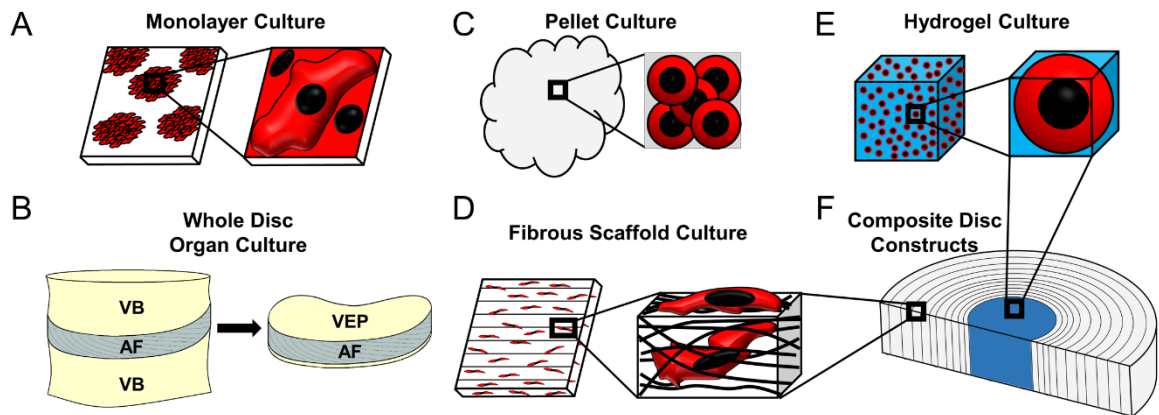


Figure 1-3 In vitro model systems (A) Monolayer culture allows for simple high-throughput studies of cell behavior. (B) Organ culture allows for studies of disc cells in their native environment. VB = vertebral body, AF = annulus fibrosus, VEP = vertebral endplate. (C) Cells can be aggregated into pellets through centrifugation for high throughput studies in a 3D environment. (D) To simulate the AF, cells can be cultured on scaffolds that mimic the organization of collagen fibers found in the AF region. (E) To simulate the NP, cells can be cultured in hydrogels so as to reproduce a spherical cell morphology. (F) A combination of fibrous AF scaffolds and hydrogel NPs allows for co-culture of cells in a simulated disc environment.

Monolayer Culture

Due to ease of manipulation and experimental assays, simple monolayer culture conditions have been used to generate the majority of our knowledge regarding mammalian cell behavior, and intervertebral disc cells are no exception. The procedure for culturing disc cells or other cell types in monolayer involves first isolating cells from donor tissue, suspending these cells in a growth medium, and plating the cell suspension onto a sterile polystyrene culture dish. Cells attach directly to the dish and can be serially passaged to expand their number. A number of outcomes can be measured; cells can be retrieved and their RNA can be extracted for gene expression analysis; cultures can be directly stained for protein and ECM components; cell appearance and morphology can be evaluated by microscopy; culture media can be extracted and its composition can be analyzed.

One or more cell-types and their interactions can be evaluated by simple modifications to a monolayer culture system. For example, the influence of NP cells on AF cells can be evaluated through co-culture; NP and AF cells can be seeded in direct apposition to study the influence of direct cell-cell communication, or seeded in culture dishes that have two tiers (one of which is porous) to study the influence of paracrine signaling between these two cell types. These are popular techniques in disc regeneration to evaluate the influence of one cell type on another; for example, to generate a NP-like phenotype in MSCs, MSCs can be co-cultured with NP cells [51].

Three-Dimensional Culture

In vivo, disc cells reside in a three-dimensional microenvironment that is not well represented by monolayer culture systems. Phenotypic differences are evident when

comparing NP cells cultured in monolayer, where they develop a fibroblast-like phenotype, to NP cells cultured in a three-dimensional environment [52, 53]. Indeed, the ‘de-differentiation’ which invariably occurs during cell expansion complicates interpretation of data acquired using monolayer culture methods.

A more realistic culture system would provide three-dimensional spatial cues for cells to promote or preserve their phenotype, and while the types of experimental assays suitable for application to cells in 3D culture are more limited than for monolayer culture, advantages include the ability to more effectively assess matrix elaboration and mechanical function. In vitro NP and AF models can be scaffold-free (as in pellet culture) or can be generated from naturally-occurring (agarose, alginate, collagen, fibrin, hyaluronic acid) or synthetic (polyethylene glycol, polyvinyl alcohol, polylactic acid, polycaprolactone) biomaterials [Fig. 1-4A].

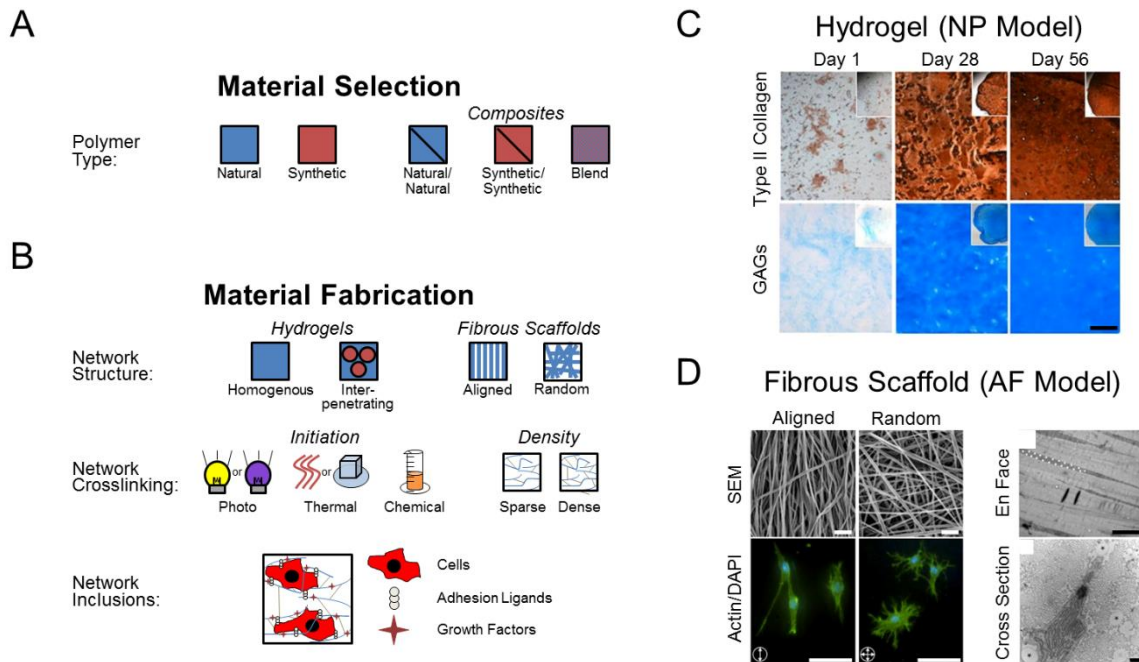


Figure 1-4 Three Dimensional Culture Systems: Material Selection, Fabrication, and Examples. (A) A variety of naturally-occurring and synthetic biomaterials, with specific physical and chemical properties, are available individually or as composite materials as a framework for cell culture. (B) Fabrication processes allow control over structural features and physical properties, and can incorporate bioactive components to better match the intervertebral niche or to elicit a desired cellular response (C) *In vitro* NP Model: NP cells cast in hyaluronic acid hydrogels develop a disc-like phenotype over 8 weeks of culture. This is evidenced by increasing levels of type II collagen and glycosaminoglycans (GAGs). (scale = 100 μm) [113] (D) *In vitro* AF Model: (Top left) SEM images of electrospun scaffold with aligned and random orientations. (scale = 10 μm). (Bottom left) MSCs seeded on aligned scaffold demonstrate preferential alignment in the fiber direction. (scale = 20 μm). (Top right) *En face* TEM image of cell bodies aligned with the fiber direction (a cell nucleus is outlined with dotted white line). (scale = 10 μm) [15] (Bottom right) Cross-sectional TEM image of a cell anchored at two electrospun fibers (starred). Collagen fibrils deposited by the cell (dark puncta) populate the space between the cell and the electrospun fibers. (scale = 10 μm) [15, 174]

Material topographies include homogenous materials, composite networks of a bulk polymer and an additional interpenetrating polymer, and aligned and randomly oriented fibrous scaffolds. These materials are typically crosslinked to infer stability to the polymer network; this can be initiated through photo, thermal and chemical stimuli, and depending on processing parameters, can lead to sparsely or densely crosslinked networks to enable tight control over the physical properties of the bulk material. Additionally, direct regulation of cellular phenotype and adhesion can be exerted by including growth factors and adhesion ligands that mimic natural extracellular matrix proteins [Fig. 1-4B].

Pellet Culture

Cells in a high density suspension can be centrifuged and concentrated in a pellet, forming a spheroid scaffold-free cell aggregate. Cell-generated extracellular matrix accumulates in the pellet over time, forming a physiologic three-dimensional microenvironment. Pellet culture is often used as a simple and more realistic alternative to monolayer culture to study basic cell functions, such as their response to inflammatory factors and hypoxia [54]. Additionally, scaffold-free aggregates are emerging for tissue engineering applications [55], where multiple pellets can be combined into large structures, or aggregation geometry can be controlled to match a defect shape like those common to the articular surface of the tibia. One could envision exploiting this method for disc tissue engineering; however these studies have not yet been conducted. One drawback of the pellet culture approach is that, in most connective tissues, cell density is low and cell-cell contact is not common; thus, high density cell aggregates produce abnormal cell-cell contact which may influence experimental findings.

Hydrogels

As an alternative to pellet culture, cells can develop and maintain a disc-like phenotype when encapsulated in hydrogels [Fig. 1-4C]. In contrast to monolayer culture, hydrogel encapsulation provides a three-dimensional environment and limits cell-cell contact.

There are a number of applications in NP regeneration in which hydrogels can be useful. Hydrogel culture systems allow for studying basic cell responses; for example, hydrogel systems are used to determine how NP cells respond to inflammatory challenge and anti-inflammatory interventions [56]. In a very active area of study, hydrogel vehicles are being used to deliver cells for NP regeneration [57-61]. Hydrogel mediated cell delivery serves as an alternative to delivery in a liquid carrier (such as saline or media), and physical parameters such as viscosity of the hydrogel can be tuned to both protect the cells during delivery as well as improve their retention at the delivery site. In addition, the chemistry of the hydrogel may be exploited to modulate cell activity; for example, a polyethylene glycol hydrogel can be modified to include cell adhesion ligands designed to influence cell phenotype [62]. Alternatively, the backbone of these hydrogels may be designed based on naturally occurring materials within the disc; another study demonstrated that the encapsulation of NP cells in hyaluronic acid, a ubiquitous extracellular matrix component, encapsulation drives cells to express NP-specific markers [63]. Hydrogels on their own (without cells) may allow for functional restoration of by restoring native tissue mechanical properties by virtue of their own physical properties in the disc space [64, 65]. This restitution of disc mechanics may have a

regenerative impact on endogenous cells by normalizing stresses and strains that they experience.

While hydrogels are largely used for the study of NP cells, they have also been used for AF regeneration studies. To study basic cell functions, AF cells can be encapsulated in hydrogels; for example, AF cells in agarose respond to growth factor stimulation and osmotic loading [66]. Others have also taken advantage of cell-mediated remodeling of hydrogels to build engineered AF-like tissues; fiber alignment can be generated by depositing cell-laden collagen around a post and allowing the gel to contract, producing circumferential fiber architecture similar to the native AF [67]; adhesive gels are also in evaluation for the repair of AF fenestrations that remain after microdissectomy [68, 69]

Fibrous Scaffolds

Given the ordered structure of the AF, scaffolds composed of aligned polymer fibers, of geometry ranging from nanoscale to microscale, are of particular interest for AF tissue engineering [Fig. 1-4D]. These scaffolds provide a topographical template; when cells are seeded on fibrous scaffolds, they will orient and elongate in the prevailing fiber direction. These topographical cues direct cells toward a phenotype similar to that of AF cells [70-72], depositing ordered extracellular matrix that acts as a mechanical reinforcement in the fiber direction. The hierarchical fiber structure in the AF, with alternating angles $\pm 30^\circ$ in apposed layers, can be constructed from sheets of aligned fibers using a layering technique [73], and this structure can be maintained after in vivo implantation [74]. This methodology has also been exploited to develop engineered

fibrous tissues composed of MSCs with mechanical properties matching the native AF [75].

Composite Disc Constructs

Beyond simple realization of the component parts of the disc, recent research efforts have expanded to include the ambitious goal of total disc replacement with an engineered, cellularized artificial disc, combining hydrogel NP regions with fibrous AF regions [Fig. 1-5].

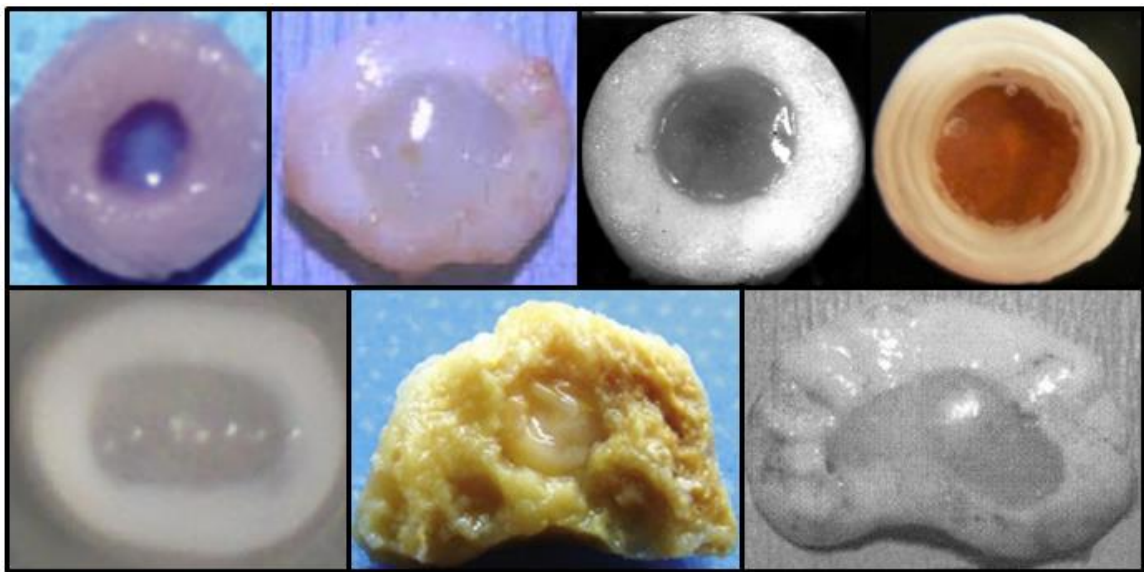


Figure 1-5 Composite engineered discs Engineered discs are fabricated from a variety of materials and cell types. **Top**, from left to right: Silk AF, fibrin and hyaluronic acid NP, porcine disc cells and chondrocytes [194]; poly(glycolic acid) AF, alginate NP, ovine disc cells [166]; poly(ϵ -caprolactone) foam AF, hyaluronic acid NP, bovine disc cells or MSCs (unpublished work from our lab); electrospun poly(ϵ -caprolactone) AF, alginate NP, bovine disc cells or MSCs [179]; **Bottom**, from left to right: collagen AF, alginate NP, ovine disc cells [31]; demineralized bone matrix gelatin AF, collagen, hyaluronic acid, chondroitin sulfate NP, lapine disc cells [254]; poly(glycolic acid) AF, alginate NP, ovine disc cells [165].

This methodology allows for evaluating co-culture of NP and AF cells, or other types of cells such as MSCs, in an anatomically correct disc-like environment. It also allows for the interrogation of total disc mechanical properties, which are of particular importance for engineered total disc replacement. NP and AF regions that comprise the total disc constructs have taken a number of forms with varying levels of complexity, ranging from 3D-printed polymer discs [76], to nanofibrous scaffold AFs wrapped around hydrogel NPs [73], to collagen gels with circumferential fiber alignment about a central hydrogel NP region [77]. Even more recently, this work has been extended to include engineered endplates into total disc constructs in order to improve potential attachment at the vertebral junction [78].

The last decade has witnessed significant advances in the development of engineered total disc replacements, with benchtop work now transitioning to in vivo total disc replacement in animal models. In some studies, these engineered discs have proven to be biocompatible and match motion segment mechanical properties [79], with early work in murine models now transitioning to large animal models [80]. These constructs have the potential to improve upon current clinical treatments for degenerative disc diseases, such as spinal fusion and metal-on-plastic arthroplasty, by restoring native spinal mechanics with a self-sustaining, cell-based, viable, and continually remodeling engineered replacement.

Organ Culture

While in vivo large animal models are an essential platform for preclinical evaluation of an engineered disc, intervertebral disc organ culture provides for the capacity to investigate therapeutic strategies in the native environment without the

expense, logistical or ethical considerations involved in large animal work [81]. Further, it can be argued that through use of live, cadaveric human disc explants, organ culture can explore unique research questions that cannot be answered with animal models, particularly in the absence of robust large animal models that accurately recapitulate the human degenerative disc phenotype. Organ culture involves isolating discs from recently deceased subjects, ranging from murine to bovine to human, and culturing the disc in standard culture media [Fig. 1-6].

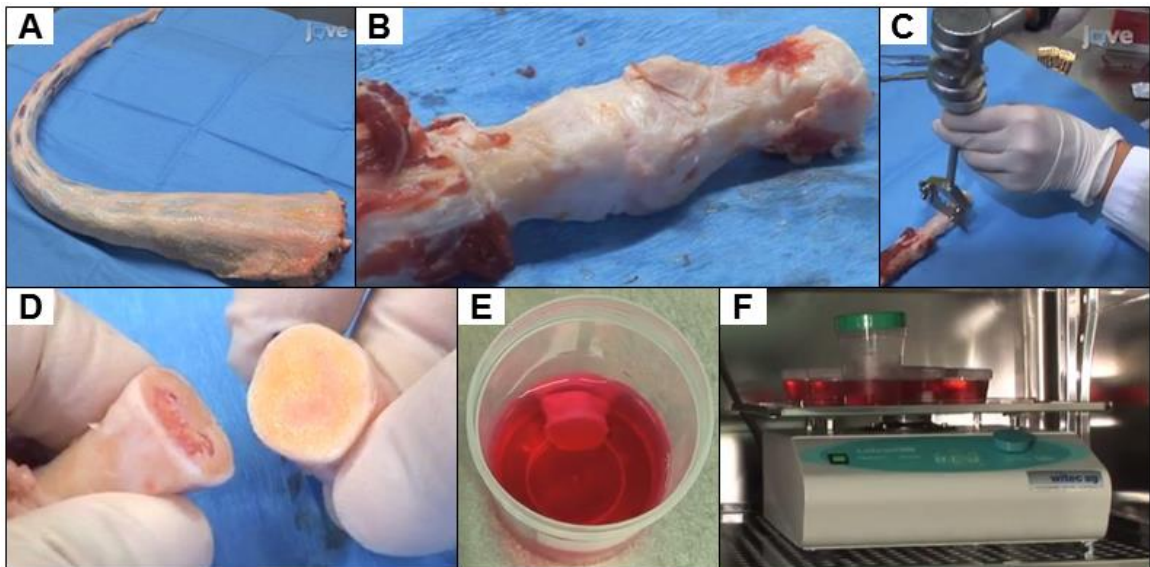


Figure 1-6 Isolation of a bovine caudal disc for organ culture The bovine caudal disc is one of the most common models used in organ culture. The procedure for isolating a bovine disc is pictured here as documented by Chan and Gantenbein-Ritter [42]. **(A)** A bovine tail is procured from a local stockyard and prepared for aseptic dissection. **(B)** The disc can be visualized after removal of the contiguous connective tissues and muscle. **(C)** A device similar to an osteotome is used to sharply dissect the disc from the tail proper, leaving a small amount of vertebral bone. **(D)** The vertebral endplate is visualized, **(E)** the disc is submerged in growth media, and **(F)** then placed on an orbital shaker plate inside an incubator for long-term culture.

Studies have shown that cells in the NP and AF of organ cultured discs can remain viable and active for periods of time on the order of months. Organ culture studies have been used to address a number of basic physiological mechanisms, such as cellular response to inflammatory factors and hypoxia [82], and also to generate disc degeneration models through chemonucleolysis [83]. Sophisticated bioreactors have been developed to apply complex static [84], dynamic [85], and impact loading [86] to identify organ- and cell-level functions.

Using organ culture systems, therapies for the treatment of degenerative disc disease can be screened for efficacy prior to their use in an animal model or human clinical trial. The delivery of cells to the disc, through direct injection [87], through hydrogel vehicle injection [88], and through cell homing [89], has demonstrated regenerative changes in organ culture models. Growth factor treatment has also been successful in organ culture models of disc degeneration [90]. Currently, there is no clinical treatment to prevent reherniation following microdiscectomy. It may be possible to mend the AF with a fibrous patch or polymer plug, as has been demonstrated successfully in organ culture [91]. One of the most exciting possibilities associated with organ culture is the ability to culture, maintain, and perform experiments on live human discs for realistic studies of physiology and regeneration [92]. However, it is still not known how well the organ culture framework can generate translatable clinical therapies; so while the technique is very promising, in vivo validation is still required.

1.8-7 Controllable External Variables

The disc microenvironment is comprised of a complex interconnected set of precisely balanced external variables that are required to maintain disc homeostasis.

These external variables are often controlled in vitro to mimic the native physiological environment and alter cell behavior. This section will discuss these relevant variables and summarize results related to their impact on disc culture.

Oxygen tension, pH, and Glucose

As the intervertebral disc is primarily avascular, it acquires oxygen by diffusion through a network of vessels in the cartilaginous endplates. Consequently, there are steep oxygen gradients in the NP and areas of low oxygen tension. This can be replicated in vitro; specialized incubators designed for oxygen regulation are available to induce a hypoxic environment similar to the intervertebral niche. Hypoxia studies have been conducted in a number of formats including monolayer [93] and hydrogel culture [94] systems. These studies collectively show that NP cells are uniquely suited to survive in strenuous conditions, deprived of both oxygen and serum, with minimal changes in viability; an ability that is closely tied to the transcription factor HIF-1 α [95]. Consequently, one school of thought suggests that preconditioning engineered replacements in a hypoxic in vitro environment will induce an NP-like phenotype and improve transplantation results, affecting in vivo survival and phenotype retention. Other cell types with potential for disc regeneration, such as MSCs, which normally reside in an oxygen-rich environment, demonstrate muted functional extracellular matrix deposition when cultured under hypoxic conditions in vitro [96], perhaps foretelling their poor performance when implanted into the disc space.

A number of factors contribute to an acidic pH in the intervertebral disc space. Due to disc avascularity and an insufficient oxygen supply, NP cells are powered primarily through anaerobic glycolysis. A byproduct of this metabolic process is lactic

acid, which accumulates in the extracellular space due to impaired transport out of the disc space as a result of poor vascular supply, resulting in a low local pH.

As demonstrated by hydrogel NP cell culture experiments, pH set at a neutral level provides an anabolic boost in extracellular matrix metabolism, while pH set at lower levels, a state with physiologic relevance to the disc, causes a profound disruption of extracellular matrix metabolism [97]. It may be necessary to examine and challenge potential therapeutic strategies, such as engineered tissue replacements, in a low pH environment prior to clinical use to ensure successful translation.

Glucose is transported into the disc through the limited vascular supply in the cartilage endplates. As a result, this important energy source for disc cells is in low supply in healthy discs and the supply is further compromised with degeneration due to changes in tissue permeability as a result of endplate calcification. The effects of low glucose are often simulated in vitro by formulating media with varying glucose concentrations. Low glucose was shown to have a significant effect on NP cells in hydrogel culture, causing decreases in many metabolic markers [98]. Similar effects of glucose deprivation have been demonstrated for MSCs as well [96].

The implications of limited glucose on tissue regeneration are important to consider. The degenerate disc space may not be able to sustain injectables with highly concentrated cells or engineered tissue replacements with a high cell density, as the finite glucose reserves may only sustain a finite number of cells. Thus, high cell concentrates may be subjected to increased levels of apoptosis soon after injection. Appropriately tuning the cell source for the in vivo environment is of critical importance for cell therapies [99].

Inflammatory Factors

For resident cells, conditions in the disc microenvironment adversely affect normal function in a healthy state and are uninhabitable in a degenerate state; the physiological niche is characterized in normal conditions by low pH, low glucose, and low oxygen (as described above), and in degeneration by disc-wide inflammation, as pro-inflammatory factors are produced by cells of both the NP and AF [41, 100-102]. These factors, which induce downstream production of collagen- and proteoglycan-degrading enzymes, create an environment of catabolism, contributing to fibrosis, compaction, and loss of structure in the NP, and are a significant hurdle for regeneration.

This pathologic inflammatory milieu will influence both injectable therapies and engineered tissue replacements. In vitro studies have confirmed that powerful pro-inflammatory cytokines, like TNF- α and IL-1 β , which are ubiquitous in disc degeneration, have a negative impact on extracellular matrix production by disc cells. Matrix synthesis can be rescued by including antagonists to these molecules, such as a soluble TNF receptor [103], the IL-1 receptor antagonist (IL-1ra) [56, 104], or an NF- κ B inhibitor [105], suggesting molecules like these have significant potential for regeneration. Co-delivery of such anti-catabolic agents at the time of cell to construct implantation may improve long term outcomes.

Mechanical Loading

The disc experiences multiaxial static and dynamic loading during routine daily activities. Loading directly affects behavior at the cell level through mechanotransduction events. In addition, loading has an effect on nutrient transport and waste removal, and in a nutrient-deficient homeostatic state, loading can have a profound impact on the

precarious balance of the intervertebral niche. Depending on the load magnitude, frequency, and duration, physical forces can positively or negatively affect cell metabolism [84, 85, 106-108], and consequently mechanical loading conditions are often replicated in in vitro studies to study these effects.

Mechanical loading events can be simulated in vitro on the organ and tissue scale to study the effects on extracellular matrix metabolism and regeneration. For tissue engineering purposes, dynamic loading is used to stimulate extracellular matrix production to generate more robust tissues for implantation. On the tissue sub-component level, dynamic compressive loading has been evaluated in hydrogel culture for both NP cells [109] and MSCs [110], and dynamic tensile loading has been evaluated for both AF cells on flexible membranes [111] and MSCs on fibrous scaffolds [112]. On the whole disc level, dynamic loading has been used for mechanical stimulation of engineered discs comprised of AF and NP cells [113] and MSCs [114], as well as in organ culture [115]. A general summary of findings from these studies is that low frequency, moderate magnitude physical forces allow for anabolic in vitro stimulation of engineered tissues and disc explants.

Growth Factors

Growth factors that regulate cell metabolism are present in the disc space, and can be applied in vitro at supra-physiological concentrations to achieve a specific cell phenotype or provide an anabolic stimulus to promote regeneration. A wealth of experiments on growth factor stimulation are available to support growth factor injections [116], as well to stimulate engineered tissues for disc repair or replacement [79]. The BMP family of growth factors is of specific interest, as two members of this family (OP-

1/BMP-7 and GDF-5/BMP-14) have demonstrated sufficient in vitro success to motivate clinical trials [117].

Growth factors have shown promising results in in vitro models, but significant hurdles must be overcome for growth factor injection to be translatable. In vitro studies allow for growth factors to be continuously supplemented by refreshing the culture media. The standard route for growth factor delivery in vivo however is by needle injection through the AF and delivery through multiple injections for continuous supplementation is not feasible. One method for prolonged growth factor delivery with a single injection is through the sustained release of these factors from biomaterials. This can be achieved through a number of mechanisms including delivery from slow-releasing microspheres, hydrogels and electrospun scaffolds. Release profiles can be tuned in vitro through polymer engineering to achieve continuous release that lasts on the order of weeks, obviating the need for multiple injections.

1.9 In Vivo Models for Disc Research

In the absence of successful treatments for degeneration and because of the scarcity and variability in human donor disc tissue, animal models are used to perform tightly controlled experiments to evaluate disc physiology, degeneration, and regeneration, to determine the efficacy of injectable therapeutics and to evaluate engineered disc tissues in situ. For the purposes of this dissertation, I will discuss three categories of animal models relevant to these experiments.

1.9-1 Altered Loading Models

The lumbar discs experience multiaxial loading during routine daily activities. These mechanical forces directly affect the tissue in a number of ways: by causing micro-failures in tissue subcomponents, by inducing the transport of nutrients through the CEPs, and through mechanobiological mechanisms in resident cells. In these ways, physical loads can directly affect disc structure, metabolism and homeostasis and can cause catabolic or anabolic stimuli that vary with the load frequency and magnitude.

Static and dynamic loading have been examined in animal models through external control of vertebrae adjacent to the disc. The caudal spines (or tails) of rats and mice are of specific interest for these types of studies, as they allow for facile access to the spine. Static loading compression and bending loads can be applied to the mouse caudal spine by fixing the vertebrae with surgical pins [49, 131]. Dynamic compression and torsion loading have been applied to the rat caudal spine using a sophisticated external mechanical system with a framework similar to the Ilizarov device for fracture fixation [Fig. 1-7] [16, 98].

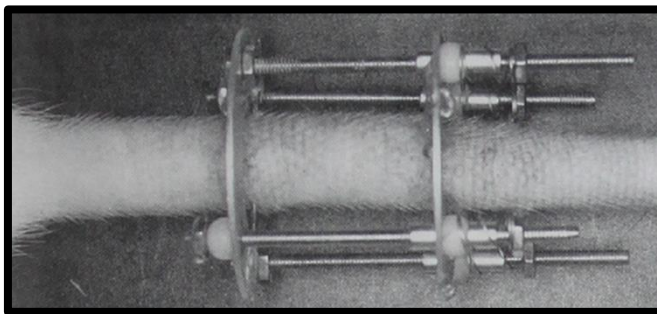


Figure 1-7 External device for simulated loading in rat model [98]. The rat tail can be instrumented with an external device used to apply static or dynamic loading to evaluate the effects of loading on disc homeostasis. Surgical wires are inserted through adjacent vertebrae and an Ilizarov ring-type fixator is secured to the pins; the rings can then be manipulated mechanically.

In addition, the rabbit lumbar spine has been instrumented for dynamic loading to evaluate the effects of cyclic compression on nutrient transport [81, 82] .

In general the results of these studies suggest that static loading is detrimental to disc health, producing a catabolic response similar to degeneration, and dynamic loading can be either catabolic or anabolic, where moderate frequency, moderate magnitude loads are anabolic and high frequency, high magnitude loads are catabolic.

1.9-3 Degeneration Models

There are three types of animal models for investigating disc degeneration: animals in which disc degeneration spontaneously occurs, animals in which degeneration is artificially-induced through disc insult, and genetically altered mice in which a degenerate phenotype develops in the disc.

Naturally Occurring Models

Degeneration naturally develops in the lumbar discs of sand rats [78] and chondrodystrophic breeds of canines, like the beagle [10]. These models closely relate to the human condition in that the degenerative phenotype slowly and naturally develops. Specifically, canine models are of interest as they represent a clinical population and may be a good and sufficiently challenging step prior to clinical trials in humans. One drawback of naturally developing disease is that it can take months to years to be evident, causing logistical issues, and does not reliably occur in specific levels, which complicates designing experiments. Recently, another naturally occurring model was described; the alpaca naturally develops disc degeneration in the caudal levels of the cervical spine [228]. This model has two advantages over other naturally occurring models, first, degeneration can be predicted by level and, second, alpacas are farmed throughout the

US and thus there is readily available supply of animals at the right ages. The work on the alpaca is still preliminary but is promising.

Injury-induced Models

To assert better experimental control in a degeneration model, a number of methods have been developed to artificially induce degeneration in individual discs. This can be done through mechanical overloading of discs with an external loading device similar to what was described above, or by creating spinal instability, by resection of the facet joints for example [110]. Similarly, scoring or partially removing the AF with a scalpel blade or needle creates instability in the motion segment by impairing the AF and depressurizing the NP [Fig. 1-8].

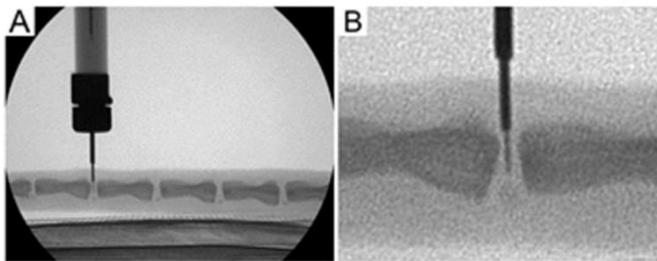


Figure 1-8 Needle puncture injury in the rat tail [76]. Fluoroscopic images of a needle inserted a controlled depth into a rat caudal disc at (A) low and (B) high magnification. The needle breeches the AF and is inserted into the central NP, where further penetration is prevented by a circumscribing stopper with a larger bore.

This technique comprises the majority of disc degeneration models as it requires a simple surgical procedure, is precise, and causes a highly reproducible degenerative condition. Annular injury models have been performed in large animals, like goats [251] and sheep [191], medium sized animals like rabbits [153], and small animals like rats [207] and mice [247]. There is a size-dependent response to the injury; larger needle diameters and scalpel defects lead to degeneration while injuries below a sizes threshold do not. Degeneration can also be cause by the injection of matrix degrading enzymes, like chondroitinase ABC [32, 88], into the disc to desiccate the nucleus pulposus. This chemonucleolysis method of producing degeneration may be preferable to annular injury methods as a smaller diameter needle can be used for the injection, the AF will remain intact, and degenerative changes will occur first in the NP, mimicking the natural degeneration process.

The primary criticism of the induced degeneration models is that the resultant degeneration processes that take place after the loading event, annulus injury, or chemonucleolysis, do not well represent the natural course of human degeneration, as it occurs over the course of weeks rather than slowly over years like natural degeneration. However, some important conclusions can be drawn from these studies. For example as a result of induced degeneration models, it is postulated that human disc degeneration is an adaptation to an altered loading pattern followed by a re-establishment of stability [130]. As a corollary, it has been suggested that the presence of sufficient mechanical perturbation is required in order for degenerative changes to take place [89]. It is likely that the physiological response to a redistribution of mechanical forces is the stabilization of the joint space through the alteration of extracellular matrix composition, a shift in the

NP composition from a cartilaginous to fibrotic. Numerous animals have shown that changes in structure or altered mechanical loads are followed by progressive changes in disc height, biochemistry, and cellular activity [32, 89, 224].

Injury-induced models play a very important role in investigating therapeutic interventions for degeneration. Typically, an insult to the disc is performed surgically and the physiologic processes that cause the degenerate phenotype are allowed to proceed for a number of weeks/months. Then, a second surgery is performed in which an injectable therapeutic, usually a cell, growth factor, or biomaterial intervention, is applied to the degenerated disc, and its ability to restore a healthy condition are evaluated. Efficacy can be monitored by fluoroscopic visualization of disc height, MR imaging to investigate disc composition, mechanical evaluation of the motion segment, histological staining for extracellular matrix alteration, RNA quantification for changes in cell behavior, etc. These studies generate critical data to screen efficacious therapies and proceed to clinical trials.

Models Induced Through Genetic Manipulation

As stated previously, the presence of degeneration is highly correlated to the presence or lack of certain genetic factors. Leveraging this strong relationship to genetics, a final subset of animal models, genetically manipulated mice, can be exploited to develop a degenerate-like condition. For example, inactivation or knockdown of genes encoding for type I [212] and type II collagen [209] leads to a musculoskeletal phenotype that includes a condition similar to disc degeneration. Polymorphisms in the collagen IX gene correlate to the presence of disc degeneration in genome wide studies, and mutations in the gene that encodes for collagen IX in mice lead to degeneration of the

cervical discs [117]. In this way, large scale, genome wide studies often pinpoint specific genetic discrepancies that correlate to degeneration in humans and follow-on studies that induce these specific mutations in mice play a role in improving our understanding of the degeneration process. The reverse process, in which many genetic phenotypes are induced in mice and these mice are screened for disc pathology, may also play a role in discovering new genetic influences on disc health.

1.9-4 Total Disc Replacement Models

Animal models have been developed for evaluating total disc replacement in a number of species, including in baboons, macaques, goats, dogs, and sheep [Fig. 1-9] [50, 51, 121, 122, 133, 230, 245].

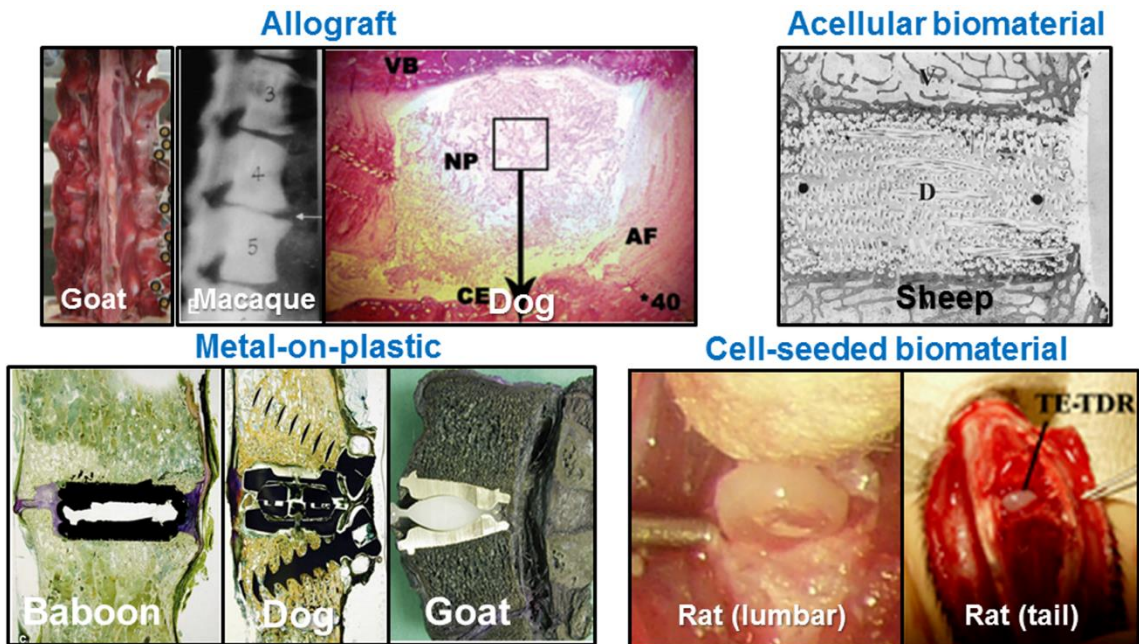


Figure 1-9 In vivo models of total disc replacement [29, 30, 50, 51, 121, 122, 133, 245]. Animal models of total disc replacement have been developed for either the cervical, lumbar, or caudal spines in species that range in size from large animals like sheep, goats and dogs, to medium sized animals like baboons and macaques, to small animals like rats. There are four general types of implants: allografts, acellular biomaterials, metal-on-plastic arthroplasty devices, and cell-seeded biomaterials.

These experiments were designed for prosthetic metal-on-plastic discs or whole-disc allografts, and generated preliminary data to motivate clinical trials. The rat or mouse caudal spine, used in many disc studies to investigate degenerative processes [146, 207] and engineered disc tissues [63, 73], is an ideal candidate for preclinical studies given the ease of surgical access and the ability to avoid critical structures (e.g., spinal cord and spinal nerves). Recently, total disc replacement with cell-seeded engineered discs was performed in the rat caudal spine [30]. These studies, performed on immunocompromised rats, demonstrated that xenogeneic cells within engineered discs were viable and produced a functional matrix over the course of months, validating the rat model for proof-of-concept design evaluation. In the context of disc tissue engineering, the rat tail model may serve as a high-throughput native environment in which to screen engineered disc designs and inform large animal studies. Thus, a rat tail model would be valuable tool to evaluate and optimize DAPS.

1.10 Acellular Biomaterials as an Alternative to Traditional Tissue Engineering

The current paradigm for regeneration of the musculoskeletal system through tissue engineering involves a two-step procedure. First, the cell source of interest is harvested from the patient in a pre-operation outpatient procedure. These cells are expanded, seeded onto an engineered scaffold, and matured for re-introduction into the body. The engineered construct is then implanted at the desired site and functions as the original tissue.

There are a number of drawbacks to this method. First, there is potential for morbidity at the donor site. For example, harvesting bone marrow from the iliac crest

results in post-operative pain and introduces the risk of infection. Second, the cells isolated from bone marrow require closely regulated culture conditions to induce and maintain a desired phenotype. AF cells, NP cells and MSCs are phenotypically unstable after a number of passages in monolayer [22, 118, 157, 240]. Finally, clinical implementation of cell-based therapy requires overcoming significant FDA regulatory obstacles and also necessitates expensive clinical trials requiring academic-industrial partnership for financial contributions from industry.

Thus, acellular biomaterials that attract and direct endogenous cells have come to the fore in the context of tissue engineering as an alternative to cell-based methods [36]. For example, acellular HA hydrogels injected into the left ventricle have improved cardiovascular function in an ovine model of myocardial infarction [Fig. 1-10][101]. Also, for the treatment of articular cartilage defects, autologous matrix induced chondrogenesis is a developing strategy that combines recruiting cells from the subchondral bone marrow through microfracture and directing the behavior of those cells once engrafted into a synthetic matrix implanted into the defect [Fig. 1-10] [21, 57].

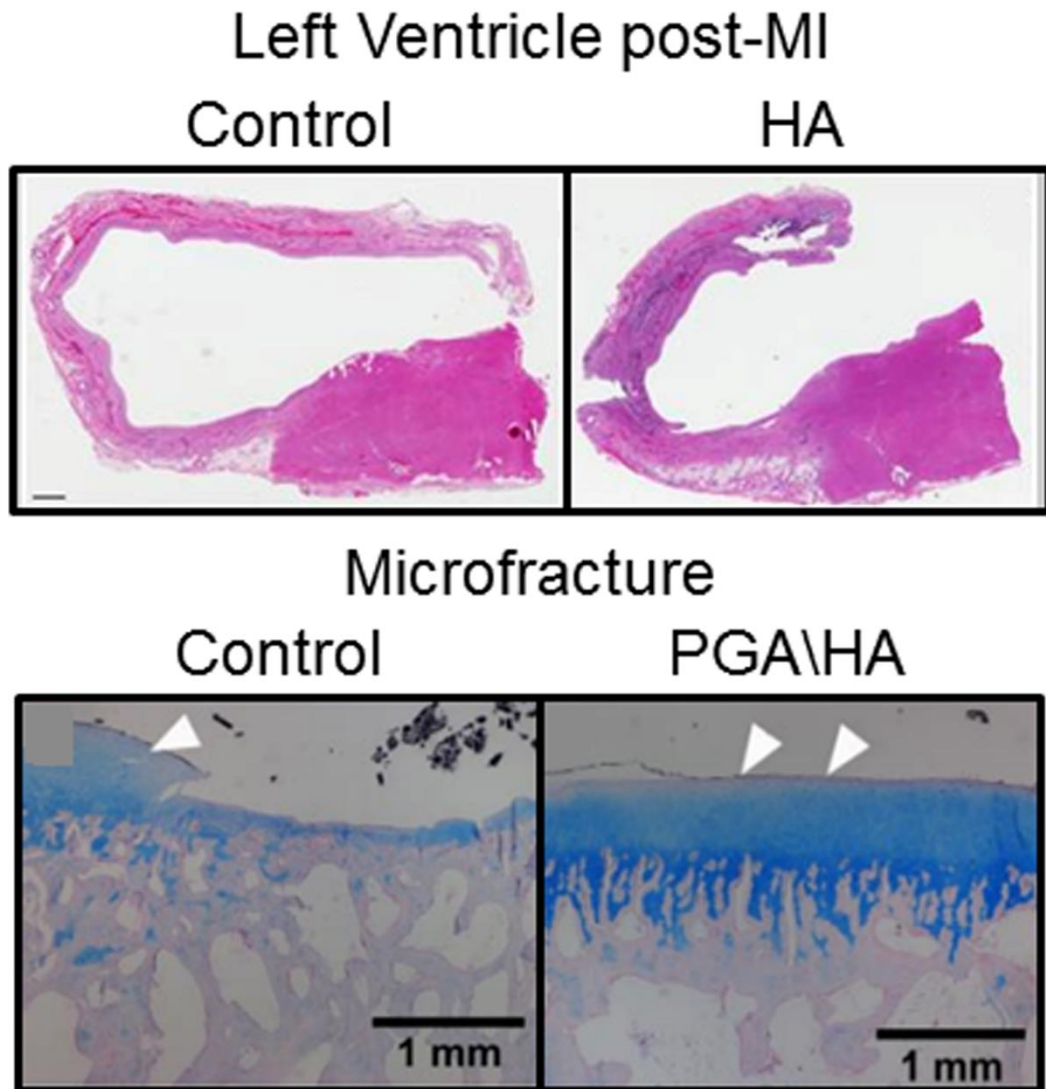


Figure 1-10 Acellular biomaterials for regenerative medicine. Two examples of acellular biomaterials for tissue repair: **(top)** the left ventricle following a simulated myocardial infarction (MI) in an ovine model. Hyaluronic acid hydrogels improved wall thickness and cardiac output. **(bottom)** The articular surface was repaired using a microfracture technique assisted by a poly(glycolic acid) and hyaluronic acid hydrogel. [21, 57, 59, 101, 113]

1.11 Current Challenges for Regenerative Therapies

The intervertebral disc and its resident cells have a difficult assignment; the disc must meet substantial functional demands, resisting physical forces that are on the order of multiple body weights in compression, shear, torsion, and bending modes, and it must do so in an avascular environment, with minimal nutritional support for healthy extracellular matrix maintenance. These two aspects, high functional demands and limited nutrition, present a challenge not only for disc survival but also for the restoration of injured or diseased discs to a healthy state. In the previous sections, we reviewed a number of potential cell sources, biomaterial frameworks, and culture systems that have advanced our knowledge of disc biology and that can serve as experimental tools towards realizing disc regeneration. However, numerous challenges remain, many of which can be addressed using in vitro experimentation. The remaining challenges are summarized as follows for each mode of regenerative therapeutic under development:

- Injectable cell therapies:
 - Low O₂, glucose, and pH
 - Inflammatory signals present in diseased tissue
 - Mechanical stress
 - Maintenance of cell regenerative phenotype after injection
 - Delivery route is damaging to AF

- Injectable growth factor therapies:
 - Limited number of endogenous cells available for regeneration
 - Resident cells have a degenerate phenotype
 - Limited activity and/or half-life of growth factors

- Growth factors may have limited activity in acidic environment
- Delivery route is damaging to AF
- Biologic NP replacements:
 - Low O₂, glucose, and pH
 - Mechanical stress
 - Maintenance of cell regenerative phenotype after implantation
- Biologic AF replacements
 - Low O₂, glucose, and pH
 - Mechanical stress
 - Mechanical properties vary with fiber orientation
 - Method of fixation to native tissue
 - Maintenance of cell regenerative phenotype after implantation
- Biologic total disc replacements:
 - Low O₂, glucose, and pH
 - Must match multiaxial mechanical properties of native tissue
 - Integration into vertebrae
 - Meet nutritional demands through diffusion over long distances
 - Impaired or degenerated interface at vertebral endplate
 - Maintenance of cell regenerative phenotype after implantation

1.12 Conclusion of Introduction

There has been substantial progress towards disc regeneration in the past 15 years and an array of strategies have been developed that show promise. From these studies, we have learned much about disc cell physiology, mechanobiology, and biomaterials,

generating a foundation for future research that will inform the implementation of new strategies. Additional work is now required to systematically evaluate the second iterations of these earlier regeneration strategies, bearing in mind the challenging environment present in the disc may counteract the regenerative potential of these approaches. These in vitro efforts, using many of the strategies documented in this chapter, are the critical experiments to define and optimize therapeutic approaches as they progress towards pre-clinical animal studies and ultimately onto clinical trials in humans suffering from degenerative disc disease.

CHAPTER 2 – Previous Work

2.1 Engineered Intervertebral Discs

My global hypothesis for this work is that engineered, cell-seeded, viable intervertebral discs can restore long-term function to the spine. Fabrication of an engineered composite disc requires replication of the structure, composition, and function two primary disc components, the NP and the AF. In our lab, we have developed a method to fabricate engineered discs from a hydrogel NP region and an electrospun nanofibrous AF region. Relevant previous work is described below.

2.1-1 Hydrogels for NP replacement

There are a number of devices on the market for NP replacement ranging from metal mechanical devices to injectable polymers that cure in situ [127]. For sustained regeneration of the native tissue, we and others have implemented biomimetic cell-seeded hydrogels [59, 68, 71, 114]. One such hydrogel, hyaluronic acid (HA), is a naturally occurring extracellular matrix component that can be remodeled by endogenous hyaluronidases and binds to cell surface receptors to influence cell behavior [159]. NP cells and Mesenchymal stem cells (MSCs) cast in HA hydrogels develop a viable NP-like phenotype as demonstrated by the improved elaboration of extracellular matrix proteins and compressive mechanical properties approaching the levels of native tissue [59, 222].

In previous work, our lab has used hyaluronic acid hydrogels to fabricate engineered tissues with a NP phenotype that mature in vitro and develop functional properties near native tissue levels [Fig. 2-1].

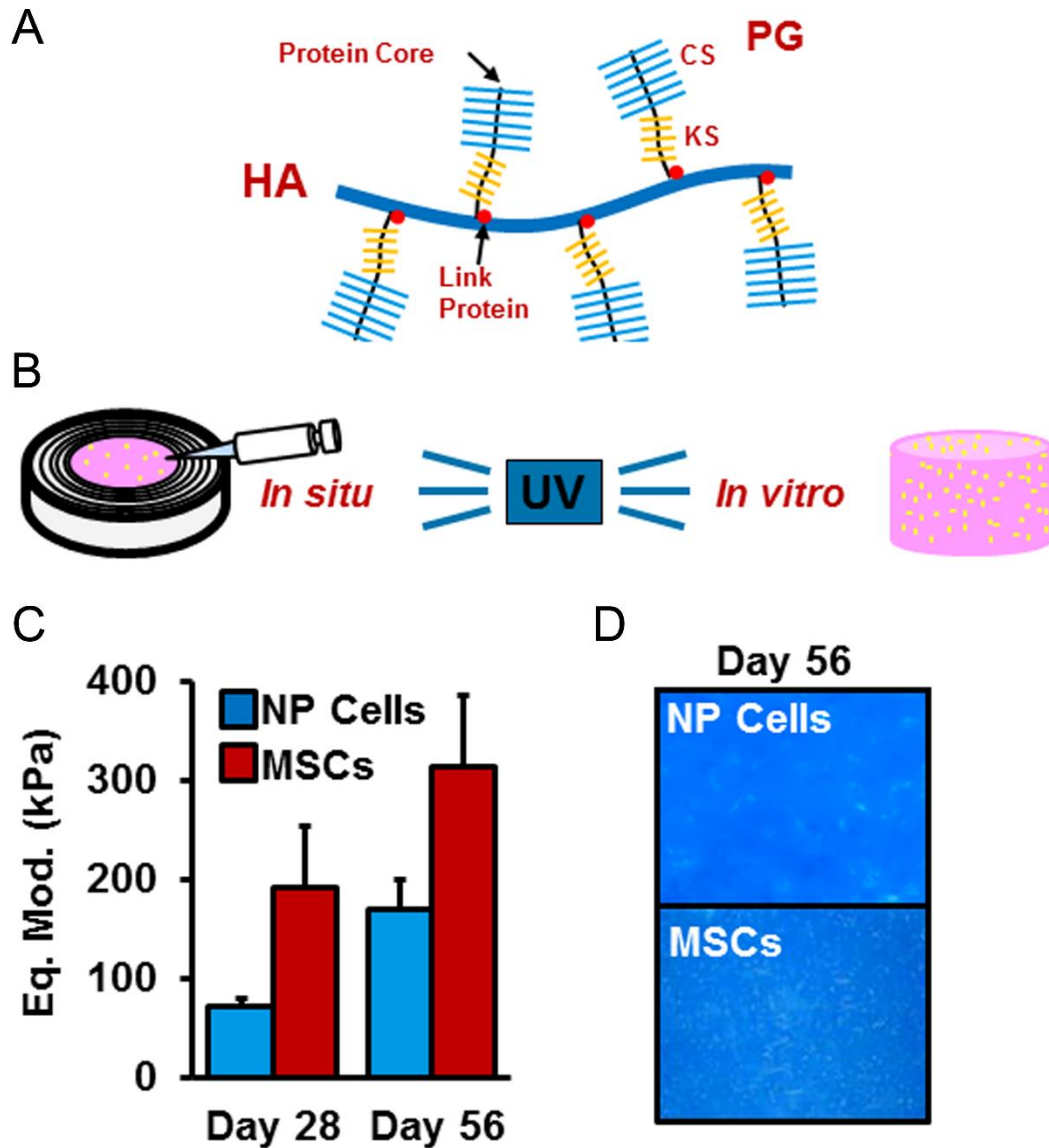


Figure 2-1 Hyaluronic acid (HA) hydrogels for NP regeneration (A) HA is a natural component of the disc extracellular matrix; it serves as the backbone substrate for the aggregation of the chondroitin sulfate (CS) and keratan sulfate (KS) that make up the proteoglycan (PG) aggregate. (B) HA can be modified to form photopolymerizable hydrophilic elastomer networks; UV crosslinking can be performed for in situ or in vitro gelation of the HA. (C) Both NP cells and MSCs encapsulated in HA hydrogels obtain a chondrogenic phenotype, maturing both functionally (left, compressive modulus) and compositionally (right, Alcian blue staining for GAG) .

Hyaluronic acid is an essential extracellular matrix component as it acts as the backbone substrate for aggrecan, the most abundant proteoglycan in the NP. Purified hyaluronic acid can be crosslinked to form a hydrophilic elastomer by adding the crosslinking molecule methacrylic anhydride. This allows for photopolymerization of the material with ultraviolet light to generate constructs of specified mechanical properties and geometry. Our lab has used this technology as a chondrogenic platform to encapsulate MSCs and NP cells with much success. **Both NP cells and MSCs respond favorably to the hyaluronic acid hydrogels, enabling long-term viability and extracellular matrix production similar to the NP phenotype.**

2.1-2 Electrospun Polymers for AF replacement

A procedure called electrospinning can be used to generate engineered materials that recreate the organized fibrous architecture of the native AF [9, 175-179]. The electrospinning process involves drawing a charged polymer solution across a voltage gradient onto a rotating collection mandrel [Fig. 2-2].

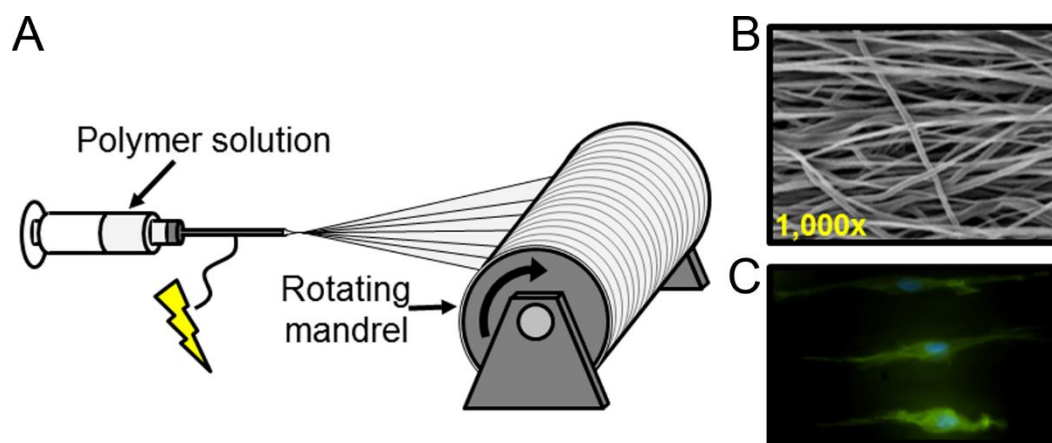


Figure 2-2 Electrospun scaffolds for AF tissue engineering (A) The electrospinning process involves charging a polymer solution with high voltage, drawing the solution across an air gap where it is collected on a grounded rotating mandrel. (B) This produces sheets of aligned nanofibers. (C) Cells seeded on these fibers orient their cytoskeleton with the fiber direction.

This produces sheets of aligned polymer nanofibers, the topography of which permits cell attachment and promotes directed extracellular matrix production for reinforcement in principal loading directions [14, 15, 54]. Strips of electrospun scaffold can be layered to create an engineered tissue with alternating fiber that matches the hierarchical structure of the native AF.

Our lab has used an electrospinning procedure to develop engineered fibrous tissues for meniscus, ligament, and AF repair and replacement. These scaffolds have mechanical properties near native tissue levels, that vary with the direction of fiber alignment [176]. When cells are seeded on these materials, they develop an elongated shape and orient their cell body in the direction of the fibers, which directs their extracellular matrix deposition [Fig. 1-5 and Fig. 2-2C]. **Electrospun poly(ϵ -caprolactone) (PCL), a polymer with sufficient physical properties for tissue engineering and with long-term in vitro and in vivo stability, can be seeded with either AF cells or MSCs and increase in functional properties with in vitro culture, approaching native tissue properties at the single and multi-lamellar length scales [54, 175, 176].**

2.1-3 Engineered Composite Discs for Total Disc Replacement

A number of studies have reported on co-cultured NP and AF components for tissue-engineered total disc replacement. These cell-seeded engineered discs have been evaluated in vitro [180, 194], in the subcutaneous space [165, 166, 254], and have recently been placed in situ between rat lumbar and caudal vertebrae [29, 30], illustrating the rapid advances in this regenerative approach to engineered disc replacement.

Our lab has developed DAPS for total disc replacement by combining HA hydrogels that act as an NP region with an electrospun PCL AF region [Fig. 2-3] [177].

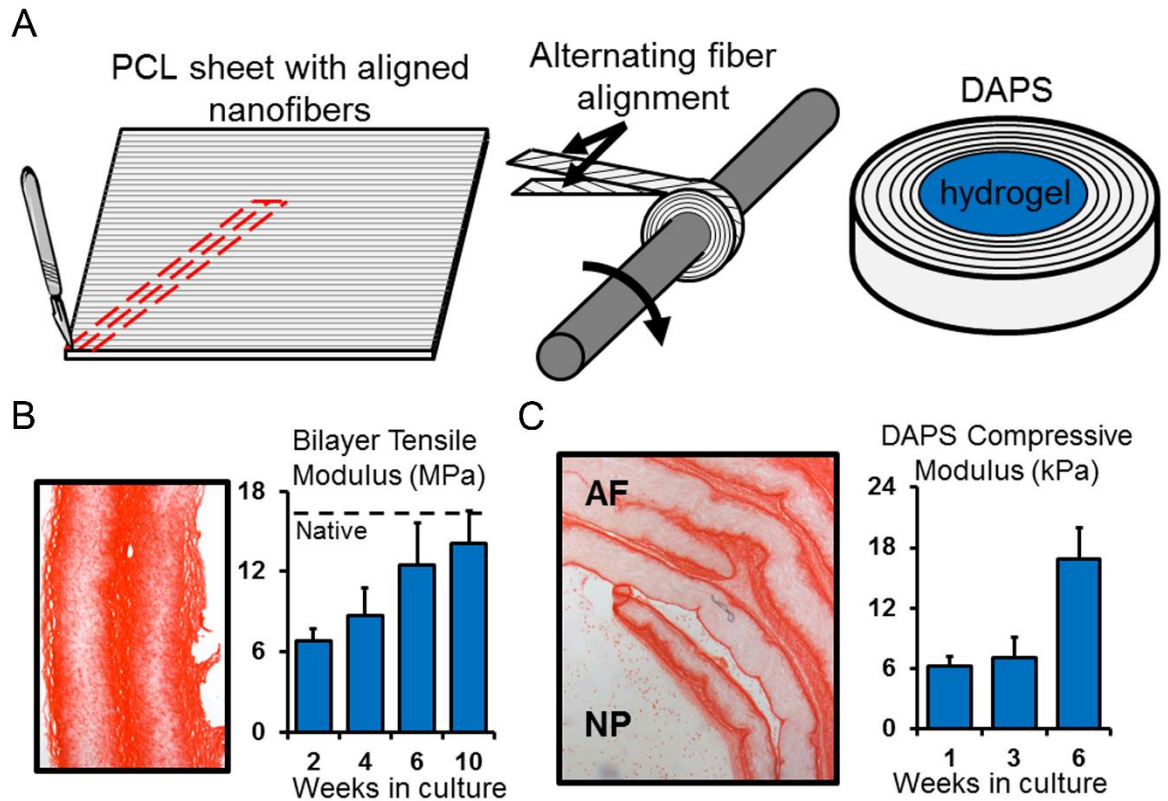


Figure 2-3 Fabrication of DAPS, an engineered composite disc (A) DAPS are fabricated by first generating a sheet of aligned nanofibers by electrospinning. The sheet is cut at an angle into strips to generate the “lamellae” of the engineered disc. These strips are wrapped with alternating fiber alignment around a post and fabrication is completed when the core is filled with an HA hydrogel. (B) Picrosirius red stained sections (for collagen) show that bilayers of PCL scaffold develop a fibrochondrogenic phenotype and mechanical properties of these bilayers are near native levels after 10 weeks in culture. (C) Similarly, DAPS mature both compositionally and functionally with time in culture [175, 179].

To do so, a sheet of aligned PCL nanofibers is generated by electrospinning, and then two strips are cut from the sheet at $\pm 30^\circ$ and wrapped as bilayers into concentric discs, precisely mimicking the alternating fiber alignment and lamellar structure of native tissue. The resultant discs, when filled with a hydrogel core, form DAPS. These constructs mature both compositionally and functionally over time when seeded with AF and NP cells or MSCs alone [175], indicating their potential for use in total disc replacement. **DAPS have yet to be evaluated in an in vivo environment; a limitation of the work which will be the major focus of this dissertation.**

2.2 Trajectory Based Tissue Engineering – Implantation at Peak Maturation State vs. Maturation Rate

Integration of an engineered disc into the native vertebrae may be the most difficult challenge facing intervertebral disc tissue engineering. One strategy to improve the integration of engineered cell-seeded materials is to culture constructs for an extended period of time and implant in vivo at their peak maturation *rate*. Engineered cell-seeded tissues go through stages of growth; an early phase of slow development, an intermediate phase of rapid development, and a late phase in which growth stabilizes [Fig. 2-4, A-B].

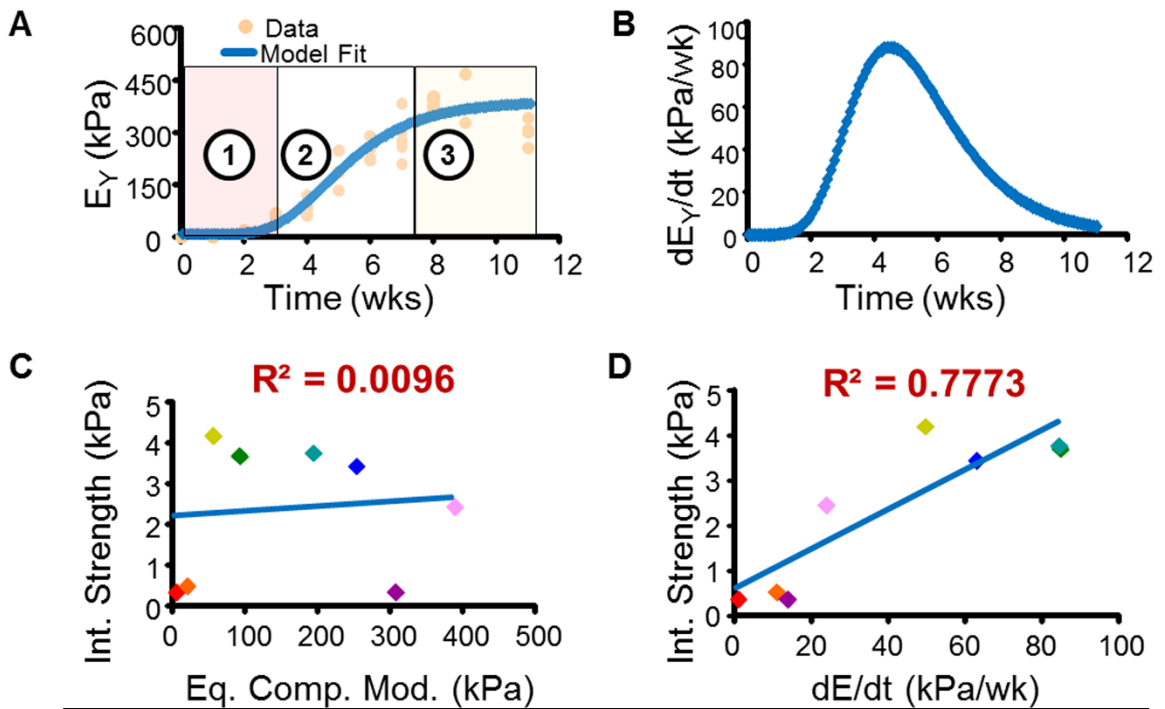


Figure 2-3 Trajectory-based tissue engineering (A) The development of an engineered tissue, as modeled here by engineered cartilage, can be defined in terms of the trajectory of its compressive modulus, E_Y , over time. There are three distinct periods of growth: (1) an early phase of slow growth, (2) an intermediate phase of rapid growth, and (3) a late phase where growth stabilizes. (B) By plotting the derivative of compressive modulus over time, a peak becomes evident where the highest maturation rate occurs. (C) In an in vitro model of in situ integration, we found no correlation between the compressive modulus and integration strength. (D) However, the rate of change in compressive modulus, or growth rate, positively correlated to integration strength, suggesting that implanting engineered tissues at their highest growth rate will improve integration into native tissue [67].

Implanting engineered discs at their peak maturation rate, in the intermediate phase where rapid growth occurs, may improve integration into the vertebral endplates.

We have demonstrated that integration potential correlates with the maturation rate of engineered cartilage [67]. One possible explanation is that the most mature constructs contain cells that are at a reduced activity level and contain tissue too dense for endogenous cells to penetrate. Thus, an emerging strategy to improve integration is to base the timepoint of implantation on the peak maturation *rate*, and recently this was successfully demonstrated in engineered cartilage in vitro [Fig. 2-4, C-D]. A fundamental concern for an engineered intervertebral disc is the ability of the disc to integrate into the native vertebral bodies. **Engineered discs implanted at their highest growth rate may integrate better into native tissue, but this hypothesis has yet to be tested.**

2.3 Summary

Collectively, these data suggest our lab has the ability to fabricate and develop in culture a cell-seeded, viable engineered disc with structural hierarchy matching the native disc. We have developed biomaterials that mimic the AF and NP and methods to isolate stem cells or disc cells, methods to seed cells on these biomaterials, and media conditions in which cells will proliferate and deposit extracellular matrix. We have also developed a strategy in which to culture these discs to improve integration into the intervertebral space using trajectory-based implantation strategy. The next step in the progression to clinical application of disc tissue engineering is the evaluation of DAPS in vivo, to test their function and viability in the physiological environment.

CHAPTER 3 – Executive Summary

The text in the following chapters describes the steps taken to design an animal model system and to evaluate the function of DAPS to the in vivo environment.

First, Ch. 4 will detail the development of a total disc replacement model using the rat tail. In preliminary studies, DAPS were displaced from the disc space, as the biomechanical environment of the tail, which has significant range of motion, was not conducive to implant engraftment. To improve upon this result, I developed an external fixation system to stabilize adjacent vertebrae and a radiopaque scaffold to track implants in vivo. External fixation provided a stable environment for implantation as evidenced by the fluoroscopic monitoring of radiopaque implants over time.

Next, Ch. 5 will be a further evaluation of the radiopaque scaffold, documenting its mechanical properties, nanostructure, and in vitro and in vivo compatibility. I found that these scaffolds were radiographically visible in both small and large joints, were cytocompatible both in vitro and in vivo and did not promote osteogenesis. These data indicated that radiopaque scaffolds have potential for improving animal model development, where they may reduce the number of iterations required to perfect new surgical procedures by allowing for in vivo monitoring of implants, and also radiopaque scaffolds may act as a substrate for engineering fibrous tissues that can be radiographically monitored.

I further investigated aspects of the rat tail disc replacement model (Ch. 6), evaluating the effects of the external fixator and the behavior of DAPS biomaterials over

long-term implantation. In a series of control groups, I found that immobilization did not affect native disc health, was conducive to fibrous tissue deposition, and eventually lead to intervertebral fusion. Acellular DAPS were implanted into the rat tail and allowed significant endogenous cell infiltration when sacrificial layers were used to create void spaces in between AF layers. Over time these implants became invested with fibrous tissue. There were, however, a few drawbacks of these implants; when acellular hyaluronic acid was used as the NP region, native cells degraded the hydrogel, and at later timepoints intervertebral fusion could not be prevented. This motivated seeding DAPS with cells to improve in vivo performance.

In the next set of studies (Ch. 7), I evaluated cellular DAPS both in vitro and in vivo. In vitro, DAPS were cultured with either AF cells in the AF region and NP cells in the NP region (AF/NP DAPS), or MSCs in the AF region and MSCs in the NP region (MSC/MSC DAPS). Both implants matured over 15 weeks of culture, with composition, structure and function matching a number of native tissue benchmarks. At 5 weeks, these implants were at an immature and highly active growth state, while at 10 weeks, implant were near fully mature. However, I hit a roadblock; when DAPS were implanted into the rat tail after either 5 weeks or 10 weeks of in vitro maturation, their resident cells underwent a substantial shift in phenotype. The DAPS, which were originally highly invested with GAG pre-implantation, were completely devoid of GAG after 5 weeks post-implantation as evident through histological and MRI evaluations (measurement details described in Appendix I). In addition, there was histological evidence that the NP was degrading in vivo. Despite these changes, motion segment mechanical (measurement

details described in Appendix II) properties matched native tissue perfectly, but it was evident that a new method for pre-maturation and a modification to the implant materials was necessary.

The final chapter with experimental data (Ch. 8) describes a series of studies in which I evaluated various pre-culture techniques to improve in vivo performance of DAPS. Interestingly, DAPS cultured in serum containing media matured very little in vitro, but had excellent in vivo performance after subcutaneous implantation into athymic rats, and, DAPS cultured in various chondrogenic media formulations with TGF- β 3 accumulated significant extracellular matrix in vitro, but could not maintain this production in vivo.

In the final chapter (Ch. 9), I express that while as a field we can develop engineered tissues that are in vivo-ready before implantation, matching native benchmarks, this tissue does not function properly in vivo. This phenomenon may certainly be related to the rat tail or rat subcutaneous implantation models, which have a number of important differences from the native intervertebral space, and suggests that another model in an environment similar to the human lumbar disc space is worth investigating. Perhaps mechanical stimulation, which is not present in this rat tail model due to the external fixation device, is necessary to maintain properties in vivo. This may be tested by remobilizing the implant after a period of integration. The specific material used for the NP region, hyaluronic acid, does not perform well in vivo, and should be modified in future work. The final issue is that integration into the vertebral endplate was not evident; this will likely require an intervening integration device. Eventually, when

moving up in scale to human-sized constructs, requirements related to nutrient diffusion over longer distances and the maintenance of human cell sources will be necessary to evaluate.

CHAPTER 4 - Translation of an Engineered Nanofibrous Disc-like Angle Ply Structure (DAPS) for Intervertebral Disc Replacement in a Small Animal Model

4.i Preface

Chapter 4 describes the development of a rat tail model of total disc replacement for in vivo evaluation of DAPS, which is published in [149]. In our first attempts at implantation, DAPS were displaced from the disc space and were found in the subcutaneous tissue. I then developed an external fixation device to unload and stabilize the implantation site and found that this improved retention of DAPS. Additionally, in this study, I introduce a method for fabricating DAPS with sacrificial layers in the AF region (sDAPS) that provide routes for cell infiltration. sDAPS are later used both in vivo to allow for endogenous cell infiltration, and in vitro as a method to improve the infiltration of seeded cells. The in vivo application of sDAPS will be elaborated on in Chapter 6 and the in vitro application will be described in Chapter 7. I also introduce a method for fabricating DAPS using a radiopaque scaffold (rDAPS). rDAPS were used in this study to track the position of the implants over time. The radiopaque scaffold has other uses in tissue engineering; this will be expanded on in Chapter 5.

4.1 Introduction

A number of therapeutic strategies have been developed for each stage of the degenerative process to preserve or restore function of the intervertebral joint. Early in the degenerative process, interventions with cell, gene, or pharmaceutical therapies may maintain disc function by reducing inflammation and preventing further matrix degradation [93, 152, 243]. A more substantial approach will likely be necessary for the treatment of end-stage disc disease, due to depletion of the endogenous cell population and irreversible deterioration of tissue structure. In such circumstances, a composite (or whole disc) approach would be required, where the entirety of disc structure and function is replicated. Towards that end, a number of studies have reported on co-cultured NP and AF components for tissue-engineered total disc replacement. These cell-seeded engineered discs have been evaluated in vitro [180, 194], in the subcutaneous space [165, 166, 254], and have recently been placed in situ between rat lumbar and caudal vertebrae [29, 30], illustrating the rapid advances in this regenerative approach to engineered disc replacement.

Current engineered discs do not replicate the hierarchical AF organization required to support multiaxial spinal loads. The AF is comprised of lamellae, discrete fibrous sheets with specialized collagen alignment. Within each lamella, fibers run in a single direction, ranging from 20° to 50° with respect to the transverse plane, and adjacent lamellae have opposing fiber orientation, producing an angle-ply structure [86]. Multi-directional load-bearing during compression, torsion, flexion/extension, lateral bending, and shear is supported by tensile reinforcement provided by fibers oriented in

these directions [227]. An engineered disc may need to incorporate aspects of this native design for proper function of the regenerated tissue.

Our lab has previously used electrospinning to generate engineered materials that recreate the organized fibrous architecture of the native AF [175-179]. Electrospun scaffolds with aligned nanofibers permit cell attachment and promote directed matrix production for reinforcement in principal loading directions [14, 15, 54]. Specifically, electrospun poly(ϵ -caprolactone) (PCL) seeded with either AF cells or mesenchymal stem cells increases in functional properties with in vitro culture, approaching native tissue properties at the single and multi-lamellar length scales [54, 175, 176]. Single strips of aligned scaffold can be arranged concentrically, precisely mimicking the alternating fiber alignment of native tissue, to form disc-like angle ply structures (DAPS) [179]. Like their single layer counterparts, these constructs mature both compositionally and mechanically over time in culture, indicating their potential for use in total disc replacement.

The objective of this study was to develop a disc replacement model in which to evaluate DAPS in vivo. The murine caudal spine, used in many disc studies to investigate degenerative processes [146, 207] and engineered disc replacements [63, 73], is an ideal candidate for preclinical studies given the ease of surgical access and the ability to avoid critical structures (e.g., spinal cord and spinal nerves). In the context of disc tissue engineering, the rat tail model serves as a high-throughput system to screen engineered disc designs and inform large animal studies. Thus, I developed a rat tail disc replacement model in which native caudal discs were removed and replaced with the electrospun AF-region of engineered DAPS. Here, our focus on the AF was to specifically assess the

potential for colonization of and matrix deposition in electrospun scaffolds in the in vivo disc environment. Given early findings of graft displacement, I also developed an external fixation system to stabilize the disc space. Further, since early studies showed poor infiltration of the AF region of the DAPS by endogenous cells, I included sacrificial layers within the DAPS structure to provide additional routes for cell migration.

4.2 Methods

4.2-1 Preparation of Disc-like Angle Ply Structures (DAPS)

DAPS were fabricated to reproduce the hierarchical structure of the native AF [Fig. 4-1A-B] [179]. Aligned nanofibrous sheets (thickness = 250 μm) were formed by electrospinning a 14.3% w/v solution of PCL (Shenzhen BrightChina Industrial Co., Hong Kong, China) dissolved in a 1:1 mixture of tetrahydrofuran (THF) and N,N-dimethylformamide (DMF) (Fisher Chemical, Fairlawn, NJ) [Fig. 4-1C]. The polymer solution was extruded at a rate of 2.5 mL/hour through a 13 kV-charged 18G needle. Fibers were drawn across a 15 cm air gap onto a grounded mandrel rotating with a surface velocity of 10 m/s. The resultant sheets of aligned nanofibers were cut into strips with fibers aligned at 30° relative to the strip long axis to mimic the native AF fiber architecture [Fig. 4-1D] [176, 179]. Two strips with opposing fiber orientation were wrapped concentrically and fixed with a spot weld to form the AF region of the DAPS [Fig. 4-1E].

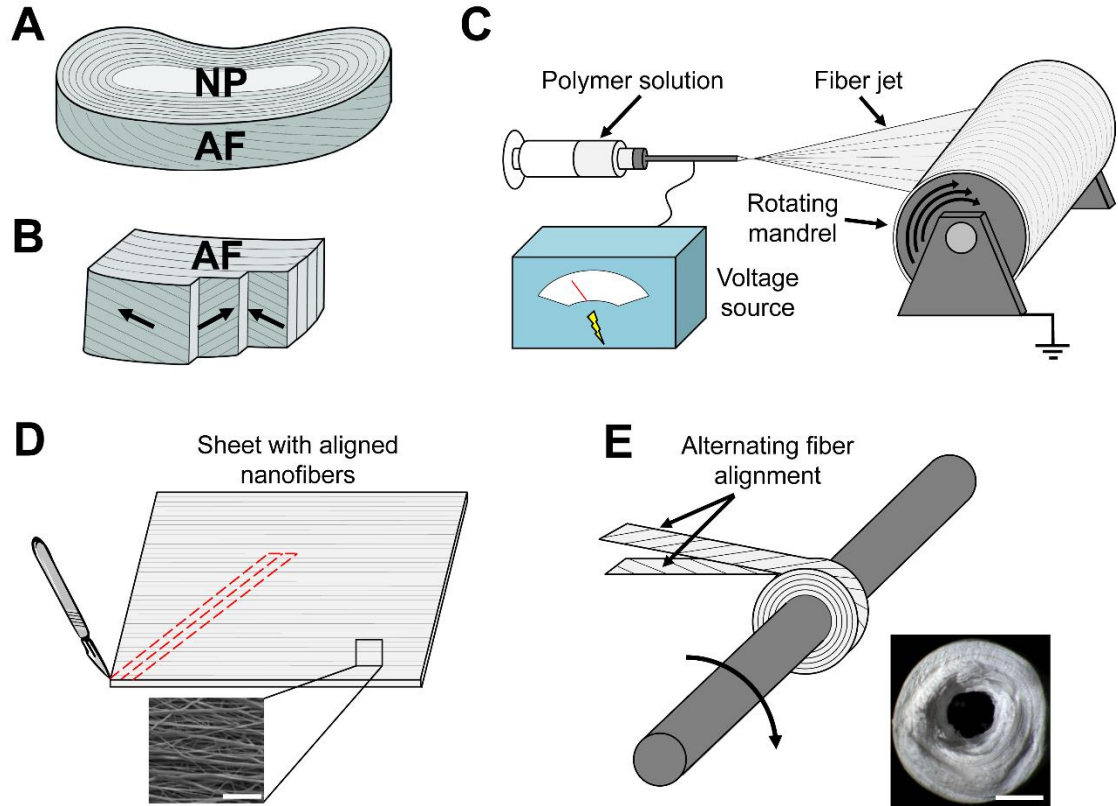


Figure 4-1 Fabrication of disc-like angle ply structures (DAPS) that replicate the intervertebral disc lamellar patterning (A) The intervertebral disc is a composite fibrocartilage that stabilizes multiaxial dynamic loading of the spine. It has two substructures that are targets for tissue engineering, the nucleus pulposus (NP) and the annulus fibrosus (AF). (B) The AF is composed of concentric lamellae with alternating $\pm 30^\circ$ collagen fiber alignment. (C) Single AF layers are replicated by electrospinning poly(ϵ -caprolactone) (PCL) nanofibers onto a rotating mandrel. (D) Aligned PCL nanofiber sheets (**bottom**) are then cut into strips at an angle (**top**) to establish a fiber arrangement consistent with native AF lamellae. (E) These strips are rolled about a post as bilayers with opposing fiber alignment (**top**) to form disc-like angle ply structures (DAPS) (**bottom**). Scale = 10 μm in panel (D, bottom) and 1mm in panel (E, bottom).

Preliminary characterization of DAPS fabricated in this manner included the measurement of DAPS geometry and compressive mechanical properties (n=7). First, a non-contact laser device was used to measure height [13] and images of DAPS were taken with a digital camera and processed in Matlab to determine inner and outer diameters [188]. DAPS were then tested in unconfined compression on an electromechanical testing system (Instron 5542, Instron, Norwood, MA). First, a 0.5 N preload was applied and allowed to relax over 300 s. Next, three consecutive compressive strain ramps of 5% magnitude were applied with a 300 s relaxation period between each ramp. The compressive equilibrium modulus was defined as the slope of a line fit through points at equilibrium after 5%, 10%, and 15% strain. The mean DAPS dimensions were: 5.1 ± 0.4 mm outer diameter, 1.0 ± 0.1 mm inner diameter, and 1.9 ± 0.3 mm height. These dimensions allow a press-fit into the (caudal) C8/C9 disc space and are comparable to the native rat caudal disc geometry (4.15 mm outer diameter, 2 mm NP diameter, 0.94 mm height [20]). The compressive equilibrium modulus was 12.6 ± 4.3 kPa and was lower than that of the native rat caudal disc (238 kPa [30]), but was expected to increase after implantation as cells infiltrate and deposit a collagenous matrix.

4.2-2 Surgical Implantation of DAPS into the Rat Caudal Spine

In a first set of surgeries, DAPS consisting of only the AF region were implanted into the caudal spines of Sprague Dawley rats (male, 7-9 months, 478 ± 11 g) in accordance with local institutional regulations. Rats were first anesthetized and, using the sacrum as an anatomical landmark, the (caudal) C8 and C9 vertebral bodies were located via fluoroscopy (Orthoscan HD, Orthoscan, Inc., Scottsdale, AZ). Then, the dorsal skin spanning the vertebral bodies was incised, the dorsal tendons were partially separated

from their bony insertions adjacent to the C8/C9 disc with a scalpel, and the native disc was removed. A double-armed non-absorbable suture was passed through the DAPS center, fed through the disc space, and tied exterior to the ventral skin to anchor the implant in place [Fig. 4-2A]. The incision was then closed with non-absorbable simple interrupted sutures. Post-surgical management included prophylactic treatment of infection (cefazolin, 15 mg/kg subcutaneous, 1 day pre-op and 2 days post-op), inflammation (meloxicam, 1 mg/kg subcutaneous, 1 day post-op), and pain (buprenorphine, 0.1 mg/kg subcutaneous, 3 days post-op). Rats were returned to normal cage activity and euthanized at either 14 (n=6) or 28 days (n=9). Additional rats were assigned to a discectomy-only control group, in which the native disc was removed in its entirety but no implant was placed. These rats were also euthanized at 14 (n=4) or 28 days (n=4).

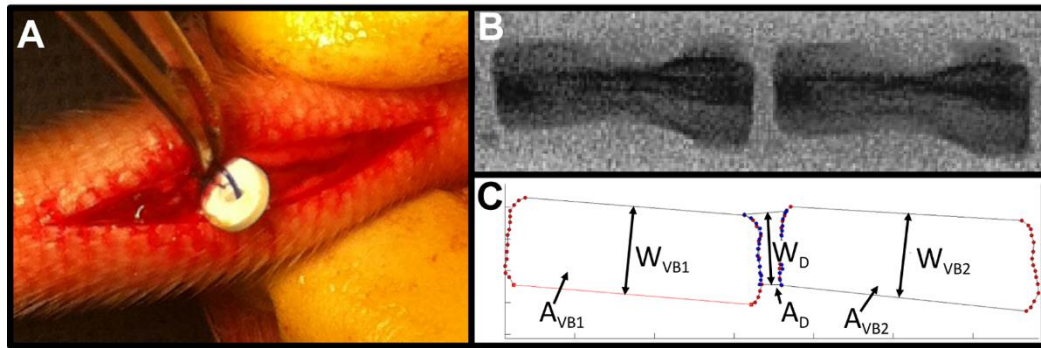


Figure 4-2 DAPS implantation into the rat caudal spine and analysis of disc height
 A rat tail model was used to evaluate DAPS integration and function. **(A)** Following a dorsal incision and discectomy, DAPS were implanted into the C8/C9 disc space and anchored to the ventral skin with a suture. **(B)** Lateral fluoroscopic images were taken at regular intervals throughout the study to analyze changes in disc height. **(C)** These changes were quantified through digital image analysis and expressed as Disc Height Index (DHI). The indicated quantities were used for calculating DHI: vertebral body 1 area, A_{VB1} , vertebral body 2 area, A_{VB2} , disc area, A_D , vertebral body 1 width, W_{VB1} , vertebral body 2 width, W_{VB2} , and disc width, W_D .

4.2-3 Evaluation of Disc Height

To evaluate implant stability, caudal spines were imaged fluoroscopically pre-operatively, immediately post-operatively and at regular intervals through 28 days [Fig. 4-2B]. Disc height index (DHI) [153], a standard technique used to normalize disc height to vertebral body length, was quantified from lateral fluoroscopic images using a custom Matlab program [Fig. 4-2C]. The disc and adjacent vertebral bodies areas (A_{VB1} , A_{VB2} , A_D) and widths (W_{VB1} , W_{VB2} , W_D) were quantified digitally. The mean vertebral body lengths (L_{VB1} , L_{VB2}) were defined as $L_{VB} = A_{VB}/W_{VB}$, the disc height (H_D) as $H_D = A_D/W_D$, and DHI as $DHI = 2H_D/(L_{VB1}+L_{VB2})$. For longitudinal analysis, DHI was expressed as a percentage of pre-operative DHI (%DHI₀). Implants were deemed ‘successful’ if 75% DHI₀ was maintained at the terminal timepoint and ‘displaced’ if this was not the case.

4.2-4 Microcomputed Tomography (μ CT)

To assess disc height and adjacent vertebral bone remodeling, μ CT scans (vivaCT 75, SCANCO Medical AG, Bruttisellen, Switzerland) of the caudal spine were acquired after euthanasia at an isotropic resolution of 20.5 μ m. Three-dimensional reconstructions were generated for visualization of the disc space and bony surfaces.

4.2-5 DAPS Implantations with External Fixation

Several DAPS were displaced from the intervertebral space in the initial surgical series; likely due to the eccentric loading conditions in the caudal spine. This motivated development of an external fixation system to improve implant retention. A radiolucent PEEK/stainless steel ring-type external fixator [98] was designed to unload and stabilize the intervertebral space [Fig. 4-3A].

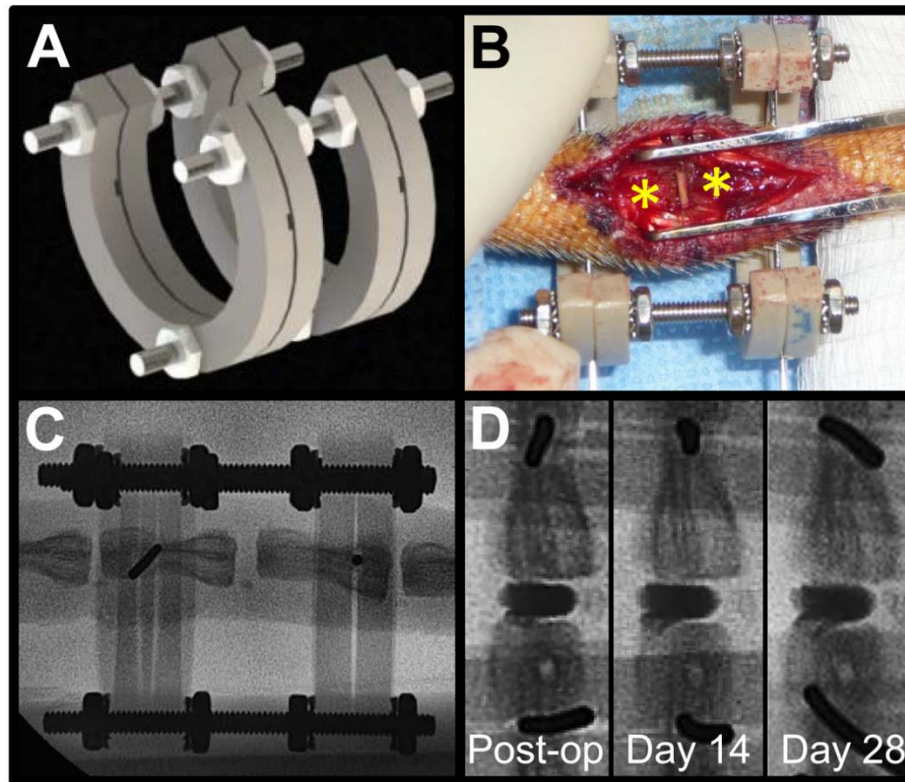


Figure 4-3 External fixation to stabilize the caudal spine and improve DAPS retention (A) Given observations of displaced implants following initial surgeries, an external fixator was designed to provide a stable environment for DAPS integration. (B) Surgical wires were passed through adjacent caudal vertebral bodies (*) and were inserted into machined grooves in the fixator. The open fixator design provided a window through which to conduct surgery. (C) The fixator ring material, PEEK, is radiolucent, allowing for visualization of the vertebral bodies by fluoroscopy and quantification of disc height over the course of the study. (D) Radiopaque DAPS (rDAPS) illustrate implant retention with external fixation over the course of 28 days.

To apply the fixator, 0.8 mm Kirschner wires (Synthes Inc., West Chester, PA) were passed laterally through the mid-height of the C8 and C9 vertebral bodies with a pneumatic wire driver, the 'C' shaped rings of the fixator were slid onto the wires ventrally leaving access to the dorsal tail, and the intervertebral height was set by adjusting the position of nuts on the threaded rods. With the fixator in place, removal of the native disc and DAPS implantations proceeded as described above, though no internal suture was used to secure the DAPS [Fig. 4-3B]. Rats received the same pre- and post-surgical medication regimen and were returned to normal cage activity until euthanasia at 14 (n=4) or 28 days (n=5). An additional external fixator plus discectomy control group was included to verify preservation of disc height with application of the fixator at 14 (n=2) and 28 days (n=4). Rats from all external fixator surgeries were subjected to serial fluoroscopy [Fig. 4-3C] and μ CT (after the fixator was removed) as described above.

To facilitate regular assessment of the position of implanted DAPS, radiopaque DAPS (rDAPS) were fabricated to enable visualization via fluoroscopy. To do so, PCL solutions were supplemented with the radiopaque nanopowder, zirconia (Zirconium(IV) Oxide Nanopowder, Sigma-Aldrich, St. Louis, MO). Nanofibrous radiopaque sheets (thickness = 250 μ m) were formed by electrospinning a 14.3% w/v solution of 50% PCL and 50% zirconia dissolved in a 1:1 mixture of THF and DMF. To monitor changes of implant position over time, rDAPS were implanted along with application of the external fixator described above [Fig. 4-3D]. Rats with rDAPS were subject to serial fluoroscopy and euthanized at 28 days for μ CT (n=2).

4.2-6 Histological Analysis

All segments from DAPS, fixation+DAPS, discectomy, and fixation+discectomy surgeries were fixed in buffered formalin and decalcified in formic acid. Vertebra-DAPS-vertebra motion segments were sectioned to 30 μm thickness in the dorsoventral plane on a cryostat microtome (Microm HM 500, Thermo Scientific, Waltham, MA). Sections were stained with hematoxylin and eosin (H&E) to visualize cell infiltration and matrix deposition. Stained sections were observed and imaged under bright field with an upright microscope (Eclipse 90i, Nikon, Tokyo, Japan). Additional samples were imaged with cross-polarized light to inspect the DAPS lamellar structure. Sections were also stained with 4',6-diamidino-2-phenylindole (DAPI) to visualize cell nuclei; these samples were imaged under fluorescence and overlaid with differential interference contrast (DIC) microscopy images to highlight the location of cells with respect to the DAPS lamellar structure.

4.2-7 Implantation of DAPS with Sacrificial Layers to Improve Cell Infiltration

After the achievement of implant stability, the slow migration of endogenous cells into the PCL-only DAPS warranted the modification of the scaffold material to include routes for cell infiltration. Sacrificial layer DAPS (sDAPS) were fabricated by sequentially electrospinning two layers of polymer, the first, a standard aligned PCL layer, and the second, a water soluble poly(ethylene oxide) (PEO) layer (200kDa, Polysciences, Inc., Warrington, PA). PEO nanofibers were electrospun from a 10% w/v solution of PEO dissolved in 90% ethanol. This solution was drawn through an 18G needle across a 10 kV gradient at 2.5 mL/hr and collected onto the rotating mandrel atop the deposited PCL layer. Strips were cut from the composite PCL/PEO mats and wrapped using the same method as described above, forming sDAPS.

To evaluate infiltration, sDAPS were first seeded in vitro with bovine AF cells and cultured for 7 days [Fig. 4-7A]. For this, a 31G needle was passed radially through the mid-height of the sDAPS to stabilize the structure. The sDAPS were then rehydrated in a series of gradient ethanol washes to remove PEO layers and coated overnight in a solution containing 20 µg/mL fibronectin (Sigma-Aldrich, St. Louis, MO) to improve cell attachment [9]. The sDAPS were then lyophilized and seeded with passage 2 bovine AF cells isolated as described previously [177]. Cells were loaded onto each surface (1×10^6 cells per side) and allowed to incubate for 1 hour per side before culture in media containing Dulbecco's modified Eagle's medium (Gibco, Invitrogen Life Sciences, Carlsbad, CA), 1% penicillin, streptomycin, and fungizone (Gibco), and 10% fetal bovine serum (Gibco) for 7 days. Three types of DAPS were included in the study (n = 3/constructs/group); PCL only DAPS (250 µm layer thickness), 'thick' sDAPS (125 µm PCL layer, 250 µm PEO layer), and 'thin' sDAPS (125 µm PCL layer, 125 µm PEO layer). Infiltration was evaluated by DAPI staining of cross sections on day 7, as described above.

Acellular sDAPS, with *intact* thick or thin PEO layers, were also implanted into the rat caudal spine (using the external fixator), and cell infiltration was evaluated after 14 days in vivo (n=3/group) [Fig. 4-7A]. Following euthanasia, motion segments were sectioned, stained with H&E or picosirius red (for collagen), and imaged by brightfield or polarized light microscopy.

4.2-8 Statistical Analysis

DHI was statistically assessed by grouping discectomy, displaced DAPS, successful DAPS, fixation+discectomy and fixation+DAPS surgeries and implementing

an ANOVA, with comparisons made among groups within each timepoint and to pooled pre-operative measurements. Tukey's post-hoc test was used for pairwise comparisons ($p < 0.05$). Statistical analyses were performed using Prism 5 (GraphPad Software Inc., La Jolla, CA).

4.3 Results

4-3.1 DAPS Implantations in the Caudal Spine: DAPS implantations using only a suture anchor successfully maintained 75% DHI₀ in 8 of 15 surgeries [Fig. 4-4A]. Immediately after implantation, an increase in DHI was noted following the press-fit of DAPS into the disc space. DHI gradually decreased over time, but, by day 28, DHI for successful implants was not different from pre-operative DHI. Following discectomy alone, the disc space also initially expanded, likely due to joint laxity caused by detachment of the dorsal tendon bundles, but collapsed to 40% of preoperative DHI by 28 days. In cases where DAPS were displaced from the intervertebral space, there was variability in the timing of implant failure, as evidenced by large standard deviations of DHI at 14 days in the displaced group. However, by day 28, there was no difference in DHI between the displaced DAPS and discectomy groups. Gross examination of tails from the displaced DAPS group revealed that the DAPS were located in the dorsal subcutaneous space at both the 14 and 28 day timepoints.

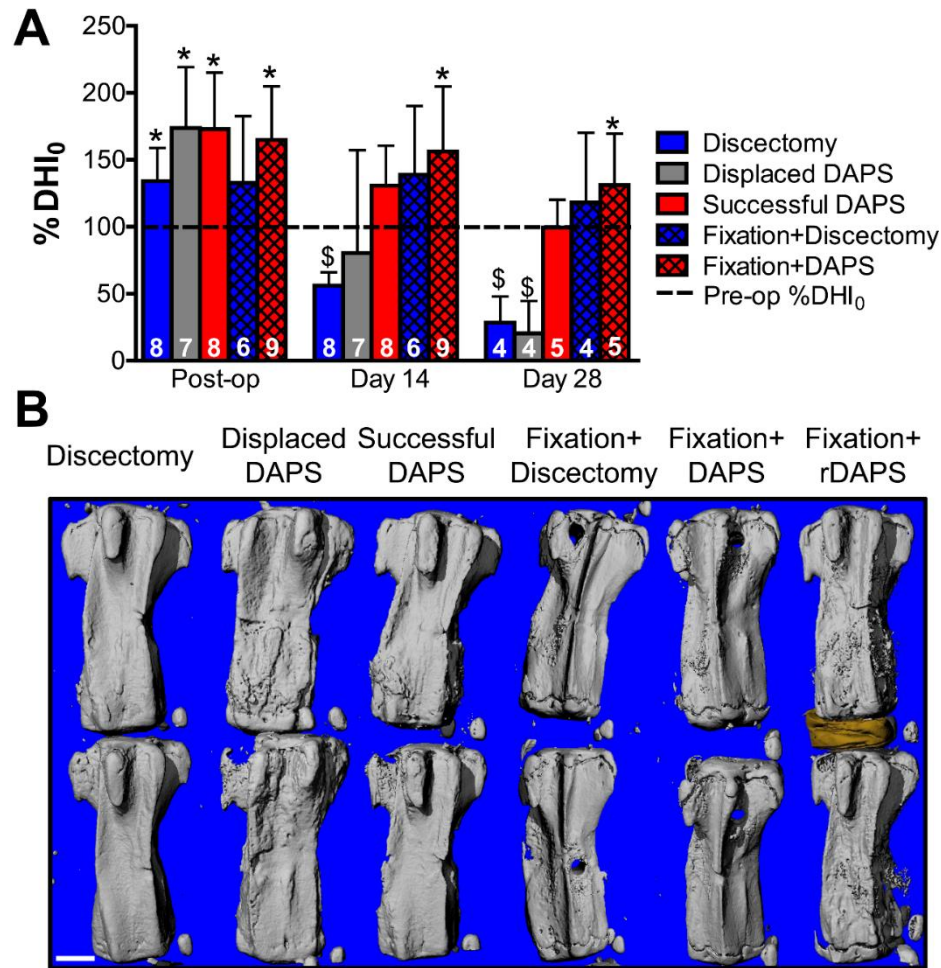


Figure 4-4 DHI and bony anatomy for DAPS implantations with or without external fixation (A) Fluoroscopic analysis of %DHI₀ for discectomy, displaced DAPS, successful DAPS, fixation+discectomy and fixation+DAPS surgeries over a 28 days. Significant differences ($p < 0.05$) are displayed as (*, vs. pre-op) and (\$, vs. successful DAPS, fixation+discectomy and fixation+DAPS groups). Sample numbers for each group are indicated at the base the corresponding bar. These decrease from day 14 to day 28 as rats were removed from the study (as scheduled) for μ CT and histological analysis. For successful DAPS and both fixation groups, the pre-op disc height was maintained over the course of the study. For DAPS that were eventually displaced, there was variation in the time at which they were displaced as evidenced by the large standard deviation at day 14. These eventually collapsed to a level similar the discectomy control group. (B) Representative μ CT reconstructions for the same groups on day 28. Both discectomy and displaced DAPS groups collapsed by day 28, with the displaced DAPS group demonstrating new bone adjacent to the disc space. Disc height is maintained with little change in the bony architecture in the successful DAPS and both fixation groups. The rightmost panel shows the morphology of an implanted rDAPS and adjacent vertebrae. Scale = 2 mm.

4-3.2 External Fixation Preserves Disc Height

External fixation caused no changes in surgical outcome or post-operative cage activity. All DAPS implanted with external fixation remained in the disc space for the duration of the study. With the fixation system in place, disc height was preserved, even in the case of discectomy. At day 14 and 28, the fixation+discectomy DHI was significantly greater than the discectomy-only DHI, and was not different from pre-operative levels. DHI was also maintained by external fixation in all fixation+DAPS surgeries; %DHI₀ post-op was set at 165% to allow room for DAPS implantation. This was significantly different from pre-operative DHI and remained so through day 28.

4-3.3 Vertebral Bone Morphology Post-DAPS Implantation

Reconstructions of μ CT scans confirmed the maintenance of disc height in successful DAPS surgeries and the collapse of disc height in displaced DAPS and discectomy surgeries at 28 days [Fig. 4-4B]. In the discectomy group, the intervertebral space collapsed, though there was no evidence of adjacent vertebral bone remodeling. Conversely, in the displaced DAPS group, bone remodeling was present adjacent to the collapsed disc space, though the reason for this new bone deposition is unclear. In successful DAPS surgeries, the intervertebral space was intact, and minor misalignment and remodeling were evident in all cases. External fixation prevented collapse with minimal superficial bone deposition at the K-wire insertion sites as illustrated in the both fixation groups. Reconstructions of rDAPS confirmed intervertebral positioning at 28 days [Fig. 4-4B].

4-3.4 Histological Appearance of DAPS and the Intervertebral Space

Histological analysis via H&E staining confirmed that disc height was maintained by the external fixator, even following discectomy, and that in all 9 fixation+DAPS surgeries, the DAPS remained in the intervertebral space. In the absence of fixation, disc height collapsed following discectomy, with remnant AF visible at both timepoints [Fig. 4-5A-B]. With the external fixator, the space left vacant by discectomy was partially filled with fibrous repair tissue by 28 days [Fig. 4-5C-D].

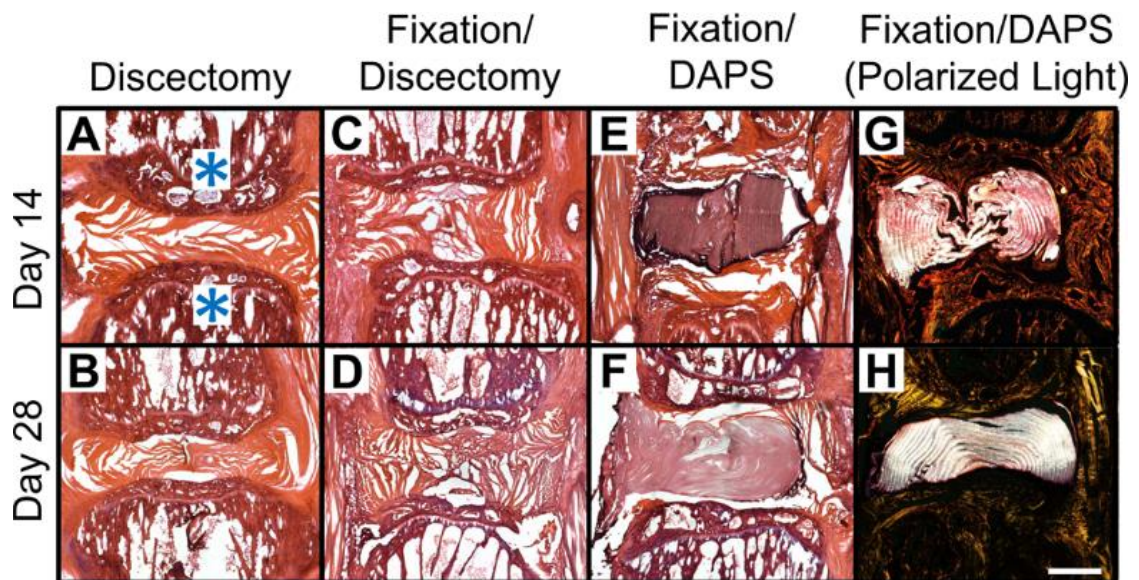


Figure 4-5 Histological appearance of DAPS in the rat caudal spine Representative H&E stained sections at 14 and 28 days for discectomy (**A**, **B**), fixation+discectomy (**C**, **D**), and fixation+DAPS groups (**E-H**). Vertebral bodies are indicated by an asterisk (*) in (A). The fixation+DAPS group was imaged in both brightfield (**E**, **F**) and polarized light (**G**, **H**) to highlight the intact DAPS lamellar structure. The discectomy group showed narrowing of the disc space at both 14 and 28 days with some remnant AF visible. The fixation+discectomy group demonstrated an expanded disc space at day 14 that was maintained through day 28, and began to fill with fibrous repair tissue. In the fixation+DAPS group, the implant filled the disc space and, at 28 days, concentric lamellae with alternating fiber orientation were observed. Scale = 1 mm in panel (A).

In fixation+DAPS surgeries, the DAPS remained in the intervertebral space at both 14 and 28 days [Fig. 4-5E-F], however, there was intense nuclear staining at the implant periphery with little or no matrix deposition between layers. Polarized light images of the H&E stained sections demonstrated that the lamellar structure (with alternating fiber angles) was intact over the course of the experiment [Fig. 4-5G-H]. DAPI staining confirmed that few cells had infiltrated the AF structure of the DAPS, with nuclei confined primarily to the boundaries of the implant and few in the interlamellar space by day 28 [Fig. 4-6A]. Cells that infiltrated had nuclei that were elongated, suggesting their interaction with the aligned nanofiber pattern [Fig. 4-6B].

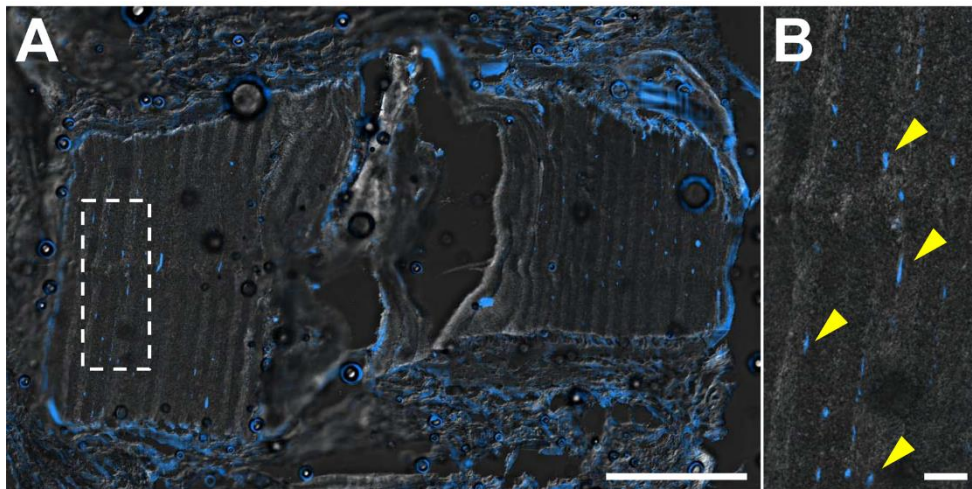


Figure 4-6 Cell infiltration into PCL-only DAPS in vivo Representative DAPI staining of cell nuclei from a fixation+DAPS implant on day 28 at low magnification (**A**) and high magnification (inset) (**B**) overlaid with a DIC image of the DAPS structure. Cells aggregated at the periphery of the DAPS, with little infiltration into the DAPS layers. Cells that did populate the interlamellar space (arrows) had elongated nuclei, indicative of their orientation with the nanofiber template. Scale = 1mm in panel (A) and 100 μ m in panel (B).

4-3.5 Improved Colonization of sDAPS

sDAPS effectively maintained interlayer gaps for cell infiltration both in vitro and in vivo. In in vitro studies, AF cells penetrated the full height of both thick and thin PEO layer sDAPS after a one week culture period [Fig. 4-7C-D]. Consistent with in vivo findings above, PCL-only DAPS were poorly infiltrated, with central areas completely devoid of cells [Fig. 4-7B]. When implanted in the caudal disc space, sDAPS remained in place and maintained their structure over time [Fig. 4-7E, H]. Along with advanced cell infiltration relative to PCL-only DAPS, collagen deposition was apparent between the remnant PCL layers, as evidenced by positive staining in both H&E [Fig. 4-7F-G] and picrosirius red sections [Fig. 4-7I-J]. Furthermore, layers with alternating fiber orientation remained intact [Fig. 4-7I-J].

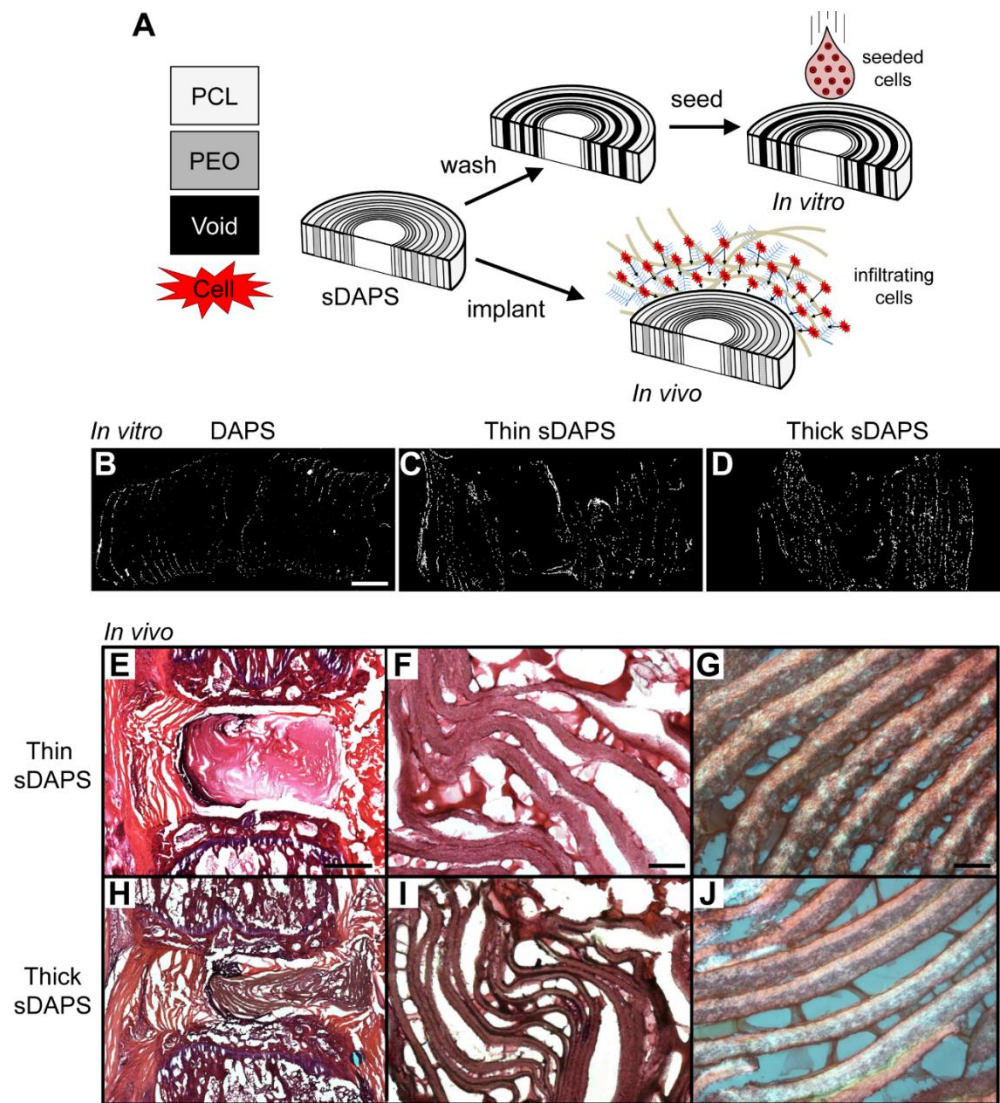


Figure 4-7 Sacrificial DAPS (sDAPS) improve cell colonization *in vitro* and *in vivo* (A) To overcome issues of poor cell infiltration, sDAPS were fabricated with a layer of PEO spun directly onto a PCL layer prior to wrapping. sDAPS were evaluated both *in vitro* (via surface seeding of constructs with bovine AF cells and 7 days of culture) and *in vivo* (via direct implantation). DAPI staining of cross sections on day 7 show increasing cell infiltration *in vitro* comparing PCL-only DAPS (B), ‘thin’ sacrificial layer sDAPS (C), and ‘thick’ sacrificial layer sDAPS (D). Implantation in the rat caudal spine (with external fixation) showed improved colonization and matrix deposition in ‘thin’ sDAPS (E-G) and ‘thick’ sDAPS (H-J). Matrix formation between lamellae was apparent at higher magnification in both formulations (F, G and I, J). Scale = 500 μ m in (B), 1 mm in panel (E), 100 μ m in panel (F), and 50 μ m in panel (G).

4.4 Discussion

Cell-based disc implants may enable reconstruction of the intervertebral disc with an engineered tissue that has the capacity to function as a living disc replacement. To further this goal, I engineered DAPS (with an AF region mirroring the hierarchical organization of the native disc), and evaluated their performance in an in vivo model of disc replacement in the rat caudal spine. This study was the first to assess an engineered disc that possessed a lamellar structure and fiber alignment similar to the native AF in vivo. In addition, I developed an external fixation system to stabilize the implant site and prevent implant extrusion, and further improved the DAPS by including sacrificial layers in the AF to improve upon poor endogenous cell infiltration.

This work validated the rat tail as a demanding, load-bearing model for disc replacement. While the axial loads experienced in the tail may be lower than the lumbar spine, the large angular displacements that occur during tail flexion (coincident with dynamic balancing activities) lead to graft displacement. Thus, in the absence of external fixation, DAPS were retained in the disc space in only 47% of surgeries, while with fixation 100% retention was achieved. Previous studies have demonstrated that a cell-seeded engineered composite disc comprised of a collagen hydrogel-based AF and an alginate hydrogel-based NP were retained in the rat lumbar and caudal disc space *without* external fixation [29, 30]. Differences in outcomes between that study and the current one may be due to differences in surgical approach, including the length of the dorsal skin incision, the treatment of dorsal tendon bundles, and the amount of annulus removed. Differences may also be due to the physical properties of the construct, where DAPS are ~4-fold stiffer in compression than the collagen/alginate implants [95], perhaps making

them more likely to displace (rather than compress) with tail flexion. Future studies could challenge such implants in a physiologic loading environment, with compressive loading and smaller angular displacements, like the lumbar or cervical spine. Alternatively, the rat caudal disc space could be subjected to controlled physiologic loads by modifying the external fixator to apply static or dynamic compressive forces [98, 244]. Such mechanical perturbation may act to increase biosynthetic activities in the implant, and encourage integration with the surrounding tissue [90, 120, 154, 244].

Another observation in this study was poor infiltration of endogenous cells, even in DAPS that were stably fixed in the disc space. Poor cell infiltration is a common drawback of electrospun scaffolds used for tissue engineering [11, 104, 167, 197] and may have been exacerbated in this case by the tight wrapping of concentric layers during DAPS fabrication. Stable PCL-only DAPS showed poor infiltration over 28 days, with an accumulation of cells at the implant periphery and little or no matrix deposition between layers. This result was independent of external fixation (i.e., fibrous encapsulation was similar in successful PCL-only DAPS with or without an external fixator) and may be a limitation of that scaffold formulation. Nevertheless, stable retention of an implant, as is enabled by an external fixator, may improve or hasten integration by preventing micromotion that would interrupt newly formed tissue bridges. Borrowing from our previous work using PEO as a water-soluble porogen, I fabricated sDAPS with a sacrificial layer interwoven between PCL layers. This allowed for rapid and complete infiltration by cells in vitro and in vivo, as well as marked collagen deposition between layers. Future work will confirm the cell type responsible for this new tissue formation, and its composition.

Our goal in initiating these studies with an acellular, AF-only DAPS was to determine the viability of the caudal disc replacement model using such materials. However, acellular biomaterials have come to the fore in the context of tissue engineering as an alternative to cell-based methods. Acellular approaches are motivated by difficulties with cell isolation, handling, and behavior, and the regulatory obstacles that may act as barriers to clinical translation of biological therapies [36]. Here, I developed a material-based (rather than a cell-based) approach in which the AF construct is populated by active endogenous cells that secrete extracellular matrix proteins to produce functional tissue. This approach requires evaluation in the target patient population, whose degenerated disc environment (with deficient vascularity, low cellularity and chronic inflammation) might limit the capacity of endogenous cells to produce functional tissue. Our in vitro data also show that DAPS can be readily pre-seeded with exogenous cells (AF cells or mesenchymal stem cells) and coupled to an acellular or cell-based NP replacement to enable total disc replacement in such scenarios.

The interface between the DAPS and the adjacent soft tissue/vertebral bodies is critical for functional restoration of the motion segment but was not specifically evaluated in this study. Integration did occur with the surrounding soft tissue, as endogenous cells transited into sacrificial layer DAPS and deposited new extracellular matrix. Soft tissue contiguity was observed histologically, particularly in those implants with sacrificial layers that were more fully invested. This soft tissue bridge is likely quite fragile at early timepoints and thus future studies are required to mechanically evaluate the forming interface as a function of time as matrix deposition continues. It is also likely that additional steps must be taken to specifically enhance integration, and this model

provides a platform to optimize both implant design and surgical strategy to promote implant integration within the motion segment.

A primary limitation of this model is the use of external fixation to unload the disc space, and so implants were not challenged or modulated by the physiologic loading environment. The current fixator design can, however, be modified to enable application of controlled static or dynamic loads [98, 205, 244]. Thus, this model provides an opportunity to investigate how the mechanical boundary conditions alter integration at the vertebral interface and guide maturation of the DAPS. Additionally, I excluded major disc structures, namely the NP and the cartilaginous/vertebral endplates, to focus on model development and the improvement of the AF region of the DAPS. Future implant design will involve DAPS inclusive of an NP region to form a composite total disc replacement.

4.5 Conclusion

This study advances the goal of biologic total disc replacement by validating a rat caudal spine model for in vivo testing of engineered disc replacements, and illustrates that a stable fixation system improves the retention of implanted discs. I evaluated the performance of a nanofibrous scaffold that was structurally equivalent to the native AF and found that the dense PCL scaffold formed by electrospinning did not permit endogenous cell infiltration. However, by modifying the design to include water soluble layers to create interlamellar spaces, endogenous cells populated the full thickness of the implant and produced a collagenous network. Future work (Ch. 7) will build upon this foundation to further the goal of a functional, tissue-engineered total disc replacement.

CHAPTER 5 - A Radiopaque Electrospun Scaffold for Engineering Fibrous Musculoskeletal Tissues: Scaffold Characterization and In Vivo Applications

5.i Preface

Chapter 5 describes a radiopaque scaffold for engineering fibrous tissues (and is published in [150]). In the previous chapter, I described the use of radiopaque DAPS (rDAPS) fabricated from this scaffold in vivo. This proved extremely useful for improving our surgical techniques and then to track implant position over time to confirm implants did not migrate from the disc space. In this chapter, I expand on the use of radiopaque scaffold, showing that it can be visible in joints with dimensions similar to humans, that it is cytocompatible, and that it does not induce osteogenesis.

5.1 Introduction

The healing capacity of musculoskeletal tissues like the intervertebral disc, meniscus, tendon, and ligament is limited, and injury or degeneration of these tissues compromises the standard of living of millions in the US [193]. While there are a number of surgical approaches for repairing diseased or damaged fibrous musculoskeletal tissues, each of these are associated with significant limitations. For example, partial meniscectomy may be indicated for tears in the avascular region of the meniscus. While in many cases this procedure provides relief of pain and mechanical symptoms, it accelerates osteoarthritis due to altered load transmission in the knee [1] and its long-term

efficacy is uncertain [106]. Spinal fusion is often performed for segmental instability resulting in stenosis or radiculopathy in the presence of a collapsed or bulging intervertebral disc. While many patients have positive outcomes following fusion, alterations in spinal kinematics after fusion are associated with accelerated degeneration of adjacent discs [85]. Rotator cuff repair is commonly performed for pain and weakness resulting in compromised upper extremity function. However, the poor healing capacity of degenerated rotator cuff tendons and high tensile loads due to tendon retraction impair healing at the bone-tendon interface [6]. For these reasons, engineering fibrous musculoskeletal tissues from cells and various natural and artificial materials has emerged as a strategy to improve the outcomes of the above procedures. In particular, tissue engineering repair strategies for disc, meniscus, tendon and ligament have transitioned over the past decade from in vitro [34, 132, 165, 179] to in vivo [30, 134, 149, 246] evaluation using a variety of animal models, and the clinical application of these emerging technologies is imminent.

Engineered fibrous tissues must meet specific design criteria related to their physical characteristics in order to effectively resist, dissipate, and transfer mechanical loads during normal daily activities. Fibrous musculoskeletal structures resist multidirectional loading by dissipating energy through collagen fibers and inter-fibrillar matrix, and, in order to ensure proper functional performance, engineered tissues must not only withstand physiologic loading and motion, but also must integrate into adjacent native tissues. In vivo visualization of engineered tissues would be a powerful method to track and confirm the performance in situ, however, the composition of most scaffold

materials does not allow for visualization by methods available to clinicians (e.g., radiography).

Visualization by fluoroscopy and radiography is routinely performed for the diagnosis of musculoskeletal conditions, surgical planning, intraoperative guidance, and postoperative assessment. Total joint replacement prostheses and fracture fixation implants have characteristic radiographic profiles due to their radiopaque components; radiopaque markers in interbody prosthetic devices for spinal fusion allow for image-guided placement and long-term confirmation of position; radiopaque bone cements derived from methyl methacrylates and heavy metal/ceramic radiopacifiers are currently used for the fixation of prostheses and in the augmentation of vertebral compression fractures. Enabling similar visualization of engineered fibrous musculoskeletal tissues is very important for repairing tissues that are subject to physiological loads and resultant deformations, as it would improve intraoperative positioning and allows post-operative tracking of scaffold location, integration and remodeling.

Electrospun scaffolds are currently being evaluated for a number of fibrous tissue engineering applications, including repair of the annulus fibrosus of the intervertebral disc [105, 176], the knee meniscus [12, 66], tendons [19, 40, 119], and ligaments [125, 211]. As these scaffolds are typically radiolucent, I developed a radiopaque nanofibrous scaffold by electrospinning a polymer/ceramic nanopowder solution [149]. Scaffolds were produced with aligned fibers to provide a template for cell attachment and to orient newly formed collagenous matrix [129, 174]. To impart radiopacity, I included radiodense nanoparticles within each fiber. In this study, I characterized the structure,

radiation attenuation, and mechanical behavior of these scaffolds as a function of nanoparticle density, as well as the behavior of bone marrow-derived mesenchymal stem cells (MSCs) seeded on the scaffolds. We further evaluated these materials in situ in the bovine knee for applications in meniscus repair and in vivo in a rat model of total intervertebral disc replacement.

5.2 Methods

5.2-1 Scaffold Fabrication

Radiopaque scaffolds were generated from a solution of poly(ϵ -caprolactone) (PCL, Shenzhen BrightChina Industrial Co., Hong Kong, China) mixed with radiodense zirconium(IV) oxide nanoparticles (Zirconia, Sigma-Aldrich, St. Louis, MO). Zirconia particles have a characteristic dimension of <100 nm, allowing for their complete encapsulation within PCL fibers that typically have a diameter greater than 300 nm [128]. PCL and zirconia were dissolved in a 1:1 mixture of tetrahydrofuran (THF) and N,N-dimethylformamide (DMF) (Fisher Chemical, Fairlawn, NJ) and the slurry was extruded at a rate of 2.5 mL/hour through a 15-20 kV-charged 18G needle while continuously mixed with a magnetic stirrer. Fibers were drawn across a 15 cm air gap onto a grounded mandrel rotating with a surface velocity of 10 m/s to create aligned nanofibrous sheets (thickness = 200 μ m). Four scaffold-types with varying zirconia concentration were fabricated with PCL/zirconia mass ratios of either 50%/50%, 75%/25%, 90%/10%, or 100%/0% [Table 5-1, Fig. 5-1]. In each case, the solution concentration was 14.3 g of PCL/zirconia in 100 mL of THF/DMF (14.3% w/v [13]).

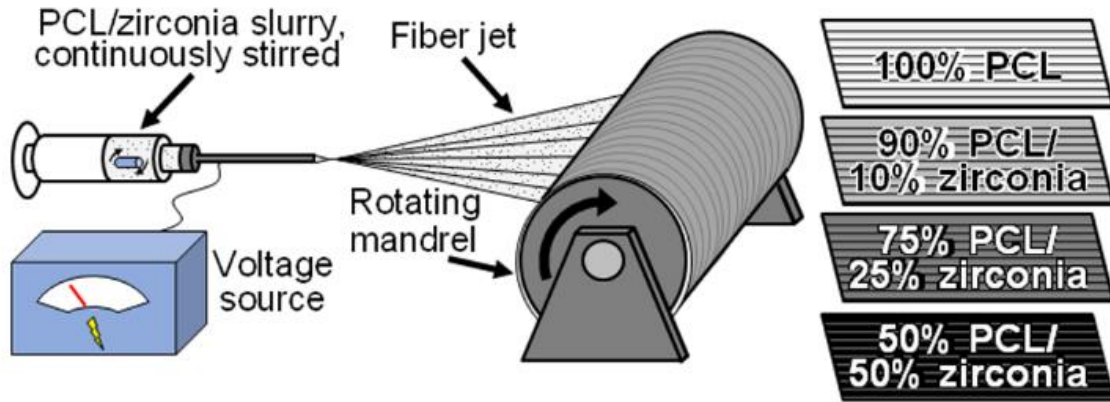


Figure 5-1 Electrospun radiopaque scaffold Radiopaque scaffolds were generated by electrospinning a mixture of PCL, a biocompatible polymer with long term in vivo stability, and zirconia, a ceramic nanopowder. The slurry was continuously mixed with a magnetic stirrer and collected onto a rotating mandrel to produce aligned nanofibrous sheets. Four different scaffold formulations were produced: 100% PCL scaffold, 90% PCL/10% zirconia scaffold, 75% PCL/25% zirconia scaffold, and 50% PCL/50% zirconia scaffold.

Table 5-1 - Composition of Solutions Used to Produce Electrospun Scaffolds

<i>Scaffold</i>	<i>%PCL by mass</i>	<i>%Zr by mass</i>	<i>PCL mass (g)</i>	<i>Zirconia mass (g)</i>	<i>THF volume (mL)</i>	<i>DMF volume (mL)</i>	<i>% w/v</i>
1	100	0	14.3	0	50	50	14.3
2	90	10	12.9	1.4	50	50	14.3
3	75	25	10.7	3.6	50	50	14.3
4	50	50	7.15	7.15	50	50	14.3

5.2-2. Scaffold Characterization

Each scaffold was assayed for structural continuity, radiodensity and mechanical properties. To assess scaffold nanostructure, samples were cut from freshly spun mats, sputter coated, and imaged at 2,000X and 10,000X magnification on a scanning electron microscope (SEM; 6400, JEOL Ltd., Tokyo, Japan) with an accelerating voltage of 10 kV. To measure radiodensity, 8 mm diameter samples were punched from each scaffold and scanned by microcomputed tomography (μ CT; vivaCT 75, SCANCO Medical AG, Bruttisellen, Switzerland) at 20.5 μ m resolution (n=5/group). The linear attenuation coefficient (volumetric average radiation attenuation) of each sample was calculated from volumetric reconstructions of the punched samples and then converted to Hounsfield Units (HU) by normalizing values to the attenuation of water. Scaffold radiation attenuation was directly compared to that of cortical bone in order to assess the potential for in situ visualization. To measure scaffold mechanical properties, scaffold strips (5 mm x 40 mm) were tested in uniaxial tension parallel to the fiber orientation using an electromechanical testing system (5542, Instron, Norwood, MA) (n=5/group). The testing protocol consisted of a 0.05 N preload followed by extension to failure at a rate of 0.1% strain/sec. The linear region tensile modulus was calculated as described previously [13].

5.2-3. In Situ Evaluation in the Bovine Meniscus

To determine whether scaffolds had radiation attenuation suitable for visualization in joints with dimensions similar in scale to human joints, a radiopaque scaffold was implanted *ex vivo* into the medial meniscus of a juvenile bovine stifle joint

and imaged with a fluoroscope (HD, Orthoscan Inc., Scottsdale, AZ). To do so, a medial parapatellar incision was made through the joint capsule, the anterior cruciate ligament was transected, and a circumferential incision was made in the medial meniscus, mimicking the location and shape of a bucket handle tear similar to those others have used in animal models [199]. The radiopaque scaffold was prepared from 50% zirconia/50% PCL solution at a thickness of 500 μm . Strips of dimensions 3 mm by 30 mm were layered into a stack of 8 and welded together with a soldering pencil. The layered scaffold was inserted into the bucket handle tear and tethered to the meniscus with 4-0 suture. The synovium and fascia were then closed with suture and anterior-posterior and medial-lateral fluoroscopic images were acquired. After this preliminary imaging, the meniscus was removed en bloc, soaked for 72 hours in Lugol's solution (Sigma-Aldrich) to enhance the radiocontrast of the meniscal tissue, and imaged via μCT at 20.5 μm resolution for visualization of both the contrast-enhanced meniscus and the radiopaque scaffold.

5.2-4 In Vitro Assessment of Cytocompatibility and Osteogenic Potential

To determine whether radiopaque scaffolds were cytocompatible, scaffolds were seeded with juvenile bovine bone marrow-derived MSCs and assayed for cell metabolic activity. MSCs were isolated from the proximal femur of 3-6 month old calves and expanded to passage 2 in a basal medium (BM) containing Dulbecco's Modified Eagle Medium (DMEM; Gibco, Invitrogen Life Sciences, Carlsbad, CA), 10% fetal bovine serum (Gibco) and 1% penicillin-streptomycin-Fungizone (Gibco). Sections were cut from each scaffold with an 8 mm biopsy punch, sterilized in ethanol, rehydrated, and then

seeded with 2×10^5 cells/scaffold (n=4/group). Metabolic activity was measured using the 3-(4,5-dimethylthiazol-2-yl)-2,5-diphenyltetrazolium bromide (MTT, Invitrogen, Carlsbad, CA) colorimetric assay at 3, 7, and 14 days after seeding. Cells were also seeded onto tissue culture plastic (TCP) and cultured in BM (n=4/group).

Previous studies have shown that nanofibrous scaffolds intended for bone tissue engineering can be optimized for osteogenic differentiation by including ceramic particles like hydroxyapatite [123, 252]. To test this potential undesirable side effect of zirconia inclusion, two additional groups, MSCs seeded on either on 100% PCL scaffold or MSCs seeded on 50% PCL/50% zirconia scaffold, were cultured for 28 days in basal media and alkaline phosphatase activity was measured. To do so, the dephosphorylation of p-nitrophenyl (pNP) phosphate by alkaline phosphatase was quantified using a colorimetric assay kit (Alkaline Phosphatase Assay Kit (ab83369); Abcam PLC, Cambridge, UK) (n=5/group). Additionally, each scaffold type (100% PCL, 90% PCL/10% zirconia, 75% PCL, 25% zirconia, and 50% PCL/50% zirconia) was seeded with MSCs, cultured for 28 days in basal media, fixed in formalin and stained with von Kossa to determine whether overt mineralization had occurred (n=1/group).

5.2-5 In Vivo Evaluation in a Rat Model of Total Disc Replacement

To examine in vivo function, disc-like angle ply structures [149] fabricated from radiopaque scaffold (rDAPS) were implanted into the coccygeal spines (tails) of Sprague Dawley rats with institutional IACUC approval (male, 440-485 g, n = 5). To fabricate rDAPS, strips were cut from aligned radiopaque scaffold 30° to the fiber direction and

two strips with alternating $\pm 30^\circ$ alignment were wrapped concentrically to form the annulus fibrosus region. Implantation of rDAPS into the rat coccygeal spine involved passing two surgical wires (0.8 mm) laterally through the mid-height of both the Co8 and Co9 vertebrae, and then fastening a radiolucent external fixator to the wires [Fig. 5-2a-b]. A dorsal incision was made, the native disc was removed, rDAPS were inserted into the disc space, and the incision was closed. Rats were then returned to cage activity and euthanized 28 days post-surgery. Two implants of varying radiodensities were evaluated: a high radiodensity implant composed of two layers of 50% PCL/50% zirconia (50/50 rDAPS, n=2), and a low radiodensity implant composed of one layer of 75% PCL/25% zirconia, 1 layer of 100% PCL and one layer of degradable 75:25 poly(lactic-co-glycolic acid) (PLGA) (multilayer rDAPS, n=3) [Fig. 5-2c]. I have previously shown that degradable layers included in DAPS provide additional routes for cell infiltration following implantation (Ch.4) [149]. In each case, the layer thickness was 125 μm .

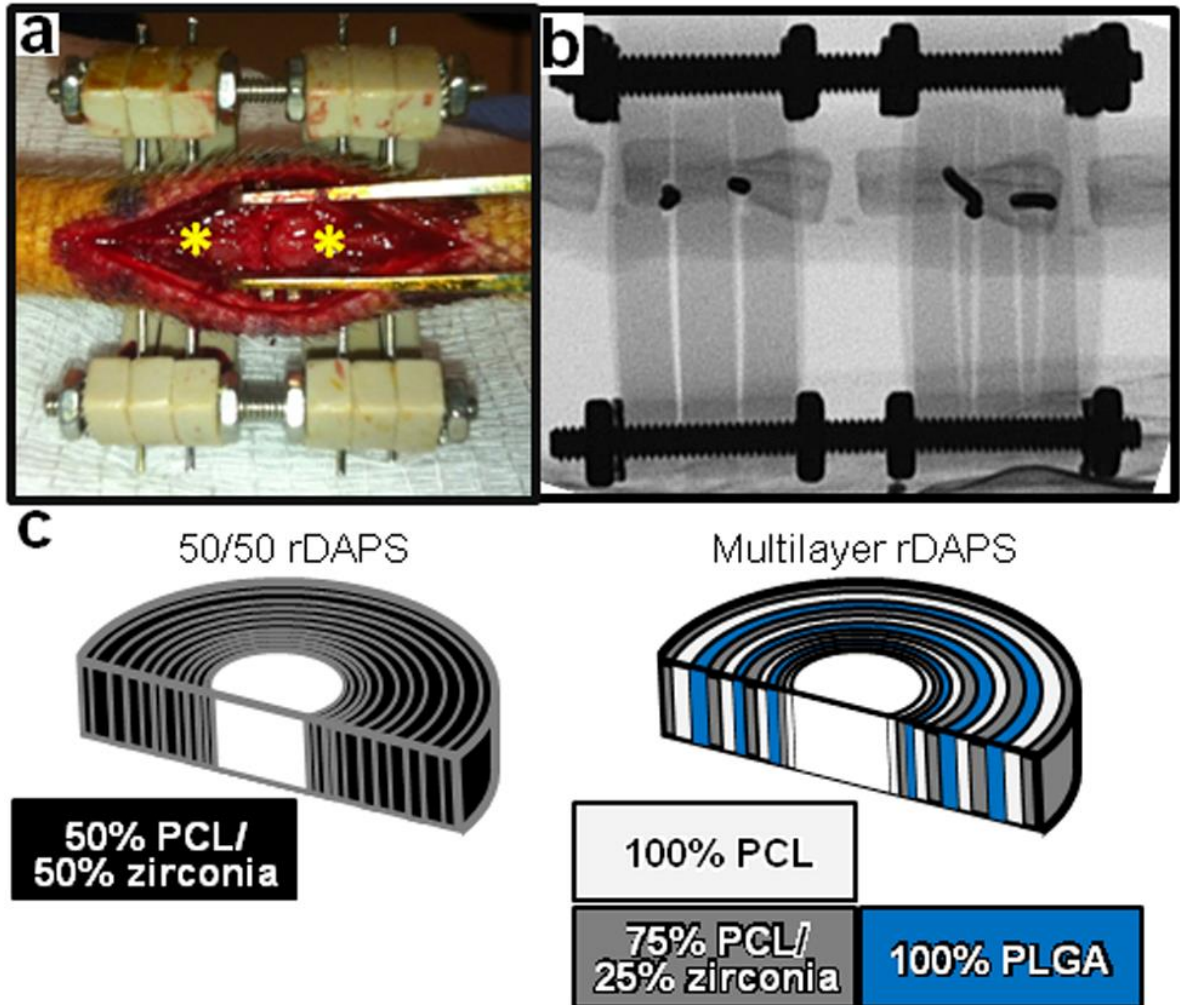


Figure 5-2 Radiopaque engineered discs in a rat model of total disc replacement (a) Rat tails were externally fixed with a custom device to provide a stable site for implantation [149]. (b) This device was radiolucent by design to allow for visualization of the disc space by fluoroscopy for longitudinal analysis. (c) rDAPS of two formulations were implanted: 50/50 rDAPS composed entirely of 50% PCL/50% zirconia layers, and multilayer rDAPS composed of three layers, a radiopaque layer of 75% PCL/25% zirconia, a radiolucent layer of 100% PCL, and a layer of 100% PLGA (designed to degrade when implanted in order to provide pathways for endogenous cell infiltration).

Implants were assessed for positioning between vertebrae, maintenance of microstructure, and integration with native tissues. To monitor implant position and structure in vivo, rat tails were imaged via fluoroscopy post-operatively and then at 3, 7, 14, 21, and 28 days through the radiolucent external fixator. Following euthanasia, the external fixator was removed and bone-rDAPS-bone motion segments were separated from the tails by sharp dissection. Motion segments were imaged via μ CT (resolution: 20.5 μ m for 50/50 rDAPS, 10 μ m multilayer rDAPS) and reconstructed in 3D to confirm implant position and visualize implant microstructure. Following imaging, motion segments were fixed in formalin, decalcified in formic acid, and sectioned at 30 μ m thickness on a cryostat microtome (Microm HM 500, Thermo Scientific, Waltham, MA). To assess implant structure and integration with native tissue, sections were double-stained with Alcian blue (for glycosaminoglycans) and picosirius red (for collagen), and were visualized via brightfield microscopy (Eclipse 90i, Nikon, Tokyo, Japan).

5.2-6 Statistical Analysis

Radiation attenuation and tensile modulus were compared between groups using one way analysis of variance (ANOVA) with zirconia concentration as the independent variable. MTT results were analyzed by two-way ANOVA with time and zirconia concentration as the independent variables. In each case, Bonferroni's post-hoc tests were used to make pairwise comparisons between groups ($p < 0.05$). Finally, alkaline phosphatase activity was compared by t-test ($p < 0.05$). Data are reported as mean \pm standard deviation.

5.3 Results

5.3-1 Scaffold structure, radiation attenuation, mechanical function, and cytocompatibility

SEM analysis revealed that all formulations of the radiopaque scaffold had continuous and aligned nanofibers [Fig. 5-3a]. Zirconia particles were embedded within the electrospun fibers and fiber morphology was not changed at lower concentrations, while at higher concentrations (25% and 50% zirconia scaffolds) zirconia aggregated as pellets exterior to the fibers. Radiation attenuation increased with zirconia content, plateauing at 25% zirconia inclusion [Fig. 5-3b]. The measured attenuation of 50% and 25% zirconia scaffolds was within the attenuation range of cortical bone [94]. PCL alone had no signal and thus 3D reconstruction of 100% PCL scaffolds was not possible. The linear region tensile modulus of the radiopaque scaffold increased with increasing zirconia content, reaching a maximum at 25% zirconia. At higher levels (50%), the tensile modulus dropped sharply to the level of 100% PCL [Fig. 5-3c].

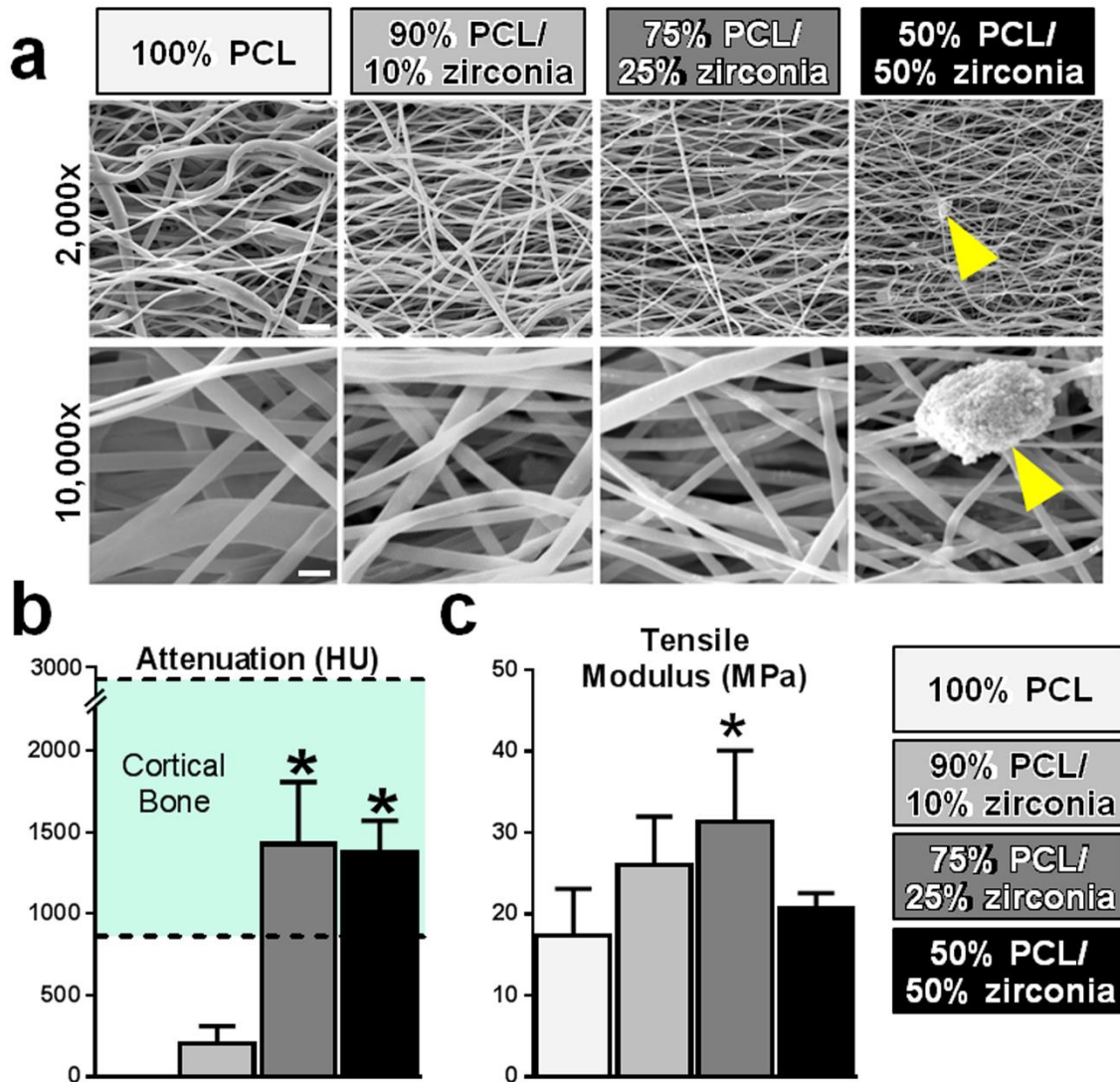


Figure 5-3 Structure, linear attenuation coefficient, and tensile modulus of radiopaque scaffolds (a) All scaffold types were aligned and nanofibrous. Structure was largely unaltered with low zirconia inclusion levels, though zirconia clusters (arrows) appeared on the fiber surfaces at the highest concentration and to a lesser extent on 75% PCL/25% zirconia scaffold. Scales – top row: 5 μ m, bottom row: 1 μ m. (b) The linear attenuation coefficients of scaffolds with high zirconia content was similar to that of cortical bone (* p <0.05 vs. 90% PCL/10% zirconia). (c) Tensile modulus was greater with increasing zirconia concentration, except for the highest concentration (* p <0.05 vs. 100% PCL).

When seeded with cells, there were no differences between scaffold variants in terms of cell proliferation which was slower on all scaffold formulations in comparison to cells seeded on TCP [Fig. 5-4a]. Additionally, there was significantly less alkaline phosphatase activity on 50% PCL/50% zirconia scaffolds when compared to 100% PCL scaffolds [Fig. 5-4b] and there was no evidence of positive von Kossa staining for any of the zirconia scaffolds. [Fig. 5-4c].

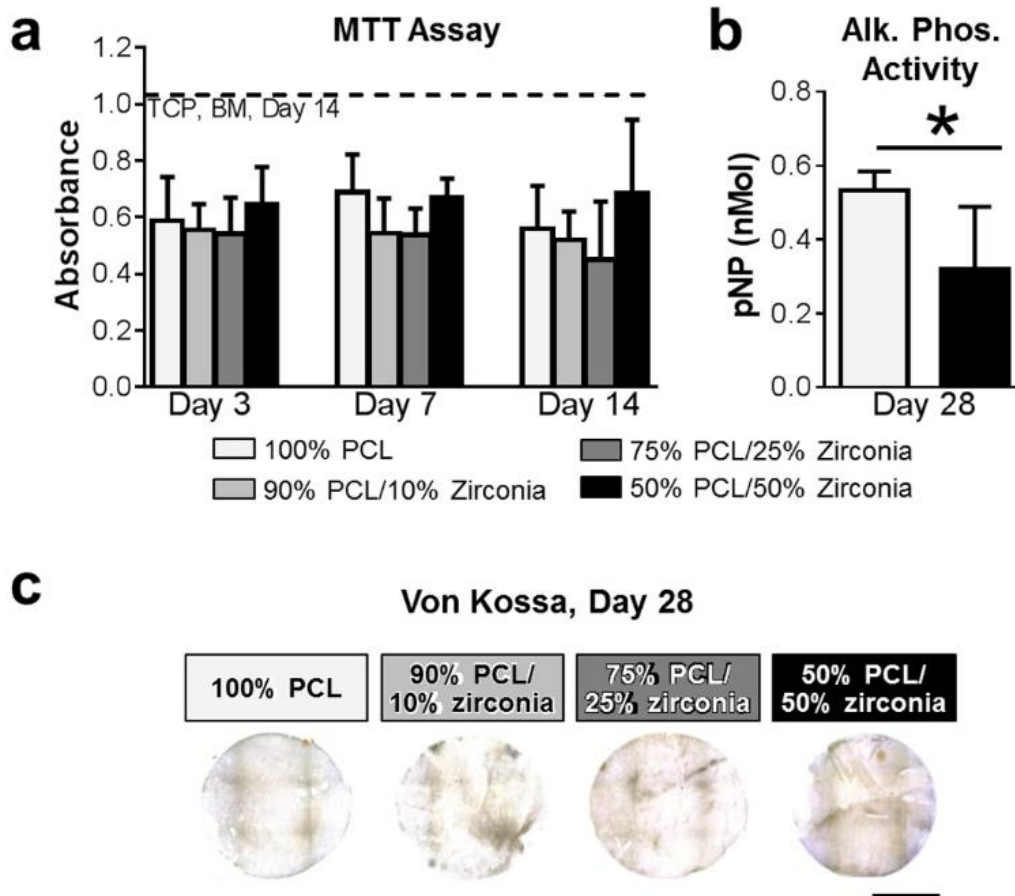


Figure 5-4 MSC viability and osteogenic potential on radiopaque scaffolds
 (a) The MTT assay for total cell metabolic activity over 14 days demonstrated no significant differences between groups and (b) quantification of alkaline phosphatase revealed diminished activity on radiopaque scaffolds (*, $p < 0.05$). (c) Furthermore, von Kossa staining revealed no evidence of calcium on any of the radiopaque scaffolds. Scale, 4mm. These data indicate that scaffolds were not cytotoxic and did not cause osteogenesis.

5.3-2 Appearance of radiopaque scaffold in situ and with long term in vivo implantation

Radiopaque scaffolds were readily visualized within the bovine meniscus in situ in both anterior-posterior and medial-lateral fluoroscopic images of the knee [Fig. 5-5a-b]. μ CT reconstructions with Lugol's solution used to enhance the contrast of the native meniscus provided anatomical information of the meniscus (the boundaries of the soft tissue were readily visualized) and positioning of the scaffold within the bucket handle tear [Fig. 5-5c-e]. The bucket handle tear was located near the boundary between the red and red-white meniscal regions and the layered scaffold was positioned within the tear, conforming to the curvature of the meniscus, with scaffold layers distinctly visible.

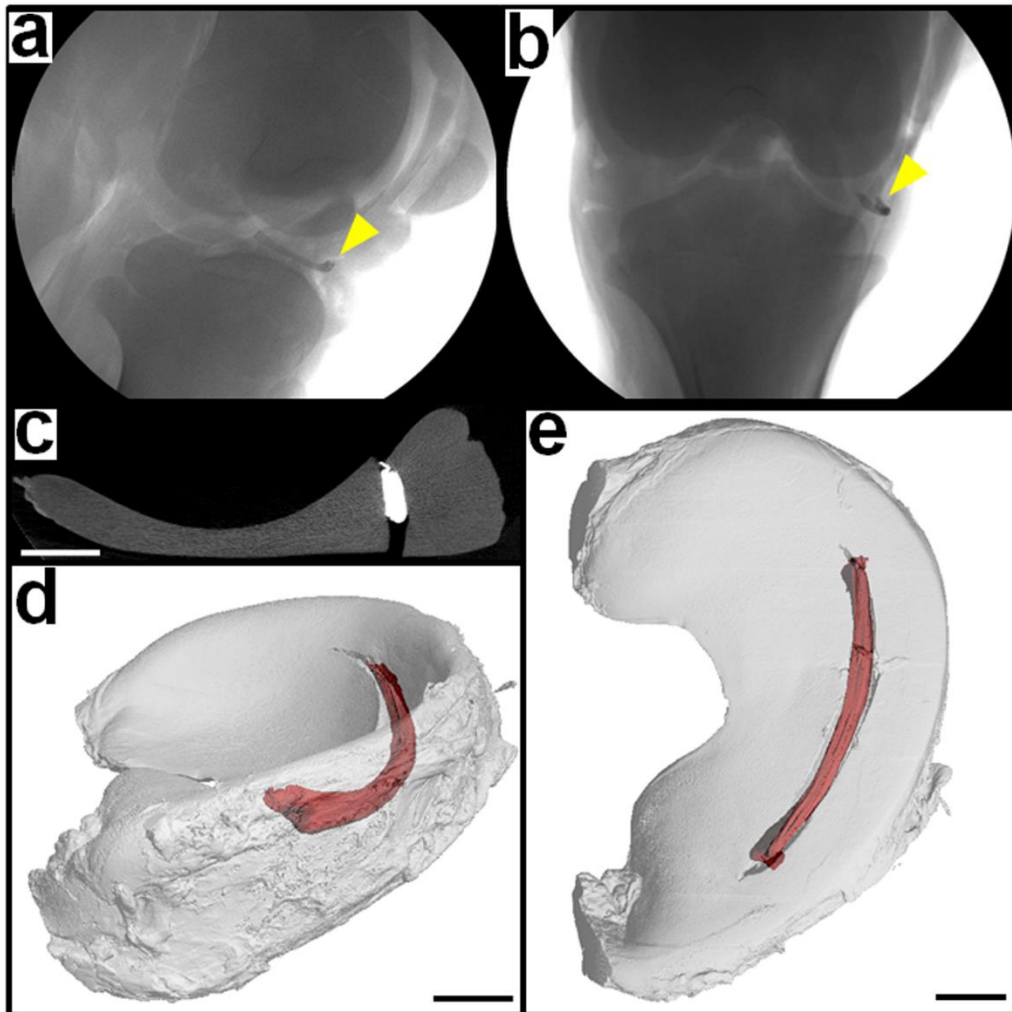


Figure 5-5 Visualization of radiopaque scaffold implanted into the bovine meniscus A layered radiopaque scaffold (arrows) was visible in an artificial tear created in the bovine medial meniscus on (a) medial-lateral and (b) anterior-posterior fluoroscopic images. Ex situ μ CT analysis, with contrast enhancement to visualize the meniscus, is shown in (c) cross section, with (d) anterior and (e) cranial views after 3D reconstruction.

Both formulations of rDAPS were visualized intra- and post-operatively by μ CT and fluoroscopy. 50/50 rDAPS had a distinct signal that allowed for segmentation of μ CT images for 3D reconstructions [Fig. 5- 6a]. Fluoroscopy revealed that the radiopaque signal of 50/50 rDAPS was more intense than that of the native bone and that there was minimal change in implant position over time [Fig. 5-6b]. Histologically, 50/50 rDAPS were located directly between vertebrae and were structurally intact, with little infiltration of local tissue [Fig. 5-6c].

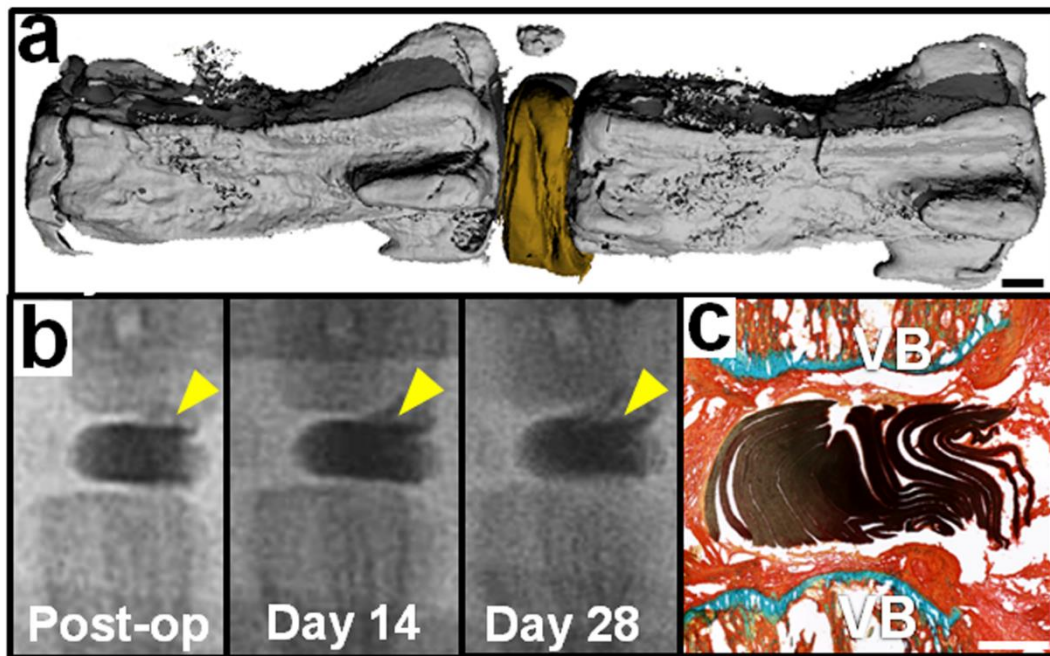


Figure 5-6 High radiopacity rDAPS in vivo (a) rDAPS (gold) were located directly between vertebrae (gray) at day 28 as visualized by μ CT. Scale, 1 mm. (b) rDAPS (arrows) attenuation was distinct from adjacent vertebrae and position did not change over time as visualized by fluoroscopy. (c) Histologically, rDAPS maintained their lamellar structure, though no tissue infiltration was apparent (as expected for DAPS without sacrificial layers). Scale, 1mm.

Multilayer rDAPS were segmented for 3D μ CT reconstructions based on their appearance, and were located directly between vertebrae [Fig. 5-7a]. The alternating radiopaque and non-radiopaque layers allowed for the visualization of the lamellar structure in transverse [Fig. 5-7b] and axial [Fig. 5-7c] cross-sections. Fluoroscopically, multilayer rDAPS were not distinguishable from adjacent vertebrae, and did not appear to migrate over time [Fig. 5-7d]. Images of histological sections confirmed that the implant lamellar structure was maintained, new collagen was deposited on PCL/zirconia layers, and that PLGA had not fully degraded by day 28 [Fig. 5-7e-f]. In addition, H&E stained sections revealed there was no endogenous response to the implanted biomaterial (not shown).

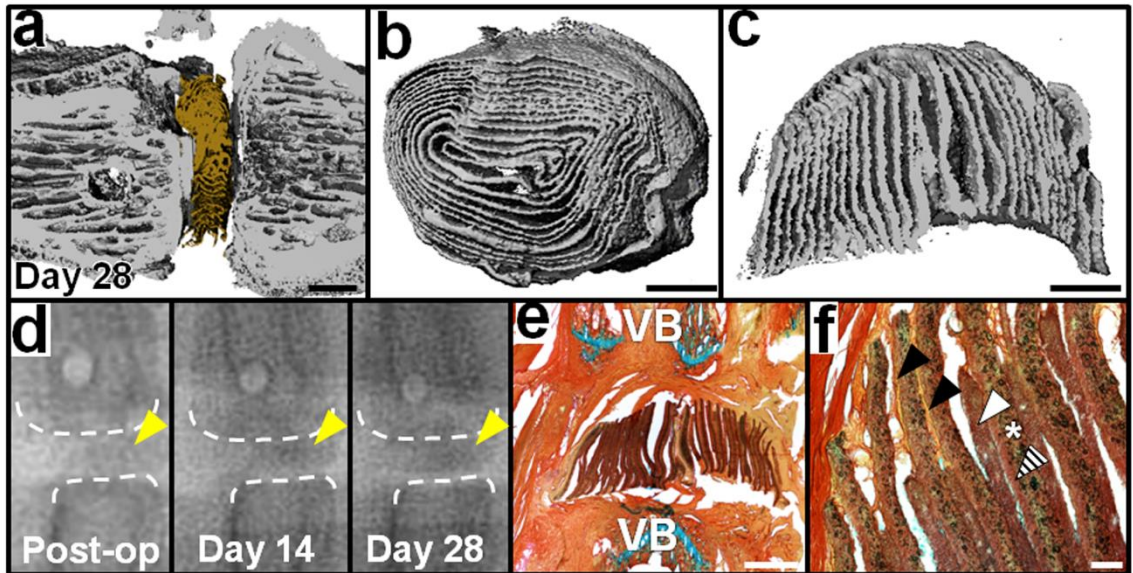


Figure 5-7 Multilayer rDAPS in vivo rDAPS were fabricated to include a radiopaque PCL/zirconia layer, a non-radiopaque semi-permanent PCL layer, and a non-radiopaque degradable PLGA layer. (a) rDAPS (gold) were located directly between vertebrae (gray) with a distinct layered structure as visualized by \square CT. Scale, 1mm. Individual layers were apparent in (b) transverse (scale, 1mm) and (a) axial (scale, 1mm) cross-sections. (d) Fluoroscopy demonstrated that low radiopacity rDAPS (arrows) were not distinct from adjacent vertebrae and that there was no change in position over time. (e) Histologically, rDAPS structure appeared intact and new tissue was deposited between layers. Scale, 1 mm. (f) Zirconia was sequestered within PCL/zirconia layers (star), while PCL-only layers (white arrow) and PLGA layers (striped white arrow) remained intact. New collagen deposits (black arrows) appeared on PCL/zirconia layers suggesting the radiopaque scaffold provides a template for fibrous tissue formation in vivo.

5.4 Discussion

In this study, I developed and characterized a radiopaque electrospun scaffolding system to enable visualization of engineered implants using clinically relevant and readily accessible imaging modalities (i.e., x-ray attenuation). Nanofibrous scaffolds were produced from PCL, a standard biodegradable polymer widely used in tissue engineering applications, coupled with nanoparticles composed of zirconia, a ceramic nanopowder. While many scaffolds for bone tissue engineering are intrinsically radiopaque, this is the first scaffold of its kind for fibrous tissue engineering applications. In developing this system, I demonstrated that scaffold radiopacity and mechanical properties could be tuned by altering the concentration of zirconia included in each fiber, that the scaffolds were visible radiographically when implanted into large joints of human dimensions, that inclusion of the radiopacifier did not influence cell viability or proliferation, and that it did not instigate osteogenic differentiation by MSCs seeded onto these scaffolds or when placed into the disc space. Radiopaque implants designed for total disc replacement were visible over 4 weeks using both fluoroscopy and μ CT. In addition, these scaffolds were compatible with the formation of collagenous tissue in vivo, establishing their utility for both animal model development and fibrous tissue engineering applications.

The linear attenuation coefficient of scaffolds was assessed in vitro and the total radiation attenuation was assessed in vivo. The linear attenuation coefficient of electrospun scaffolds changed as a result of inclusion of the zirconia nanoparticles. Specifically, the linear attenuation coefficient increased with zirconia content, reaching a

plateau at 25% zirconia. This may suggest that the maximum packing density of zirconia in the nanofibers is in the range of 25%. Thus, while scaffolds were nominally 50%, 25%, 10% or 0% zirconia, at the highest concentration phase separation may have occurred during the electrospinning procedure as evidenced by the extrafibrillar accumulation of zirconia in SEM images. The linear attenuation coefficient reported here is a property intrinsic to the scaffold material. It represents the volumetric average of radiation attenuation and consequently is not a function of scaffold geometry. As it is a material property it allows for direct comparisons between samples independent of scaffold geometry. Fluoroscopic images however are a visualization of total radiation attenuation, which *is* a function of scaffold geometry. For our in vivo studies, the 50/50 rDAPS were composed of 100% radiopaque layers, while the multilayer (75/25) rDAPS consisted of only 33% radiopaque layers. This resulted in a difference in the total radiation attenuation of the two implant types, despite 75/25 and 50/50 layers have a similar linear attenuation coefficient. For future studies, by controlling the zirconia content, scaffold radiopacity could be tuned for a specific application. For example, if an electrospun scaffold is used to repair a deeper tissue, such as a tissue inside a synovial joint [41], the abdomen [87], or within the lumbar spine [149], a high radiodensity scaffold may be required for adequate visualization. However, in a subcutaneous model, a less radiodense scaffold may be useful, since the superficial nature of a subcutaneous model lends itself to less obstructed visualization.

Scaffold mechanical properties were also affected by increasing the concentration of zirconia nanoparticles. Tensile modulus initially increased with increasing zirconia

content but declined at the highest concentration. This phenomenon has also been observed in electrospun scaffolds containing hydroxyapatite inclusions that have been investigated for bone tissue engineering [236], and may be related to a loss of fiber continuity at high filler concentrations. The aggregation of zirconia on the surface of the 50% zirconia scaffolds may also have an effect on the mechanical response (by altering fiber-to-fiber interactions), and further suggests that zirconia concentration within PCL had reached a saturation point at this high percent weight.

To assess *in vivo* potential, radiopaque implants formed with high and low concentrations of zirconia were visualized in the rat coccygeal spine. Previous work with this model demonstrated that the retention of engineered discs can be improved by stabilizing the implant site with an external fixation device [149]. Visualization by fluoroscopy in this context was useful for intraoperative positioning of the implant and to confirm that there was no migration of scaffolds over time. Likewise, imaging of the scaffold *in situ* in the bovine knee demonstrated the potential utility of these radiopaque scaffolds in large animal and human applications. Subsequent μ CT analyses on explanted tissues offered high resolution scaffold imaging and dimensioning that could be coupled with other outcome measures (such as histology) to better monitor scaffold localization, integration, and degradation with time after implantation. These features may enable the conservation of animals in future studies by eliminating the number of iterations required for improving surgical techniques during model development.

The inclusion of zirconia into the PCL fibers did not alter cell viability and appeared to not be a factor in promoting osteogenesis. While other polymer/ceramic

composite scaffolds have been used to promote an osteogenic phenotype, I did not observe additional alkaline phosphatase activity or calcium deposition on scaffolds containing zirconia cultured in vitro. Furthermore, when these scaffolds were implanted into the rat coccygeal spine after discectomy (a location that is prone to fusion), I did not find any evidence of increased mineral density in adjacent to the intervertebral space (by μ CT) after 4 weeks. Other osteogenic scaffolds are composed of minerals like hydroxyapatite or calcium phosphate [72, 84] which are naturally present in bone and provide raw materials that cells can utilize to form mineral deposits; in contrast, zirconia is foreign to the body and should not play a role in this process. Future work is required to fully characterize MSCs and other cell types after seeding onto these scaffolds, including measurements of extracellular matrix production and the expression of genes relevant to the osteogenic and fibrochondrogenic phenotype. Over a one month implantation time, multilayer rDAPS were compatible with the formation of new collagenous tissue by endogenous rat cells in the coccygeal spine. Taken together these data suggest that PCL/zirconia scaffolds may be useful for both developing engineered fibrous tissues and evaluating these tissues in in vivo models.

As PCL will degrade in vivo, implanted scaffolds fabricated from PCL and zirconia will release zirconia once the slowly degrading PCL begins to break down, thus introducing a potential contaminant into the local microenvironment. A previous report demonstrated that the zirconia nanoparticles have the physical properties of a biologically inert material, and when zirconia nanoparticles were directly included in the culture media of 3T3 fibroblasts in monolayer, there was no effect on cell morphology or

viability [111]. Our study confirmed there was no effect of zirconia at any concentration on cell viability in vitro. In addition, H&E stained sections from rDAPS implanted in vivo showed no aberrant cellular response to two implant types with high or low concentrations of zirconia. This provides strong evidence that zirconia within the PCL fibers are not cytotoxic at the implant site. However, these studies are limited in that the timepoints evaluated are too early for the PCL degradation process to have occurred, thus little release of zirconia into the media or into the disc space would be expected. An additional limitation of this scaffold system may be that the radiopacity could change after the release of zirconia through the normal degradation of PCL, which could limit ability to radiographically visualize and track scaffolds after long-term implantation. Scaffold displacement usually occurs relatively soon after implantation, and at these longer time points, one would expect that the scaffold would be fully integrated in the surrounding native tissue. Future studies will focus on these potential changes in scaffold radiopacity, as well as the potential for systemic and local inflammatory responses to zirconia, after long-term degradation of the PCL fibers (on the order of months to years). These studies will identify whether the scaffold is best used for shorter term optimization of scaffold placement and surgical methods, or whether it may be considered for long term applications as well.

5.5 Conclusions

Taken together, these data show that zirconia-embedded polymer scaffolds can be visualized radiographically in both small and large animal models and can serve as a framework for the development of an engineered fibrous tissue. The material was

cytocompatible and did not promote osteogenesis as demonstrated both in vitro, using a cell source with a pliable phenotype, and in vivo, where collagenous tissue was deposited into the scaffold. A scaffold with these characteristics will allow for the image-guided implantation and non-invasive assessment of engineered fibrous tissues.

CHAPTER 6 - Intermediate and long-term outcomes of an acellular disc-like angle ply structure (DAPS) for intervertebral disc replacement in a small animal model

6.i. Preface

In chapters 4 and 5, I described the development and analysis of a rat model of total disc replacement. Building off this work, here, I describe the development of an **acellular** engineered total disc replacement, evaluating acellular DAPS with sacrificial layer (sDAPS) in the rat tail (1) to evaluate their ability to functionally replace discs and (2) to improve our understanding of the biomaterials (PCL and HA) response in the in vivo space.

6.1. Introduction

The current paradigm for regeneration of the musculoskeletal system through tissue engineering involves a two-step procedure. First, the cell source of interest is harvested from the patient in a pre-operative outpatient procedure; these cells are expanded, seeded onto an engineered scaffold, and matured for re-introduction into the body. There are a number of drawbacks to this method. First, there is potential for morbidity at the donor site. For example, harvesting bone marrow from the iliac crest results in post-operative pain and introduces the risk of infection. Second, the cells isolated from bone marrow require closely regulated culture conditions to induce and

maintain a desired phenotype. AF cells, NP cells and MSCs are phenotypically unstable after a number of passages in monolayer [22, 118, 157, 240]. Finally, clinical implementation of cell-based therapy necessitates overcoming significant regulatory hurdles, along with expensive clinical trials and the requisite academic-industrial partnership for financial contributions from industry.

Thus, acellular biomaterials that attract and direct endogenous cells have come to the fore in the context of tissue engineering as an alternative to cell-based methods [36]. For example, acellular hydrogels injected into the left ventricle have improved cardiovascular function in an ovine model of myocardial infarction [101]. Also, for the treatment of articular cartilage defects, autologous matrix induced chondrogenesis is a developing strategy that combines recruiting cells from the subchondral bone marrow through microfracture and directing the behavior of those cells once they have engrafted into a synthetic matrix implanted into the defect [21, 57]. An acellular engineered total disc replacement may establish healthy spine function while also eliminating the need for evaluating complicated cell-based tissue replacement strategies.

For the treatment of end-stage disc pathology, our lab developed disc-like angle ply structures (DAPS) for total disc arthroplasty that include an electrospun nanofibrous annulus fibrosus (AF) that matches the structural hierarchy of the native AF and a hydrogel core nucleus pulposus (NP). When seeded with disc cells or stem cells, DAPS mature in vitro, recapitulating native compositional and mechanical properties [175, 179]. In previous work, I implanted *acellular* DAPS into the rat tail for short durations and established that endogenous cell infiltration and tissue deposition was possible (Ch. 4), indicating that the topographical template provided by the nanofibrous structure of the

electrospun AF region guides the natural remodeling response to establish an “organized scar” and ultimately a functional tissue. This strategy is likely translatable, as fibrous tissue deposited around total disc arthroplasty devices in human surgeries has substantial mechanical properties, nearing those of the native AF and NP [70]. While significant tissue deposition between AF layers was evident in this model histologically, mechanical competence of the resultant DAPS/repair-tissue hybrid was not measured. In addition, long-term timepoints, where the risk for intervertebral fusion is high, were not evaluated, and the role of an acellular NP replacement was not investigated.

To expand on this previous study (Ch. 4), here I generated acellular DAPS composed an eletrospun AF region and a hydrogel NP region and evaluated their intermediate and long-term function after implantation in the rat tail model. A number of control groups were also evaluated so as to assess the local wound remodeling process in the intervertebral space and its potential for populating an acellular DAPS with functional tissue. In addition, the role of fixation in this model was more closely examined to determine its effect on tissue health.

6.2. Methods

6.2-1 Formation of acellular sacrificial layer DAPS (sDAPS) for total disc replacement

DAPS with sacrificial layers (sDAPS) [Fig. 6-1a] were fabricated with geometry compatible with the rat tail: outer diameter of 5 mm, NP diameter of 1.5 mm, and height of 2 mm. The AF regions of these constructs had 3 repeating concentric layers: a 125 um layer of a cytocompatible polymer with longterm stability, a 125 um layer of the same

polymer with opposing fiber orientation, and a 250 um layer of a polymer designed to degrade after implantation to provide channels for cell infiltration [149]. The center of the construct was filled with a bioactive hydrogel core.

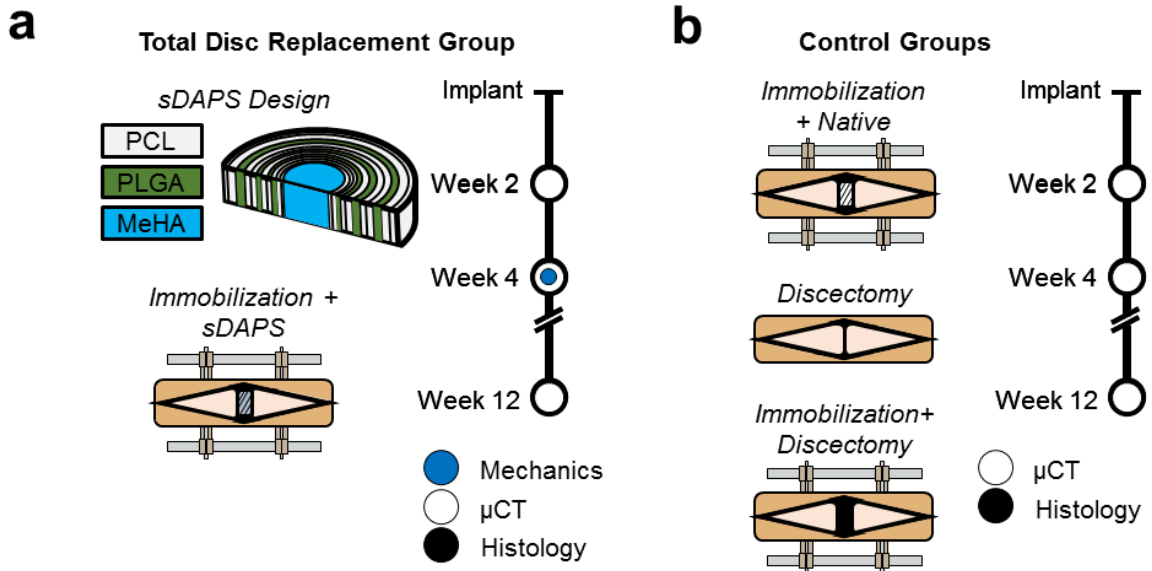


Figure 6-1 Study design: evaluation of acellular engineered discs (a) Engineered disc-like angle ply structures with sacrificial layers for cell infiltration (sDAPS) were fabricated with an AF region consisting of PCL, a cytocompatible polymer with long term stability, and PLGA, a degradable polymer designed to allow cell infiltration, and an NP region consisting of photopolymerizable HA, an essential component of the NP extracellular matrix. These constructs were implanted into the rat caudal spine and the implantation site was immobilized with an external fixation device. Spinal segments were assayed by μ CT, histology and mechanical testing over the course of 12 weeks. (b) Additional control groups were evaluated over the same time period to explore the role of immobilization on functional outcomes.

Specifically, AF regions were fabricated from oriented electrospun nanofibrous sheets that included layers of poly(ϵ -caprolactone) (PCL; Shenzhen Bright China Industrial Co., Hong Kong, China), and resorbable layers of poly(lactic-co-glycolic acid) (PLGA; 50:50 DL-PLG, LACTEL, Birmingham, AL)]. To enable electrospinning, PCL was dissolved in a 1:1 mixture of tetrahydrofuran (Fisher Chemical, Fairlawn, NJ) and N,N-dimethylformamide (Fisher Chemical), generating a 14.3% w/v solution, and PLGA was dissolved in 1:1 THF/DMF at 35.1% w/v. PCL solution was loaded into a syringe, extruded through an 18G needle at 2.5 mL/hr across a 12-15 kV voltage gradient, and collected on a mandrel positioned 15 cm from the needle tip, which was rotating at a surface velocity of 10 m/s. A layer of PLGA was electrospun atop the accumulated PCL at 2.5 mL/hr and 13 kV. These PCL/PLGA sheets were cut with a scalpel at 30°, replicating the angled fiber alignment of an individual lamella, and strips with alternating fiber alignment were wrapped concentrically about a post, generating an artificial AF region with hierarchical fiber structure similar to the native AF.

NP regions consisted of hyaluronic acid, an essential component of the disc extracellular matrix, which was processed as a photopolymerizable hydrogel. Methacrylated hyaluronic acid (MeHA) was generated by reacting sodium hyaluronate (65 kDA, Lifecore, Chaska, MN) with methacrylic anhydride (Sigma Aldrich, St. Louis, MO). A 5% w/v solution of MeHA in PBS was modified with 0.05% photoinitiator (Irgacure 2959, (2-methyl-1-[4-(hydroxyethoxy)phenyl]-2-methyl-1-propanone, Ciba-Geigy, Tarrytown, NY) to allow for photocrosslinking of the polymer network. The centers of the PCL/PLGA AF regions were removed with a 1.5 mm biopsy punch and 10 μ L of MeHA solution was pipetted into the core. An airtight container was filled with

nitrogen gas at 2 psi, the composite PCL/PLGA AF regions with MeHA NP regions were inserted into the container, and the MeHA NP regions were photopolymerized through a window by exposure to ultraviolet light at 5 mW/cm² for 20 minutes.

6.2-2 Implantation of sDAPS into the rat caudal spine

sDAPS were implanted into the tails of retired breeder Sprague Dawley rats (male, 7-9 months, 507 +/- 32g) with local institutional approval [Fig. 6-1a]. Rats were anesthetized with isoflurane, two surgical wires were passed through both the C8 and C9 (caudal) vertebrae, and a PEEK/stainless steel ring-type external fixator was secured to the embedded wires to immobilize the implantation site [149, 150]. The fixator was distracted slightly to expand the disc space and provide room for the implant. A dorsal skin incision was made, a scalpel and micro-curette were used to remove the native C8-C9 disc and sDAPS were implanted into the open intervertebral space. The skin was closed with suture and rats were returned to normal cage activity. Several additional control groups were included: an immobilized intact disc, a group with immobilization and discectomy, and a non-immobilized discectomy only control [Fig. 6-1b]. Rats from each group were euthanized at 2, 4 or 12 weeks after surgery; sample sizes for each group are listed in Table 6-1.

Table 6-1 – sDAPS and Control Group Sample Sizes

	Week 2	Week 4	Week 12
Immobilization		3 (μ), 3 (H)	3 (μ), 3 (H)
Discectomy	2 (μ), 2 (H)	2 (μ), 2 (H)	4 (μ), 4 (H)
Immobilization + Discectomy	2 (μ), 2 (H)	3 (μ), 3 (H)	5 (μ), 5 (H)
Immobilization + sDAPS	2 (μ), 2 (H)	8 (μ), 4 (H), 4 (M)	4 (μ), 4 (H)

μ : micro-computed tomography, H: histology; M: mechanical testing

6.2-3 Microcomputed tomography (μ CT), histology, and mechanical function

After euthanasia, external fixation devices were removed, and the C8 through C9 spinal section was dissected en bloc and assayed by μ CT and histology. Segments were scanned by μ CT (vivaCT 75, SCANCO Medical AG, Bruttisellen, Switzerland) at an isotropic resolution of 20.5 μ m and three-dimensional reconstructions were performed. The segments were then fixed in formalin, decalcified in formic acid, and either embedded in optimum cutting temperature gel for sectioning on a cryostat microtome (2 week and 4 week groups, 30 μ m sections) or processed for paraffin infiltration for sectioning on a paraffin microtome (12 week groups, 10 μ m sections). Sections were stained with a combination of Alcian blue and picosirius red to evaluate proteoglycan (PG) and collagen content. Immunohistochemical staining for types I and II collagen was performed by first incubating sections in proteinase K and the blocking with 10% NGS. Primary antibodies were applied overnight followed by a 1 h incubation with secondary antibodies at room temperature. Staining was visualized using the DAB chromogen reagent. In each case, images were acquired in brightfield (Eclipse 90i, Nikon, Tokyo, Japan).

Additional segments from the sDAPS group were tested in compression to evaluate their ability to function at physiologically relevant loads. Vertebra-sDAPS-vertebra motion segments were isolated from the tail, the skin was removed, and the dorsal soft tissue was cleared away with a micro-curette to expose the vertebrae. The proximal and distal vertebrae were marked with ink directly adjacent to the vertebral endplates and the motion segment was inserted into custom fixtures installed on an electromechanical testing system (5948; Instron, Norwood, MA). The testing protocol consisted of 20 cycles of compression from 0 to -3N (~0.3 MPa, 60% body weight). During testing, a digital camera (acA3800-14um; Basler AG, Ahrensburg, Germany) fit with a close-focusing macro video lens (Zoom 7000; Navitar Inc., Rochester, NY) was used to record the motion of the segment, and a custom texture tracking program was used to optically track displacement [146]. The linear region compressive modulus and maximum strain were extracted from the 20th compressive loading cycle using a bilinear fit routine. Mechanical properties were normalized to sDAPS geometry,[20] which was measured after the mechanical test. Cross-sectional area was measured from a digital image and height was measured using a non-contact laser-based device [13, 149]. Intact native discs proximal to the external fixator served as controls.

6.3 Results

The mechanical properties of sDAPS very closely matched that of the native disc after 4 weeks of implantation, while at 12 weeks, intervertebral fusion precluded mechanical analysis. [Fig. 6-2].

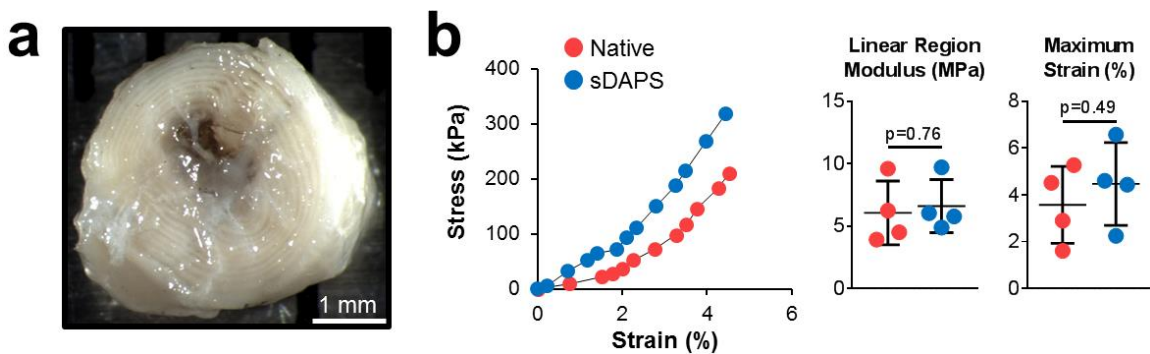


Figure 6-2 Mechanical properties and gross appearance at 4 weeks (a) sDAPS appearance after 4 weeks *in vivo*. Layers of the AF region are intact and invested with tissue, while the NP region appears to have degraded or contracted. (b) Representative stress-strain curves and mechanical properties for vertebra-sDAPS-vertebra and native motion segments. sDAPS nearly matched native mechanics, with the exception of a stiffer response at strains < 2%. sDAPS properties were not significantly different than that of the native motion segments. Data are displayed as mean +/- standard deviation.

The stress-strain curves of native discs and sDAPS nearly overlapped, as the calculated compressive moduli and maximum strains were not significantly different (compressive modulus, $\beta = 0.94$; maximum strain, $\beta = 0.90$). The key mechanical difference was that the sDAPS response to strain was very nearly linear (2 of 4 samples tested were completely linear, the other 2 of 4 were slightly nonlinear), whereas that of the native disc was nonlinear with a distinct low stiffness “toe” region and a high stiffness “linear” region. Upon gross inspection of sDAPS explanted after 4 weeks, layers in the AF region appeared to be intact and invested with tissue, though there was evidence that the NP region had degraded or contracted.

Reconstructions from μ CT scans revealed no evidence of intervertebral fusion at 2 or 4 weeks for the sDAPS and control groups [Fig. 6-3]. However, by 12 weeks, there was evidence of intervertebral bone deposits after either immobilizing and performing a discectomy or immobilizing and inserting an sDAPS. The sDAPS group had more aberrant intervertebral bone formation in comparison to the immobilization with discectomy group, suggesting that the implant accelerated the fusion process. Complete intervertebral bridging did not occur in all motion segments with implanted sDAPS, though intervertebral bone deposition was present in all. There was no evidence of fusion after immobilizing an intact disc or after discectomy alone (i.e., without immobilization).

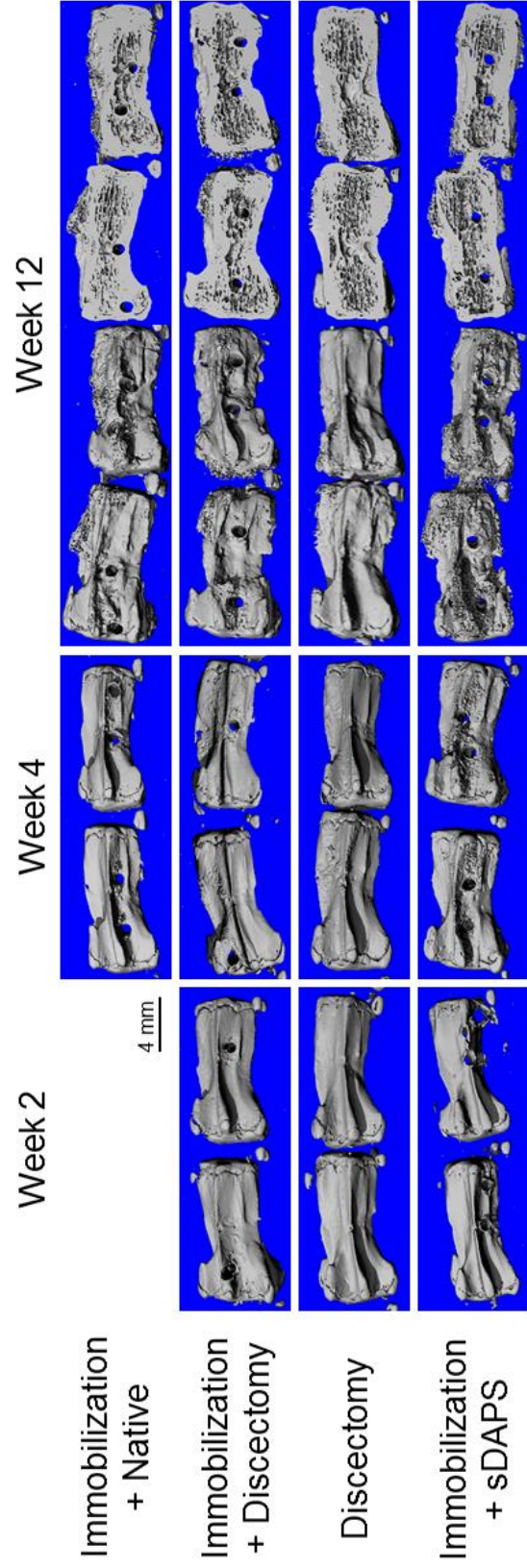
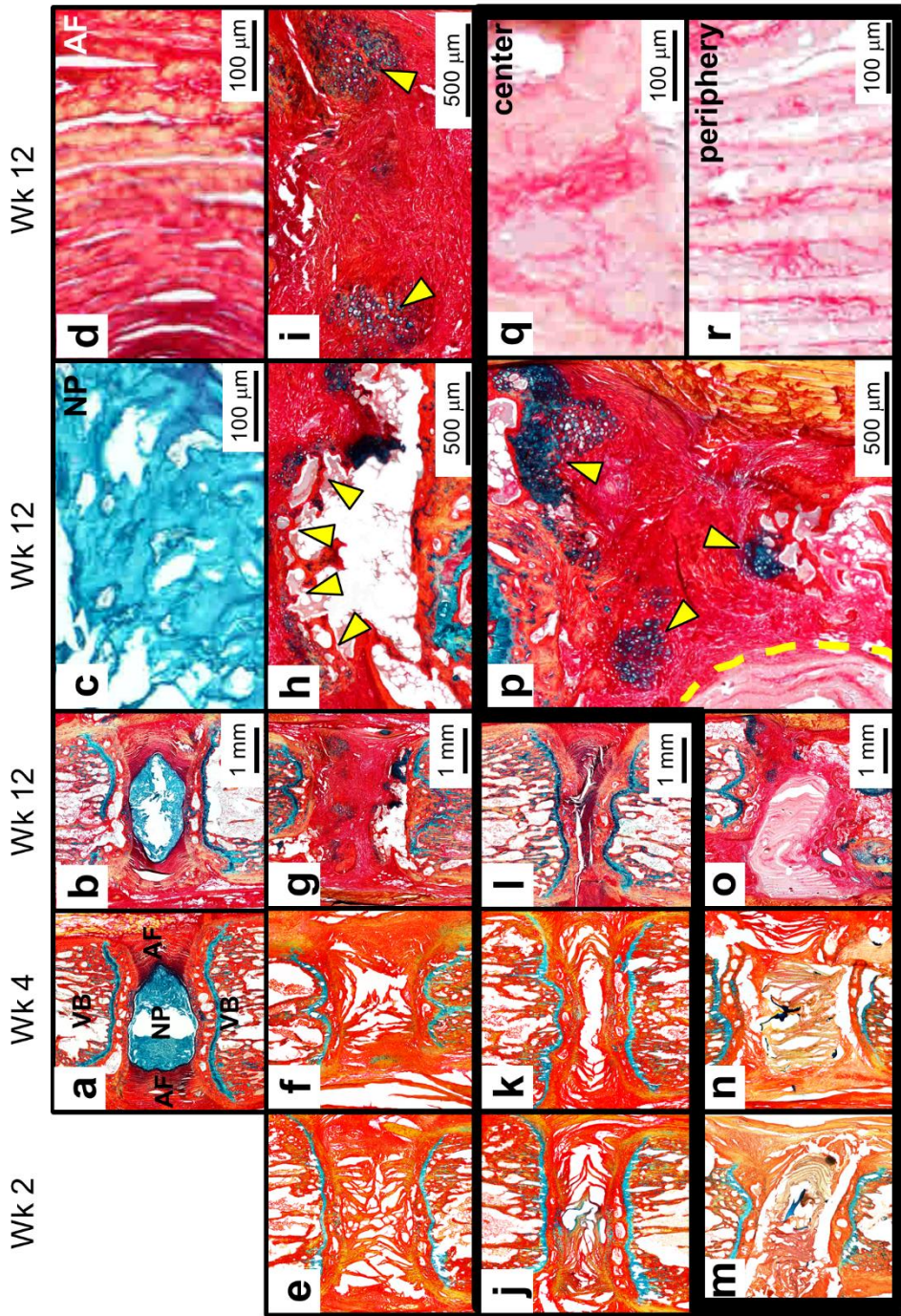


Figure 6-3 Three-dimensional μ CT reconstructions at 2, 4 and 12 weeks. At 2 and 4 weeks, immobilization groups appear normal with some small bone deposits adjacent to the surgical wire holes, while the discectomy-only group has already lost disc height. By week 12, in all immobilization groups, there was significant bone deposition on the periosteal surfaces, and, in the immobilization and discectomy and immobilization and sDAPS groups, intervertebral bone deposition had occurred, with complete bridging in the sDAPS group. The features of vertebrae from the discectomy-alone group appeared normal, despite the collapsed disc space and possibly some mechanical wear at the vertebral endplate.

Histologically, it was apparent that immobilization had little effect on the native tissue, but did seem to promote fibrous tissue deposition in the intervertebral space after discectomy [Fig. 6-4]. After externally fixing a healthy disc, there were no gross changes in disc appearance and the NP and AF regions appeared normal. After immobilizing the segment and then performing a discectomy, the empty intervertebral space accumulated picrosirius-red-positive tissue, starting from the periphery at 4 weeks and completely filling the space by 12 weeks. In this group there was also histological evidence of early fusion, as the boundaries of the vertebral endplates expanded into the intervertebral space and additional Alcian-blue positive staining was present in some intervertebral areas indicating a pre-osteogenic, hypertrophic phenotype. This did not occur after performing a discectomy without immobilizing the segment; this group lost disc height gradually over time, without an immediate collapse. By week 12, vertebral bodies in this discectomy group were in contact, but the disc space did not fill with new fibrous tissue.



Immobilization + Native

Immobilization + Discectomy

Discectomy

Immobilization + sDAPS

Figure 6-4 – Alcian blue and picrosirius red stained histological sections at 2, 4, and 12 weeks (a, b) Immobilizing the native disc had little effect on histological appearance, with normal appearance of both the (c) NP and (d) AF regions. (e-g) When the segment was immobilized and the disc was removed, remnant AF left after surgery occupied the intervertebral space, and the space was eventually filled with fibrous repair tissue. (h) The boundary of the vertebral endplates (yellow arrows) expanded into the intervertebral space in some cases (i) where local areas of chondrogenesis were apparent (yellow arrows), indicating that the process of fusion was occurring through an endochondral mechanism. (j-l) Removing the native disc without external fixation resulted in a gradual decrease in the intervertebral height, though no fusion was apparent at this time point. (m-o) Implanted sDAPS were situated between vertebrae, and fibrous tissue began filling the layers as early as week 2. There was little MeHA NP apparent histologically at 2 and 4 weeks, and none at 12 weeks, suggesting the material had degraded *in vivo*. (o-p) At 12 weeks, intervertebral bridging was apparent in the sDAPS group, (p) with ossification fronts (yellow arrows) observed at multiple intervertebral locations, especially along the implant (yellow dotted line). (q) The central portion of the sDAPS collapsed, (r) while the AF region remained intact with parallel layers. Both intra- and inter-lamellar picrosirius red staining was apparent, indicating collagenous tissue was deposited throughout the construct.

sDAPS successfully promoted cell infiltration and tissue deposition in vivo. However, at week 12 there was evidence of intervertebral bridging and degradation of the hydrogel core [Fig. 4]. At timepoints as early as 2 weeks, sDAPS began filling with collagenous tissue, and, by week 12, sDAPS appeared to have cohesive layers. There was evidence of the hydrogel core at 2 and 4 weeks, but by 12 weeks, there was no hydrogel apparent and the volume that the hydrogel NP had originally filled had collapsed. Also at 12 weeks, just adjacent to the sDAPS boundary, bridging of the vertebrae proximal and distal to the implant occurred, and while there was no evidence of direct integration of sDAPS into the vertebrae, there was significant integration into the adjacent soft tissue.

In terms of specific collagens, there was little evidence of type I collagen in native discs after long-term immobilization, while type II collagen was distributed as expected, concentrated centrally and dissipating radially outwards [Fig. 6-5]. After removal of the native disc and 12 weeks of immobilization, types I and II collagen were distributed throughout the intervertebral space, with type II collagen concentrated in areas that also stained for proteoglycan, further indicating a hypertrophic phenotype. Similar results were seen in sDAPS group, with types I and II collagen distributed throughout the disc space and throughout the implant.

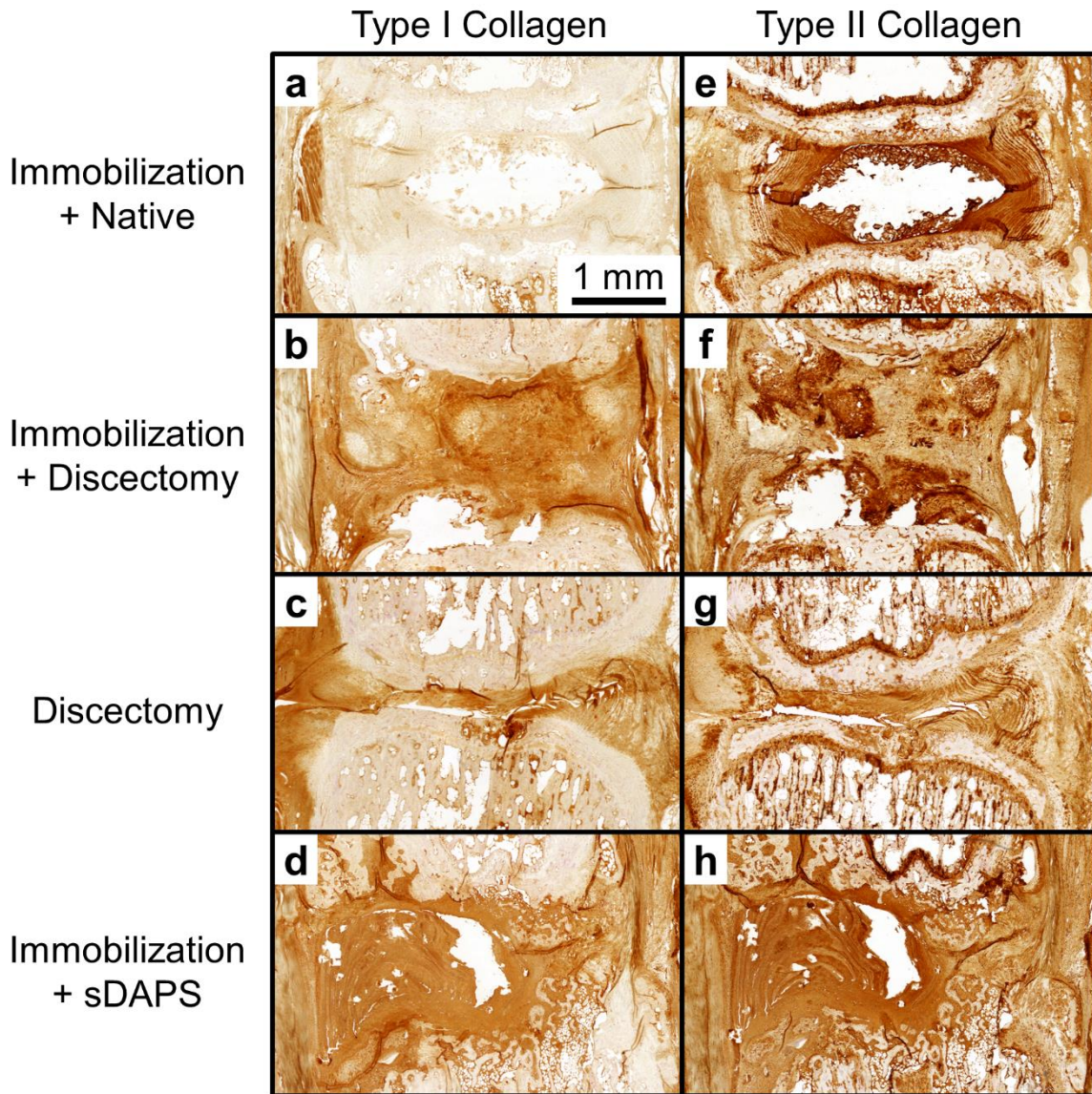


Figure 6-5 – Immunostaining of types I and II collagen at 12 weeks (a-d) Sections from each group stained for type I collagen. After 12 weeks of fixation only mild type I collagen staining was evident in native discs, while there was strong type I collagen staining throughout the intervertebral space in the immobilization with discectomy and the immobilization with sDAPS groups. (e-h) Sections from each group stained for type II collagen. Type II collagen staining started from the NP and dissipated radially in native discs after 12 weeks of immobilization, while in the immobilization with discectomy group, type II collagen filled the intervertebral space and concentrated in areas that matched concentrations of proteoglycan staining, indicating a pre-osteogenic, hypertrophic phenotype. sDAPS stained strongly for type II collagen as well, suggesting a fully infiltrated engineered tissue.

6.4 Discussion

Constructs that replicate the structure of the native disc were implanted into the rat caudal spine. These constructs, which are designed to organize the remodeling process by allowing cells to infiltrate between layers and engraft onto an aligned topographical framework, were effectively invested with tissue and reached mechanical properties equal to that of the native disc. In a series of control groups, I found that immobilization did not affect native disc health, and (following discectomy) was conducive to fibrous tissue deposition and lead to intervertebral fusion. Placement of the engineered construct seemed to expedite this process, suggesting that additional measures, including cell and/or growth factor delivery from the implant, may be required to harness the regenerative capacity of the disc space while preserving the fibrocartilaginous nature of the tissue that forms.

Endogenous cells colonized the implanted sDAPS and filled the construct with fibrous tissue; consequently sDAPS had compressive moduli equivalent to native intervertebral discs. The hydrogel NP region degraded or contracted after implantation, however, rendering the surrogate NP ineffective. In previous work with these constructs, cell-seeded DAPS showed robust growth in both the NP and AF regions, and had mechanical properties that were strongly nonlinear both in vitro and in vivo [147]. Testing sDAPS after implantation, when the hydrogel core was no longer intact or was too weak to provide the mechanical functions of the NP, revealed that the stress-strain response was linear. Previous studies have established that the NP dominates the neutral zone response, or the low-stiffness region of the stress-strain curve. Thus, when the NP is altered as a consequence of nucleotomy [214], chemonucleolysis [33], or by

degeneration [163] there is an increase in compliance at low strains. Previous work with in vivo implantation of acellular crosslinked HA hydrogels has demonstrated that this material can be degraded in the physiological environment. For instance, in a porcine model where HA gels were used to fill a full thickness cartilage defect, no sign of remaining HA implant was apparent at 6 weeks, suggesting the potential for rapid degradation in vivo [64]; endogenous hyaluronidase activity resulting from surgery-related inflammation may be responsible for disappearance of HA in these models. In the rat tail model, the NP disappeared along with the neutral zone response of sDAPS; this suggests that the design of the DAPS successfully reproduces the load-sharing interactions of the AF and NP, but that it may be necessary to modify the hydrogel to better meet physiological demands after implantation.

The requirement for external fixation is a limitation of this rat model, as implants are not challenged by the physiological mechanical environment. However, immobilization had a number of significant effects in this model that have broader implications. For example, immobilization was required for fibrous tissue deposition; even in this highly metabolically active rodent model. It appears that motion at the joint (the discectomy-only group) did not allow fibrous remodeling after removal of the disc. With implications for spinal fusion surgeries, these findings suggest that improper fixation at the intervertebral joint is a risk factor for non-union. The application of pedicle screws or locking plates to assist in interbody fusion is a technically complicated procedure, thus variability in fixation quality, segmental rigidity and consequently incomplete intervertebral fusion may be unavoidable. Another observation in this study was that the fusion process appeared to be accelerated with sDAPS implantation.

Interestingly, a similar finding was reported previously when a small intestinal submucosa patch was used for annular repair in a sheep model [124]. In that study, the patch was affixed to adjacent vertebrae with bone screws, thus interrupting the periosteum and initiating bleeding from the vertebra. Similarly, the rat caudal disc replacement model requires interrupting the periosteum with surgical wires for the external fixation device. Breaching the cortical shell and including a material that bridges the vertebrae are both factors that may accelerate fusion in these models.

Altered loading is also a risk factor for degenerative changes to the disc [131, 239, 249]; a previous report in the rat tail model compared immobilization to compressive loading and demonstrated that while static compression caused remodeling in the loaded discs, there were no changes to immobilized discs [98]. The histological results from the current study are consistent with those findings, as there was no gross change in appearance after long-term immobilization. Dynamic loading affects fluid transport into and out of the disc [81, 82] and the disc is predominantly avascular. Restriction of dynamic loading through immobilization would restrict fluid convection into and waste removal from the disc, and so the disc would be required to rely on diffusion for these processes. In larger discs, such as those of human dimensions where diffusion distances are long, immobilization would likely produce degenerative changes. However, in the rat tail model, where diffusion distances are relatively shorter, the effect appears to be minimal. This reinforces the role of diffusion for nutrient transport into the rat disc.

The effects of immobilization described herein also have implications for disc tissue engineering. Total disc replacement with an engineered tissue will likely require a period of integration into adjacent vertebrae just after implantation; this may be

facilitated by immobilization. That immobilization did not cause degenerative effects after 12 weeks suggests that an engineered tissue composed of disc cells or cells with a disc phenotype may have some tolerance to immobilization and suggests that diffusion alone may be sufficient for maintenance of the engineered disc through a period of fixation to enhance integration immediately post-operatively. The duration of this integration period must be closely controlled, however, so as to reduce the potential for spinal fusion, as was noted here with long-term immobilization. Remobilization after a period integration may prevent fusion from occurring. Likewise, local delivery of factors from the scaffold in a temporally or spatially controlled manner [103, 234], including pro-chondrogenic factors that resist progenitor cell hypertrophy, may help to limit fusion in this scenario.

6.5 Conclusion

In these experiments, the rat caudal disc was immobilized using an external fixation device and the potential for an acellular construct to functionally replace the native disc was investigated. This construct was designed to permit endogenous cell infiltration and tissue deposition. These constructs were successfully implanted and integrated into the intervertebral space, as evidenced by robust tissue formation within the construct and mechanical properties that matched that of the native disc. Immobilization, which is a requirement for successful implant retention in this model, had no discernible effect on the histological appearance of native discs and provided a stable site for the fibrous tissue formation necessary for the implants success. However,

in cases of discectomy, immobilization eventually lead to intervertebral fusion. Indeed, this fusion appeared to be promoted by the sDAPS under these immobilized conditions. Limitations of the current implant include the volatility of the hydrogel NP region and the inability to prevent intervertebral fusion. However, with modifications in material design and the adoption of an implantation, integration, and then remobilization strategy, these limitations can likely be overcome.

CHAPTER 7 - In Vitro Growth Trajectory and In Vivo Function of Cell-Based Disc-like Angle Ply Structures (DAPS) for Total Disc Arthroplasty

7.i Preface

This chapter describes the culmination of much work: the development and validation of the rat tail model of total disc replacement, the development of methods to fabricate cellular DAPS, and the development of assays to track and evaluate DAPS composition and function after in vivo implantation. Here, cellularized DAPS were cultured in vitro and a detailed analysis of their growth trajectory was performed. These were then implanted into the rat tail at either a mature or an immature state of growth and their performance was tracked by MRI, histological and mechanical analyses.

7.1 Introduction

To treat severely degenerated discs, our group has developed engineered implants that replicate the hierarchical structure of the native disc. These implants are comprised of an organized multi-lamellar nanofibrous scaffold that replicates the annulus fibrosus (AF) and a hydrogel that replicates the central nucleus pulposus (NP). In previous work, I showed that multilayer AF constructs support tissue development when seeded with mesenchymal stem cells (MSCs) and match the mechanical properties of native tissue [175]. I have also shown that various hydrogels that serve as the NP region can promote a chondrogenic phenotype in both MSCs [59] and NP cells [113] and drive NP cells to express genetic markers indicative of a healthy NP phenotype [113]. When combined

together, these subunits form a disc-like angle ply structure (DAPS) for total disc replacement and DAPS seeded with MSCs or disc cells mature with in vitro culture [179], emphasizing their potential for disc regeneration. In previous work (Ch. 4), I also developed an in vivo model to evaluate DAPS biocompatibility and integration, using the rat caudal spine (or tail) along with an external fixation system to stabilize vertebrae adjacent to the implantation site [149]. Implantation of the acellular AF region of the DAPS showed them to be biocompatible, with constructs maintaining their lamellar and fiber structure over time, further illustrating the potential of these constructs for disc regeneration. To further this line of inquiry, the primary objective of this study was to take the next step in this regenerative process by evaluating cell-seed DAPS in this in vivo environment.

One strategy for implanting engineered cell-seeded materials is to culture constructs for an extended period of time and then implant these constructs in vivo at their peak maturation *state*. These mature constructs are fully invested with tissue and contain cells with a stable phenotype that are likely to survive the difficult transition to the in vivo space. Recent studies, however, have demonstrated that integration potential does not correlate with the maturation state of engineered cartilage, but rather that integration with native tissue occurs to the greatest extent when constructs are implanted at their peak maturation *rate* [67]. Thus, an emerging strategy to improve the integration of engineered tissues is to implant constructs at a pre-culture timepoint corresponding to the peak maturation *rate*. This strategy may likewise be useful for disc tissue engineering, as integration into the adjacent vertebrae is paramount to the success of the procedure.

In this study, I hypothesized that in vivo integration potential is related to the in vitro growth trajectory (i.e., the maturation rate) of the engineered tissue. To test this hypothesis, I established the in vitro growth trajectory of DAPS seeded with either AF and NP cells or MSCs over a 15 week period. After establishing this profile, I next tested, after short- or long-term pre-culture durations, the ability of DAPS to integrate and function in the rat tail in vivo. Results from this study showed that when transitioning from the in vitro culture environment to the in vivo space, there was marked shift in cell phenotype and function, with loss of disc constituents as evidenced by histological, MRI, and mechanical analyses. These data highlight the difficult transition from in vitro studies to in vivo application, and identify new challenges that must be overcome to improve the stability in composition and function of engineered tissues after implantation into a challenging microenvironment.

7.2 Materials and Methods

7.2-1 Study Design

These experiments were broken into 3 distinct studies. In Study 1, DAPS were seeded with either MSCs or AF and NP cells, cultured for up to 15 weeks in vitro, and assayed for mechanical, compositional, and histological characteristics [Fig. 7-1a,b; pg. 150]. Doing so, I developed the in vitro growth trajectory of cellular DAPS, defining in immature and mature states of growth. In Study 2, using this established growth trajectory, AF/NP DAPS were implanted in to the caudal spines of athymic rats after 5 weeks of in vitro pre-culture, representing an immature/rapidly-growing state of maturation. Over the course of 5 weeks, vertebra-DAPS-vertebra motion segments were evaluated mechanically, imaged by MRI, and examined histologically to determine the functional and compositional maturation of DAPS after implantation [Fig. 7-3a; pg. 155]. Finally, in Study 3, AF/NP DAPS were implanted the caudal spines of athymic rats after pre-culture for either 5 or 10 weeks, comparing the effects of pre-maturation duration on the implant phenotype. These were assayed by μ CT and histology after 5 weeks in vivo [Fig. 7-5s; pg. 160]. To evaluate the effects of the implantation site, DAPS were also implanted in dorsal subcutaneous pockets in athymic rats an analyzed histologically. The following sections (7.2-2 to 7.2-10) provide a technical description of the assays performed.

7.2-2 Cell Isolation and Expansion

Bovine MSCs were isolated from femoral and tibial bone marrow, while bovine AF and NP cells were isolated from caudal discs as described previously [113, 155]. In preparation for seeding, all cell types were expanded to passage 2 or 3 in a basal medium

(BM) that included Dulbecco's Modified Eagle Medium (DMEM; Gibco, Invitrogen Life Sciences, Carlsbad, CA), 10% fetal bovine serum (Gibco) and 1% Antibiotic-Antimycotic (Gibco).

7.2-3 DAPS Fabrication, Cell Seeding, and In Vitro Culture

The AF portions of DAPS were fabricated from an electrospun nanofibrous scaffold to match the rat caudal disc geometry [149, 179]. Layers of poly(ϵ -caprolactone) (PCL) nanofibers and poly(ethylene oxide) (PEO) were sequentially electrospun onto a rotating mandrel as aligned multilayer sheets. This scaffold was cut at an angle into strips in which fibers ran 30° to the strip length, replicating the structure of an individual lamella. Strips with alternating alignment were wrapped around a post into concentric discs with final dimensions 5 mm diameter by 2 mm height. Scaffolds were rehydrated and sterilized through a gradient of ethanol washes, which removed water-soluble PEO layers to provide routes for infiltrating cells, and then coated with a 20 $\mu\text{g}/\text{mL}$ fibronectin solution (Sigma-Aldrich). Bovine MSCs or AF cells from primary isolation were seeded on the top and bottom side of the constructs (2×10^6 cells per construct), allowing for 1 hour of cell attachment per side.

The NP portions of DAPS were generated using a photocrosslinkable bioactive hydrogel [35, 58]. Methacrylated hyaluronic acid (MeHA) was produced by reacting 65 kDA sodium hyaluronate (Lifecore, Chaska, MN) with methacrylic anhydride (Sigma Aldrich, St. Louis, MO). A 1% w/v solution of MeHA in PBS was sterilized by 30 minutes of UV light exposure, after which 0.05% photoinitiator (Irgacure 2959, (2-methyl-1-[4-(hydroxyethoxy)phenyl]-2-methyl-1-propanone, Ciba-Geigy, Tarrytown,

NY) was added. Bovine MSCS or NP cells were suspended in the MeHA solution (20M cells/mL, 6×10^5 cells per construct), which was poured into a mold and photopolymerized with UV light exposure for 10 minutes. The mold was punched to create cell-laden cylindrical gels of final dimensions 2 mm diameter by 1.5 mm height.

Following fabrication and seeding, AF and NP regions were cultured separately for 2 weeks, at which point a 2 mm core was punched from the center of the AF and the NP was inserted to form DAPS [Fig. 7-1a]. Throughout this study, DAPS were cultured in a chemically defined medium [108] consisting of DMEM supplemented with 1% penicillin, streptomycin, and amphotericin B (Antibiotic-Antimycotic; Gibco), 40 ng/mL dexamethasone (Sigma-Aldrich), 50 $\mu\text{g/mL}$ ascorbate 2-phosphate (Sigma-Aldrich), 40 $\mu\text{g/mL}$ L-proline (Sigma-Aldrich), 100 $\mu\text{g/mL}$ sodium pyruvate (Corning Life Sciences, Corning, NY), 0.1% insulin, transferrin, and selenious acid (ITS Premix Universal Culture Supplement; Corning), 1.25 mg/mL bovine serum albumin (Sigma-Aldrich), 5.35 $\mu\text{g/mL}$ linoleic acid (Sigma-Aldrich), and 10 ng/mL TGF- β 3 (R&D Systems, Minneapolis, MN). This media was replenished every 3 days.

7.2-4 Geometric and Mechanical Characterization of DAPS

DAPS geometry and compressive mechanical properties were measured at each timepoint (n=4). DAPS were geometrically characterized for total cross-sectional area by evaluating digital images with a custom MATLAB program [149, 188]. Mechanical properties were evaluated in unconfined compression on an electromechanical testing system (5542; Instron, Norwood, MA) with a protocol used to assay native tissue [20, 146]. First a 0.05 N preload was applied, and the platen-to-platen distance was used to

define the DAPS height. Next, 20 cycles of compressive loading from 0.05 N to 3.0 N were applied at a rate of 0.5 Hz. This was followed by a return to 0.05 N, and then, to characterize creep behavior, a 1.5 second step load to 3.0 N was applied, with this load held for 10 minutes.

7.2-5 Compositional and Histological Characterization of DAPS

Following mechanical testing, AF and NP regions were separated and total glycosaminoglycan (GAG) and collagen contents were measured for each region (n=4). GAG content was evaluated using the dimethylmethylene blue (DMMB) technique [61], and collagen content (following acid hydrolysis) using the p-diaminobenzaldehyde/chloramine-T technique for hydroxyproline [226]. Results are reported as normalized to AF or NP region wet weight.

An additional group of DAPS without prior mechanical testing was used for histological analysis (n=2). These were prepared by fixation in formalin at room temperature and embedding in paraffin at 55°C (below the melting temperature of PCL). Sections were cut at 10µm, stained with alcian blue (GAG) or picrosirius red (collagen) and imaged in bright-field. Immunohistochemical staining for types I and II collagen was performed by first incubating sections in proteinase K and the blocking with 10% NGS. Primary antibodies were applied overnight followed by a 1 h incubation with secondary antibodies at room temperature. Staining was visualized using the DAB chromogen reagent and imaged in brightfield.

7.2-6 DAPS Implantation Procedure

DAPS were implanted into the caudal spines of athymic rats (Foxn1^{mu} retired breeders, 465±41g; Harlan Laboratories, Inc., Indianapolis, IN) using an external fixator designed to unload and stabilize the rat caudal disc space [149]. To do so, two surgical wires were passed laterally through both the C8 and C9 vertebrae and the external fixator was secured to the wires. A dorsal skin incision was made, the native C8/C9 disc was removed, and DAPS were implanted into the disc space. Rats were returned to normal cage activity, pair-housed after a 2 week recovery period, and euthanized after 5 weeks.

7.2-7 Mechanical Testing of Implanted DAPS

Vertebra-DAPS-vertebra and native motion segments were tested in compression using an electromechanical testing system (5948; Instron, Norwood, MA) and an optical displacement tracking technique (n=4). In preparation for testing, the skin around the motion segment was carefully removed, while adjacent muscle and tendons were left intact. The ventral bony surface adjacent to the disc space was cleared of soft tissue using a micro-curette. Ink spots drawn onto the vertebral surfaces proximal and distal to the disc space served as markers for optical tracking. A digital camera (acA3800-14um; Basler AG, Ahrensburg, Germany) fit with a close-focusing macro video lens (Zoom 7000; Navitar Inc., Rochester, NY) and custom software were used to record images during testing. The mechanical testing protocol consisted of 20 cycles of compression from 0 to -3N at 0.05 Hz, with images of the segment recorded at 10 Hz. Texture tracking was performed in MATLAB [146] and the 20th cycle of stress-strain was analyzed using a bilinear fit routine. Mechanical properties were normalized to cross-sectional area measurements from digital images and disc height from MR images as described previously [20].

7.2-8 Mechanical Data Analysis

The 20th cycle of the load/displacement curve was analyzed for toe and linear region modulus, transition strain, and total compressive range of motion (ROM). First, load and displacement were converted to stress and strain, by dividing by the total cross-sectional area and height, respectively. Then, toe and linear region stiffnesses were calculated using a bilinear fit routine in MATLAB.

The creep response was fit to a 5 parameter viscoelastic constitutive model [Eq. 7-1] [146] that defines the compressive strain (ϵ) and stress (σ) as a function of time (t) and includes an early damping modulus and time constant (E_1 and τ_1), a late damping modulus and time constant (E_2 and τ_2), and an instantaneous damping modulus (E_3).

[Eq. 7-1]
$$\epsilon(t) = \frac{\sigma}{E_1} \left(1 - e^{-\frac{t}{\tau_1}}\right) + \frac{\sigma}{E_2} \left(1 - e^{-\frac{t}{\tau_2}}\right) + \frac{\sigma}{E_3}$$

Creep strain, or the total change in strain from 1.5s to 10 minutes, was also calculated.

7.2-9 μ CT and Histological Analysis of Implanted DAPS

Vertebra-DAPS-vertebra segments were imaged by μ CT (vivaCT 75; SCANCO Medical AG, Bruttisellen, Switzerland) and evaluated histologically (n=6). Segments were scanned at an isotropic 20.5 μ m resolution to evaluate the appearance of the vertebral bodies and potential bony fusion across the disc space. Then, segments were fixed in formalin, decalcified in formic acid and embedded in paraffin at 55°C. Sections were cut to 10 μ m and stained with both AB and PR, and imaged in brightfield.

7.2-10 MRI Analysis of Implanted DAPS

MRI was performed at 4.7T on intact rat tail discs and AF/NP constructs 5 weeks after implantation into the rat caudal spine (n=3-6). A multi-echo-multi-spin sequence was used to acquire quantitative coronal T2 maps (three 0.5 mm thick slices, 16 echoes, TE/TR = 7.84 ms/2,000 ms, FOV = 15x15 mm², matrix = 128x128, 4 averages). Timepoint average T2 maps were generated by scaling T2 maps to a normalized grid and averaging the T2 signals at each of each disc within a timepoint [145]. Mean NP T2 signals for individual discs were calculated after manual segmentation of the NP.

7.2-11 Subcutaneous Implantation of DAPS

DAPS were implanted into the dorsal subcutaneous space of athymic retired breeder rats (n=2). Incisions were made 1 cm lateral to the spine and 1 cm caudal to the scapula and a subcutaneous pocket was opened. DAPS were inserted into the pocket which was then closed with suture.

7.2-11 Statistical Analysis

In vitro and in vivo DAPS compositional measurements and mechanical properties were compared by one or two-way ANOVA. Post-hoc pairwise analyses were made using the method of Bonferroni (p<0.05). Data are displayed as mean ± standard deviation.

7.3 Results

7.3-1 Study 1: DAPS In Vitro Growth Trajectory

I fabricated two versions of DAPS constructs [Fig. 7-1a], either DAPS with AF cells in the AF region and NP cells in the NP region (AF/NP DAPS) or DAPS with

MSCs in both regions (MSC/MSC DAPS). Both construct types were cultured in defined media with the chondrogenic growth factor TGF- β 3 for up to 15 weeks [Fig. 71b]. Both MSC/MSC and AF/NP DAPS matured compositionally with time in culture [Fig. 7-1c] and grew physically larger [Fig. 7-2a]. For the AF region, picosirius red (PR) staining for collagen and alcian blue (AB) staining for GAG began at the AF boundaries at 2.5 weeks and gradually infiltrated to deeper regions by 10 weeks. GAG was distributed diffusely through the AF, while collagen was localized to specific areas in the interlamellar spaces. By 15 weeks, a peripheral concentration of dense extracellular matrix indicated encapsulation. In the NP region, both collagen and GAG-positive staining increased with time, with collagen staining concentrated at the center of the NP, and GAG staining evenly distributed throughout the NP. Immunostaining for type I and type II collagens indicated a fibro-chondrogenic phenotype, rich in type II collagen deposition in both regions [Fig. 7-1c].

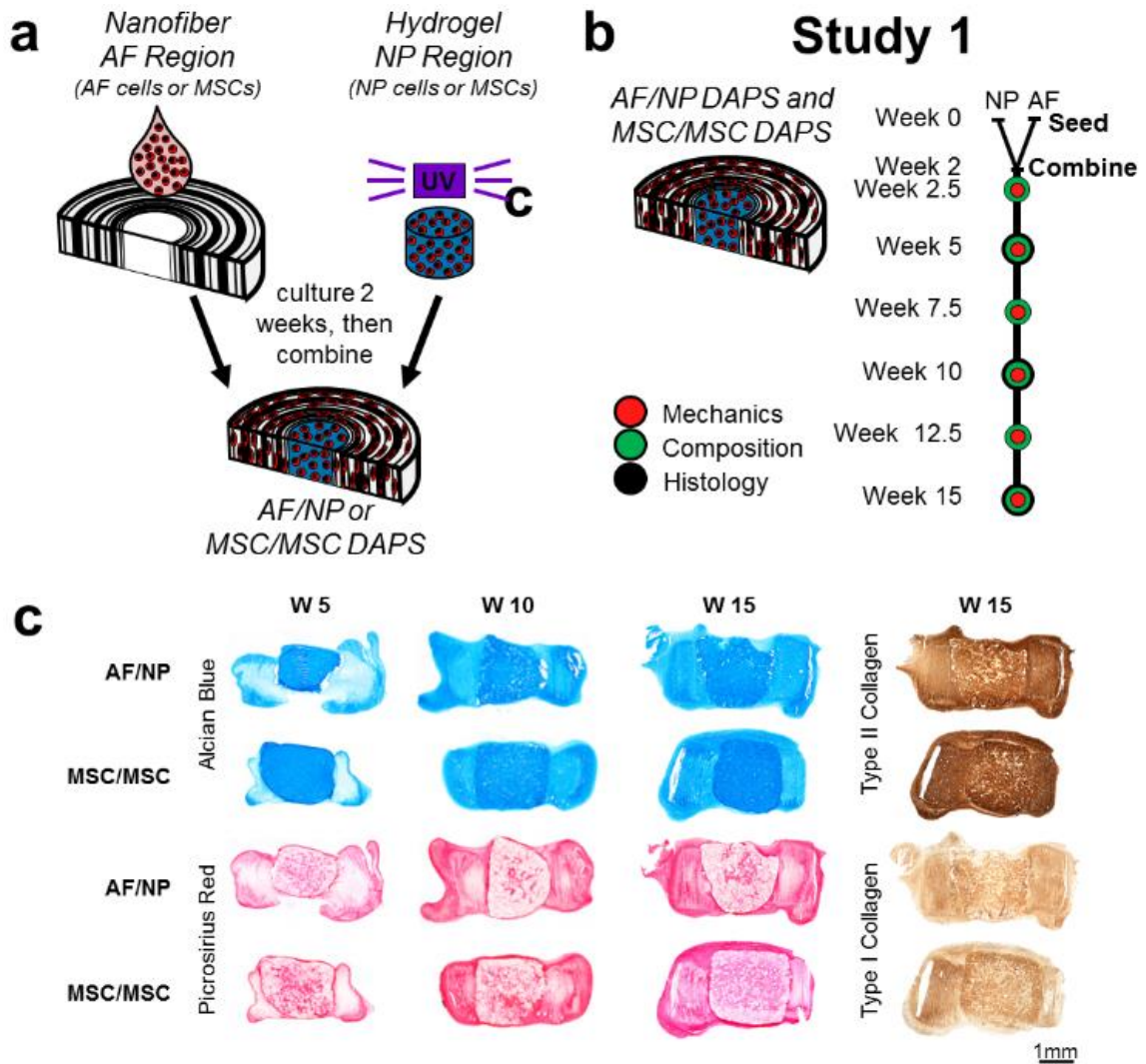
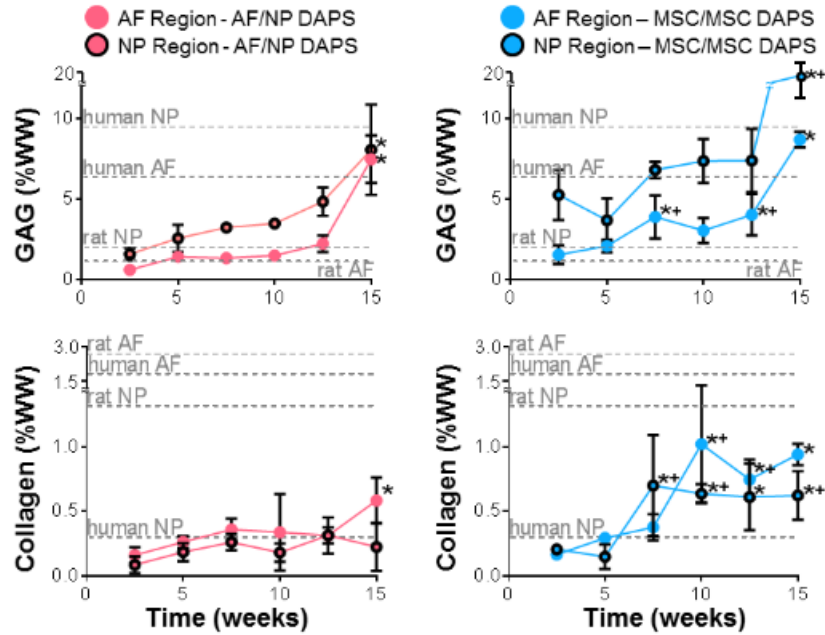


Figure 7-1 Study 1: *In vitro* growth trajectory of cell-seeded DAPS: design and results
 (a) Engineered intervertebral disc analogs, DAPS, composed of a nanofibrous AF and a hydrogel NP, were seeded with either AF and NP cells or MSCs and cultured in chemically defined media with TGF- β 3 separately for 2 weeks and then combined. (b) The *in vitro* maturation of DAPS was evaluated mechanically, compositionally, and histologically at regular intervals over the course of 15 weeks. (c) DAPS matured compositionally in terms of proteoglycan (alcian blue) and collagen (picrosirius red) staining over this time period, and stained strongly for type II collagen after 15 weeks. (continued on following page...)

d Composition



e Mechanical Function

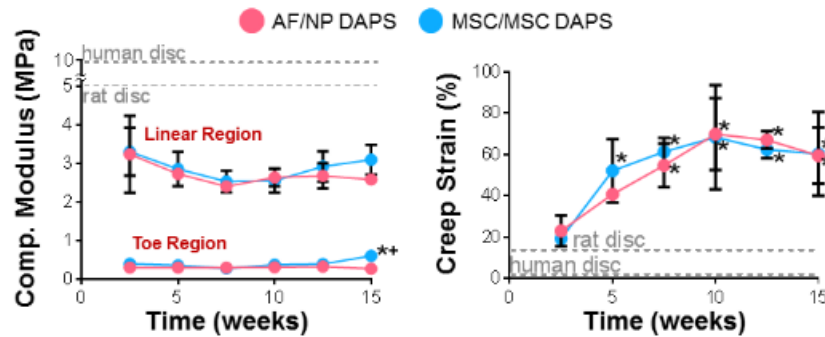


Figure 7-1 Study 1: *In vitro* growth trajectory of cell-seeded DAPS: design and results (cont.) (d) This was confirmed by measurements of GAG and collagen content, which exceeded or was within range of native tissue values in every case. GAG content consistently increased over 15 weeks, while collagen content increased early and then reached a plateau. Native values from [20, 30]. (*, p < 0.05 vs Wk. 2.5; +, p < 0.05 vs. AF/NP at corresponding timepoint) (e) DAPS demonstrated a nonlinear stress/strain response in compression, and elastic mechanical properties (moduli) were stable over 15 weeks. Viscoelastic properties (creep strain) became more dominant over the 15 week period, stabilizing by 10 weeks. In both cases there were no differences between AF/NP and MSC/MSC DAPS and mechanical properties were within range of native tissue mechanical properties. Native values from [20, 30, 113]. (*, p < 0.05 vs Wk. 2.5; +, p < 0.05 vs. AF/NP at corresponding timepoint).

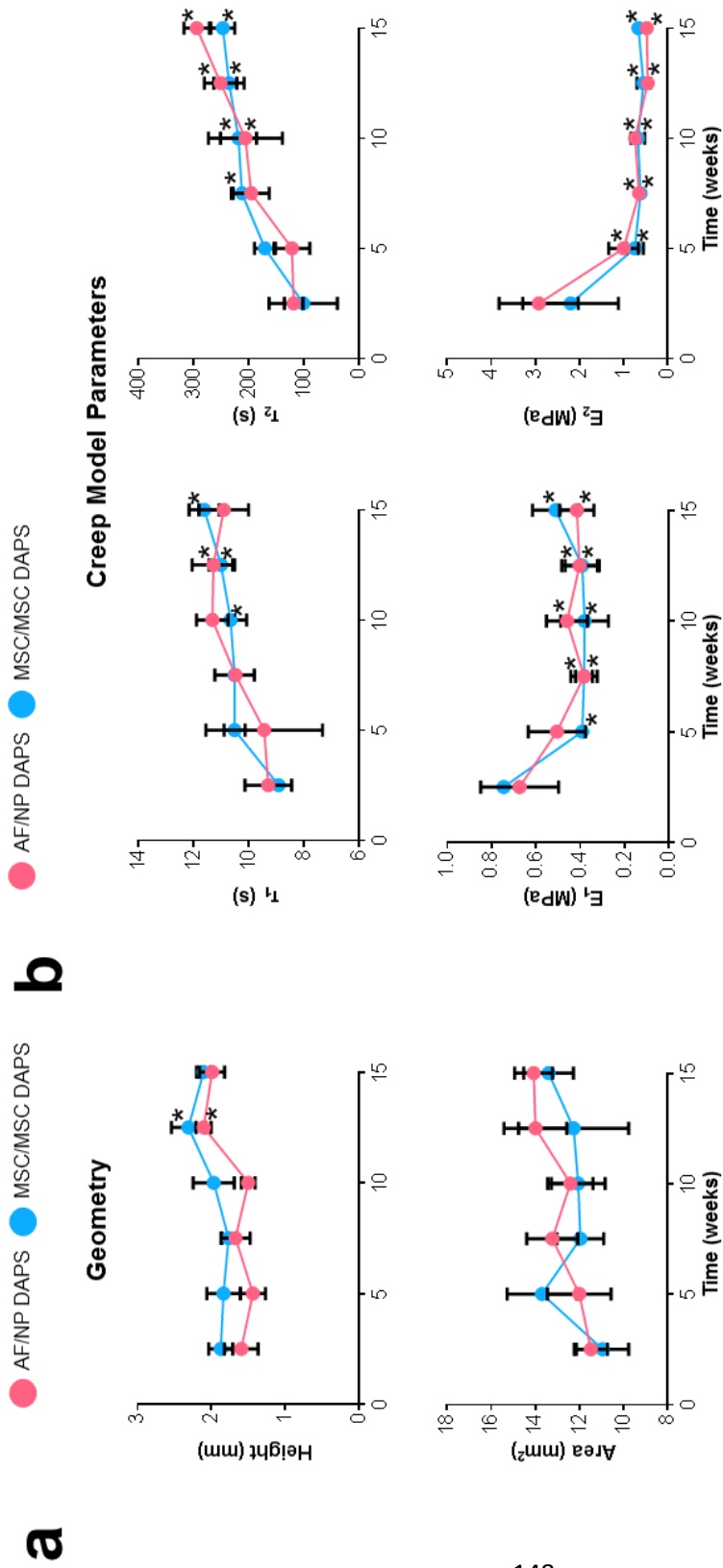


Figure 7-2 Geometry and Creep Model Parameters of Cultured DAPS (a) The height of both AF/NP and MSC/MSC DAPS significantly increased by week 12.5, while there was no change in cross-sectional area (*, $p < 0.05$ vs. week 2.5). (b) Time constants, τ_1 and τ_2 , representing the early and late response to creep loads, continuously increased with time, while damping moduli, E_1 and E_2 , increased over the first 5 weeks, where they remained after 15 weeks. The combination of these findings suggests DAPS become increasingly viscous over time, and more similar to native tissue (*, $p < 0.05$ vs. week 2.5).

The maturational changes evident by histology were confirmed by measurement of GAG and collagen content [Fig. 7-1d]. GAG content steadily increased in the NP region of both AF/NP and MSC/MSC DAPS, reaching significance by week 15. GAG production in NP region of MSC/MSC DAPS was significantly greater than that of the same region of AF/NP DAPS at 15 weeks. GAG content also increased in the AF region of both AF/NP and MSC/MSC DAPS, reaching significance by 7.5 weeks for MSC/MSC DAPS and 15 weeks for AF/NP DAPS. GAG production in the AF region by MSC/MSC DAPS again outpaced that of AF/NP DAPS, and was significantly different at 7.5 and 12.5 weeks, but not different at 15 weeks. Collagen content in both the AF and NP regions of MSC/MSC DAPS significantly increased over time and was significantly different than collagen content in the AF and NP regions of AF/NP DAPS. There was an increase in collagen in the AF region of AF/NP DAPS over time, reaching significance at 15 weeks, while there was no change in collagen content in the NP region of AF/NP DAPS.

Functional properties of MSC/MSC and AF/NP DAPS were not different from one another over 15 weeks of culture. Indeed, for both DAPS types, elastic mechanics were primarily unchanged and viscoelastic effects steadily become more dominant. Toe and linear region compressive moduli did not change significantly over 15 weeks, with no differences between MSC/MSC and AF/NP DAPS [Fig. 7-1e]. There was a significant increase in creep strain over the first 10 weeks that plateaued between 10 and 15 weeks, with no differences between cell types [Fig. 7-1e]. Both the early and late response to creep load became stronger, as evidenced by viscoelastic parameters extracted from the

creep curves [Fig. 7-2b], suggesting that DAPS were increasingly viscous with time, progressing from a cell-seeded biomaterial to an engineered tissue.

7.3-2 Study 2: Trajectory-based In Vivo DAPS Implantation

Using the in vitro growth trajectory defined by the study described above, I determined a timepoint that corresponded to an immature, rapidly growing state of the DAPS, which I hypothesized would integrate better into the native vertebrae than a mature DAPS based on [67]. Thus, DAPS were precultured for 5 weeks and implanted into the caudal spines of athymic rats. An external fixation device was used to stabilize adjacent vertebrae to provide a patent site for implantation and further in vivo maturation [149] [Fig. 7-3a]. After 5 weeks in the in vivo environment, bone-DAPS-bone motion segments were subjected to compression loading in order to evaluate their in situ mechanical response. To do so, motion segments with DAPS were cyclically loaded from 0 to 3 N (≈ 0.3 MPa) in compression, using an optical displacement tracking technique and, subsequently, a digital texture tracking program to evaluate the mechanical response. [Fig. 7-3b]. Both implanted DAPS and native discs had a similar non-linear stress/strain response [Fig. 7-3c]; DAPS were mechanically functional at physiologically-relevant loads, with toe and linear region compressive moduli matching that of the native disc (toe region compressive modulus, $\beta = 0.89$; linear region compressive modulus, $\beta = 0.86$) [Fig. 7-3d]. While these toe and linear moduli were comparable between DAPS and native discs, DAPS implants exhibited a significantly later transition between the toe and linear regions, the primary difference between groups [Fig. 7-3d].

a

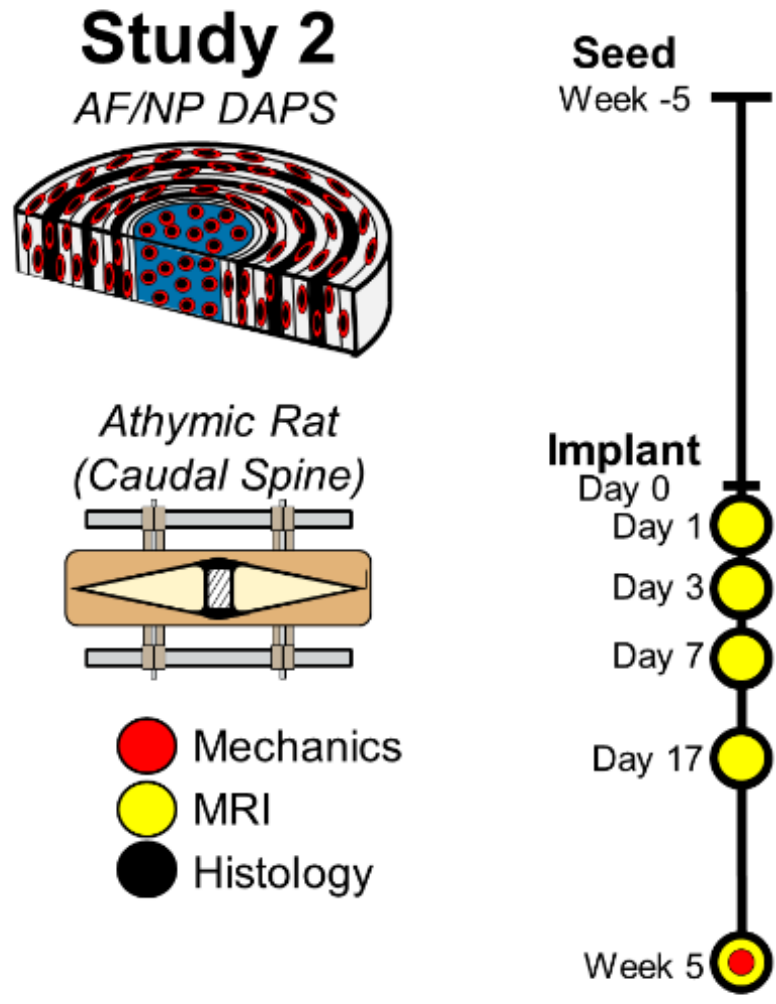


Figure 7-3 Study 2: *In vivo* implantation of immature, rapidly growing DAPS (a) After 5 weeks of *in vitro* culture, AF/NP DAPS were implanted into the caudal spines of athymic rats, an *in vivo* model of total disc replacement.

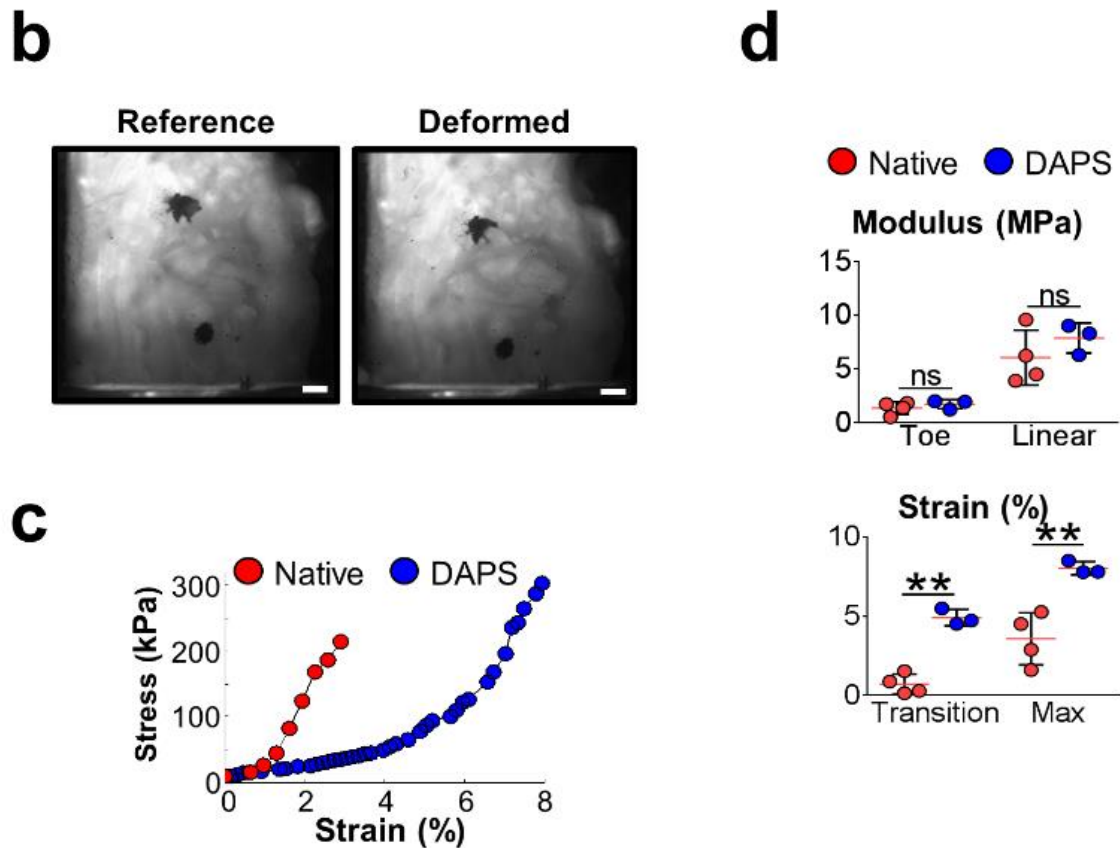


Figure 7-3 Study 2: *In vivo* implantation of immature, rapidly growing DAPS (cont.) (b) After 5 weeks *in vivo*, vertebra-DAPS-vertebra motion segments were tested in compression, using an optical displacement tracking technique to measure deformations. (c) Similar to native motion segments, DAPS had a nonlinear stress-strain response with separate toe and linear regions, as shown in these representative curves. (d) After extracting mechanical parameters, it was evident that there were no significant differences between toe and linear region moduli of DAPS implants and native discs. The primary difference mechanically was in the transition and maximum strains, which were higher in the DAPS group. (ns, nonsignificant, $p > 0.05$, **, $p < 0.01$).

To investigate adaptations in DAPS composition post-implantation, T2 MRI maps (which are indicative of GAG and water content) were generated using a multi-echo multi-spin sequence at 4.7T. Quantification of the AF and NP T2 signal showed that the NP T2 signal of implanted DAPS was higher than native tissue at early timepoints, but progressively decreased over 5 weeks [Fig. 7-4a]. This was confirmed visually by timepoint average maps [145] [Fig. 7-4b, left column]. Alterations in composition were mirrored in histological sections [Fig. 7-4b, middle and right columns]. Pre-implantation, the NP composition was initially proteoglycan- and collagen-rich after 5 weeks of in vitro culture [Fig. 7-1c]. However, within 5 weeks post-implantation, DAPS lost proteoglycan staining, and became composed primarily of collagen rich tissue. This alteration in phenotype initiated in the NP at days 1 and 3, with infiltration by host cells apparent by day 7. By day 35, the original implanted NP was difficult to distinguish, while the AF region retained its structure over time, but similarly lost proteoglycan content and was primarily comprised of collagen at day 35. In addition, there was little evidence of integration into adjacent vertebrae. In terms of specific collagens, at post-implantation day 1, the NP region stained for types I and II collagen in some areas, while the AF region stained strongly for both collagens [Fig. 7-4c]. By 35 days post-implantation, both the AF and NP region stained positively and homogeneously for types I and II collagen, possibly indicating a shift in implant phenotype or the infiltration of endogenous cells that deposited fibrous repair tissue throughout the intervertebral space.

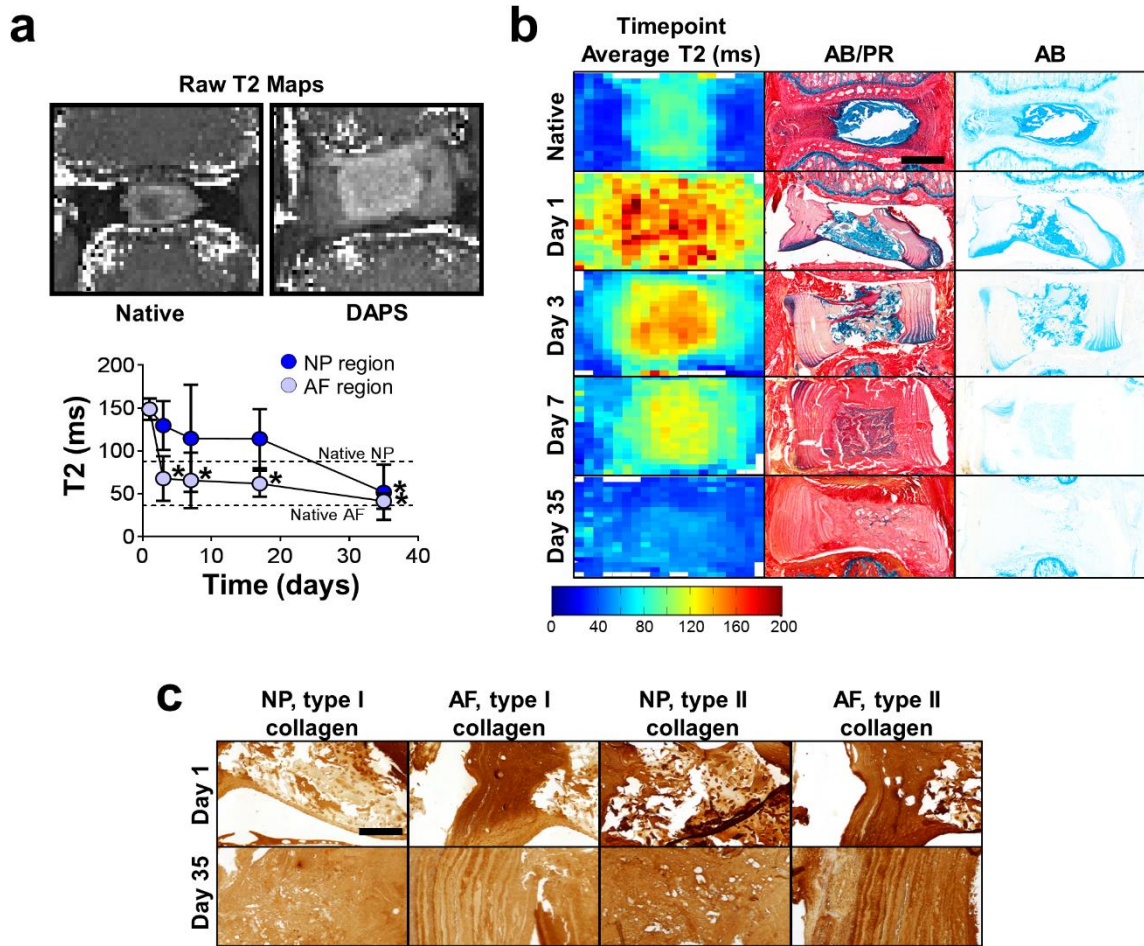


Figure 7-4 Study 2 (cont.): Compositional analysis of implanted DAPS (a) T2 MRI mapping was performed over the 5 week implantation period, and the T2 relaxation time (which is indicative of water and GAG content) was calculated after manual segmentation of the AF and NP regions. The AF and NP T2 both decreased significantly after implantation (*, $p < 0.05$). (b) Timepoint average T2 maps were generated and compared to Alcian blue (AB) and picosirius red (PR) stained histological sections. Corresponding with the decrease in T2, AB positive staining decreased over time in both the AF and NP regions. Dynamic modifications to the NP region took place over this time period. (c) At day 1, was mildly and heterogeneously stained for types I and II collagen, while the AF stained strongly for both. By day 35, collagens were distributed homogeneously throughout both the AF and NP regions.

7.3-3 Study 3: Implantation of Fully Mature DAPS

Given these findings with immature DAPS constructs, I next hypothesized that a more mature construct may be better suited to retain its composition the in vivo environment. DAPS were thus precultured for 10 weeks (to a mature state) and implanted into the caudal spines of athymic rats, as above [Fig. 7-5a]. Microcomputed tomographical (μ CT) reconstructions revealed normal vertebral morphology, with only mild bone formation around the surgical wire holes and no bone formation in the intervertebral space, indicating that fusion had not occurred. Alcian blue/picrosirius red stained vertebra-DAPS-vertebra sections showed that these more mature DAPS maintained their lamellar structure after 5 weeks. However, again, the majority of implants were positive for collagen staining throughout the entire construct, but showed little evidence of proteoglycan [Fig. 7-5b]. In only two of 12 implants was significant GAG staining apparent in the NP region [Fig 7-5b, 'Mature: Best'] and in some cases implants stained yellow as a result of bleeding from an inadvertent fracture at the growth plate [Fig 7-5b, 'Immature: Intermediate and Worst', Fig 7-5b 'Mature: Best and Worst']. Integration into the adjacent bone was not apparent for any of these implants, and upon gross dissection, the vertebral motion segment separated at the DAPS/vertebra interface, suggesting that earlier success in mechanical testing was likely due to integration into adjacent soft tissue.

a Study 3

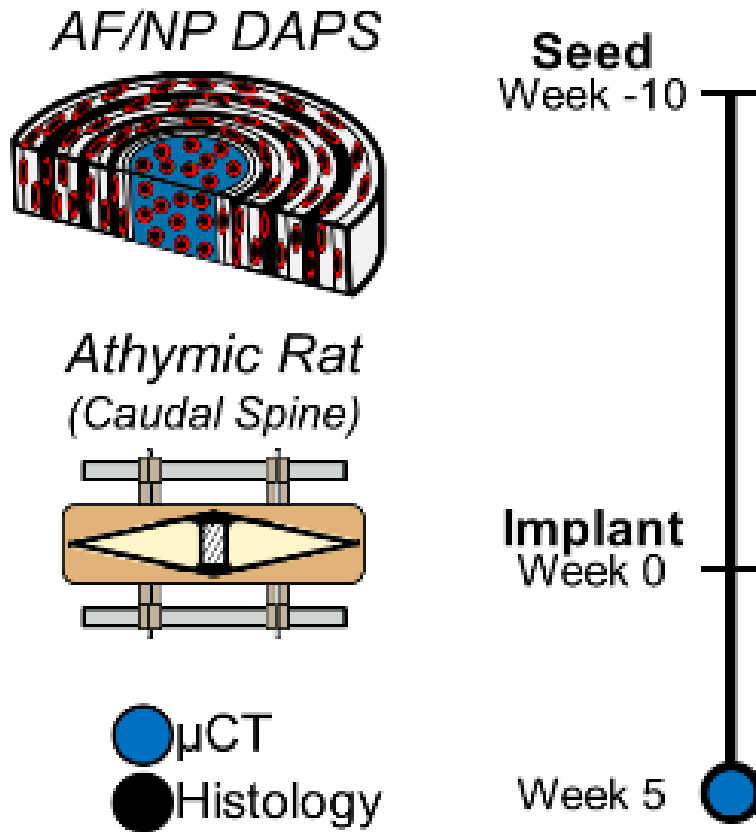


Figure 7-5 Study 3: *In vivo* implantation of fully matured DAPS AF/NP DAPS were pre-matured for 10 weeks and implanted into the caudal spines of athymic rats. (continued on following page...)

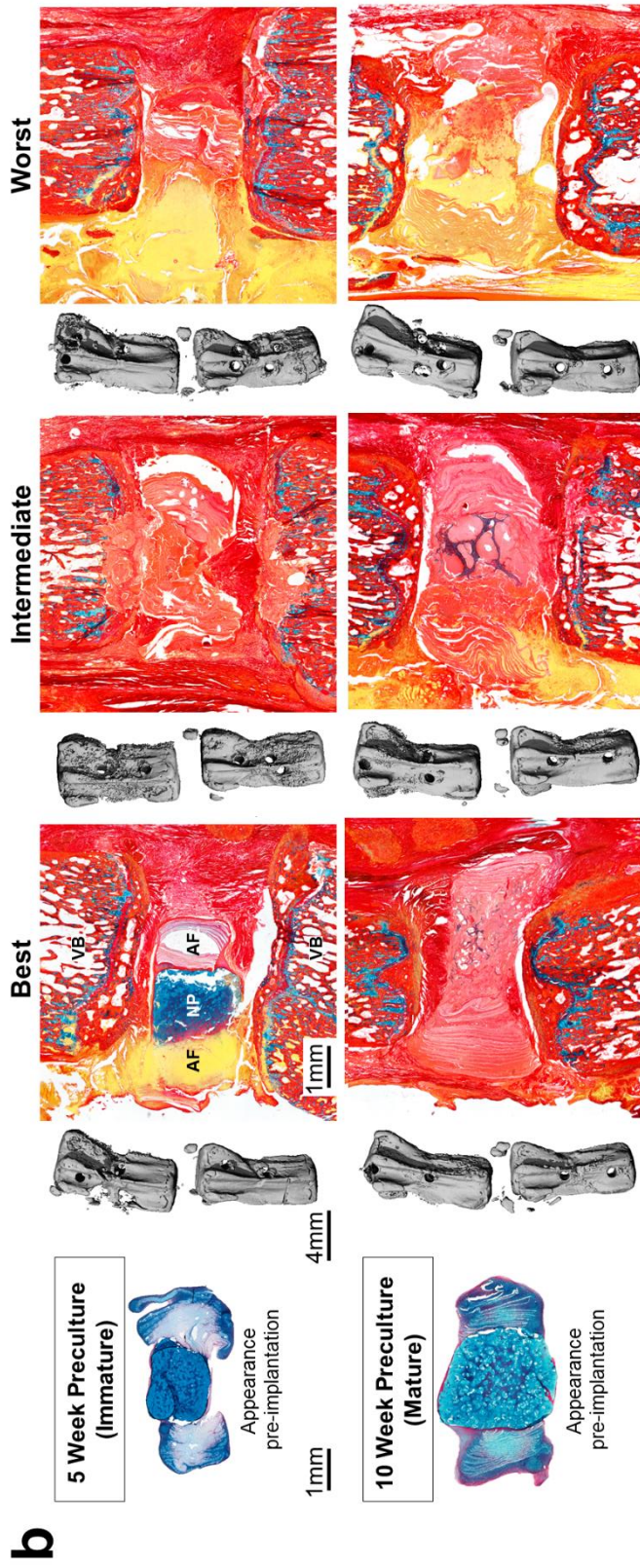


Figure 7-5 Study 3: *In vivo* implantation of fully matured DAPS (cont.) (b) Micro-CT reconstructions and Alcian-blue/picrosirius-red stained sections of DAPS with the best, intermediate and worst appearance are displayed along with the 5 week pre-cultured group for comparison. There was no evidence of fusion in any case and, in all but one case, GAG-positive staining was absent from the AF and NP. (continued on following page ...)

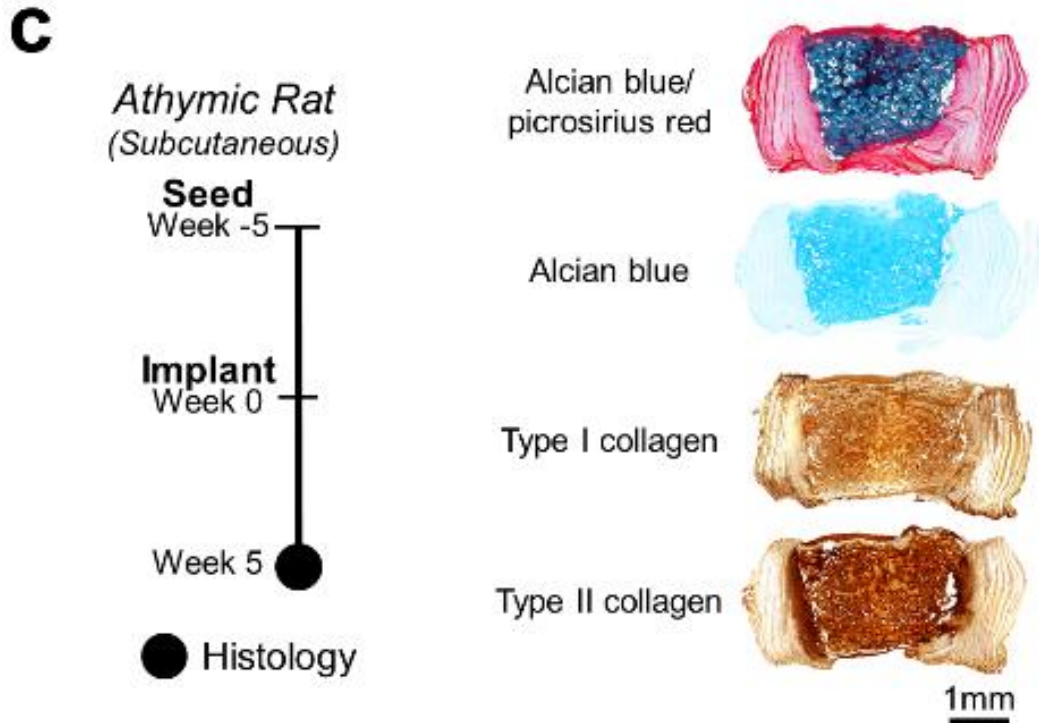


Figure 7-5 Study 3: *In vivo* implantation of fully matured DAPS (cont.) (c) To compare between implantation sites, DAPS were pre-matured for 5 weeks and implanted into the dorsal subcutaneous space of athymic rats. Again, GAG staining decreased over 5 weeks of implantation, though not to the extent that occurred in the disc space, while types I and II collagen stained strongly in the NP region, and in the interlamellar spaces of the AF.

To determine whether these phenotypic changes were due to in vivo implantation in general, or a consequence of implantation in the intervertebral space specifically, AF/NP DAPS were next implanted in the subcutaneous space of athymic rats. After 5 weeks of implantation subcutaneous, a similar shift from GAG-rich to GAG-deficient occurred, as evidenced by histologically sections [Fig. 7-5c]. However, in this case, the NP structure was still intact and retained some proteoglycan as well as types I and II collagen. The AF region was devoid of proteoglycan but did stain for collagen; thus the matrix distribution in the AF following subcutaneous implantation was very similar to the native disc [Fig. 7-4b]. Thus, while the transition from in vitro culture to in vivo implantation is deleterious to the in vitro phenotype, the infiltration of endogenous tissue and adaptations to the NP structure appear to be specific to intervertebral implantation.

7.4 Discussion

This study details the compositional and functional growth trajectory of an engineered disc composed of an electrospun AF and a hydrogel NP, and subsequent in vivo characteristics of the engineered disc after implantation in a rat model of total disc replacement. In vitro, DAPS demonstrated composition and nonlinear, viscoelastic mechanical properties similar to native tissue, and supported a viable cell population of either disc cells or stem cells over 15 weeks in culture. After 5 weeks of in vivo implantation, DAPS maintained their structure and did not instigate intervertebral fusion. However, both histological and MRI results suggested a shift in phenotype after the transition from in vitro culture to the in vivo space, a phenomenon that was independent

of the pre-culture duration. Despite these changes, key mechanical features of the native disc were fully replicated, strongly implicating the potential of this strategy for total disc replacement.

Current metal-on-plastic engineered replacements for total disc arthroplasty aim to restore the natural kinematics of the spine but are composed of materials that have physical properties that do not match native tissue. In this study, I demonstrated that the complete rescue of healthy spine function in compression is possible by replacement with living engineered tissues, such as the DAPS constructs. I applied physiologically relevant loading (approximately 60% rat body mass) and found that DAPS demonstrated full recapitulation of healthy disc compressive mechanics, with the exception of an elongated toe region. Histologically, a significant amount of fibrous tissue was evident between the DAPS and the adjacent vertebrae, which likely is engaged and contributes to the functional response at low loads, lengthening the toe region. Future work will seek to improve integration at the endplate to eliminate this region of fibrous tissue at the interface of the DAPS and the vertebrae, while at the same time improving anchorage at the implant site. Improved integration would enable further mechanical characterization of these implants at higher loads and other physiologically relevant loading modalities, including bending and torsion.

With extended in vitro growth, the compositional and functional properties of the DAPS reached levels comparable to native human and rat discs [4,5]. Measurements of GAG and collagen content showed a progressive increase in matrix deposition in the AF and NP regions for both cell types, with deposition rate in MSC-seeded DAPS outpacing that of disc-cell seeded DAPS. GAG content of MSC/MSC and AF/NP DAPS

approached human levels in the AF and NP regions, while collagen content was 40% of the human AF and exceeded or matched that of the human NP. Interestingly, single GAG molecules that are not attached to aggrecan core protein have a molecular weight an order of magnitude lower than collagens (chondroitin sulfate: 0.5 Da, keratan sulfate: 1 kDa vs. type I collagen: 140kDa, type II collagen: 140kDa). These charged species appeared spread throughout the construct while collagen was localized to the interlamellar spaces in the AF and the central region of the NP. This suggests that GAG molecules themselves, or potentially smaller breakdown products of the larger aggrecan molecule, might diffuse more readily than collagens through the biomaterials, poly(ϵ -caprolactone) (PCL) and hyaluronic acid (HA), used in these implants. Collagen-positive staining was strongest in the center of the NP of DAPS of both cell types, not at the periphery where cells are closest to culture media. This may be related to oxygen tension, which would be lower in the central NP when compared to the peripheral NP, as previous studies have shown that collagen production increases in hypoxic conditions [138].

While the in vitro elastic mechanical properties of DAPS were generally unaltered over time in culture, the development of time-dependent mechanical properties, along with improvements in extracellular matrix content, demonstrated the transition of the construct from a cell-seeded biomaterial to an engineered tissue. DAPS possessed nonlinear stress/strain behavior and moduli within 70% of the native rat disc, an improvement over previous reports of engineered discs [30, 96, 179]. Despite increasing extracellular matrix content over time, compressive mechanical properties did not change. Electrospun PCL has a tensile modulus in the MPa range [13] and slowly degrades [128]. Thus, PCL may be likely the dominant factor in the elastic mechanical

response over 15 weeks *in vitro*. Additionally, DAPS mechanical properties became increasingly more viscous over time, while the overall response to creep loads exceeded that of native tissue. Thus, while DAPS resembled native tissue in their elastic mechanical behavior, there were differences in their time dependent mechanisms compared to native, perhaps driven by differences in the ability to retain water under load or plastic deformation in the AF region.

Given that the DAPS cultured *in vitro* met or exceeded many compositional and mechanical design criteria for native tissue, there is little room for improvement in terms of generating a more *in-vivo*-ready engineered tissue. However, after implantation, a significant shift in phenotype occurred. This suggests that the standard tissue engineering techniques employed to generate a functional construct *in vitro* (cell isolation, expansion and seeding techniques, media conditions for differentiation and growth) do not generate a construct whose phenotype is sustainable *in vivo*. Specifically, upon implantation, there was marked depletion of GAGs in the NP region, suggesting there was an inability to continuously produce and retain GAG *in vivo* or there was a catabolic shift in cell behavior. This may be a result of the surgical procedure, as post-operative inflammation may have caused an increase in catabolic cell activities. It may also be a limitation of the rat tail model; externally fixing the tail does not allow the normal course of physiological loads, which may be an anabolic stimulus [244], to act on the engineered implant. Likewise, the lack of loading may have compromised load-induced convective diffusion mechanisms that are necessary to maintain cell function. Phenotypic transformations after implantation of either fully differentiated cells or stem cells into the subcutaneous space have been documented in a number of studies [52, 53, 195, 237]. Such changes may be

related to the abrupt removal of media components such as glucose, TGF- β 3, or dexamethasone upon implantation. Glucose deficiency causes a depletion in the functional capacity of disc cells [27], though less is known in terms of the sudden removal of the other media components, a possible area for future study. The effects of transitioning from the amenable in vitro culture conditions to the harsh in vivo conditions on other cell sources with potential for regeneration, such as MSCs, may comparatively be exaggerated, as disc cells are known to be uniquely suited to function in challenging environments [204]. However, based on our findings, new strategies for transitioning engineered tissues in vitro to in vivo will be required for sustained function post-implantation.

One notable observation in the implant post-implantation was that the HA hydrogel NP began degrading within the first few days after implantation and was completely absent after five weeks. HA is a naturally occurring component of the extracellular matrix and can be turned over by cells; hyaluronidase production, as a result of a catabolic shift in cell phenotype after implantation or as a result of surgery-related inflammation, may have caused the loss of HA. Invading endogenous cells that take part in the wound healing response are also likely a factor in HA turnover. Certainly, these materials are meant to degrade after implantation, but the rapidity of HA breakdown was somewhat unexpected, as HA is sufficiently stable in the subcutaneous environment as demonstrated both in this study and in previous work [25, 26], though it was absent after polymerization in a porcine osteochondral defect [64]. A modification to the NP biomaterial may improve in vivo stability, improve implant performance, and better support and sustain the implanted cell population.

7.5 Conclusion

In these experiments, an engineered disc composed a fibrous AF region and a hydrogel NP region supported the compositional and functional growth of seeded cells, and reproduced the compressive mechanical functions of the native disc after implantation *in vivo*. Degeneration of the intervertebral disc leads to a loss of function in disc structures, and ultimately inferior mechanical performance at the motion segment level. Tissue engineering is one strategy to replace degenerate tissue with a functional substitute, and in these preclinical experiments, I demonstrated that, through tissue engineering, recapitulation of disc mechanical properties was possible *in situ*. These data strongly support tissue engineering for functional restoration of spine health. Furthermore, I also detailed an important limitation of current tissue engineering strategies, that culture in a chemically-defined media formulation with TGF- β 3, a staple of the field, does not produce an engineered tissue that is prepared for transition the *in vivo* environment. This finding was demonstrated in two locations, both *in situ* in the rat tail and *ex situ* in the subcutaneous space. While the former resulted in more dramatic declines in GAG content, both showed reduced content within five week. As such, modifications to the pre-culture strategy and the NP biomaterial may be necessary to ensure the viability of the engineered disc after implantation; future work should first focus on these challenges. Finally, engineered discs must be evaluated at a larger scale and in a physiologically relevant mechanical environment, such as the lumbar spine of a large animal model, and in an environment relevant to disc degeneration, such as an animal model of disc degeneration. Ultimately, this will need to be addressed with human

cells, demonstrating their ability to mature in vitro and survive in vivo, for this DAPS technology to transition forward to clinical trials.

CHAPTER 8 - Optimization of in vitro pre-culture to maximize in vivo performance of a cell-seeded disc-like angle ply structure (DAPS) for total disc replacement

8.i Preface

In the previous chapter, I described that DAPS development matched many compositional and mechanical benchmarks of native tissue after in vitro culture. However, in vivo, DAPS deteriorated and lost the GAG content that had developed in vitro. I hypothesized that this may be due to the sharp transition in environments, moving DAPS from an in vitro space rich in chondrogenic factors to an in vivo space where these do not exist. Thus, in this chapter, I will describe the analysis of a pre-culture method with the potential to improve upon these results.

8.1 Introduction

The development of engineered tissues has progressed over the past twenty years from in vitro characterization to in vivo implementation, particularly for the musculoskeletal system, where in vitro metrics of engineered constructs regularly meet or exceed native tissue benchmarks for bone [74, 141], cartilage [24, 59, 185], and fibrocartilage [167, 175, 232]. The emphasis of many of these studies was to select conditions to maximize functional and compositional gains in vitro; however, the transition from the favorable in vitro culture environment to a less favorable in vivo environment has proven difficult. That is, in many cases, engineered tissues do not retain their pre-implantation phenotype after even short periods in vivo [52, 53, 195, 237].

Developing a successful pre-culture strategy that allows for functional extracellular matrix production in vitro which continues after implantation in vivo is critical to the translation of these technologies.

While DAPS recapitulate important mechanical parameters of the native disc in vivo, consistent with other studies in the field, I found that after implantation of DAPS proteoglycans that had accumulated in the AF and NP regions during pre-culture diminished markedly post-implantation [148]. This shift in phenotype may be due to inflammation related the surgical procedure or to limitations of the biomaterials, or issues with transition from nutrient and growth factor rich pre-culture media to the challenging nutrient- and growth-factor poor in vivo environment. In the current studies, I focus on the transition from the in vitro culture conditions to the in vivo space. The culture medium used for these studies was designed for MSC chondrogenesis [108], and is a chemically-defined, serum-free formulation that includes potent factors for extracellular matrix production, including transforming growth factor β 3 (TGF- β 3), ascorbate-2-phosphate, proline and dexamethasone. This formulation has been useful for engineering a number of musculoskeletal tissues, including cartilage [46, 62], meniscus [12, 65], as well the intervertebral disc [179], using both multipotent and fully differentiated cell sources. While this formulation has proven successful in developing tissues that meet native tissue benchmarks in vitro, there are some drawbacks. For example, MSCs differentiated using this formulation do not match the gene expression profiles of articular chondrocytes [91], and the phenotype imprinted on MSCs following culture in this medium dissipates when media components are selectively removed [115]. Thus, this chemically defined medium likely does not instill a cell phenotype that is truly

chondrogenic or one that is sufficiently stable to be carried forward through the challenging in vivo environment.

A modification to the media formulation may better prepare engineered implants for the in vivo environment. For example, a growing number of studies suggest culture in serum-containing media before implantation successfully primes cells for in vivo environment where they maintain a healthy chondrogenic phenotype; this has been true for AF cells, NP cells, and chondrocytes in implantation sites that include the subcutaneous space, the disc space, and articular cartilage defects for a number of species [30, 43, 63, 137, 166, 208, 254]. Combining the benefits of pre-culture in media with chondrogenic factors with those of serum-containing media may therefore improve extracellular matrix deposition in vitro while at the same time fostering phenotype retention in vivo. Others have reported that transient stimulation with TGF- β 3, a method that models the rapid formation of tissue during fetal development, improves the chondrogenesis of MSCs and chondrocytes in vitro [38, 83, 114, 181]. While the biomolecular mechanisms that drive this phenomenon are unknown, the phenotype imprinted by transient doses of TGF- β 3 appears to be maintained over an extended period of time. In one study, chondrogenic features of engineered cartilage based on MSCs remained intact 8 weeks after the cessation of TGF administration [114]. While it is unknown whether the imprinted phenotype will persist after in vivo implantation, this strategy of ‘weaning’ constructs off of a dependence on TGF- β 3 may be effective in developing extracellular matrix in vitro and then retaining phenotype in vivo.

In these experiments, I tested six different pre-culture strategies for their ability to preserve DAPS composition and metabolic activity during the transition from in vitro culture to in vivo implantation in an athymic rat subcutaneous model. Based on the strategies described above and our previous in vitro success with TGF- β 3, I tested three hypotheses: (1) that pre-culture in serum-containing media with TGF- β 3 would improve in vivo performance, (2) that a transient high dose of TGF- β 3 would improve phenotype retention in vivo and (3) that, just prior to implantation, a gradual transition from chemically-defined media to serum-containing media would facilitate a stable in vivo transition.

8.2 Methods

8.2-1 DAPS Fabrication and Cell Seeding

DAPS were fabricated to match the natural hierarchical features of the intervertebral disc, including an electrospun nanofibrous AF region, with layers of aligned fibers that, similar to the AF lamellar structure, alter in apposed layers +/- 30° to the transverse plane, and a hydrogel NP region. The AF region was assembled from layers of a soluble polymer between layers of a cytocompatible, backbone polymer with long-term in vivo stability. These soluble layers would be washed away before seeding, providing channels for seeded cells to penetrate and then engraft onto the backbone polymer. The NP was fabricated from hyaluronic acid (HA), an essential component of the disc extracellular matrix, as a photopolymerizable hydrogel network.

Specifically, AF regions were composed of poly(ϵ -caprolactone) (PCL; Shenzhen Bright China Industrial Co., Hong Kong, China) as the core polymer, and poly(ethylene

oxide) (PEO; 200kDa, Polysciences, Inc., Warrington, PA) as the sacrificial polymer. PCL was dissolved in a 1:1 mixture of tetrahydrofuran (THF) and N,N-dimethylformamide (DMF) (Fisher Chemical, Fairlawn, NJ) to form a 14.3% w/v solution. PCL was electrospun onto a grounded rotating mandrel to produce a sheet of aligned fibers; PEO was dissolved in 90% ethanol at 10% w/v and electrospun atop the PCL layer. The PCL/PEO layers were then cut to produce strips with a 30° fiber angle, and two strips with opposing alignment were rolled concentrically about a post and spot welded with a soldering pencil. A 31G needle was passed radially through the mid-height of the construct to provide the implant with initial stability and hold the formed layers together during removal of PEO. The final construct had two 125 µm layers of PCL for every one 250 µm layer of PEO, a diameter of 5 mm diameter and a height of 2 mm. Prior to cell seeding, constructs were washed in a gradient ethanol series for both sterilization and to remove PEO layers, and then coated in 20 µg/mL fibronectin (Sigma-Aldrich, St. Louis, MO).

The NP regions of DAPS were filled with a photocrosslinkable methacrylated HA (MeHA) hydrogel. Sodium hyaluronate (65kDa, Lifecore, Chaska, MN) and methacrylic anhydride (Sigma Aldrich, St. Louis, MO) were reacted to produce MeHA, which was dissolved in phosphate buffered saline at 1% w/v, sterilized by UV light, and combined with 0.05% photoinitiator (Irgacure 2959, (2-methyl-1-[4-(hydroxyethoxy)phenyl]-2-methyl-1-propanone, Ciba-Geigy, Tarrytown, NY).

To harvest AF and NP cells, caudal intervertebral discs were dissected from adult bovine tails obtained from local abattoir with institutional approval. The disc tissue was isolated in aseptic conditions and the AF and NP regions were separated and then

digested, first in pronase at a concentration of 2.5 mg/mL for 1 h, and subsequently in collagenase at 0.5 mg/mL (4 h for NP tissue, 8 h for AF tissue). AF and NP cells were then expanded in a serum-containing medium consisting of Dulbecco's Modified Eagle's Medium (DMEM; Gibco, Invitrogen Life Sciences, Carlsbad, CA), 10% fetal bovine serum (FBS; Gibco), and 100 U/mL penicillin, 0.1 mg/mL streptomycin, 0.25 µg/mL amphotericin B (Antibiotic-Antimycotic, Gibco). At passage 2-3, cells were trypsinized and then seeded, AF cells onto the top and bottom of the electrospun AF region (1×10^6 cells per side) and NP cells in MeHA solution (20×10^6 cells/mL or $\sim 6 \times 10^5$ cells/NP) that was subsequently photopolymerized with UV light exposure for 10 min and then punched to 2 mm diameter.

8.2-2 Study Design

AF and NP regions were cultured separately for 2 weeks in one of 6 media conditions, at which point they were combined to form DAPS, cultured an additional 3 weeks, and then implanted into dorsal subcutaneous pockets of athymic rats for 5 weeks or cultured for an additional 5 weeks in vitro [Fig. 8-1]. At 2.5, 5, 6, and 10 weeks after in vitro culture, the metabolic activity (n=3), composition (n=3), and histological appearance (n=1-2) of DAPS were analyzed. Similar assays were performed 1 and 5 weeks after in vivo implantation (corresponding to in vitro weeks 6 and 10) for metabolic activity (n=3), composition (n=3), and histological appearance (n=1-2).

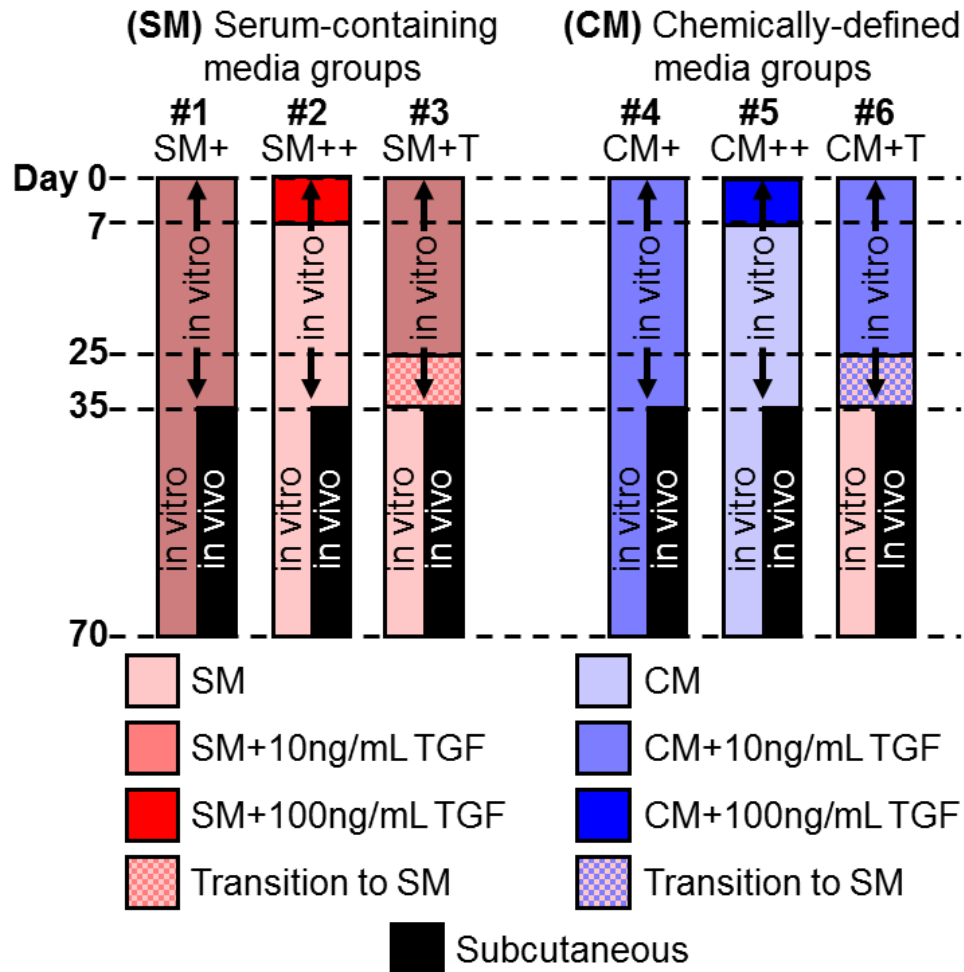


Figure 8-1 Study design: Optimization of pre-culture strategies Cell-seeded disc-like angle ply structures (DAPS) for engineered total disc replacement were cultured in one of six pre-culture conditions and implanted into the subcutaneous space of athymic rats; conditions were directly compared to evaluate which was the best for *in vivo* performance.

There were 3 serum-containing media pre-culture conditions:

#1, SM+: serum-containing media plus TGF- β 3;

#2, SM++: serum-containing media plus a one week high dose of TGF- β 3;

#3, SM+T: serum-containing media plus TGF- β 3 and then a transition to serum-containing media without TGF- β 3 over 10 days.

There were 3 chemically-defined media pre-culture conditions:

#4, CM+: chemically-defined media plus TGF- β 3;

#5, CM++: chemically-defined media plus a one week high dose of TGF- β 3;

#6, CM+T: chemically-defined media plus TGF- β 3 and then a transition to serum-containing media without TGF- β 3 over 10 days.

The base media formulations were a serum-containing medium (SM) [116, 168] with DMEM, 10% FBS, 100 U/mL penicillin, 100 µg/mL streptomycin, 2.5 µg/mL amphotericin B (Gibco), 1% MEM vitamin solution (Gibco), 25 mM HEPES Buffer (Gibco), and 40 µg/mL ascorbate 2-phosphate (Sigma-Aldrich) and a chemically-defined medium (CM) [59, 108] containing DMEM, 100 U/mL penicillin, 0.1 mg/mL streptomycin, and 0.25 µg/mL amphotericin B, 40 ng/mL dexamethasone (Sigma-Aldrich), 50 µg/mL ascorbate 2-phosphate, 40 µg/mL L-proline (Sigma-Aldrich), 100 µg/mL sodium pyruvate (Corning Life Sciences, Corning, NY), 0.1% insulin, transferrin, and selenious acid (ITS Premix Universal Culture Supplement; Corning), 1.25 mg/mL bovine serum albumin (Sigma-Aldrich), 5.35 µg/mL linoleic acid (Sigma-Aldrich). Transforming growth factor-β3 (TGF- β3; R&D Systems, Minneapolis, MN) was included at either a normal dose (10 ng/mL) or a high dose (100 ng/mL).

DAPS maturation and in vivo phenotype were evaluated after culture in 3 SM conditions and 3 CM conditions. Two groups had media with a normal dose of TGF- β3 (SM+, CM+ groups), two groups had a high dose of TGF- β3 for one week followed by culture in SM or CM (SM++, CM++ groups), and two groups were cultured in SM+ or CM+ and then transitioned over 10 days (4 media changes) to SM just prior to week 5 (SM+T, CM+T groups). Specifically, the transitioning strategy is as follows: Day 24 (100% SM+ or CM+), *Media Change 1* at Day 25 (75% SM+ or CM+, 25% SM), *Media Change 2* at Day 28 (50% SM+ or CM+, 50% SM), *Media Change 3* at Day 31 (25% SM+ or CM+, 75% SM), *Media Change 4* at Day 34 (100% SM).

8.2-3 Implantation Surgery

DAPS were implanted into the dorsal subcutaneous space of athymic retired breeder rats (male, 9-10 months, $463\text{g} \pm 45\text{g}$) with local institutional approval. Rats were anesthetized with isoflurane and dorsal subcutaneous pockets were opened with small incisions at 6-7 positions 1 cm lateral to the spine. DAPS were inserted into the pocket, which was then closed with suture. Rats were returned to normal cage activity after the procedure.

8.2-4 T2 Magnetic Resonance Imaging (MRI), Metabolic Activity, and Histological Analyses

T2 relaxation time generated from MRI correlates to the spatial distribution of water within a tissue and is a non-invasive, clinically-relevant method for assessing intervertebral disc health. A 4.7T MRI spectrometer was used to generate T2 maps of DAPS using a multi-slice, multi-echo acquisition (three 500 μm thick slices, 16 echoes, TE/TR = 7.84 ms/2,000 ms, FOV = $15 \times 15 \text{ mm}^2$, matrix = 128×128 , 4 averages). AF and NP regions were manually segmented from T2 maps and the mean T2 signal was calculated for each region.

Metabolic activity was assayed using the 3-(4,5-dimethylthiazol-2-yl)-2,5-diphenyltetrazolium bromide (MTT) colorimetric assay (n=3). To do so, DAPS were sectioned in half axially, submerged in a solution of DMEM and MTT at 0.5 mg/mL, and incubated for 5h at 37°C and 5% CO₂. AF and NP regions were then separated, minced, and the formazan product was solubilized in dimethyl sulfoxide and read on a microplate reader.

For histological analysis, DAPS were fixed in formalin, embedded in paraffin, sectioned axially at 10 μm , stained with either Alcian blue or picosirius red to identify collagens and proteoglycans, respectively, and then imaged in brightfield (Eclipse 90i, Nikon, Tokyo, Japan).

8.2-5 Statistical Analysis

For both MRI and MTT measurements, results after 5 Weeks subcutaneous implantation were normalized to either the pre-implantation CM+ measurements, to determine their relationship to the control group, or to the pre-implantation measurements within each group, to determine changes after implantation. It was important for DAPS maturation to outperform the standard growth conditions (CM+) and to improve over time after in vivo implantation. Data were analyzed by analysis of variance, and Bonferroni's method was used to make post-hoc comparisons ($p < 0.05$). Data are displayed as mean \pm standard deviation.

In order to draw conclusions from this large data set, a simple scoring system was devised to determine the best media condition for pre-maturation. Categories were based on each assay (T2, MTT, Alcian blue staining, picosirius red staining) and for each, two comparisons were made (to the CM+ group at week 5, and within the group to W5). Points were assigned to each category based on a statistically significant difference (MTT, MRI) or an increase in staining intensity; "+1" was added for an increase in MTT absorbance (increase in metabolic activity), decrease in T2 relaxation time (increase in matrix accumulation), or increase in staining intensity (increase in collagen or GAG); "-

1” was assigned for a decrease in these measurements; “0” was added to indicate no difference in the comparison. The scores were tallied for both the AF and NP regions to develop a cumulative score indicative of the success of the pre-culture to implantation strategy.

8.3 Results

8.3-1 Histological appearance of DAPS before and after implantation

Overall, CM conditions were most conducive to DAPS in vitro growth, SM conditions improved DAPS maturation after implantation, and DAPS cultured in the CM++ condition performed well both in vitro and in vivo [Fig. 8-2]. There were substantial differences in SM groups compared to CM groups with in vitro culture. DAPS from CM conditions were considerably larger at every timepoint, especially in the NP region, suggesting that CM is better for the in vitro growth of these constructs. After implantation, DAPS cultured in every condition increased in collagen staining in the AF. For the CM+ and CM++ groups, the only groups with significant NP growth in vitro, there was also an increase in NP collagen staining post implantation. The CM++ group demonstrated substantial AF and NP growth in vitro and continued with this trend after implantation, where both GAG and collagen staining in the AF and NP either persisted or increased.

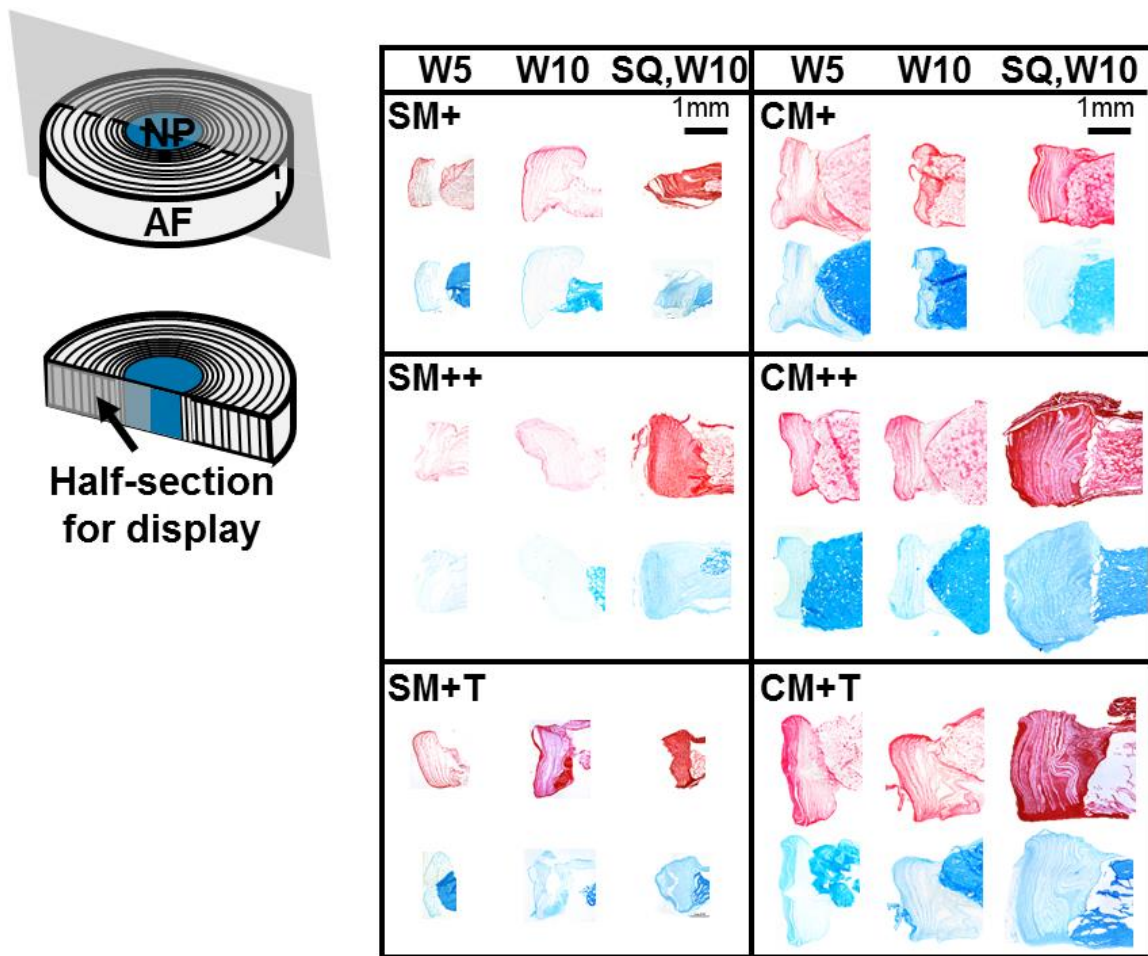


Figure 8-2 – Picrosirius red (collagen) and Alcian blue (proteoglycan) staining DAPS were sectioned after 5 and 10 weeks of *in vitro* culture (W5, W10) or after 5 weeks *in vitro* and an additional 5 weeks of subcutaneous implantation (SQ, W10). Sections were stained with picrosirius red for collagen and Alcian blue for proteoglycans. One half-section is displayed for each condition. Each of the six pre-culture conditions are represented here; the difference in size and staining intensity between SM and CM groups is evident; SM conditions were not conducive to growth *in vitro*. All implants demonstrated increased collagen staining after the implantation; GAG staining after implantation was dependent on the pre-culture condition. The CM++ condition produced DAPS with the best histological characteristics after implantation.

For the SM conditions, there was little to no growth in DAPS size and minimal accumulation of extracellular matrix in vitro. There was, however, an increase in GAG and collagen in both the AF and NP regions after implantation. For the CM groups, CM+ was favorable for DAPS growth in vitro, but these constructs either did not retain the GAG and collagen produced in vitro or did not produce new GAG and collagen in vivo. The CM++ condition outperformed all others, with successful in vitro growth and maintenance/improvement in histological appearance after implantation. The CM+T condition, similar to the other serum conditions, was not conducive to growth in the NP region, but showed positive results in the AF region after implantation.

8.3-2 Measurements of DAPS metabolic activity before and after implantation

The transition to the in vivo environment proved difficult for cells within DAPS to maintain pre-culture levels of metabolic activity [Fig. 8-3]. In all groups except SM+ and CM+, there was a decrease in metabolic activity between weeks 5 and 6. However, in most cases, levels either rebounded or were maintained after week 6. Conversely, in both the SM+ and CM+ groups, the effect of transitioning in vivo was not detrimental, as the SM+ group actually improved after implantation, while the CM+ maintained pre-implantation levels. The negative impact of transitioning may have actually been due to withdrawal from TGF- β 3, as DAPS in the SM++, SM+T, CM++, and CM+T conditions cultured in vitro in parallel to the subcutaneous implantations (which had TGF- β 3 removed from media prior to implantation) also decreased between weeks 5 and 6.

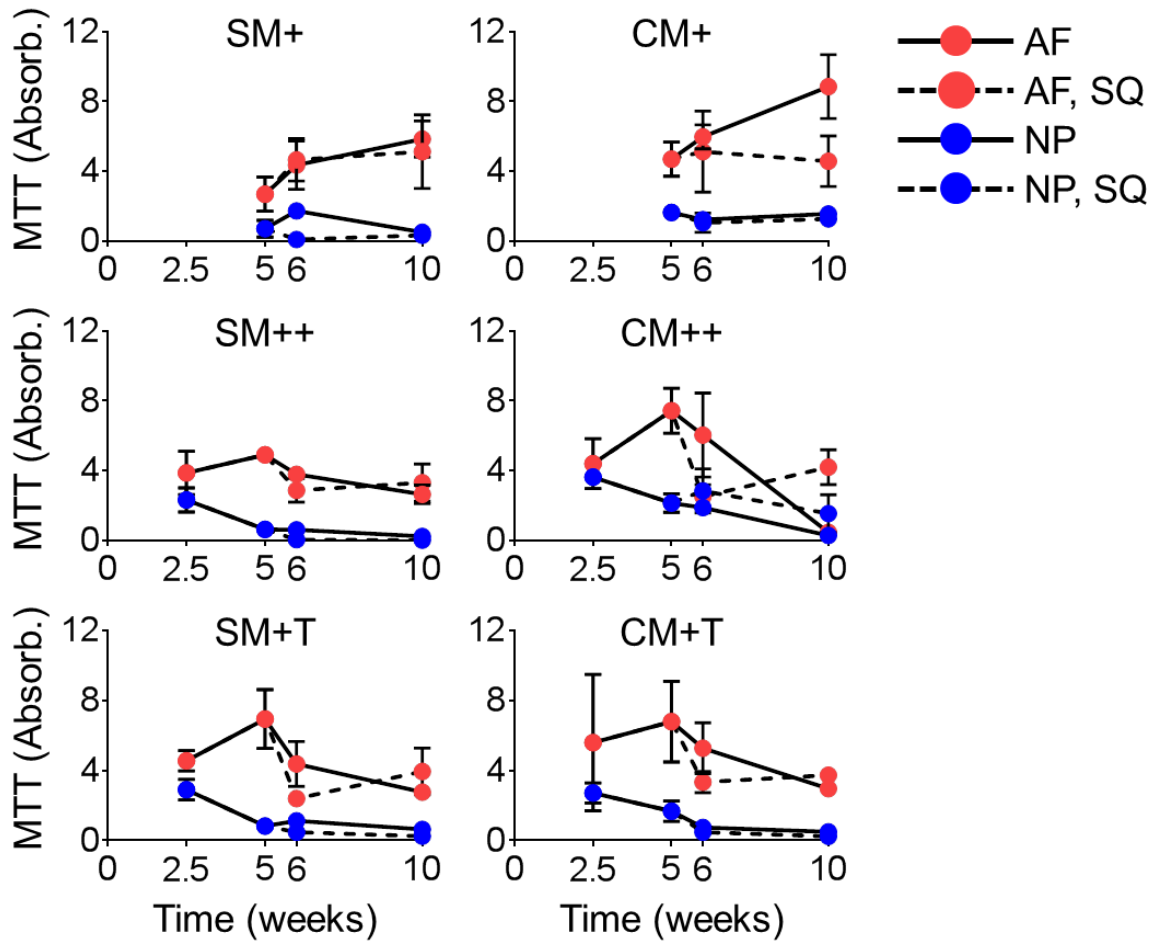


Figure 8-3 Detailed MTT (metabolic activity) results The MTT assay was performed on the DAPS AF and NP regions at each timepoint to measure changes in metabolic activity in each media condition; an increase in absorbance indicates higher metabolic activity. Statistical analysis is displayed in Figure 8-4.

A summary of these results with statistical analysis [Fig. 8-4a-b] demonstrates that, in comparison to the standard growth condition (CM+), over 5 weeks of implantation there are no decreases in metabolic activity in the AF for all groups, while in the NP region there are significant decreases in every group except CM+ and CM++ [Fig. 8-4a]. In looking at the change after implantation within each group, there were moderate decreases in metabolic activity in the AF region of all groups except SM+ and CM+, and no significant changes in the NP region in the SM+, SM+T, CM+ and CM++ groups [Fig. 8-4b].

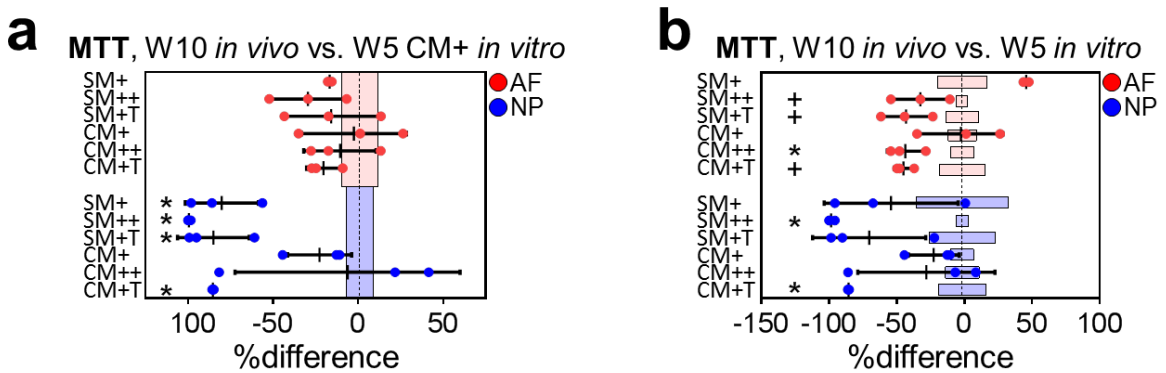


Figure 8-4 Summary of MTT (metabolic activity) results Metabolic activity was measured over time and comparisons were drawn to either the week 5 CM+ group or within each group from week 5 to week 10 to track changes after implantation. Light blue and red bars about 0 indicate the standard deviation of the control group. In all cases: *, $p < 0.05$ and +, $p < 0.1$ vs. control. **(a)** Compared to CM+ growth, there were no differences in metabolic activity in the AF region after implantation, while in the NP region, there was significantly less activity in all groups that included serum (SM+, SM++, SM+T, and CM+T groups). **(b)** After implantation, there were decreases in metabolic activity in the AF region when TGF was removed *in vitro* (SM++, SM+T, CM++, CM+T), while in the NP region there were decreases in the SM++ and CM+T groups.

8.3-3 DAPS matrix accumulation before and after implantation as quantified by T2 MRI

The T2 relaxation time, which correlates to the amount of water within the construct, decreased as extracellular matrix was deposited and replaced free water as the construct matured. This is evidenced by decreases in the AF region T2 after implantation for all groups and the concurrent increase in collagen-positive staining in the same region [Fig. 8-5]. Thus, T2 can be used as a numerical quantification and confirmation of histological findings.

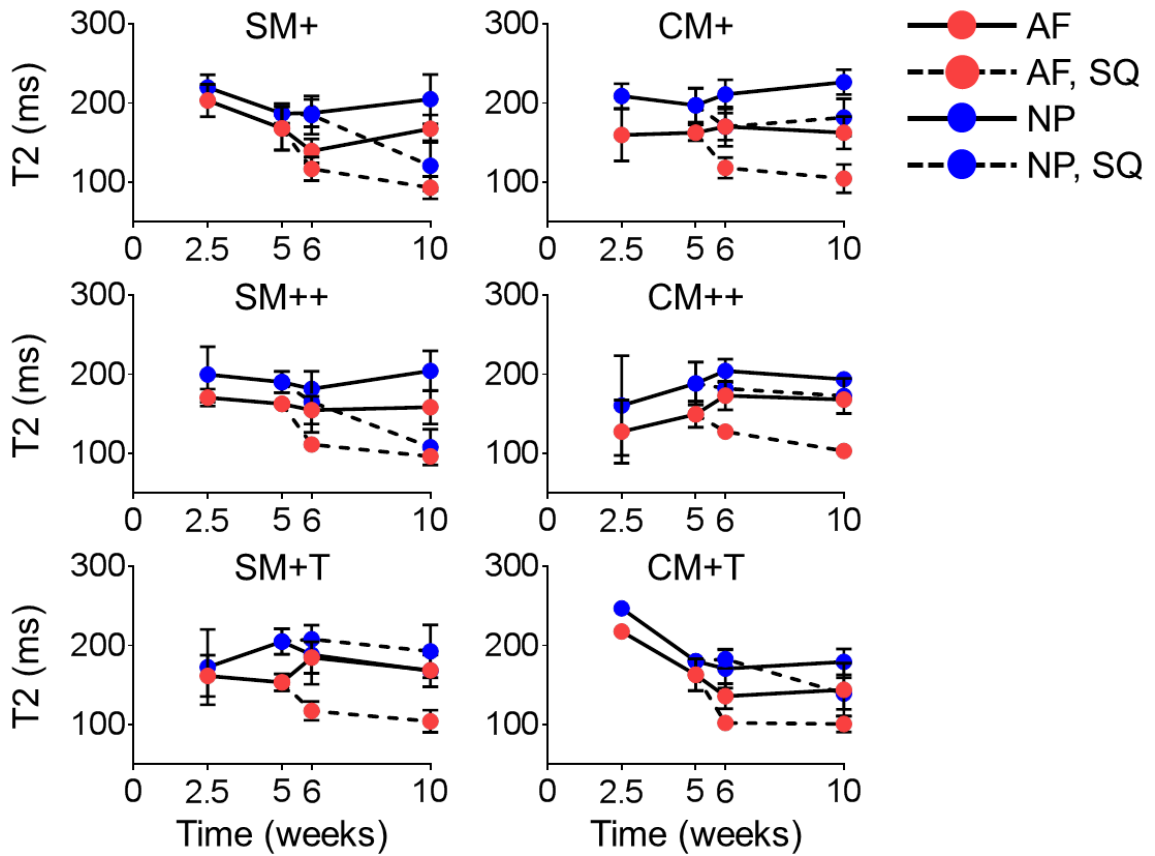


Figure 8-5 Detailed T2 MRI (composition) results The mean T2 relaxation time was calculated for the DAPS at each timepoint by manually segmenting the AF and NP region; a decrease in T2 signified an increase in matrix deposition.

For further validation of the use of T2 in this capacity, in the SM+ group, T2 decreased in both the NP and AF regions during in vitro culture from weeks 2.5 to 5, and then continued to decrease after implantation, which corresponds to increased GAG and collagen staining. In addition, long term in vitro culture of this group revealed increases in T2, matching the lack of matrix deposition demonstrated in histological sections from week 10. In the CM+ group, the results also matched what was demonstrated histologically, as after implantation T2 decreased in the AF region, where more collagen was present, but did not change in the NP region, where NP deposition did not improve.

A summary of the T2 results with statistical analysis [Fig. 8-6] shows that T2 decreased in the AF region of all groups after implantation, matching histological outcomes of increased collagen in this region in all groups. In the NP region, there was a decrease in T2 in the SM+ and SM++ groups, and a trend towards a decrease in the CM+ group after implantation. Pre-implantation levels were maintained in the SM+T, CM++ and CM+T groups.

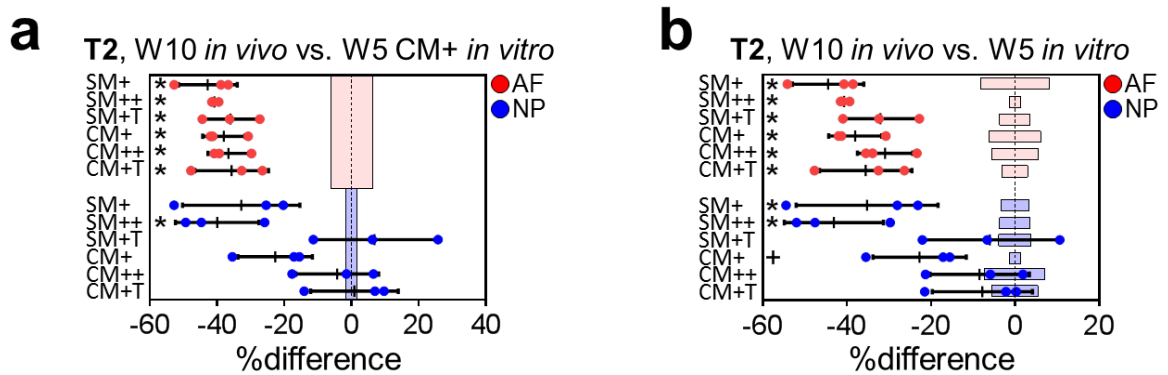


Figure 8-6 Summary of T2 MRI (composition) results Composition was quantified over time through T2 MRI scanning and comparisons were drawn to either the week 5 CM+ group or within each group from week 5 to week 10 to track changes after implantation. Light blue and red bars about 0 indicate the standard deviation of the control group. In all cases: *, p < 0.05 and +, p < 0.1 vs. control. **(a)** In all groups, T2 was lower (more matrix accumulation) in the AF region after implantation in comparison to the CM+ week 5 control group. In the NP region, T2 was lower only in the SM++ group. **(b)** After implantation, T2 decreased in the AF region of all groups (again, indicating more matrix accumulation) and decreased in the NP region in the SM+, SM++ and CM+ groups.

8.3-4 Summary of results based on scoring system

In order to draw conclusions from this large data set, a simple scoring system was used to compare groups [Table 8-1]. DAPS cultured via the CM++ strategy outperformed all others with uniformly distributed collagen in both the AF and NP regions, high proteoglycan content in the NP, and stable metabolic activity and T2 signal. All strategies were conducive to growth in the AF region after implantation, but only the CM+ and CM++ strategies were conducive to a healthy NP phenotype, though they both mildly decreased in GAG staining after subcutaneous implantation.

Table 8-1 Scoring System For Determining Best Pre-culture Condition

AF	MTT, W10 in vivo vs. W5 in vitro	MTT, W10 in vivo vs. W5 CM+ in vitro	T2, W10 in vivo vs. W5 in vitro	T2, W10 in vivo vs. W5 CM+ in vitro	Alcian Blue Intensity, W10 in vivo vs. W5 in vitro	Alcian Blue Intensity, W10 in vivo vs. W5 CM+ in vitro	Picrosirius Red Intensity, W10 in vivo vs. W5 in vitro	Picrosirius Red Intensity, W10 in vivo vs. W5 CM+ in vitro	AF Score
SM+	=	=	+	+	-	+	+	+	4
SM++	-	=	+	+	+	=	+	+	4
SM+T	-	=	+	+	+	+	+	+	5
CM+	=	=	+	+	-	-	+	+	2
CM++	-	=	+	+	+	+	+	+	5
CM+T	-	=	+	+	+	=	+	+	4

NP	MTT, W10 in vivo vs. W5 in vitro	MTT, W10 in vivo vs. W5 CM+ in vitro	T2, W10 in vivo vs. W5 in vitro	T2, W10 in vivo vs. W5 CM+ in vitro	Alcian Blue Intensity, W10 in vivo vs. W5 in vitro	Alcian Blue Intensity, W10 in vivo vs. W5 CM+ in vitro	Picrosirius Red Intensity, W10 in vivo vs. W5 in vitro	Picrosirius Red Intensity, W10 in vivo vs. W5 CM+ in vitro	NP score	Total score
SM+	=	-	+	=	-	-	-	-	-4	0
SM++	-	-	+	+	+	-	+	-	0	4
SM+T	=	-	=	=	-	-	+	-	-3	2
CM+	=	=	+	=	-	-	+	+	1	3
CM++	=	=	=	=	=	-	+	+	1	6
CM+T	-	-	=	=	-	-	-	-	-6	-2

8.4. Discussion

In many cases, engineered tissues do not retain their pre-implantation phenotype after introduction in vivo. This is likely due to the stark differences between the amenable in vitro culture environment, with high concentrations of media components conducive to cell proliferation and metabolism, and the harsh inflammatory and nutrient deprived in vivo environment. Six strategies were evaluated to identify pre-culture conditions conducive to maturation in vitro and phenotype maintenance in vivo, using DAPS (an engineered intervertebral disc) and a subcutaneous implantation model. I found that a scheme incorporating a transient high dose of TGF- β 3 in a chemically-defined media (CM++ group) promoted the best deposition of GAG and collagen in DAPS in vitro, maintenance of accumulated matrix in vivo, and minimal changes in the metabolic activity of cells within the construct.

Subcutaneous implantation was conducive to collagen formation in all implants, while GAG production was dependent on the pre-culture medium formulation. After implantation, there was an increase in AF collagen staining in all media conditions, and an increase in NP collagen staining in conditions conducive to NP growth (CM+ and CM++). In terms of GAG production, it may be that a single, powerful phenotype driving event (a one week high dose of TGF- β 3) imparts a sustainable phenotype, whereas a continuous, less powerful series of events (continuous supplementation of low dose TGF- β 3) does not. This was this case in studies on chondrocytes and MSCs in hydrogel culture with a transient high dose of TGF- β 3, which was sufficient to lock in the chondrogenic phenotype over a period of months, even though TGF- β 3 was only administered for 1-2

weeks [114, 181]. This may explain the success of the CM++ group after implantation and future work should characterize mRNA expression before and after implantation using this strategy. Another explanation is that the abrupt removal of TGF- β 3 (CM+ group) at implantation diminishes a cells potential in vivo, a phenomenon that does not occur when culturing in serum-containing media. This was true of human MSCs pre-differentiated in chemically-defined media with TGF- β 1 for 3 weeks and implanted subcutaneous as a micromass. In that study, there was a decrease in toluidine blue (GAG) staining and a decrease in cell viability after implantation [52]. In another study, MSCs were pre-differentiated in chemically-defined media with TGF- β 3 and BMP-6; these cells also lost their phenotype after subcutaneous implantation, with a reduction in GAG and type II collagen, and an increase in alizarin red indicative of hypertrophy [53]. This was also true of fully differentiated cells; chondrocytes encapsulated in hydrogels pre-cultured in chemically-defined media with TGF- β 3 maintained the collagen produced during pre-culture, but showed a depletion of GAG after implantation [237]. Taken together, these data suggest that culture using the CM+ formulation, while important for identifying aspects of chondrogenesis in vitro, may not be practical or useful for in vivo translation of engineered tissues.

In vitro culture with serum is not conducive to functional and compositional maturation, while chemically-defined media enhance matrix accumulation, increase physical size, and improve metabolic activity in cultured engineered discs. In another study, NP cells encapsulated in hydrogels were cultured with TGF- β 3 in either chemically-defined or serum-containing media; gels in chemically-defined media with

TGF- β 3 developed a chondrogenic phenotype and compositionally and functionally outperformed gels cultured in parallel in serum-containing media [202]. It may be that serum increases the turnover rate of extracellular matrix components, as high levels of cleaved aggrecan were measured after culture of NP cells in serum-containing media with TGF- β 3 [203]. FBS contains many growth factors that contribute to cell proliferation, differentiation, and matrix production, including those of the Insulin-like growth factor family, fibroblast growth factor family, as well as the factors from the TGF family [253]. It may be that, in serum, finite resources within the cell are diverted to respond to these other signals, interfering with the main action of TGF- β 3. In contrast, in defined media, TGF- β 3 may be able to drive chondrogenesis and matrix accumulation without interruption. In addition, FBS contains lipopolysaccharides, which are implicated in rheumatoid arthritis [92] and provoke an inflammatory response in NP cells [135]; this molecule may oppose the anabolic signal from TGF- β 3. Though TGF- β 3 was originally employed as a molecule to induce differentiation of mesenchymal stem cells, it has a significant effect on the behavior of fully differentiated cells, an effect that is mitigated in serum.

In two chemically-defined media conditions, CM⁺ and CM⁺⁺, DAPS maintained a healthy NP phenotype after implantation while, in all other cases (where DAPS were exposed to serum), cells in the NP region did not produce matrix. In serum conditions, cells may have actively contracted or degraded the gel, as histological sections show a decrease in NP dimensions after culture (radius <1 mm in all cases) as compared Day 0 (1 mm). In other cases when this hydrogel was exposed to serum, for example, in an in

vivo rat tail disc replacement model [147] and an in vivo pig osteochondral defect model [64], HA was also degraded, while in subcutaneous models such as this one and others [25, 26], where little bleeding occurs surgically, the hydrogel remains intact. In these in vivo systems, it may be that local inflammation, as communicated through the blood within the wound site, induces the activation of hyaluronidase by implanted cells or local endogenous cells to break down the gel. Circulating hyaluronidase in the blood may also play a role. Hyaluronidase activity in these constructs should be measured in future work for confirmation, and a more stable hydrogel, such as agarose, which is not susceptible to hyaluronidase-mediated degradation, may be useful as a substitute for HA for tissue replacement.

There are three primary limitations of this study; the infiltration of endogenous cells, which may affect matrix accumulation after implantation, was not characterized, and T2 MRI, an indirect method of quantifying extracellular matrix deposition, was used to evaluate DAPS maturation, and a subcutaneous implant model was adopted for high throughput. Implanted DAPS with little matrix accumulation in vitro have significant space available for the infiltration of endogenous cells; DAPS cultured with the SM strategies had poor matrix production in vitro. Thus these implants were at risk for colonization by host cells, which would subsequently engraft and produce collagen. However, the inability of these conditions to mature constructs in vitro precludes serum conditions from being useful for translation. Cell-tracking methods with fluorescent dyes and proteins are available for this purpose, and will necessarily be performed in future work. For the analysis of matrix accumulation by T2 MRI, I made the assumption that water is replaced during maturation of the engineered tissue with extracellular matrix,

and that high T2 values correspond to high water content and consequently an immature tissue. There is one complicating factor, however; increased GAG content with maturation would likely increase water content as GAGs are highly hydrophilic. Early Day 0 measurements of DAPS T2 revealed that T2 values in the AF and NP were between 250-300 ms (data not shown), much higher than those measured after maturation. Water sequestered by GAGs after maturation does not seem to generate a T2 signal as high as free water within the hydrogel. Further confirmation of this by direct measurement of GAG and collagen is necessary. In addition, T2 is a non-invasive and clinically-relevant method for evaluating matrix content of a tissue, and a method that is useful for in vivo animal models and ultimately clinical trials. For these reasons, T2 is an important tool for these experiments. A final limitation is that implants were evaluated in a subcutaneous implantation model, which allows for multiple implants per rat and reduces the number of animals required for these studies, but does not have all the characteristics of an orthotopic disc replacement model, for example the juxtaposition of vertebrae. Future work will evaluate the best strategy, CM++, as a pre-culture method before in situ total disc replacement.

8.5. Conclusion

Previous results demonstrated that a transient high dose of TGF- β 3 improves the in vitro chondrogenesis and matrix production of MSCs and chondrocytes. Here, this strategy (CM++ group) improved both in vitro maturation and in vivo phenotype retention of disc-cell-laden DAPS. Other strategies were not as effective; DAPS cultured

in serum improved compositionally in vivo, but did not mature in vitro, especially in the NP region. Additionally, transition strategies (SM+T and CM+T groups) reinforced that serum was not compatible with maturation of the NP region. Interestingly, all groups showed increased collagen production after implantation, possibly in response to factors secreted by endogenous cells or as a result of infiltration by immune cells or fibroblasts. These findings define the most favorable pre-culture strategy (CM++) for DAPS development before and after implantation. In the future, another student should quantify proteoglycan and collagen composition for each condition, evaluate the CM++ strategy in terms of mRNA expression, and ultimately determine whether the CM++ pre-culture strategy improves the in vivo performance of engineered discs that are implanted into the intervertebral space.

CHAPTER 9 – Summary, Future Directions and Conclusions

9.1 Summary

My global hypothesis for this work was that engineered, viable intervertebral disc replacements can restore normal spine function. Building off earlier work from our lab in which disc-like angle ply structures (DAPS) for total disc replacement were designed and evaluated preliminarily in vitro, in this series of experiments, I developed a rat model of total disc replacement to evaluate DAPS in vivo. In developing this model, I designed an external fixation device to stabilize adjacent vertebrae of the rat tail and a radiopaque scaffold to fluoroscopically confirm implant retention. Radiopaque DAPS were implanted using external fixation and tracked fluoroscopically; no migration occurred after 4 weeks, confirming the utility of this model for evaluating engineered discs. I next focused on cell-seeding and in vitro culture of DAPS, using either AF and NP cells or MSCs, and found that DAPS seeded with disc cells or stem cells both compositionally and functionally matured reaching or exceeding many native tissue benchmarks. Over long-term culture, timepoints related to an immature/rapidly-growing phase of growth and a mature/stable phase of growth were identified and AF/NP cell-seeded DAPS were implanted into the rat tail using these pre-culture criteria. There were dynamic alterations to the DAPS after implantation; there was a depletion in GAG that had accumulated in vitro, remodeling of the NP region, infiltration of endogenous cells and tissue, and minimal vertebral integration. Despite these changes, vertebra-DAPS-vertebra motion

segments matched native tissue mechanical properties in compression. In tackling the first of these issues, the reduction in GAG after implantation, I evaluated six pre-culture strategies to identify which best prepared the implant for the in vivo environment, confirming that pre-culture in chemically-defined media with a high, transient dose of TGF- β 3 best prepared cells within DAPS for the harsh in vivo conditions. To conclude, in my work, the most promising finding was that DAPS matched the compressive moduli of the native disc, and though I have identified some limitations of the implant design, this mechanical competency validates my global hypothesis that engineered biological disc replacement is a real possibility for functional restoration of the intervertebral joint.

9.2 Future Directions

To realize the ultimate goal of biologic total disc replacement, future work must focus on the implant deficiencies described above: phenotype retention, NP degradation, and vertebral integration. The biostimulatory effects of dynamic, multidirectional mechanical loading on live DAPS should be evaluated, DAPS must be evaluated in a large animal model, and finally DAPS scaled up to human size with human cell sources must be evaluated.

In terms of phenotype retention, I took the first step in solving this problem by identifying a useful pre-culture strategy and determining its success in a subcutaneous model. Confirming the efficacy of this strategy in situ, where exposure to blood, circulating cells, and serum components appears to be an impediment to implant performance, is the most relevant next step for evaluating this pre-culture strategy.

The hyaluronic acid (HA) hydrogel that formed the NP degraded after implantation, and while degradation and replacement of the biomaterials with endogenous tissue is warranted after long-term implantation, the rate at which degradation occurred was unfavorable for implant performance. HA degradation may be a result of a local inflammatory process and the production of hyaluronidase; quelling inflammation may result in improved HA performance. Also, it may be useful to modify HA; increasing the number of crosslinks and thus reducing the number of exposed sites for hyaluronidase-mediated degradation will improve the in vivo stability of the implant, but may affect cell viability, proliferation, and matrix production, as cell-HA interactions are known to be bioactive. New materials, particular those that are not degradable in vivo, may be useful in pre-clinical models to better evaluate implant performance. There is an ever-growing list of biomaterials that may be useful for the NP region, as well as the AF region. The material selection should be optimized to promote successful in vitro growth, sufficient in vivo mechanical support and phenotype retention, and minimize the endogenous foreign body response. Some biomaterials of particular interest at this stage are silk, agarose, and dextran, but more will likely be identified. One additional point, in terms of the AF materials, electrospun PCL as-spun is very dense and cells have a difficult time penetrating the layers. One way to speed this process, as demonstrated previously by our lab, is to fabricate mats with stable PCL and soluble PEO fibers within one layer. Removing the PEO layers increases the porosity, and may speed tissue infiltration and improve the overall nutrient permeability of the engineered tissue.

The integration of engineered soft tissues into native bone is currently a highly active area of study in musculoskeletal tissue engineering, and will be important for disc tissue engineering. Implanted DAPS integrate well into the adjacent soft tissue, but no integration was evident into the adjacent vertebrae, a significant limitation of the current technology. Engineered endplates that are osteoconductive may be attached or cultured in apposition with DAPS to improve integration. Some preliminary results that I have generated (not shown) suggest that a porous PCL foam cultured in apposition with DAPS will form tissue at the DAPS/foam interface during *in vitro* culture.

Dynamic mechanical loading, which was neglected in these studies due to use of the external fixation system, will play an important role in evaluating the engineered disc moving forward. Pre-maturation of the construct can be enhanced through dynamic loading *in vitro*; it may shift the growth trajectory, increase the overall rate maturation, reduce the pre-culture duration and improve *in vivo* integration. A combination compression-torsion bioreactor may be useful for these purposes [Fig. 9-1].

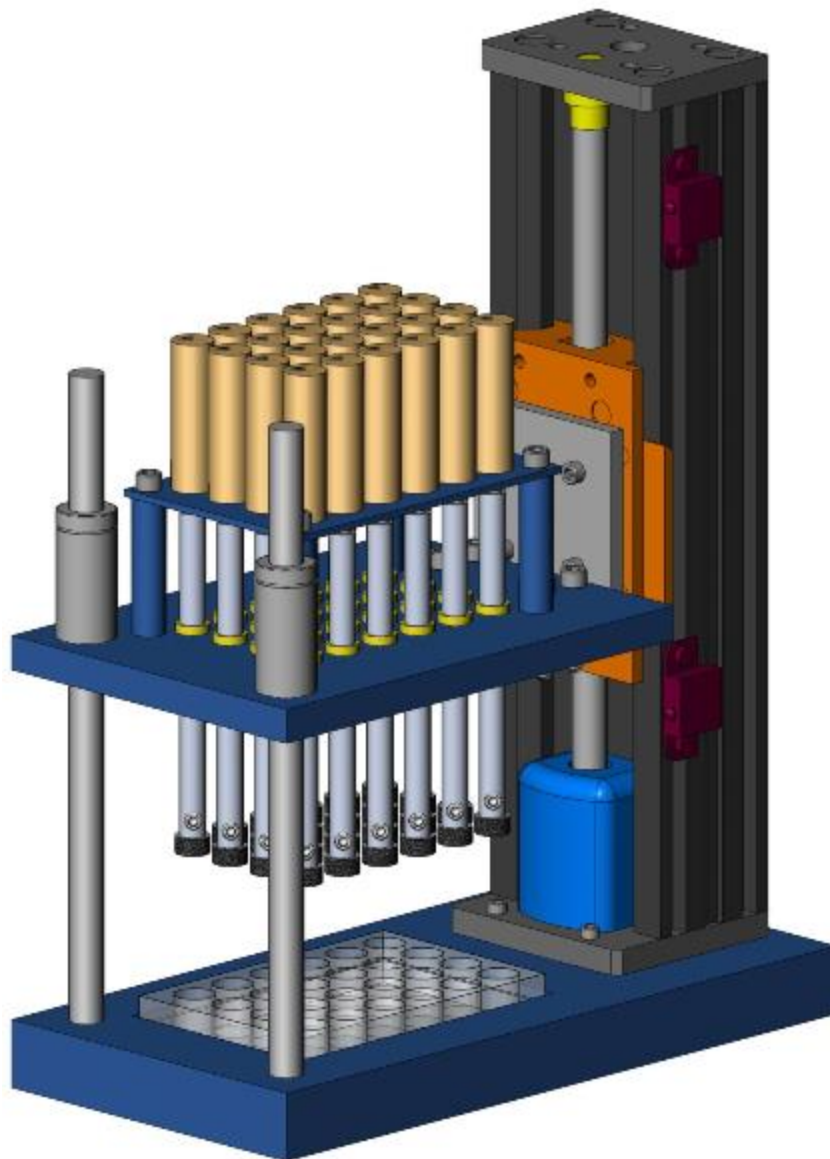


Figure 9-1 Combination Compression-Torsion Bioreactor Here, I demonstrate the design of a bioreactor system that combines compression and torsion load for mechanical stimulation of DAPS in vitro. An array of 24 stepper motors provides oscillatory motion for torsional loading, while a single larger stepper motor raises and lowers a stage to apply compression loads.

Dynamic loading will also play an important role in vivo; for example, remobilization of the implantation site by removing the external fixation device will resume physiological loading and may have a biostimulatory effect. A period of integration after implantation will first be required, perhaps 5 weeks (when DAPS demonstrated mechanical competency ex vivo), at which point the external fixation device can be removed. DAPS support of long-term in vivo loading has yet to be evaluated in terms of mechanical fatigue, as well; this may be a future direction for mechanical analysis.

Before moving to clinical trials, a cervical or lumbar spine of a large animal model is a critical next step for in vivo evaluation of DAPS. This will open up new avenues of implant evaluation through functional outcome measures like gait analysis and joint kinematics, which were not possible using the aphysiologic externally-fixed rat tail model. My personal opinion is that the complete restoration of joint kinematics is likely the most important outcome for musculoskeletal tissue engineering. Of course, patients report to clinic because they have pain, and pain reduction and return to activity are the ultimate clinical goals. The restoration of joint kinematics is the foundation on which pain can be relieved; inappropriate kinematics causes stress in other tissues and joints, wearing of articular cartilage, inflammation and ultimately the tissue degeneration. It may be that, following tissue replacement, spinal nerve sensitization, muscle weakness, or arthritis in adjacent joints still linger; restoring joint kinematics is the first priority for total disc replacement, but secondary treatments may be necessary to resolve these problems.

Eventually, DAPS must be formed to match human dimensions and seeded with human cells for clinical translation. The maturation of engineered tissues in vitro is

closely tied to the ability of nutrients from the media to diffuse through the tissue and reach the deepest regions. Increasing the size of an engineered tissue increases the diffusion distance and limits nutrients to deeper areas. Scaling DAPS to human size will certainly create this problem. Assuming restrictions to diffusion occur along the shortest dimension, in the case of DAPS, height will be the limiting factor to diffusion; currently, our lab has grown rat-sized implants (2 mm height, as in this dissertation) and rabbit-sized implants (3 mm height, [179]) with much success. Human-sized implants will be on the order of 10 mm in height, greatly increasing the diffusion distance. It remains to be seen whether this will limit growth, though some strategies are available to deal with this potential problem; mechanical stimulation is known to improve nutrient flow into tissues through convection, DAPS permeability can be improved by including channels or electrospinning an additional sacrificial fiber layer to improve porosity, and perhaps cells can be primed to function in oxygen and glucose deprived conditions. Human cell sources will need to be evaluated in future work. Some directions research on human cell sourcing could take include evaluating human MSCs, evaluating cells from degenerated human discs and methods to restore a healthy phenotype, and evaluating induced pluripotent cells and their ability to adopt a disc-like phenotype. This is an exciting area for future research.

9.3 Conclusions

When I arrived in the lab, an engineered intervertebral disc had been developed and preliminary in vitro culture had been performed to demonstrate its compatibility with cells. I built upon this innovative work by characterizing the long-term in vitro

performance of the disc and evaluating it in an animal model of total disc replacement. There were some very promising results, for example, the implant matched the compressive mechanical properties of the native disc. In addition, along the way, I developed some tools that will be useful for future studies: an animal model of total disc replacement, a radiopaque scaffold, an optimized pre-culture strategy, and mechanical and MRI analysis protocols. There are also some areas in which these engineered discs require improvement, namely, phenotype retention, vertebral integration, and NP stability. I have confidence that by solving the problems I laid out above, engineered disc replacement will be a real clinical alternative to intervertebral fusion in the future.

APPENDIX I – Development of a Quantitative MRI Analysis Protocol: Population Average T2 MRI Maps Reveal Quantitative Regional Transformations in the Degenerating Rabbit Intervertebral Disc that Vary by Lumbar Level

I.i Preface

In Appendices I and II, I describe two side projects I worked on, developing two disc degeneration models, one in rabbits and one in mice. These studies are published in [145, 146]. While the specific results of these studies are not directly related my work with DAPS, the assays I developed for MRI and mechanical analysis were later applied to evaluate DAPS after in vivo implantation. In Appendix I, I describe a method for developing average T2 MRI maps for a population of rabbit lumbar discs degenerated by needle puncture. Averaging T2 maps will later to be used to develop timepoint average T2 maps to track changes in DAPS composition over time.

I.1 Introduction

Towards developing therapies for disc degeneration, animal models are commonly used to assess degenerative changes and the efficacy of proposed therapeutics. In these models, degeneration can be induced by injuring the annulus fibrosus (AF) with a scalpel or needle, which depressurizes the nucleus pulposus (NP) and triggers a

physiological response that closely resembles human disc degeneration. AF injury has been conducted and validated in many species [89, 109, 146, 191], with the rabbit model among the most common [153, 171, 210, 224].

Rabbit discs closely resemble human discs in composition and structure, and their response to puncture injury closely resembles human degeneration. Glycosaminoglycan (GAG)[20] and collagen [213] contents of both the NP and AF of healthy rabbit lumbar discs are similar to non-degenerate human lumbar discs. In addition, puncture injury results in compositional, cellular, structural, and mechanical changes that resemble human degeneration. Specific examples of puncture-induced modifications similar to human degeneration include the loss of NP GAG [126, 172], pro-fibrotic changes in mRNA expression [172], structural changes inclusive of a shift from bulging AF lamellae to serpentine lamellae [45], and mechanical changes at both the whole disc level [126, 164] and the tissue level [77].

Magnetic resonance imaging (MRI) allows for the quantitative, non-invasive assessment of soft tissues like the intervertebral disc and, consequently, is used to identify pathological changes in the disc. In the healthy disc, signal intensity on T2-weighted MR images is highest in the central, hydrated NP and dissipates radially with transition to the fibrocartilaginous AF [196]. With degeneration, there is a characteristic loss of NP signal intensity and consequently the NP and AF become indistinguishable [196]. These abnormalities are typically assessed by visual inspection of MR images or by qualitative evaluations on an integer scale, like the Pfirrmann or Thompson grading frameworks [196, 231]. In addition, clinicians routinely evaluate candidates for surgery

using MRI to identify disc abnormalities in the presence of radicular and/or low back pain, and, while these scoring systems provide some level of discrimination between degenerative states, they do not provide quantitative information on T2 signal or positional information regarding the location of the compositional changes.

T2 relaxation time is a physical property related to tissue water content and can be quantitatively measured in vivo with MR imaging. This has been well described in articular cartilage [136, 169, 170, 221], and more recently, the disc [142, 143]. Rigorous spatial quantification of T2 MR images may allow for improved discrimination between age-based sub-populations or degenerate sub-populations (populations with early versus advanced degeneration) by identifying changes in disc shape, structure and composition. Furthermore, the development of quantitative outcomes that enable non-invasive assessment of degeneration is critical for longitudinally evaluating therapeutics.

The objective of this study was to spatially map changes in T2 relaxation time as a result of puncture-initiated degeneration in the rabbit. To do so, rabbits were imaged before and after puncture to generate population average T2 maps of the healthy and post-injury state. Additionally, an auto-segmentation procedure was developed to enable objective observer-independent isolation of the NP. I hypothesized that population composite images would identify specific changes with degeneration as a function of disc level (i.e., change in NP area and T2 values), as well as morphologic changes such as the disappearance of the intranuclear cleft, a region of lower T2 signal intensity at the center of the NP [3].

I.2 Methods

I.2-1 Surgical procedure

With local institutional approval, 20 New Zealand White rabbits (3 mos., 2.5-3.0 kg, Charles River Laboratories, Wilmington, MA) underwent a procedure in which four lumbar discs (L3/L4 to L6/L7) were injured by needle puncture to induce degeneration [171, 218-220]. Rabbits were tranquilized and anesthetized, and a retroperitoneal approach to the lumbar spine was achieved by incising the skin at the left flank and then the external oblique, and bluntly developing a plane between the paraspinal and psoas muscles. An 18G needle was inserted through the lateral AF a depth of 5 mm controlled by a stopper. Rabbits were returned to normal cage activity and medicated for pain (meloxicam, 0.2 mg/kg) and infection (cefazolin, 22 mg/kg).

I.2-2 Radiographic Analysis

Lateral radiographs were acquired preoperatively and 4 weeks postoperatively for disc height and of spinal curvature analysis [Fig. I-1a]. Resultant images were digitally processed in Matlab to calculate Disc Height Index (DHI) [151, 153] and the relative angles of rotation between vertebrae in the sagittal plane. First, each disc and its corresponding adjacent superior and inferior vertebrae were manually traced for area quantification (A_D , A_{VB1} , A_{VB2}) [Fig. I-1b-c]. Then, a principal components analysis[139] was performed on individual disc and vertebrae shapes. The principal axes generated by this analysis point in the direction of minimum distribution of pixels within the shape, and thus the widths of the vertebrae (W_{VB1} , W_{VB2}) and disc (W_D) could be defined along

the principal axes [Fig. I-1c]. Disc height (H_D) and vertebral length (L_{VB1} , L_{VB2}) were defined as $H_D = A_D/W_D$ and $L_{VB} = A_{VB}/W_{VB}$. DHI was defined as $DHI = 2H_D / (L_{VB1} + L_{VB2})$.

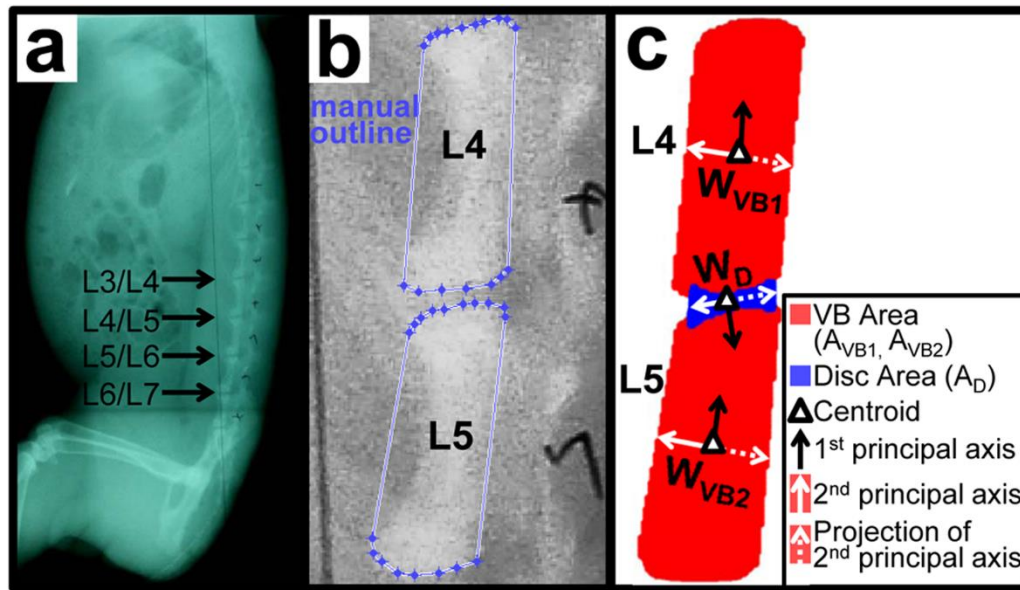


Figure I-1 Radiographic analysis of response to injury (a) Representative lateral radiograph with the location of punctured lumbar discs identified. (b) Manual outline of vertebrae for disc height analysis. (c) Features used for the analysis of disc height, vertebral width (W_{VB1} , W_{VB2}) and disc width (W_D), vertebral area (A_{VB1} , A_{VB2}) and disc area (A_D), and 1st and 2nd principal axes generated by principal components analysis.

I.2-3 MRI Acquisition

In vivo T2 mapping was performed pre-injury and 4 weeks post-injury on each rabbit. A custom MR coil [Fig. I-2a] and a 3.0 T MRI spectrometer (Medspec S300; Bruker Instruments, Ettlingen, Germany) were used to generate coronal T2 maps as measured from a multi-slice, multi-echo acquisition (three 2mm-thick slices, 17 Echoes, TE/TR=7.55ms/2000ms, FOV=16.5x16.5cm², matrix=384x384, 2 averages).

I.2-4 Population Average T2 Maps

Week 0 and Week 4 T2 maps [Fig. I-2b-c] were processed in Matlab to enable quantitative comparisons between groups. Discs were initially manually segmented from coronal slices and mapped to a coordinate system normalized to disc dimensions [Fig. I-2d-f].

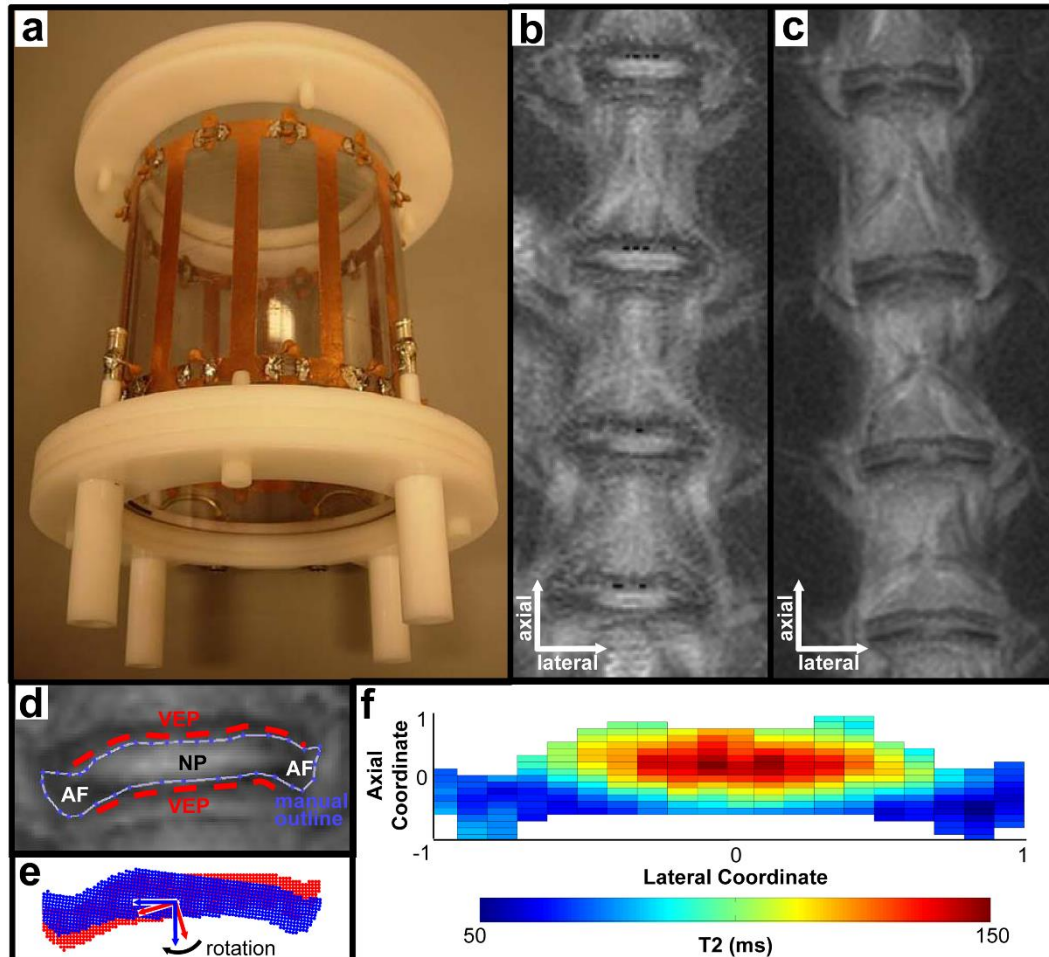


Figure I-2 MRI analysis of response to injury (a) Custom MR coil for imaging the rabbit spine. (b) Week 0 and (c) Week 4 coronal T2 maps. Example of (d) manual segmentation (AF, annulus fibrosus; NP, nucleus pulposus; VEP, vertebral endplate) and (e) rotation of a disc based on axes generated by principal components analysis. (f) Interpolation of a disc T2 map to a regularly spaced grid. The aspect ratio represents the average ratio of disc length to disc width.



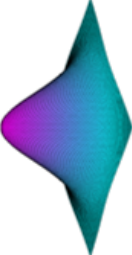
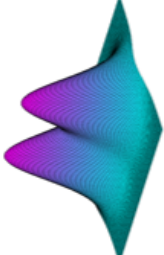
The mapping process began with a principal components analysis of the manually segmented disc shape to identify the long and short axes. Then, the centroid of the disc was set as the origin and the disc axes were rotated to match the vertical and horizontal axes of a rectangular coordinate system. Finally, a grid was defined spanning -1 to 1 in both the axial and lateral disc dimensions, and the T2 map was linearly interpolated to these regularly spaced grid points. By mapping each disc to a grid, population average T2 maps could be developed by averaging the T2 values of discs from the Week 0 or Week 4 groups at each grid point. In addition, T2 difference maps were constructed by subtracting (and subsequently taking the absolute value of) the Week 0 population average map from (1) the Week 4 population average map (to identify the average change post injury), (2) from the Week 4 L3/L4, L4/L5, L5/L6 and L6/L7 population average maps (to identify average change as a function of level), or (3) from Week 4 individual disc maps (to identify deviations of individual discs from the population average). In case (3), for an individual disc, the T2 difference at each pixel was averaged to generate a single numerical quantity that described the degenerative changes following puncture injury.

I.2-5 Auto-Segmentation of the NP by T2 Signal

An automatic procedure was developed to enable non-biased segmentation of the NP based on T2 signal. The area surrounding the NP was first manually segmented to provide an initial guess for curve fitting (lateral boundaries at mid AF, axial boundaries at vertebral endplates). This area was mapped to a normalized grid as described above. Then, to evaluate fitting techniques, four modified Gaussian distribution functions [Table

I-1], two 2-D functions (a *unimodal, univariate* function and a *bimodal, univariate* function) and two 3-D functions (a *unimodal, bivariate* function and a *bimodal, bivariate* function), were fit to T2 data at the disc mid-height along the lateral axis (2-D) or to the full T2 surface along the lateral and axial axes (3-D). This was done for each disc in the Week 0 and Week 4 groups [Fig. I-3]. The mean and standard deviation associated with the Gaussian functions are determined from the fitting procedure and describe the distribution of the NP signal. Using the concept of full width at half maximum, NP boundaries were defined as points where 50% of the max NP T2 signal had dissipated as defined by the curve fit [Fig. I-3a,c]. This concept was expanded to determine NP dimensions with bimodal or bivariate fits [Fig. I-3b,d].

Table I-1 - Modified Gaussian functions used for NP T2 curve and surface fits
 $V_{12} = 1,2$ component of the x,y covariance matrix

Name	Dimensionality	Characteristic shape	Equation	Fit Parameters
Unimodal, Univariate	2D		$T2 = \frac{A}{\sigma\sqrt{2\pi}} \exp\left(-\frac{(x-\mu)^2}{2\sigma^2}\right) + B$	A, B, σ , μ
Bimodal, Univariate	2D		$T2 = \frac{A}{\sigma_1\sqrt{2\pi}} \exp\left(-\frac{(x-\mu_1)^2}{2\sigma_1^2}\right) + \frac{B}{\sigma_2\sqrt{2\pi}} \exp\left(-\frac{(x-\mu_2)^2}{2\sigma_2^2}\right) + C$	A, B, C, σ_1 , μ_1 , σ_2 , μ_2
Unimodal, Bivariate	3D		$T2 = \frac{A}{2\pi\sigma_1\sigma_2\sqrt{1-\rho^2}} \exp\left[-\frac{z}{2(1-\rho^2)}\right] + B$ $z = \frac{(x-\mu_1)^2}{\sigma_1^2} - \frac{2\rho(x-\mu_1)(y-\mu_2)}{\sigma_1\sigma_2} + \frac{(y-\mu_2)^2}{\sigma_2^2}$ $\rho = \frac{V_{12}}{\sigma_1\sigma_2}$	A, B, C, σ_1 , μ_1 , σ_2 , μ_2
Bimodal, Bivariate	3D		$T2 = \frac{A}{2\pi\sigma_{11}\sigma_{22}\sqrt{1-\rho_1^2}} \exp\left[-\frac{z_1}{2(1-\rho_1^2)}\right] + \frac{B}{2\pi\sigma_{21}\sigma_{22}\sqrt{1-\rho_2^2}} \exp\left[-\frac{z_2}{2(1-\rho_2^2)}\right] + C$ $z_1 = \frac{(x-\mu_{11})^2}{\sigma_{11}^2} - \frac{2\rho_1(x-\mu_{11})(y-\mu_{12})}{\sigma_{11}\sigma_{12}} + \frac{(y-\mu_{12})^2}{\sigma_{12}^2}$ $z_2 = \frac{(x-\mu_{21})^2}{\sigma_{21}^2} - \frac{2\rho_2(x-\mu_{21})(y-\mu_{22})}{\sigma_{21}\sigma_{22}} + \frac{(y-\mu_{22})^2}{\sigma_{22}^2}$ $\rho_1 = \frac{V_{12}}{\sigma_{11}\sigma_{12}} \quad \rho_2 = \frac{V_{12}}{\sigma_{21}\sigma_{22}}$	A, B, C, σ_{11} , μ_{11} , σ_{12} , μ_{12} , σ_{21} , μ_{21} , σ_{22} , μ_{22}

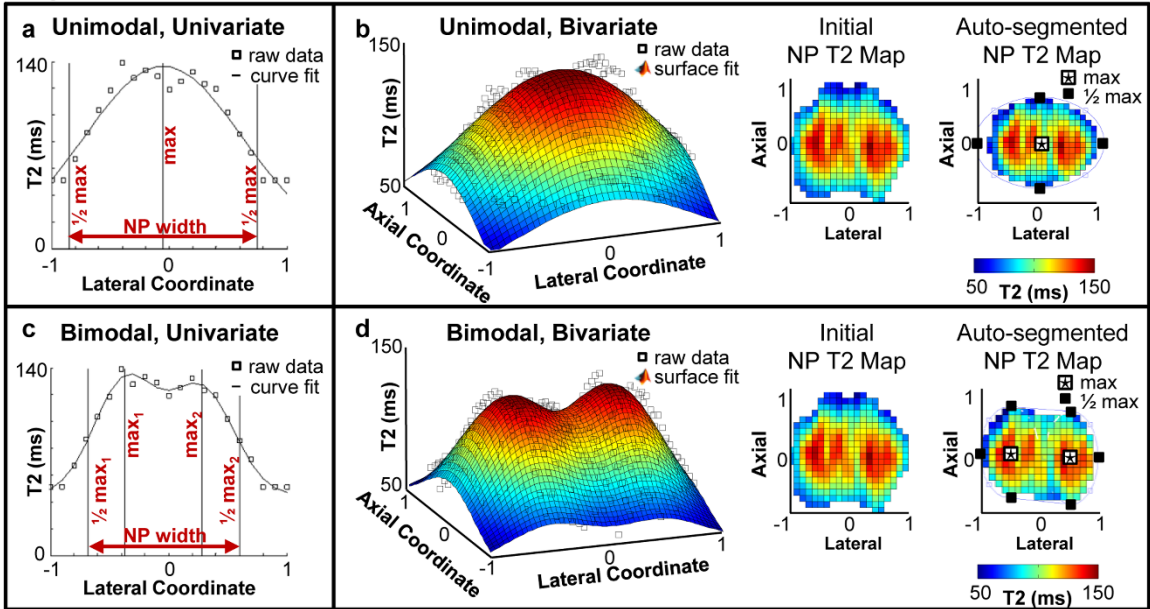


Figure I-3 Gaussian distribution functions for NP auto-segmentation Gaussian distribution functions fit to the NP T2 signal: (a) unimodal, univariate, (b) unimodal, bivariate, (c) bimodal, univariate, and (d) bimodal, bivariate. On each plot, the max and $\frac{1}{2}$ max points are labeled. These landmarks were used to determine the boundaries of the NP. Details on these functions are provided in Table I-1. In (b, d) NP T2 maps are shown before (*Initial NP T2 Map*) and after (*Auto-segmented NP T2 Map*) application of a Gaussian function to determine the NP boundaries.

I.2-6 Calculation of Mean T2 Signal and T2 Volume

From the original raw T2 maps, the mean T2 signal was calculated for the whole disc, the AF, and the NP of all discs. The mean signal from the whole disc T2 map (isolated by manual selection) was quantified by averaging the T2 value at all pixels within the disc. The mean signal from the NP T2 map (isolated by bimodal, bivariate segmentation) was quantified by averaging pixels within the segmented region. The pixels within the disc excluded by auto-segmentation were used to define the AF and the mean AF signal was defined by the average of T2 values in the excluded region. The T2 volume (or volume under the T2 surface) of the whole disc, AF, and NP regions was determined using a method analogous to numerical integration, summing the volume at each pixel, where dimensions are: axial resolution by lateral resolution by T2 value. T2 volume is comparable to the MRI Index (the *average* T2 volume or the product of the total NP area and the mean NP signal intensity) which decreases following puncture injury as both the NP area and NP T2 signal decrease.

To examine inter-observer reliability of the automatic segmentation procedure, two researchers (a PhD student with 6 years experience in spine research and an attending orthopaedic spine surgeon) independently analyzed 10 sets of images from the pre-injury and post-injury groups. Pearson correlation coefficients were calculated to determine the linear correlation between each set of observations. To demonstrate reliability, correlations related to manual outlining were compared to those from automatic segmentation using the bimodal, bivariate Gaussian function, specifically for measurements of mean NP T2 values.

I.2-7 Measurement of Disc Geometry from MR Images

Area, width, and height for the whole disc, the AF, and the NP were determined from the original raw T2 maps for all discs [Fig. I-4]. Whole disc area was defined as the number of pixels within the manually segmented whole-disc region multiplied by the scan resolution. Whole disc width was defined as the maximum distance across the lateral axis of the disc; whole disc height was defined as the whole disc area divided by the whole disc width. NP area, width and height were defined in the same way using the NP area isolated from by bimodal, bivariate segmentation. AF area was defined as the difference between the disc area and NP area, AF width as the difference between the disc width and NP width, and AF height as the AF area divided by the AF width. AF width is reported as half the measured width to indicate the thickness of the right or left lateral AF.

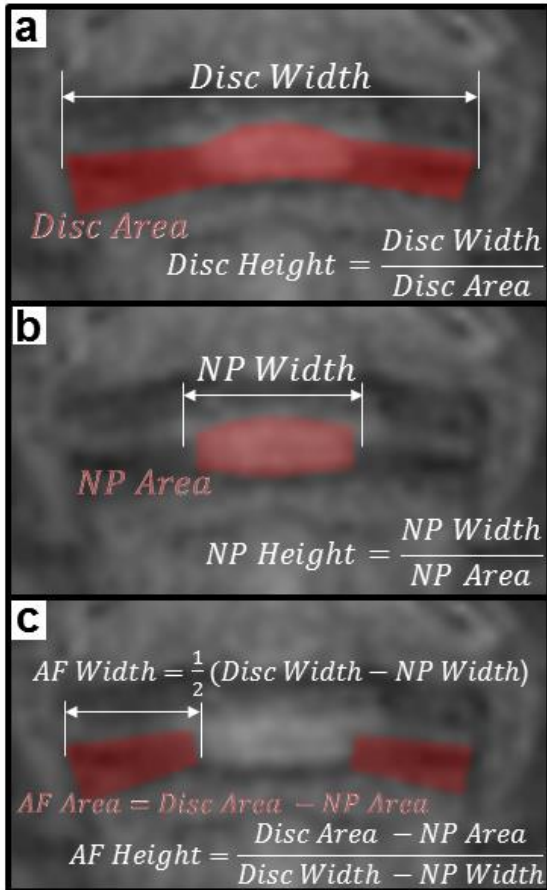


Figure I-4 Geometry analysis for MR images. (a) Whole disc dimensions as estimated by manual tracing, (b) NP dimensions as determined by bimodal, bivariate auto-segmentation, (c) AF dimensions as the regions excluded by auto-segmentation.

I.2-8 Statistical Analysis

Measurements of four discs from each rabbit were averaged for Week 0 (n=80, 4 discs/rabbit, 20 rabbits) and Week 4 (n=76, 4 discs/rabbit, 19 rabbits) groups to determine the effect disc injury on disc geometry and T2 signal. Paired t-tests were used to determine significant differences ($p < 0.05$). To evaluate NP segmentation functions, the mean coefficient of determination (R^2) for each of the 4 Gaussian functions was calculated for Week 0 (n=80) and Week 4 (n=76) groups and a two-way ANOVA was implemented. Post-hoc Bonferroni analysis was employed to determine differences between groups at each timepoint ($p < 0.05$). To analyze discs by level, measurements from each disc level were averaged for Week 0 (n=20 discs/level) or Week 4 (n=19 discs/level) groups and a one-way ANOVA was performed with post-hoc Bonferroni analysis used to determine differences between groups at each timepoint ($p < 0.05$).

I.3 Results

All rabbits survived surgery and maintained healthy body weight postoperatively. One rabbit was removed from the study due to skin necrosis and resultant wound complication.

Quantitative T2 mapping was used to generate spatial maps of the T2 relaxation rate of each disc. Upon fitting these data, the bimodal, bivariate method was most effective for NP segmentation, as determined by the mean R^2 of all fits (Table 1). For Week 0 fits, there were no differences between the bimodal, bivariate method and the univariate methods, while the unimodal, bivariate method mean R^2 was less than the

bimodal, bivariate method. For Week 4 fits, the bimodal, bivariate function fit data more accurately than all other methods. Thus, all reported NP dimensions and T2 values were determined by bimodal, bivariate segmentation.

	Unimodal, Univariate	Bimodal, Univariate	Unimodal, Bivariate	Bimodal, Bivariate
Week 0	0.88 ± 0.076	0.94 ± 0.043	0.79 ± 0.086	0.87 ± 0.053
Week 4	0.68 ± 0.28	0.74 ± 0.26	0.70 ± 0.16	0.85 ± 0.080

Table I-2 - Coefficient of Determination (R^2) for 4 modified Gaussian distribution functions fit to NP T2 Maps

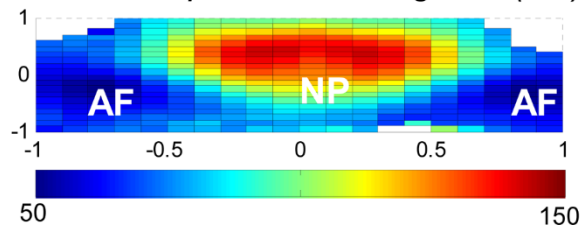
Bold font, $p < 0.05$ vs. Bimodal, Bivariate at corresponding timepoint
 Values are listed as mean ± standard deviation

There were no differences between independent observers in terms of mean NP T2 values both pre- and post-injury for either manual outlining or bimodal, bivariate segmentation. In addition, I found that Pearson coefficients were identical between manual outlining and auto-segmentation (Pre-injury: manual outlining $r^2 = 0.86$, auto-segmentation $r^2 = 0.83$; Post-injury: manual outlining $r^2 = 0.44$, auto-segmentation, $r^2 = 0.44$). Thus, automatic segmentation was equivalent to manual outlining, while having the additional benefit of a rigorously defining NP boundaries and potentially eliminating user bias.

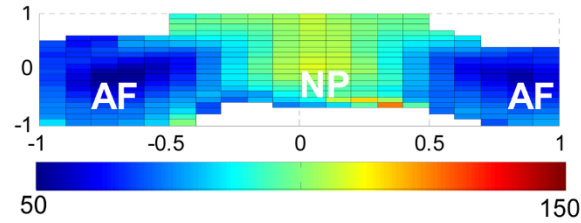
Population average T2 maps showed quantitative differences in T2 values across healthy discs and revealed specific transformations following injury [Fig. I-5a]. Before injury, T2 relaxation time was lowest in the AF and increased gradually towards the NP. The pre-injury map identified that the intranuclear cleft (bilateral T2 peaks at the center of the NP) is a consistent anatomical feature preserved across all discs. At Week 4, NP T2 values decreased and the T2 difference map showed that this reduction occurred at the periphery of the NP.

The T2 relaxation time decreased in the NP but not in the AF. Between Weeks 0 and 4, the mean T2 decreased in the NP and the whole disc, while there was no change in the AF [Fig. I-5b]. T2 volume also decreased in the whole disc and NP, and increased in the AF [Fig. I-5c].

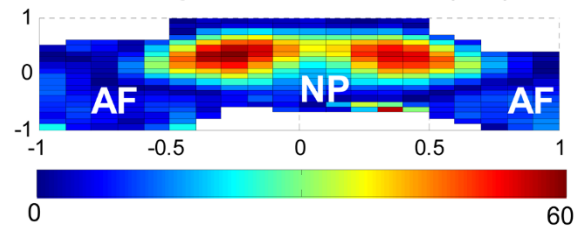
a Week 0 Population Average T2 (ms)



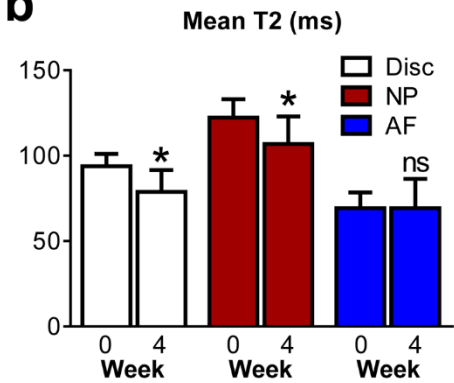
Week 4 Population Average T2 (ms)



Average T2 Difference (ms)



b



c

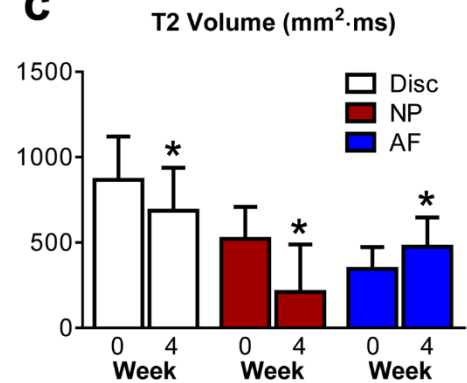


Figure I-5 Population average T2 maps and T2 quantification by disc region (a) Population average T2 maps were generated for discs from Week 0 (n=80, top) and Week 4 (n=76 discs, middle) groups. Map of T2 difference (bottom) between Week 0 and Week 4 population averages. (b) Mean T2 values for the whole disc, the NP, and the AF at each timepoint (*, p<0.05 vs. Week 0). (c) Mean T2 volume (volume under T2 surface) for the whole disc, the NP, and the AF at each timepoint (*, p<0.05 vs. Week 0). Data is shown as the mean \pm standard deviation.

Needle injury also resulted in changes in disc shape. Whole disc area remained constant from Week 0 to Week 4 while NP area decreased and AF area increased [Fig. I-6a]. Whole disc width increased, while NP width decreased and AF width increased [Fig. I-6b]. In addition, whole disc and AF heights decreased, while there was no change in NP height [Fig. I-6c]. While MRI measurements confirmed disc height decreased in the coronal plane, radiographs demonstrated that disc height decreased in the sagittal plane [Fig. I-6d].

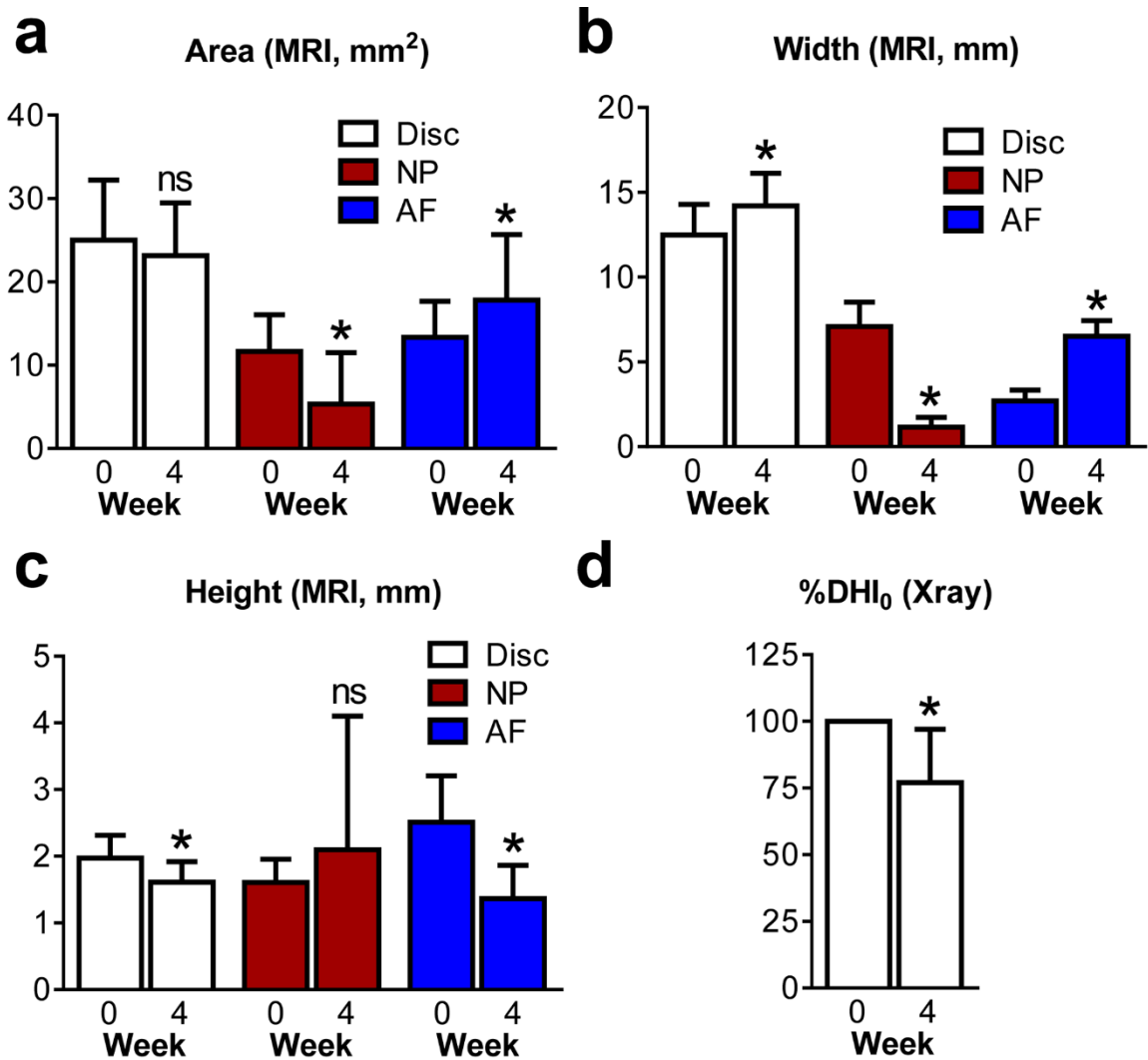


Figure I-6 Disc geometry pre- and post-injury MRI measurement of whole disc, NP, and AF (a) area, (b) width, and (c) height from Week 0 (n=80) and Week 4 (n=76) discs (*, p<0.05 vs. Week 0). Note: AF Width refers to the AF radial thickness; see Figure I-4 for details. Radiographic measurement of (d) Disc Height Index (DHI) reported as % of Week 0 DHI and (e) vertebral offset angle in the sagittal plane. Data is shown as the mean \pm standard deviation.

Population average T2 maps revealed differences in how discs at different lumbar levels responded to injury. Specifically, level-by-level analysis showed that the L4/L5, L5/L6 and L6/L7 discs were less responsive to injury than the L3/L4 discs [Fig. I-7].

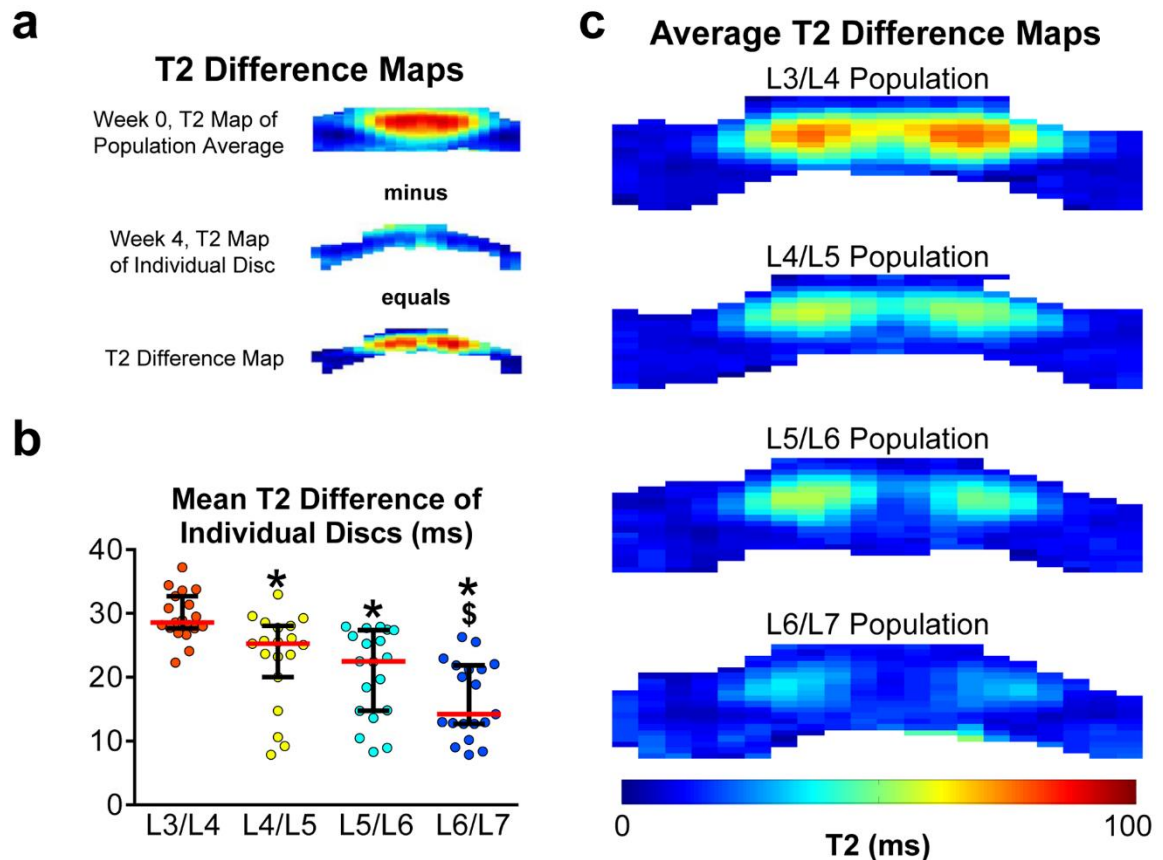


Figure I-7 T2 difference as a function of level T2 difference maps were used to identify the location of T2 transformation within each disc. (a) These were defined by subtracting the individual T2 maps of Week 4 discs from the Week 0 population average map (n=19 discs/level). (b) T2 difference maps of individual discs were averaged at each point on the grid to quantify changes in T2 values with injury. Individual data points represent the mean T2 difference for an individual disc and are displayed with the median and interquartile range (*, p<0.05 vs. L3/L4 and \$, p<0.05 vs. L4/L5). (c) Population average T2 maps of discs at each level confirm the variability in response to needle puncture injury, with less difference observed at lower levels.

With progression along the spine, the T2 difference in individual discs showed an increasing range, indicating that the response to injury was not only less severe, but was less repeatable at these lower levels. The mean NP T2 signal in the L3/L4 and L4/L5 discs was significantly decreased between Weeks 0 and 4, while the mean NP T2 value in both the L5/L6 and L6/L7 discs did not change over the same time period and was significantly greater than the L3/L4 NP T2 [Fig. I-8]. In addition, while DHI changed for all levels from 0 to 4 weeks, the amount it changed was significantly less for L6/L7 discs compared to L3/L4 discs [Fig. I-8b]. Interestingly, the mean NP T2 signal in the L6/L7 discs was significantly greater than the mean NP T2 signal in L3/L4 discs at Week 0 [Fig. I-8c], and the mean AF width of the L5/L6 and L6/L7 discs was significantly greater than the mean AF width of the L3/L4 discs [Fig. I-8d].

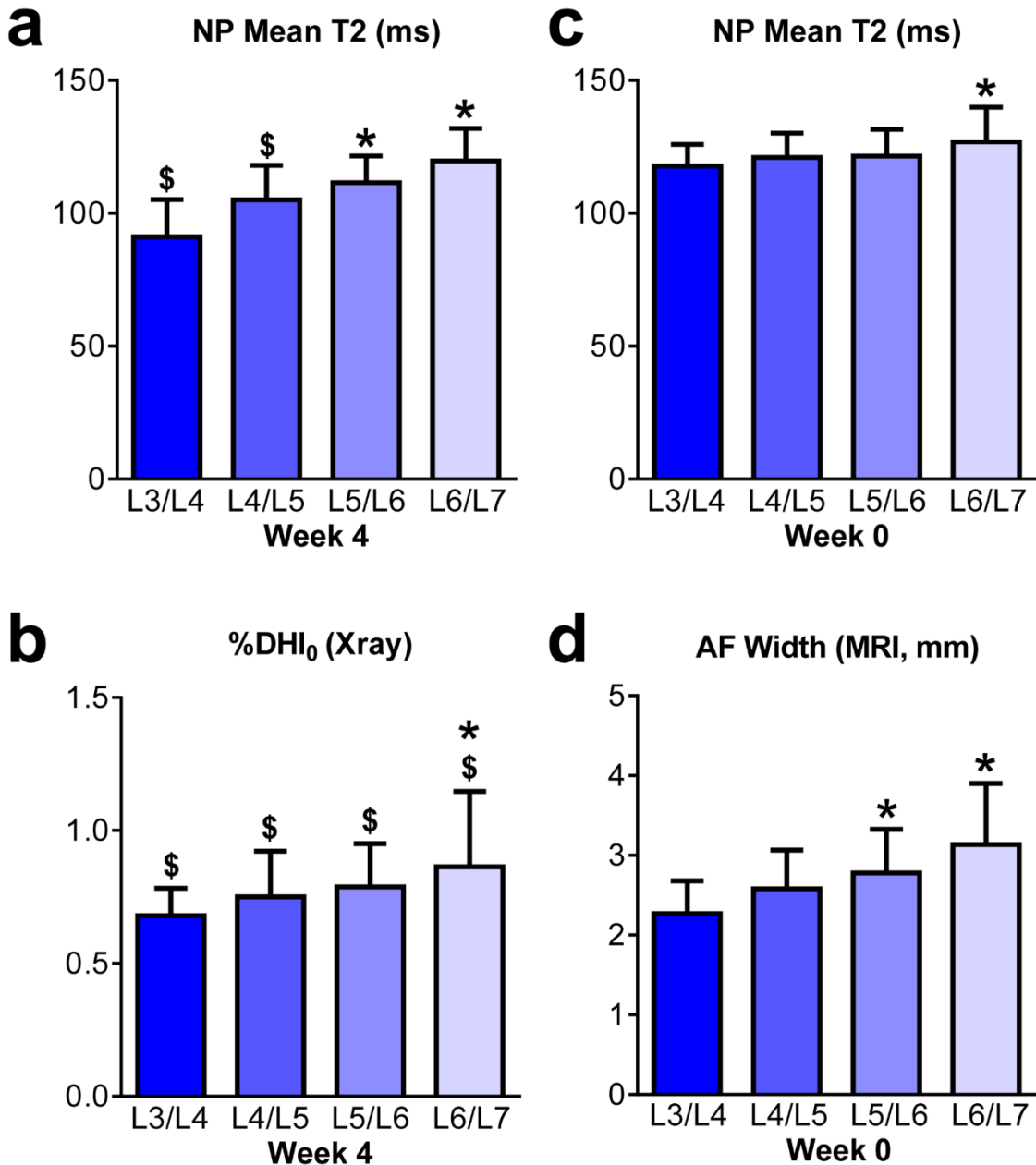


Figure I-8 Effects of puncture by level and baseline differences (a) Mean NP T2 and (b) %DHI₀ by level after injury. (\$, <0.05 vs. corresponding Week 0 group and *, p<0.05 vs. Week 4 L3/L4). (c) Mean NP T2 signal and (d) AF width by level before injury (*, p<0.05 vs. Week 0 L3/L4).

I.4 Discussion

Rabbit lumbar discs were injured using the needle puncture method established by Masuda and et al. [153], and changes in T2 MRI maps were quantified. I generated population average T2 maps before and after injury which demonstrated that transformations in T2 signal occurred primarily in the NP, with the intranuclear cleft disappearing as a result of injury. This method also identified transformations in disc geometry, as quantified by MRI and radiographs, analogous to those observed in the human degeneration process. Finally, analysis by level showed that lower lumbar discs were protected from injury, illustrating how anatomical differences (AF thickness) mediate the response to a standardized injury.

Overall, this study showed that lumbar disc injury led to MRI and geometric transformations consistent with those previously reported in both animal models and human disc degeneration. A standard MR definition of disc degeneration, the loss of T2 signal in the NP, is consistently replicated in this and previous animal models [79, 224, 229, 250]. Through quantitative analysis of MR images, this study also demonstrated the disappearance of the NP intranuclear cleft following injury, a feature of the rabbit puncture model that was not previously defined, but is consistent with human disc pathology [3]. Geometric changes like disc height loss and the disappearance of hydrated tissue in the NP are well documented for human disc degeneration and are similarly exhibited in this rabbit puncture model [224, 229]. This study revealed additional geometric transformations not previously described in the rabbit puncture model. Specifically, the increase in the coronal disc width following puncture supports the idea

that disc bulging occurs in this model, a common finding in epidemiological studies of the human disc [18].

Another feature of this methodology was its sensitivity in identifying degeneration as a function of level. Level-by-level analysis illustrated the limits of set needle puncture depth (5mm) with respect to the increasing disc dimensions at lower lumbar levels. The heterogeneity in response to injury at L4/L5 and lower may suggest that needle insertion depth should be a function of disc level. Many studies support that structural perturbation is only apparent when the injury is of sufficient size relative to disc geometry [56, 89, 146, 158]. The specific findings of Michalek and Iatridis, who demonstrated computationally that disc mechanics were sensitive to the ratio of needle diameter to AF width, is particularly relevant to our result that increased AF width was protective in the context of a standardized needle injury [161]. Because initiating degeneration in the rabbit lumbar disc with an 18G needle is a standard model in disc research, we believe this information is important to take into account for future experiment planning, especially in light of the NIH call for improvements in the experimental reproducibility in animal research [47]. Careful selection of puncture depth and validation of the effects are critical to proper interpretation of experimental outcomes in multi-segment experiments.

Auto-segmentation of the NP using a modified Gaussian function was successful in both pre- and post-injury discs, with the bimodal, bivariate function providing the best fit at both timepoints. Univariate functions along the lateral disc coordinates fit the pre-injury data well, but failed to capture post-injury transformations in signal, likely because

the spatial distribution of T2 signal was plateau-shaped (rather than peak-shaped) in the post-injury situation. Post-injury, the T2 signal transformed from bimodal T2 peaks along a left-right line at the disc mid-height to bimodal T2 peaks at the superior and inferior margins of the NP. Thus, the bimodal, bivariate function provided the best fits, as expected for a bimodal function fit to bimodal data. In all cases, Gaussian functions produced meaningful boundaries for defining the NP geometry.

Use of bimodal, bivariate NP segmentation was an objective approach to defining internal boundaries. This method has less potential for bias relative to other NP isolation methods (i.e. by the absolute position within the disc [241], by using the geometry of a predefined region of interest [28], or by tracing the NP at its boundaries [183]). A comparable auto-segmentation procedure delineates the NP based on T2 pixel intensity by defining a T2 threshold based on the mean T2 signal within a region of interest in a control NP and selecting pixels above this threshold [79]. This method warrants direct comparison to the bimodal, bivariate method in future studies.

The rabbit AF response to needle puncture was different from human degeneration. In human degeneration the AF T2 relaxation times decreases with increasing degeneration grade [7, 241], while for the rabbit disc, there was no change in AF T2 following needle puncture. This suggests that biochemical changes that occur immediately following puncture are primarily in the NP and not the AF. Similar findings have been described for this model previously. Miyamoto et. al showed there were no changes in AF DNA, proteoglycan or collagen contents 8 weeks after needle puncture, while significant changes in composition occurred in the NP [164]. We propose that in

disc puncture models compositional modifications in the AF are preceded by structural modifications in the AF. Evidence for AF structural disorganization in the rabbit puncture model was provided by Sakai et. al who demonstrated lamellar disorganization 6 weeks after puncture [210], and also by Gregory et. al who reported a decrease in interlamellar shear strength at 12 weeks [77]. Future work must evaluate later time points to confirm the effects of puncture on AF composition in the rabbit model and its relation to changes in the human AF.

The primary criticism of disc injury models is that the rapid advancement of degeneration does not replicate changes seen in human degeneration, which develop over the course of years. These models, however, have a number of features that mimic the human condition: disc height collapse [146] and bulging [255], the disappearance of the NP T2 signal [224], and the presence of a number of molecular markers [225, 247]. Because the endpoints of both injury-initiated degeneration and human degeneration are comparable, injury-mediated degeneration is a powerful technique to study the basic science of disc degeneration and develop therapeutic strategies to regenerate tissue. Another limitation of this study is the inability of the MR analysis to detect subtle changes in disc geometry due to limited scan resolution. For example, at the segmentation boundaries there is volume averaging within each voxel, and consequently, evaluating the AF dimensions by T2 signal may overestimate AF geometry. Relative changes in AF and NP geometry resulting from puncture injury were detectable despite limited resolution, and, in addition to changes in T2 signal, measurement of these parameters enables monitoring of the degeneration process quantitatively.

I.5 Conclusion

Population average T2 maps enable the quantification of the deviation of an individual disc from a population norm, providing new information on the degree of degeneration that is not available with standard ordinal grading methods. Furthermore, the spatial discrimination of changes implicit in this approach provides additional information on alterations in regional disc structure. This is exemplified here by the disappearance of the intranuclear cleft after injury, a potential early indicator of degeneration, which may be obscured in grading standard T2-weighted clinical MR images. Future work will determine whether these population average T2 and corresponding T2 difference maps are useful in a clinical population to assess the degree of degeneration, to predict pain/disability, and to quantify the adjacent segment degeneration.

APPENDIX II – Development of a Precision Mechanical Testing Protocol: Needle Puncture Injury Causes Acute and Long-Term Mechanical Deficiency in a Mouse Model of Intervertebral Disc Degeneration

II.i Preface

In Appendix II, I describe a method for precision mechanical analysis of degenerated mouse caudal discs through optical displacement tracking. This method will be used to quantify the mechanical properties of DAPS after implantation.

II.1 Introduction

While current surgical and non-surgical interventions may relieve discogenic pain, they do not restore disc function. An *in vivo* disc degeneration model can provide the necessary platform for evaluating therapies aimed at reducing pain *and* restoring function. Because the primary function of the disc is mechanical, consideration of disc mechanics is critical in such models.

Intervertebral disc injury in animal models consistently produces an acute response that progresses to resemble key features of disc degeneration [99, 130]. Injury models provide repeatable results and have controlled specificity in comparison to global gene knockouts and spontaneous development models. Thus, injury studies have been conducted in many species including the sheep, pig, rabbit, and rat [89, 109, 153, 164,

191, 207]. Methods for inducing degeneration through injury include scalpel incision, defect creation (box, cruciate), and needle puncture and, of these methods, needle puncture is used frequently as puncture depressurizes the nucleus pulposus (NP), a primary factor for creating instability, while also minimizing annulus fibrosus (AF) damage [89, 153, 164]. Recently, the mouse caudal disc was shown to degenerate as a result of needle puncture, displaying changes in morphology, cellularity and composition consistent with those in humans [247]. Puncture-initiated degeneration of the rodent caudal disc requires only minor surgery; thus it is an excellent alternative to lumbar surgery in which access requires an invasive and technically challenging peritoneal or dorsolateral approach [32]. In addition, the mouse caudal disc is comparable mechanically to the human lumbar disc when accounting for geometry despite different physiological loading environments [55, 213]. These factors, along with the wide commercial availability of mouse-specific biological assays, indicate that the mouse caudal disc model can be a powerful tool for investigating degeneration.

Mechanical function is the primary metric for studying the efficacy of potential therapies as restoring function is the end-goal of such therapies. Mechanical changes immediately following puncture injury [56, 89, 160] and over time due to biological effects such as inflammation [109, 164] have been assessed in separate studies; however no study has linked the immediate mechanical changes following puncture with progressive mechanical deterioration or recovery. In addition, a needle diameter to disc height ratio of 40% is required to cause changes in the mechanics of *lumbar* discs [56], while much larger defects are required to alter rat *caudal* disc mechanics [89, 160]. By

evaluating acute and long-term disc mechanics, changes caused by the initial puncture can be distinguished from those caused by physiological processes, and by evaluating needle sizes, an appropriate injury for a degeneration model can be selected.

Mechanical data for the degenerate mouse disc is currently limited to bending and creep [49, 192]; however, compression and torsion are also primary mechanical modes, and to date have not been measured. Compression and torsion are governed by different structural mechanisms; compression through the interactions between the NP and AF and torsion primarily through loading of the AF fiber network. Quantification of the compressive and torsional mechanical behavior of healthy and degenerate discs will aid in understanding alterations in mechanics of the individual disc tissues.

The objective of this study was to quantify the acute and long-term effects of needle puncture injury on mouse caudal disc function. Injuries were surgically induced with one of two needle sizes and were evaluated for changes in disc structure, mechanics, and composition both immediately and after eight weeks. We hypothesized that the initial puncture would decrease compressive and torsional mechanical properties and that these changes would be amplified by subsequent structural and compositional deterioration.

II.2 Methods

II.2-1 Surgical Procedure

With institutional IACUC approval, 26 C57BL/6 retired breeder mice (7.5-9 months, 32.7±5.1g) were obtained from Jackson Laboratories (Bar Harbor, ME) and allocated to two timepoints: zero weeks (n=12) and eight weeks (n=14). Mice were

anesthetized in an aseptic setting and the surgery was fluoroscopically guided. The C6/C7 and C8/C9 discs were exposed with a 2.5 mm dorsal longitudinal scalpel incision and puncture injuries were created at one randomly assigned level with either a 29G (65% of disc height) or 26G (90% of disc height) needle, while the other exposed disc served as a sham control. Needles were inserted at the dorsal annulus through the NP center and partially through the ventral annulus (controlled depth of 1.75 mm or 90% of the dorsoventral width) for 30 seconds and removed. The injured level was marked with India ink and both incisions were closed with suture. Mice were returned to normal cage activity and euthanized after eight weeks. Zero-week mice were euthanized and their discs were punctured in vitro following the same procedure.

II.2-2 Microcomputed Tomography

Microcomputed tomography (μ CT) (vivaCT 40, SCANCO Medical AG, Bruttisellen, Switzerland) was used to measure disc area and mean disc height of zero-week control and eight-week control and punctured groups (n=7/group). The C6 through C9 section the caudal spine was removed and imaged en bloc at an isotropic 21 μ m resolution. Volumetric image data was converted to stacks of cross-sectional vertebral body slices and disc area and mean disc height were measured from a 3D reconstruction of slices that spanned disc space [32] [Fig. II-1a-c]. Polar moment of inertia, J_z , about the spinal longitudinal axis was measured from a cross-sectional slice directly distal to the disc space for use in normalizing torsional mechanical properties [Fig. II-1d-f].

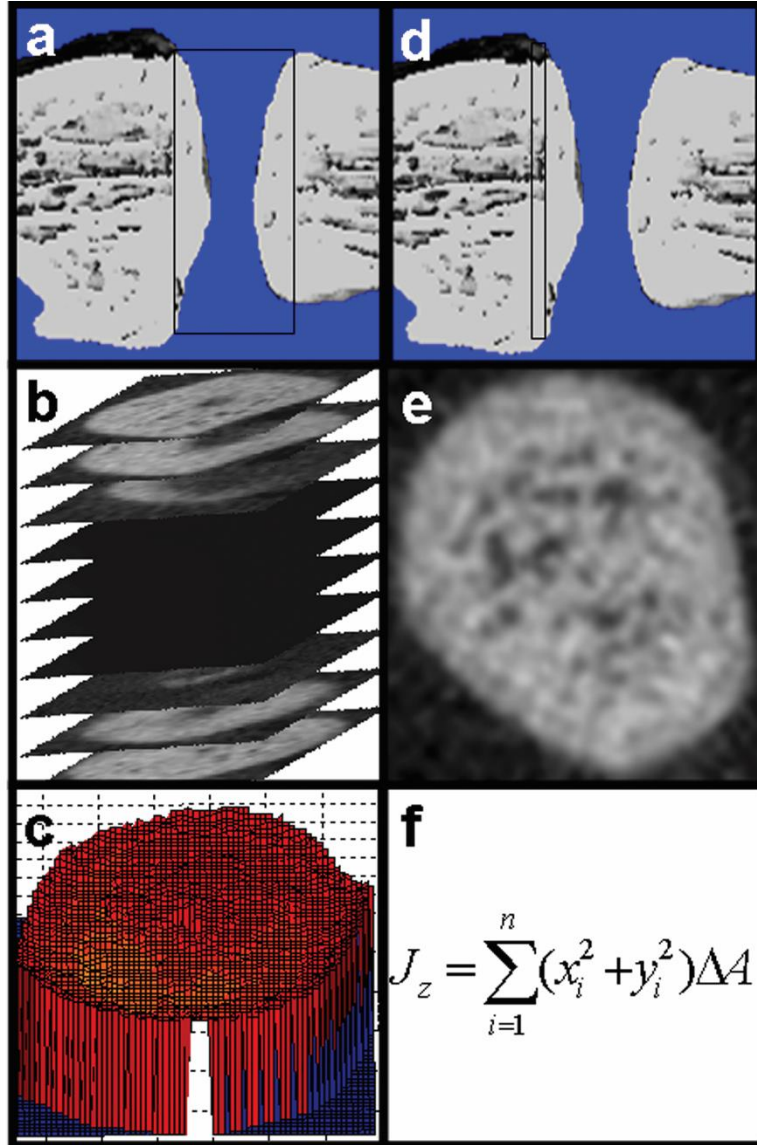


Figure II-1 μ CT analysis of disc geometry Disc area and mean disc height were measured by (a) isolating the intervertebral space and (b) converting to cross-sectional image stacks. (c) Stacks were analyzed in Matlab by differentiating between pixels that corresponded to bone and pixels that corresponded to disc [32]. Polar moment of inertia, J_z , was measured by (d) isolating a cross-sectional image directly adjacent to the disc space, determining the centroid, and (f) numerically integrating over n pixels (where n is equal to the number of pixels within the boundary of the vertebral body cross-section), each with coordinate (x_i, y_i) and area ($\Delta A = 21\mu\text{m} \times 21\mu\text{m}$, based on μ CT resolution).

II.2-3 Mechanical Testing

Mechanical function was assessed with an electromechanical testing system (Instron 5542, Instron, Norwood, MA) fit with a custom torsion device consisting of a stepper motor (AM1524; MicroMo Electronics, Inc., Clearwater, FL) and a 5 in-oz (35 mNm) torsional load cell (TFF400; Futek, Irvine, CA) [Fig. II-2]. A custom LabVIEW (LabVIEW 8.5; National Instruments, Austin, TX) program was used to control the angular displacement of the stepper motor and read the torsional reaction force. While the electromechanical testing system and stepper motor were used to directly control the compressive and rotational displacements, two digital cameras (A602f; Basler, Exton, PA) were used to optically track the extension and rotation of each vertebral body. Axial position (mm) was defined simply as the difference in the z -position of points in camera 1, while rotational position (radians) was measured by recording the x -position of a point in camera 1 and the y -position of the same point in camera 2 and defined as $\tan^{-1}(y/x)$ [Fig. II-2c].

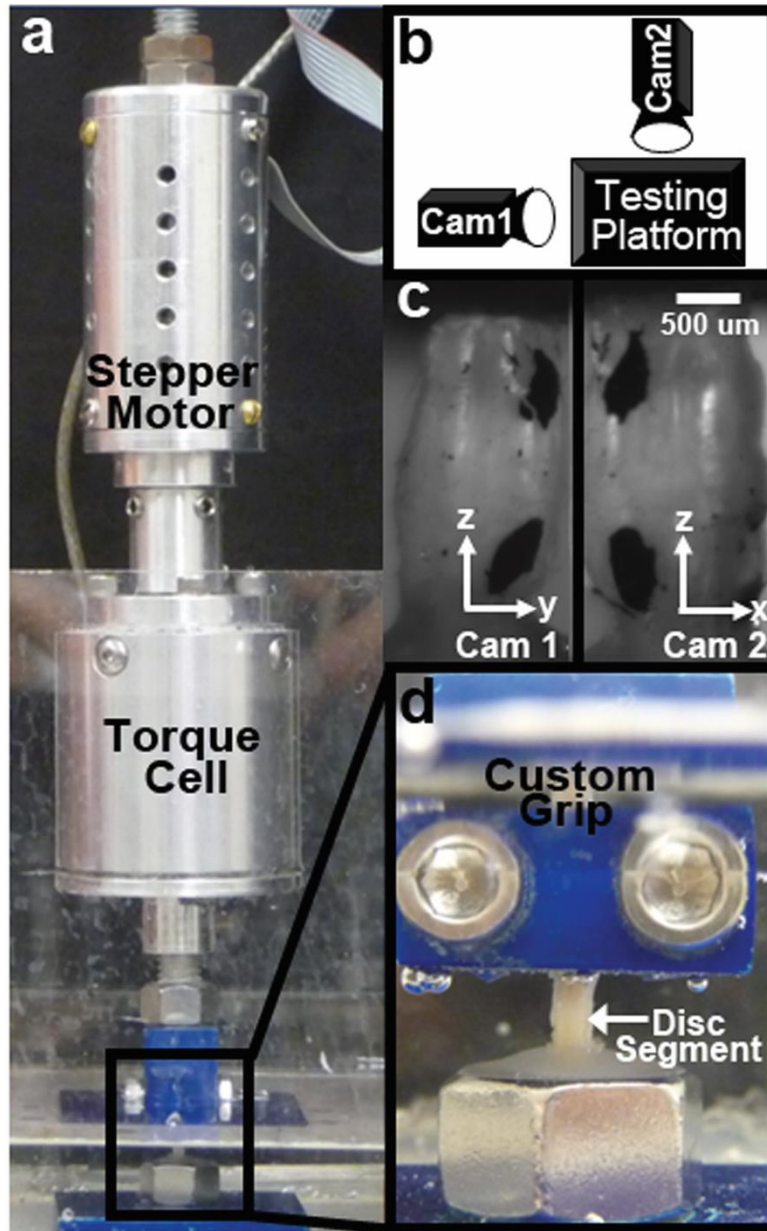


Figure II-2 Mechanical testing and optical displacement tracking setup (a) A custom torsion device consisting of a stepper motor and torque cell was installed on a uniaxial mechanical testing system. (b) Two digital cameras positioned 90° apart were used to record the 3-dimensional position of the vertebral bodies. (c) Markings on the vertebral bodies were tracked using custom software. (d) Samples were fixed to the upper machine grip, lowered into a pot filled with dental cement and, when cured, the mechanical test was started.

A significant portion of machine-reported displacement was a contribution of unavoidable motion at spots along the load string (for example slipping at the grips or minor motions between bolted connections to the load cell). These errors are likely present in all disc compression tests, but because the rodent disc is small, minor motions have a relatively large impact. Thus, it was necessary to eliminate displacement error through optical tracking with the dual camera system and a custom texture tracking program written in Matlab. Preliminary evaluations of this technique demonstrated that axial displacements and rotations were successfully captured as $85.4 \pm 12.4\%$ and $75.4 \pm 38.4\%$ of their machine-reported counterparts respectively [Fig. II-3]. These optical measures of displacement and rotation were then used in post-test mechanical parameter calculations.

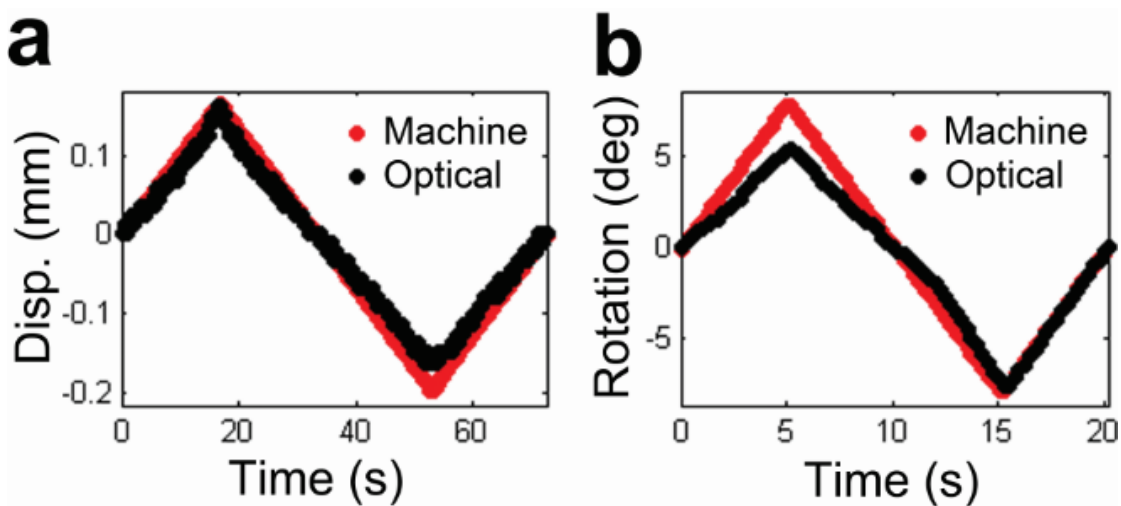


Figure II-3 Optical displacement vs. machine reported displacement
Representative plots of machine-reported and optically-tracked (a) displacement and (b) rotation over one loading cycle.

Discs from zero-week and eight-week control and punctured groups (n=5/group) were exposed to a mechanical testing regimen including compressive, creep, and torsional loads. Caudal spines were prepared as bone-disc-bone segments by cutting through adjacent unused discs (leaving the entire vertebral body surface area to grip for mechanical testing) and gently clearing extraneous tendon and muscle with a scalpel. The testing protocol consisted of 20 cycles of compression/tension from -1.5 N to +0.5 N at 0.5 Hz [20] (causing compression/extension of the disc from approximately 70% to 130% of the initial height), a one hour creep load of -1.5 N [20], and 10 cycles of torsion of $\pm 8^\circ$ at 0.05 Hz [213]. All testing was conducted in phosphate buffered saline bath at room temperature.

Compression/tension data was analyzed for compressive stiffness and range of motion (ROM), and neutral zone (NZ) stiffness and ROM by fitting data to a sigmoid function [217] (an S-shaped curve with well-behaved first and second derivatives that represents displacement as a functional of applied load) [Fig. II-4]. Compressive and NZ stiffness were normalized to disc geometry by multiplying by the disc height and dividing by the disc area [20], and ROM measurements were normalized by dividing by the disc height [20]. Torsion data was analyzed for torsional stiffness, torque range, torsional NZ stiffness and torsional NZ ROM using the same curve fitting procedure [Fig. II-4]. Torsional stiffness, torsional NZ stiffness, torque range were normalized to disc geometry by multiplying by the disc height and dividing by J_z [213].

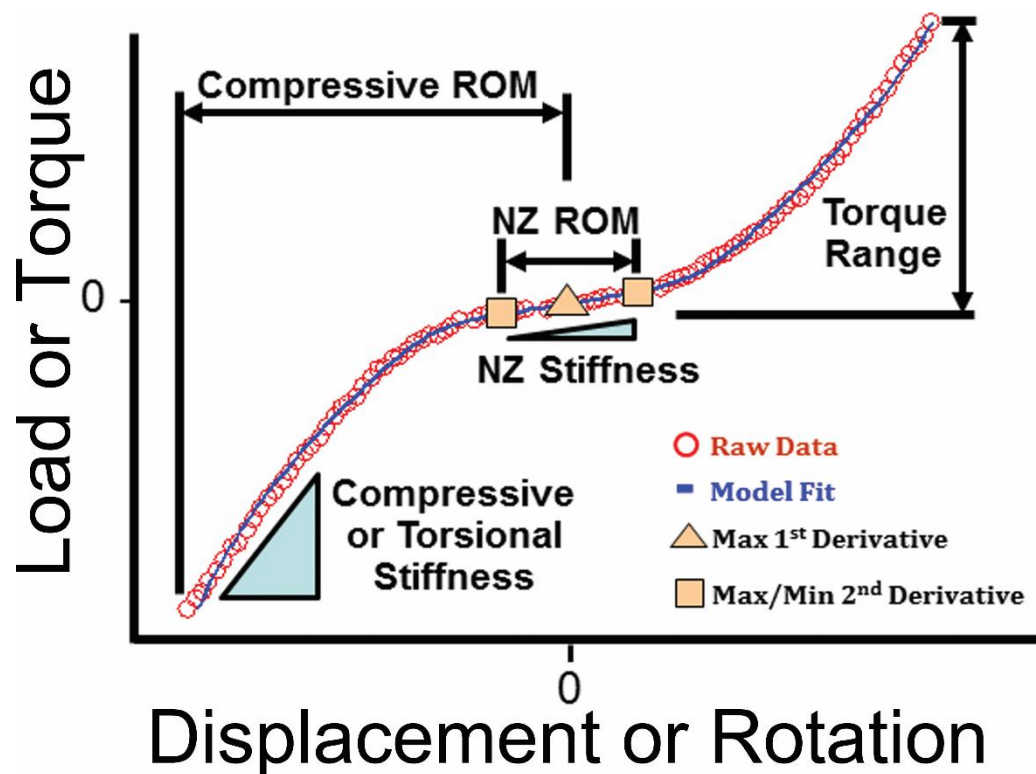


Figure II-4 Data analysis for compression and torsion response Loading curves were isolated from the final test cycle to analyze (a) compression and (b) torsion data. Positive loading curves (tension or counter-clockwise rotation) and negative loading curves (compression or clockwise rotation) were made to intersect by shifting each to the load axis to form a composite curve, which was subsequently fit to a sigmoid function. The maximum of the first derivative (maximum compliance) of the sigmoid function represents the transition from positive to negative loading regions. The extremum of the second derivative of the sigmoid function represent the boundaries of the NZ. (a,b) Neutral zone stiffness (for both compression/tension and torsion) was defined as the slope of the line connecting the point at each boundary of the neutral zone. (a,b) Neutral zone ROM (for both compression/tension and torsion) was defined as the displacement between these points. (a) Compressive ROM was defined as the displacement between the inflection point of the curve and the displacement at -1.3 MPa, a value of stress which consistently occurred just prior to the peak stress (the peak stress varied slightly from test to test). (a) Compressive stiffness was defined from the raw data as the slope of the line fit from -1.3 MPa to -0.5 MPa (a value that consistently occurred after the transition region). (b) Torque range was defined as the change in torque from the inflection point of the curve to the maximum torsional load. (b) Torsional stiffness was defined from the raw data by fitting a line from 40% - 90% of the maximum torque for both positive and negative rotations and then averaging the two.

Creep behavior was fit to a 5-parameter viscoelastic constitutive model[186]

$$d(t) = \frac{L}{S_1} (1 - e^{-t/\tau_1}) + \frac{L}{S_2} (1 - e^{-t/\tau_2}) + \frac{L}{S_3} \quad (1)$$

describing the displacement (d) at time (t) for constant load (L). The material response consists of an elastic stiffness (S_3) and two exponential decays with one time constant (τ_1 , τ_2) and damping stiffness (S_1 , S_2) each. This model provided a simple but reasonable method to compare the time-dependent response across groups. In addition, creep displacement was measured from raw optical displacement. Damping stiffnesses were normalized by disc geometry by multiplying by disc height and dividing by disc area, and creep displacement was normalized by dividing by disc height [20].

II.2-4 NP Glycosaminoglycan and Collagen Content

Following mechanical testing, discs from zero-week control and eight-week control and punctured groups (n=5/group) were isolated for NP GAG and collagen content analysis. First, a scalpel was used to cut through a vertebral body adjacent to the disc above the vertebral endplate. The remaining vertebral body-disc segment was embedded in optimum cutting temperature compound on a cryostat microtome, and consecutive sections through the partial vertebral body exposed the underlying disc. A 100 μm section of disc was then isolated and the NP was removed with 0.75 mm biopsy punch (the approximate NP diameter). This dissection technique facilitated precise control of the volume of tissue obtained. Isolated NPs were subsequently digested in papain at 60°C. Glycosaminoglycan (GAG) content was measured using the dimethylmethylene blue (DMMB) technique [61], and collagen content (following acid

hydrolysis) using the p-diaminobenzaldehyde/chloramine-T technique for hydroxyproline [226] assuming a ratio of hydroxyproline to collagen of 1:10 [182]. Results are reported as normalized to NP wet weight.

II.2-5 Histology

Discs from eight-week sham and punctured groups (n=2/group) were fixed in formalin, decalcified, and embedded in paraffin. Sagittal, 8 μ m sections were stained with alcian blue/picosirius red for GAG/collagen and imaged under bright field and cross-polarized light.

II.2-6 Statistics

Differences in disc height, GAG content and collagen content were analyzed by one-way ANOVA comparing the zero-week control group to the eight-week control and punctured groups. Differences in mechanical properties were analyzed by two-way ANOVA comparing zero-week control and punctured groups to the eight-week control and punctured groups with needle size and time as the main effects. Tukey's post-hoc test was used for pairwise comparisons with significance defined as $p \leq 0.05$ and a trend as $0.05 < p \leq 0.10$. Results are reported as mean \pm standard deviation.

II.3 Results

Mice survived the minor surgical procedure and recovered with no change in body weight over 8 weeks. Disc height eight weeks after 26G puncture was less than the zero-week control group (37%, $p \leq 0.05$), the eight-week control group (29%, $p \leq 0.05$) and the 29G group (28%, $p \leq 0.05$), and there was no significant effect of the sham surgery or

29G needle puncture [Fig. II-5a]. Nucleus pulposus GAG content followed a similar trend as at eight weeks the 26G group was 41% less than the zero-week control group ($p \leq 0.05$), with no change in eight-week control or 29G groups [Fig. II-5b]. Nucleus pulposus collagen content for the 26G group was not significantly different from zero-week control but was 45% greater than both the eight-week control and 29G groups ($p \leq 0.10$) [Fig. II-5c].

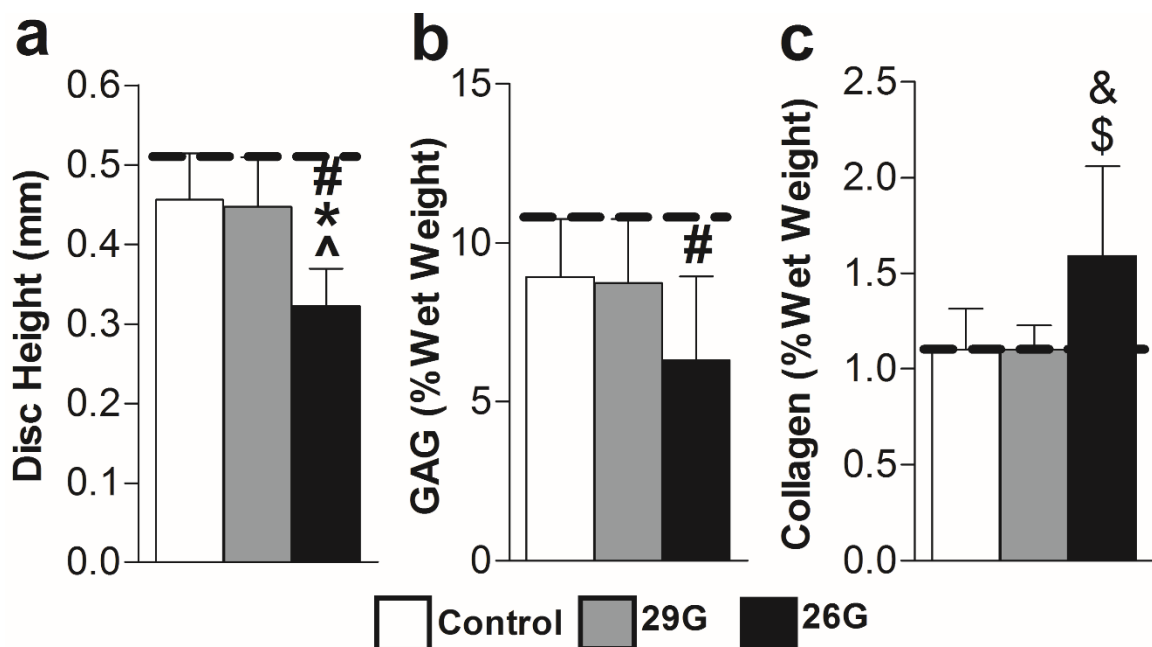


Figure II-5 Disc height, GAG content, and collagen content at week 8 (a) Disc height ($n=7$ /group/timepoint), (b) NP GAG content ($n=5$ /group/timepoint) and (c) NP collagen content ($n=5$ /group/timepoint) were altered after eight weeks. Significant differences ($p < 0.05$) are labeled: from zero-week control (represented by dotted line) (#), from eight-week control (*), and from 29G (^). Significant trends ($p < 0.10$) are labeled: from eight-week control (&) and from 29G (\$).

Histologically, there were no qualitative differences between control and 29G puncture groups at eight weeks, while the 26G group had a collapsed disc space, disorganized lamellae, and collagenous NP [Fig. II-6].

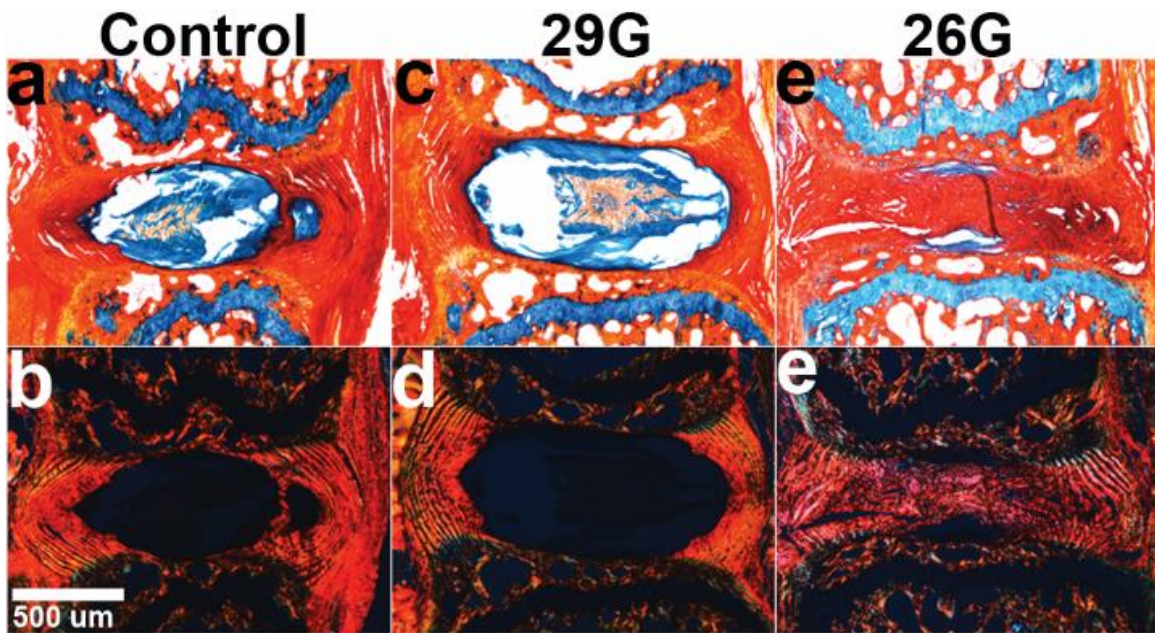


Figure II-6 Histological results at week 8 Alcian Blue/Picrosirius Red stained sagittal sections of eight-week mice viewed under (a-c) brightfield and (d-f) polarized light (n=2/group/timepoint). (a,d) Control and (b,e) 29G discs were no different at eight weeks, while (c,f) 26G discs had collapsed height and disorganized lamellae with the presence of collagen-positive stain and lack of GAG-positive stain in the NP.

The baseline mechanical response in both compression and torsion consisted of an elongated low stiffness NZ that transitioned with increasing strain to a high stiffness linear region [Fig. II-7]. A two-way ANOVA revealed that changes in compressive and torsional mechanical properties (normalized compressive stiffness, normalized torsional stiffness, normalized torque range) were a function of puncture size only ($p \leq 0.05$) and not time [Fig. II-7]. Compressive stiffness of the 26G group was less than the control groups at week zero (62%, $p \leq 0.05$) and week eight (62%, $p \leq 0.05$), but there were no differences across timepoints [Fig. II-7a]. In addition, there were no significant changes in compressive ROM for any treatment [Fig. II-7b]. Torsional stiffness for the 26G group was significantly less than the control group at week zero (60%, $p \leq 0.05$) and at week eight (71%, $p \leq 0.05$), but again there were no differences across timepoints [Fig. II-7c]. Torque range of the 26G puncture group was less than the control group at week eight (51%, $p \leq 0.05$) [Fig. II-7d]. The sham surgery and the 29G needle puncture had no effect and there were no differences in either compressive or torsional NZ mechanics for any of the groups.

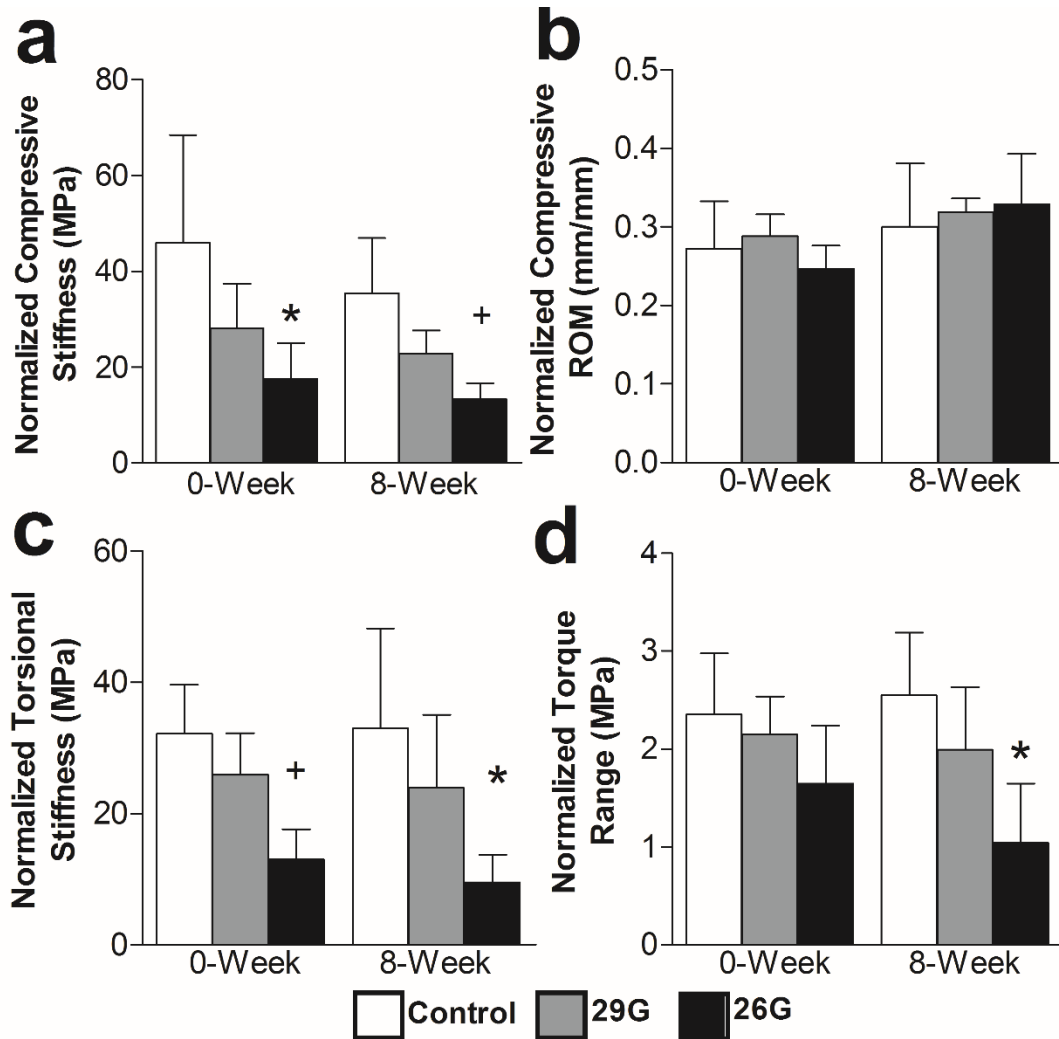


Figure II-7 Elastic mechanical parameters before and 8 weeks after puncture injury (a) Normalized compressive stiffness, (b) normalized compressive ROM, (c) normalized torsional stiffness, and (d) normalized torque range (n=5/group/timepoint). Differences from control at each timepoint are labeled as significant (*, $p < 0.05$) and trend (+, $p < 0.10$).

The response to creep loading was characterized by an initial high strain rate over the first 60 seconds and slower strain rate thereafter, equilibrating by approximately 40 minutes. Again, a two-way ANOVA revealed that changes in creep mechanical properties (normalized S_1 , τ_1 , τ_2) were a function of puncture size only ($p \leq 0.05$) and not time [Fig. II-8]. Puncture with 26G needle caused a faster, magnified creep response [Fig. II-8a]. The early damping stiffness, S_1 , of the 26G puncture group was significantly less than the control group at week zero (84%, $p \leq 0.05$) and week eight (84%, $p \leq 0.05$) [Fig. II-8d], and there were similar statistical trends for τ_1 and τ_2 [Fig. II-8b-c]. There were no differences in the late damping stiffness, S_2 , the elastic stiffness, S_3 , or creep displacement [Fig. II-8e].

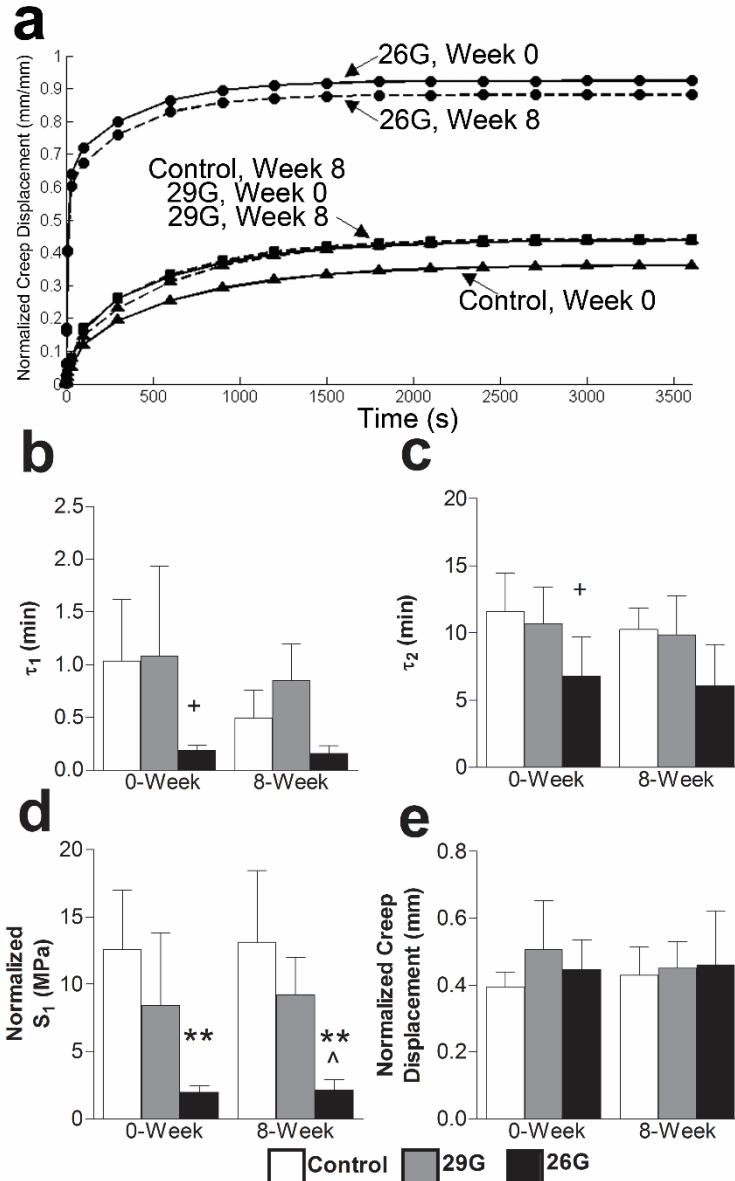


Figure II-8 Viscoelastic mechanical response before and 8 weeks after puncture injury
 (a) Average creep curves calculated from mean parameter values in Eq. 1. The total response (initial step displacement plus creep displacement) was magnified by puncture while the creep displacement did not change. The data are displayed as: control (triangles), 29G (squares), 26G (circles) with zero-week (solid line) and eight-week (dotted line). (b) Early time constant, τ_1 , (c) late time constant, τ_2 , (d) normalized creep displacement, (e) normalized early damping stiffness, S_1 , (f) normalized late damping stiffness, S_2 , (g) and normalized elastic stiffness, S_3 ($n=5$ /group/timepoint). Differences from control at each timepoint are labeled as highly significant (**, $p<0.001$), significant (*, $p<0.05$), and trend (+, $p<0.10$). Significant differences from 29G are labeled as (^, $p<0.05$).

II.4 Discussion

Compression, torsion, and creep mechanics of the mouse caudal disc were assessed both immediately and eight weeks following the needle injury described here. In each loading modality, stiffness was decreased after puncture with the large needle and remained at those levels at eight weeks. Conversely, the classical signs of degeneration progressed over eight weeks; disc height and NP GAG content decreased, while NP collagen content increased and histological signs of degeneration were present. Thus, needle puncture had an acute effect on mechanics that neither improved nor deteriorated over time despite other compositional changes. In addition, the mouse disc was insensitive to puncture with the smaller needle size. Thus, the injection of therapeutics into the nucleus pulposus with a minimal needle size may limit damage due to the needle insertion.

With disc degeneration the NP undergoes structural and compositional alterations, shifting to a fibrocartilaginous phenotype. This fibrocartilaginous shift was observed in this study; needle puncture triggered compaction of the disc space with subsequent increase in collagen content and reduction in GAG content. This is consistent with findings reported by Yang *et al.*, where, following needle injury, the mouse caudal NP transitioned from gelatinous to fibrocartilaginous, shifting from collagen II dominant to collagen I dominant [247]. Results from our study and that of Yang *et al.* are consistent with the well-defined alterations in internal composition in degenerative disc disease [233]. Thus, it is possible that the mouse disc post-injury exhibits a distorted internal strain field similar to that of the human degenerate disc [189]. However, bulk segment

mechanics declined immediately following puncture, but not over time. The NP transition to fibrocartilage observed here and in human degeneration may represent an adaptation to the loss of AF structural integrity, a physiological response to preserve segment mechanics or mitigate their decline. Future work should evaluate changes in tissue level mechanics following disc injury.

The immediate effect of needle puncture depends upon the spinal region, as caudal and lumbar discs respond differently to a given defect size. A needle with diameter equivalent to 40% disc height is required to alter the mechanical response of *lumbar* discs in compression[56]. In the *caudal* disc, compressive and torsional mechanics following a 90% disc height disruption (26G) were diminished acutely, while a 65% disc height disruption (29G) had no significant effect. In the rat *caudal* disc Michalek *et al.* demonstrated that a 21G needle (80% disc height, assuming disc height of 1 mm[188]) decreased compressive and torsional mechanical properties, while 25G and 30G (50% and 30% disc height) needles affected compression only [160]. Similarly, Hsieh *et al.* showed that in the rat *caudal* disc an 18G needle (100% disc height) affected compressive properties while 22G and 26G needles (70% and 45% disc height) had no effect [89]. Our results are consistent with these studies [89, 160], confirming that in the *caudal* disc the defect size threshold is in the range 80% disc height. This may be due to lower NP pressure and lower residual AF tension in tail discs compared to lumbar discs, as lumbar levels experience considerable loads due to muscle forces for stance and ambulation [216].

The immediate changes in torsion mechanics following needle puncture are considered to be needle size-dependent [160]. Torsion is primarily governed by AF fiber tension, which decreases with increasing needle size. The changes in torsion mechanics we measured for the mouse caudal disc are consistent with those of the rat caudal disc [160]. However, there is not consensus regarding the acute changes in compression mechanics following needle puncture, which have been suggested to be both needle size-dependent [56] and size-independent [160]. The underlying theory behind size-independence in compression is that compression mechanics are primarily governed by NP pressure, which may be reduced by puncture regardless of needle size. In this study of the mouse caudal disc, I could not confirm size-independence in compression. This difference may be due to animal size effects or differences in puncture techniques and mechanical testing protocols. However, changes in compression mechanics may also depend on needle size since, in compression, both NP pressure and AF tension play a fundamental role.

Needle puncture affects the response of the caudal disc to creep loading, although at eight weeks, the behavior did not match that of the degenerate human lumbar disc. Puncture with the 26G needle caused a magnified, faster creep response relative to control discs, predominantly seen in the early damping stiffness, S_I . This is similar to the behavior of the rat caudal disc [89]. The stiffness, S_I , dominated the response only over the short term τ_I (9.3 ± 4.5 s), supporting the idea that puncture results in a pressure vent [161] in which fluid can immediately leave at the onset of load. However, in the human lumbar disc, degeneration causes a magnified and slower response [187]. In that study,

the late time constant, τ_2 , increased with human disc degeneration [187], which was not the case following needle puncture in the mouse caudal disc.

All animal models have limitations. In this model, while the mechanical effects were immediate and do not represent the slow progressive nature of the human disease, other characteristics of degeneration were controlled and consistent. In addition, unlike the human disc, the mouse disc retains a notochordal cell population throughout its lifespan [223] and caudal discs experience different physiological mechanical loading than lumbar discs. Finally, our experiment was not able to reveal a difference in mechanical function following small needle puncture because, for the small effect caused by the 29G needle, the study was underpowered. However, the primary goal of the study was to initiate a degenerative state and measure the resultant change in mechanics and the 29G group did not meet any of the criteria for a degenerative state (loss of disc height, loss of NP GAG, change in histological appearance). Thus, our primary finding that disc height, NP GAG and collagen contents, and mechanical function did not recover eight weeks after large needle puncture is valid, supporting the mouse caudal injury model for certain studies.

II.5 Conclusion

The effects of needle injury in the mouse caudal disc were examined using rigorous mechanical outcomes. Injury caused an immediate change in mechanics that were not altered over time despite progressive compositional changes. Sufficient mechanical perturbation is required for degenerative changes to take place [89]. Consistent with this theory, changes in mechanics from a large needle injury were

associated with downstream alterations in disc height, NP composition, and histological characteristics of degeneration.

BIBLIOGRAPHY

- [1] Abrams GD, Frank RM, Gupta AK, Harris JD, McCormick FM, Cole BJ. Trends in meniscus repair and meniscectomy in the United States, 2005-2011. *Am J Sports Med* 2013;41:2333-9.
- [2] Acaroglu ER, Iatridis JC, Setton LA, Foster RJ, Mow VC, Weidenbaum M. Degeneration and aging affect the tensile behavior of human lumbar annulus fibrosus. *Spine (Phila Pa 1976)* 1995;20:2690-701.
- [3] Aguila LA, Piraino DW, Modic MT, Dudley AW, Duchesneau PM, Weinstein MA. The intranuclear cleft of the intervertebral disk: magnetic resonance imaging. *Radiology* 1985;155:155-8.
- [4] United States Bureau of Economic Analysis. Current-dollar and "real" GDP. 2014; <http://www.bea.gov/national/index.htm#gdp>
- [5] Andersson GB. Epidemiological features of chronic low-back pain. *Lancet* 1999;354:581-5.
- [6] Angeline ME, Rodeo SA. Biologics in the management of rotator cuff surgery. *Clin Sports Med* 2012;31:645-63.
- [7] Antoniou J, Epure LM, Michalek AJ, Grant MP, Iatridis JC, Mwale F. Analysis of quantitative magnetic resonance imaging and biomechanical parameters on human discs with different grades of degeneration. *J Magn Reson Imaging* 2013;38:1402-14.
- [8] Antoniou J, Steffen T, Nelson F, Winterbottom N, Hollander AP, Poole RA, et al. The human lumbar intervertebral disc: evidence for changes in the biosynthesis and

- denaturation of the extracellular matrix with growth, maturation, ageing, and degeneration. *J Clin Invest* 1996;98:996-1003.
- [9] Attia M, Santerre JP, Kandel RA. The response of annulus fibrosus cell to fibronectin-coated nanofibrous polyurethane-anionic dihydroxyoligomer scaffolds. *Biomaterials* 2011;32:450-60.
- [10] Bach FC, Willems N, Penning LC, Ito K, Meij BP, Tryfonidou MA. Potential regenerative treatment strategies for intervertebral disc degeneration in dogs. *BMC Vet Res* 2014;10:3.
- [11] Baker BM, Gee AO, Metter RB, Nathan AS, Marklein RA, Burdick JA, et al. The potential to improve cell infiltration in composite fiber-aligned electrospun scaffolds by the selective removal of sacrificial fibers. *Biomaterials* 2008;29:2348-58.
- [12] Baker BM, Nathan AS, Huffman GR, Mauck RL. Tissue engineering with meniscus cells derived from surgical debris. *Osteoarthritis Cartilage* 2009;17:336-45.
- [13] Baker BM, Nerurkar NL, Burdick JA, Elliott DM, Mauck RL. Fabrication and modeling of dynamic multipolymer nanofibrous scaffolds. *J Biomech Eng* 2009;131:101012.
- [14] Baker BM, Shah RP, Huang AH, Mauck RL. Dynamic tensile loading improves the functional properties of mesenchymal stem cell-laden nanofiber-based fibrocartilage. *Tissue Eng Part A* 2011;17:1445-55.
- [15] Baker BM, Shah RP, Silverstein AM, Esterhai JL, Burdick JA, Mauck RL. Sacrificial nanofibrous composites provide instruction without impediment and enable functional tissue formation. *Proc Natl Acad Sci U S A* 2012;109:14176-81.

- [16] Barbir A, Godburn KE, Michalek AJ, Lai A, Monsey RD, Iatridis JC. Effects of torsion on intervertebral disc gene expression and biomechanics, using a rat tail model. *Spine (Phila Pa 1976)* 2011;36:607-14.
- [17] Battie MC, Videman T, Kaprio J, Gibbons LE, Gill K, Manninen H, et al. The Twin Spine Study: contributions to a changing view of disc degeneration. *Spine J* 2009;9:47-59.
- [18] Battie MC, Videman T, Parent E. Lumbar disc degeneration: epidemiology and genetic influences. *Spine (Phila Pa 1976)* 2004;29:2679-90.
- [19] Beason DP, Connizzo BK, Dourte LM, Mauck RL, Soslowsky LJ, Steinberg DR, et al. Fiber-aligned polymer scaffolds for rotator cuff repair in a rat model. *J Shoulder Elbow Surg* 2012;21:245-50.
- [20] Beckstein JC, Sen S, Schaer TP, Vresilovic EJ, Elliott DM. Comparison of animal discs used in disc research to human lumbar disc: axial compression mechanics and glycosaminoglycan content. *Spine (Phila Pa 1976)* 2008;33:E166-73.
- [21] Benthien JP, Behrens P. The treatment of chondral and osteochondral defects of the knee with autologous matrix-induced chondrogenesis (AMIC): method description and recent developments. *Knee Surg Sports Traumatol Arthrosc* 2011;19:1316-9.
- [22] Bertolo A, Mehr M, Janner-Jametti T, Graumann U, Aebli N, Baur M, et al. An in vitro expansion score for tissue-engineering applications with human bone marrow-derived mesenchymal stem cells. *J Tissue Eng Regen Med* 2013.
- [23] Best BA, Guilak F, Setton LA, Zhu W, Saed-Nejad F, Ratcliffe A, et al. Compressive mechanical properties of the human annulus fibrosus and their relationship to biochemical composition. *Spine (Phila Pa 1976)* 1994;19:212-21.

- [24] Bhumiratana S, Eton RE, Oungouljian SR, Wan LQ, Ateshian GA, Vunjak-Novakovic G. Large, stratified, and mechanically functional human cartilage grown in vitro by mesenchymal condensation. *Proc Natl Acad Sci U S A* 2014;111:6940-5.
- [25] Bian L, Guvendiren M, Mauck RL, Burdick JA. Hydrogels that mimic developmentally relevant matrix and N-cadherin interactions enhance MSC chondrogenesis. *Proc Natl Acad Sci U S A* 2013;110:10117-22.
- [26] Bian L, Zhai DY, Tous E, Rai R, Mauck RL, Burdick JA. Enhanced MSC chondrogenesis following delivery of TGF-beta3 from alginate microspheres within hyaluronic acid hydrogels in vitro and in vivo. *Biomaterials* 2011;32:6425-34.
- [27] Bibby SR, Jones DA, Ripley RM, Urban JP. Metabolism of the intervertebral disc: effects of low levels of oxygen, glucose, and pH on rates of energy metabolism of bovine nucleus pulposus cells. *Spine (Phila Pa 1976)* 2005;30:487-96.
- [28] Blumenkrantz G, Zuo J, Li X, Kornak J, Link TM, Majumdar S. In vivo 3.0-tesla magnetic resonance T1rho and T2 relaxation mapping in subjects with intervertebral disc degeneration and clinical symptoms. *Magn Reson Med* 2010;63:1193-200.
- [29] Bowles RD, Gebhard HH, Dyke JP, Ballon DJ, Tomasino A, Cunningham ME, et al. Image-based tissue engineering of a total intervertebral disc implant for restoration of function to the rat lumbar spine. *NMR Biomed* 2012;25:443-51.
- [30] Bowles RD, Gebhard HH, Hartl R, Bonassar LJ. Tissue-engineered intervertebral discs produce new matrix, maintain disc height, and restore biomechanical function to the rodent spine. *Proc Natl Acad Sci U S A* 2011;108:13106-11.

- [31] Bowles RD, Williams RM, Zipfel WR, Bonassar LJ. Self-assembly of aligned tissue-engineered annulus fibrosus and intervertebral disc composite via collagen gel contraction. *Tissue Eng Part A* 2010;16:1339-48.
- [32] Boxberger JI, Auerbach JD, Sen S, Elliott DM. An in vivo model of reduced nucleus pulposus glycosaminoglycan content in the rat lumbar intervertebral disc. *Spine (Phila Pa 1976)* 2008;33:146-54.
- [33] Boxberger JI, Sen S, Yerramalli CS, Elliott DM. Nucleus pulposus glycosaminoglycan content is correlated with axial mechanics in rat lumbar motion segments. *J Orthop Res* 2006;24:1906-15.
- [34] Brophy RH, Cottrell J, Rodeo SA, Wright TM, Warren RF, Maher SA. Implantation of a synthetic meniscal scaffold improves joint contact mechanics in a partial meniscectomy cadaver model. *J Biomed Mater Res A* 2010;92:1154-61.
- [35] Burdick JA, Chung C, Jia X, Randolph MA, Langer R. Controlled degradation and mechanical behavior of photopolymerized hyaluronic acid networks. *Biomacromolecules* 2005;6:386-91.
- [36] Burdick JA, Mauck RL, Gorman JH, 3rd, Gorman RC. Acellular biomaterials: an evolving alternative to cell-based therapies. *Sci Transl Med* 2013;5:176ps4.
- [37] Bydon M, De la Garza-Ramos R, Abt NB, Gokaslan ZL, Wolinsky JP, Sciubba DM, et al. Impact of smoking on complication and pseudarthrosis rates after single- and 2-level posterolateral fusion of the lumbar spine. *Spine (Phila Pa 1976)* 2014;39:1765-70.
- [38] Byers BA, Mauck RL, Chiang IE, Tuan RS. Transient exposure to transforming growth factor beta 3 under serum-free conditions enhances the biomechanical and

biochemical maturation of tissue-engineered cartilage. *Tissue Eng Part A* 2008;14:1821-34.

[39] Callaghan JP, McGill SM. Intervertebral disc herniation: studies on a porcine model exposed to highly repetitive flexion/extension motion with compressive force. *Clin Biomech (Bristol, Avon)* 2001;16:28-37.

[40] Chainani A, Hippensteel KJ, Kishan A, Garrigues NW, Ruch DS, Guilak F, et al. Multilayered electrospun scaffolds for tendon tissue engineering. *Tissue Eng Part A* 2013;19:2594-604.

[41] Chainani A, Hippensteel KJ, Kishan A, Garrigues NW, Ruch DS, Guilak F, et al. Multilayered Electrospun Scaffolds for Tendon Tissue Engineering. *Tissue Eng Part A* 2013.

[42] Chan SC, Gantenbein-Ritter B. Preparation of intact bovine tail intervertebral discs for organ culture. *J Vis Exp* 2012.

[43] Chawla K, Klein TJ, Schumacher BL, Jadin KD, Shah BH, Nakagawa K, et al. Short-term retention of labeled chondrocyte subpopulations in stratified tissue-engineered cartilaginous constructs implanted in vivo in mini-pigs. *Tissue Eng* 2007;13:1525-37.

[44] Choi KS, Cohn MJ, Harfe BD. Identification of nucleus pulposus precursor cells and notochordal remnants in the mouse: implications for disk degeneration and chordoma formation. *Dev Dyn* 2008;237:3953-8.

[45] Chujo T, An HS, Akeda K, Miyamoto K, Muehleman C, Attawia M, et al. Effects of growth differentiation factor-5 on the intervertebral disc--in vitro bovine study and in vivo rabbit disc degeneration model study. *Spine (Phila Pa 1976)* 2006;31:2909-17.

- [46] Cigan AD, Nims RJ, Albro MB, Esau JD, Dreyer MP, Vunjak-Novakovic G, et al. Insulin, ascorbate, and glucose have a much greater influence than transferrin and selenous acid on the in vitro growth of engineered cartilage in chondrogenic media. *Tissue Eng Part A* 2013;19:1941-8.
- [47] Collins FS, Tabak LA. Policy: NIH plans to enhance reproducibility. *Nature* 2014;505:612-3.
- [48] Costi JJ, Stokes IA, Gardner-Morse MG, Iatridis JC. Frequency-dependent behavior of the intervertebral disc in response to each of six degree of freedom dynamic loading: solid phase and fluid phase contributions. *Spine (Phila Pa 1976)* 2008;33:1731-8.
- [49] Court C, Colliou OK, Chin JR, Liebenberg E, Bradford DS, Lotz JC. The effect of static in vivo bending on the murine intervertebral disc. *Spine J* 2001;1:239-45.
- [50] Cunningham BW, Hu N, Zorn CM, McAfee PC. Bioactive titanium calcium phosphate coating for disc arthroplasty: analysis of 58 vertebral end plates after 6- to 12-month implantation. *Spine J* 2009;9:836-45.
- [51] Cunningham BW, Lowery GL, Serhan HA, Dmitriev AE, Orbegoso CM, McAfee PC, et al. Total disc replacement arthroplasty using the AcroFlex lumbar disc: a non-human primate model. *Eur Spine J* 2002;11 Suppl 2:S115-23.
- [52] De Bari C, Dell'Accio F, Luyten FP. Failure of in vitro-differentiated mesenchymal stem cells from the synovial membrane to form ectopic stable cartilage in vivo. *Arthritis Rheum* 2004;50:142-50.
- [53] Dickhut A, Pelttari K, Janicki P, Wagner W, Eckstein V, Egermann M, et al. Calcification or dedifferentiation: requirement to lock mesenchymal stem cells in a desired differentiation stage. *J Cell Physiol* 2009;219:219-26.

- [54] Driscoll TP, Nerurkar NL, Jacobs NT, Elliott DM, Mauck RL. Fiber angle and aspect ratio influence the shear mechanics of oriented electrospun nanofibrous scaffolds. *J Mech Behav Biomed Mater* 2011;4:1627-36.
- [55] Elliott DM, Sarver JJ. Young investigator award winner: validation of the mouse and rat disc as mechanical models of the human lumbar disc. *Spine (Phila Pa 1976)* 2004;29:713-22.
- [56] Elliott DM, Yerramalli CS, Beckstein JC, Boxberger JI, Johannessen W, Vresilovic EJ. The effect of relative needle diameter in puncture and sham injection animal models of degeneration. *Spine (Phila Pa 1976)* 2008;33:588-96.
- [57] Erggelet C, Endres M, Neumann K, Morawietz L, Ringe J, Haberstroh K, et al. Formation of cartilage repair tissue in articular cartilage defects pretreated with microfracture and covered with cell-free polymer-based implants. *J Orthop Res* 2009;27:1353-60.
- [58] Erickson IE, Huang AH, Sengupta S, Kestle S, Burdick JA, Mauck RL. Macromer density influences mesenchymal stem cell chondrogenesis and maturation in photocrosslinked hyaluronic acid hydrogels. *Osteoarthritis Cartilage* 2009;17:1639-48.
- [59] Erickson IE, Kestle SR, Zellars KH, Farrell MJ, Kim M, Burdick JA, et al. High mesenchymal stem cell seeding densities in hyaluronic acid hydrogels produce engineered cartilage with native tissue properties. *Acta Biomater* 2012;8:3027-34.
- [60] Fagan AB, Sarvestani G, Moore RJ, Fraser RD, Vernon-Roberts B, Blumbergs PC. Innervation of annulus tears: an experimental animal study. *Spine (Phila Pa 1976)* 2010;35:1200-5.

- [61] Farndale RW, Sayers CA, Barrett AJ. A direct spectrophotometric microassay for sulfated glycosaminoglycans in cartilage cultures. *Connect Tissue Res* 1982;9:247-8.
- [62] Farrell MJ, Comeau ES, Mauck RL. Mesenchymal stem cells produce functional cartilage matrix in three-dimensional culture in regions of optimal nutrient supply. *Eur Cell Mater* 2012;23:425-40.
- [63] Feng G, Zhang Z, Jin X, Hu J, Gupte MJ, Holzwarth JM, et al. Regenerating nucleus pulposus of the intervertebral disc using biodegradable nanofibrous polymer scaffolds. *Tissue Eng Part A* 2012;18:2231-8.
- [64] Fisher MB, Belkin NS, Milby AH, Henning EA, Bostrom M, Kim M, et al. Cartilage repair and subchondral bone remodeling in response to focal lesions in a mini-pig model: implications for tissue engineering. *Tissue Eng Part A* 2015;21:850-60.
- [65] Fisher MB, Henning EA, Soegaard N, Bostrom M, Esterhai JL, Mauck RL. Engineering meniscus structure and function via multi-layered mesenchymal stem cell-seeded nanofibrous scaffolds. *J Biomech* 2015;48:1412-9.
- [66] Fisher MB, Henning EA, Soegaard N, Esterhai JL, Mauck RL. Organized nanofibrous scaffolds that mimic the macroscopic and microscopic architecture of the knee meniscus. *Acta Biomater* 2013;9:4496-504.
- [67] Fisher MB, Henning EA, Soegaard NB, Dodge GR, Steinberg DR, Mauck RL. Maximizing cartilage formation and integration via a trajectory-based tissue engineering approach. *Biomaterials* 2014;35:2140-8.
- [68] Francisco AT, Mancino RJ, Bowles RD, Brunger JM, Tainter DM, Chen YT, et al. Injectable laminin-functionalized hydrogel for nucleus pulposus regeneration. *Biomaterials* 2013;34:7381-8.

- [69] Freburger JK, Holmes GM, Agans RP, Jackman AM, Darter JD, Wallace AS, et al. The rising prevalence of chronic low back pain. *Arch Intern Med* 2009;169:251-8.
- [70] Freeman AL, Buttermann GR, Beaubien BP, Rochefort WE. Compressive properties of fibrous repair tissue compared to nucleus and annulus. *J Biomech* 2013.
- [71] Frith JE, Cameron AR, Menzies DJ, Ghosh P, Whitehead DL, Gronthos S, et al. An injectable hydrogel incorporating mesenchymal precursor cells and pentosan polysulphate for intervertebral disc regeneration. *Biomaterials* 2013;34:9430-40.
- [72] Gandhimathi C, Venugopal J, Ravichandran R, Sundarrajan S, Suganya S, Ramakrishna S. Mimicking nanofibrous hybrid bone substitute for mesenchymal stem cells differentiation into osteogenesis. *Macromol Biosci* 2013;13:696-706.
- [73] Gebhard H, James AR, Bowles RD, Dyke JP, Saleh T, Doty SP, et al. Biological intervertebral disc replacement: an in vivo model and comparison of two surgical techniques to approach the rat caudal disc. *Evid Based Spine Care J* 2011;2:29-35.
- [74] Gershovich JG, Dahlin RL, Kasper FK, Mikos AG. Enhanced osteogenesis in cocultures with human mesenchymal stem cells and endothelial cells on polymeric microfiber scaffolds. *Tissue Eng Part A* 2013;19:2565-76.
- [75] Gilbert HT, Hoyland JA, Millward-Sadler SJ. The response of human anulus fibrosus cells to cyclic tensile strain is frequency-dependent and altered with disc degeneration. *Arthritis Rheum*;62:3385-94.
- [76] Gorth DJ, Martin JT, Dodge GR, Elliott DM, Malhotra NR, Mauck RL, et al. In vivo retention and bioactivity of IL-1ra microspheres in the rat intervertebral disc: a preliminary investigation. *Journal of Experimental Orthopaedics* 2014;1.

- [77] Gregory DE, Bae WC, Sah RL, Masuda K. Disc degeneration reduces the delamination strength of the annulus fibrosus in the rabbit annular disc puncture model. *Spine J* 2014.
- [78] Gruber HE, Johnson T, Norton HJ, Hanley EN, Jr. The sand rat model for disc degeneration: radiologic characterization of age-related changes: cross-sectional and prospective analyses. *Spine (Phila Pa 1976)* 2002;27:230-4.
- [79] Grunert P, Hudson KD, Macielak MR, Aronowitz E, Borde BH, Alimi M, et al. Assessment of intervertebral disc degeneration based on quantitative magnetic resonance imaging analysis: an in vivo study. *Spine (Phila Pa 1976)* 2014;39:E369-78.
- [80] Grunhagen T, Wilde G, Soukane DM, Shirazi-Adl SA, Urban JP. Nutrient supply and intervertebral disc metabolism. *J Bone Joint Surg Am* 2006;88 Suppl 2:30-5.
- [81] Gullbrand SE, Peterson J, Ahlborn J, Mastropolo R, Fricker A, Roberts TT, et al. ISSLS Prize Winner: Dynamic Loading-Induced Convective Transport Enhances Intervertebral Disc Nutrition. *Spine (Phila Pa 1976)* 2015;40:1158-64.
- [82] Gullbrand SE, Peterson J, Mastropolo R, Roberts TT, Lawrence JP, Glennon JC, et al. Low rate loading-induced convection enhances net transport into the intervertebral disc in vivo. *Spine J* 2015;15:1028-33.
- [83] Gupta MS, Nicoll SB. Duration of TGF-beta3 Exposure Impacts the Chondrogenic Maturation of Human MSCs in Photocrosslinked Carboxymethylcellulose Hydrogels. *Ann Biomed Eng* 2015;43:1145-57.
- [84] He C, Xiao G, Jin X, Sun C, Ma PX. Electrodeposition on nanofibrous polymer scaffolds: Rapid mineralization, tunable calcium phosphate composition and topography. *Adv Funct Mater* 2010;20:3568-76.

- [85] Helgeson MD, Bevevino AJ, Hilibrand AS. Update on the evidence for adjacent segment degeneration and disease. *Spine J* 2013;13:342-51.
- [86] Holzapfel GA, Schulze-Bauer CA, Feigl G, Regitnig P. Single lamellar mechanics of the human lumbar annulus fibrosus. *Biomech Model Mechanobiol* 2005;3:125-40.
- [87] Hong Y, Takanari K, Amoroso NJ, Hashizume R, Brennan-Pierce EP, Freund JM, et al. An elastomeric patch electrospun from a blended solution of dermal extracellular matrix and biodegradable polyurethane for rat abdominal wall repair. *Tissue Eng Part C Methods* 2012;18:122-32.
- [88] Hoogendoorn RJ, Wuisman PI, Smit TH, Everts VE, Helder MN. Experimental intervertebral disc degeneration induced by chondroitinase ABC in the goat. *Spine (Phila Pa 1976)* 2007;32:1816-25.
- [89] Hsieh AH, Hwang D, Ryan DA, Freeman AK, Kim H. Degenerative anular changes induced by puncture are associated with insufficiency of disc biomechanical function. *Spine (Phila Pa 1976)* 2009;34:998-1005.
- [90] Huang AH, Farrell MJ, Kim M, Mauck RL. Long-term dynamic loading improves the mechanical properties of chondrogenic mesenchymal stem cell-laden hydrogel. *Eur Cell Mater* 2010;19:72-85.
- [91] Huang AH, Stein A, Mauck RL. Evaluation of the complex transcriptional topography of mesenchymal stem cell chondrogenesis for cartilage tissue engineering. *Tissue Eng Part A* 2010;16:2699-708.
- [92] Huang QQ, Pope RM. The role of toll-like receptors in rheumatoid arthritis. *Curr Rheumatol Rep* 2009;11:357-64.

- [93] Huang YC, Leung VY, Lu WW, Luk KD. The effects of microenvironment in mesenchymal stem cell-based regeneration of intervertebral disc. *Spine J* 2013;13:352-62.
- [94] Hubbell JH, Seltzer SM. Tables of X-Ray Mass Attenuation Coefficients and Mass Energy-Absorption Coefficients from 1 keV to 20 MeV for Elements Z = 1 to 92 and 28 Additional Substances of Dosimetric Interest. National Institute of Standards and Technology, Reference Database 126 1996.
- [95] Hudson KD, Mozia R, Bonassar LJ. Dose-dependent response of tissue engineered intervertebral discs to dynamic compressive loading. *Transactions of the Annual Meeting of the Orthopaedic Research Society* 2013.
- [96] Hudson KD, Mozia RI, Bonassar LJ. Dose-dependent response of tissue-engineered intervertebral discs to dynamic unconfined compressive loading. *Tissue Eng Part A* 2015;21:564-72.
- [97] Humzah MD, Soames RW. Human intervertebral disc: structure and function. *Anat Rec* 1988;220:337-56.
- [98] Iatridis JC, Mente PL, Stokes IA, Aronsson DD, Alini M. Compression-induced changes in intervertebral disc properties in a rat tail model. *Spine (Phila Pa 1976)* 1999;24:996-1002.
- [99] Iatridis JC, Michalek AJ, Purmessur D, Korecki CL. Localized Intervertebral Disc Injury Leads to Organ Level Changes in Structure, Cellularity, and Biosynthesis. *Cell Mol Bioeng* 2009;2:437-47.

- [100] Iatridis JC, Setton LA, Foster RJ, Rawlins BA, Weidenbaum M, Mow VC. Degeneration affects the anisotropic and nonlinear behaviors of human annulus fibrosus in compression. *J Biomech* 1998;31:535-44.
- [101] Ifkovits JL, Tous E, Minakawa M, Morita M, Robb JD, Koomalsingh KJ, et al. Injectable hydrogel properties influence infarct expansion and extent of postinfarction left ventricular remodeling in an ovine model. *Proc Natl Acad Sci U S A* 2010;107:11507-12.
- [102] Inoue H. Three-dimensional observation of collagen framework of intervertebral discs in rats, dogs and humans. *Arch Histol Jpn* 1973;36:39-56.
- [103] Ionescu LC, Lee GC, Huang KL, Mauck RL. Growth factor supplementation improves native and engineered meniscus repair in vitro. *Acta Biomater* 2012;8:3687-94.
- [104] Ionescu LC, Mauck RL. Porosity and cell preseeding influence electrospun scaffold maturation and meniscus integration in vitro. *Tissue Eng Part A* 2013;19:538-47.
- [105] Iu J, Santerre JP, Kandel RA. Inner and outer annulus fibrosus cells exhibit differentiated phenotypes and yield changes in extracellular matrix protein composition in vitro on a polycarbonate urethane scaffold. *Tissue Eng Part A* 2014;20:3261-9.
- [106] Jarvinen TL, Sihvonen R, Malmivaara A. Arthroscopic partial meniscectomy for degenerative meniscal tear. *N Engl J Med* 2014;370:1260-1.
- [107] Johannessen W, Elliott DM. Effects of degeneration on the biphasic material properties of human nucleus pulposus in confined compression. *Spine (Phila Pa 1976)* 2005;30:E724-9.
- [108] Johnstone B, Hering TM, Caplan AI, Goldberg VM, Yoo JU. In vitro chondrogenesis of bone marrow-derived mesenchymal progenitor cells. *Exp Cell Res* 1998;238:265-72.

- [109] Kaigle AM, Holm SH, Hansson TH. 1997 Volvo Award winner in biomechanical studies. Kinematic behavior of the porcine lumbar spine: a chronic lesion model. *Spine (Phila Pa 1976)* 1997;22:2796-806.
- [110] Kaigle AM, Holm SH, Hansson TH. Experimental instability in the lumbar spine. *Spine (Phila Pa 1976)* 1995;20:421-30.
- [111] Karunakaran G, Suriyaprabha R, Manivasakan P, Yuvakkumar R, Rajendran V, Kannan N. Screening of in vitro cytotoxicity, antioxidant potential and bioactivity of nano- and micro-ZrO₂ and -TiO₂ particles. *Ecotoxicol Environ Saf* 2013;93:191-7.
- [112] Katz JN. Lumbar Disc Disorders and Low-Back Pain: Socioeconomic Factors and Consequences. *The Journal of Bone & Joint Surgery* 2006;88-A (Supplement 2):21-4.
- [113] Kim DH, Martin JT, Elliott DM, Smith LJ, Mauck RL. Phenotypic stability, matrix elaboration and functional maturation of nucleus pulposus cells encapsulated in photocrosslinkable hyaluronic acid hydrogels. *Acta Biomater* 2014;Epub Ahead of Print.
- [114] Kim M, Erickson IE, Choudhury M, Pleshko N, Mauck RL. Transient exposure to TGF-beta3 improves the functional chondrogenesis of MSC-laden hyaluronic acid hydrogels. *J Mech Behav Biomed Mater* 2012;11:92-101.
- [115] Kim M, Garrity S, Burdick JA, Dodge GR, Mauck RL. Media Components Regulate Functional Properties of MSC-laden Hyaluronic Acid Hydrogel in Long-term Culture. *Transactions of the Orthopaedic Research Society, 60th Annual Meeting, New Orleans, LA 2014.*
- [116] Kim M, Kraft JJ, Volk AC, Pugarelli J, Pleshko N, Dodge GR. Characterization of a cartilage-like engineered biomass using a self-aggregating suspension culture model: molecular composition using FT-IRIS. *J Orthop Res* 2011;29:1881-7.

- [117] Kimura T, Nakata K, Tsumaki N, Miyamoto S, Matsui Y, Ebara S, et al. Progressive degeneration of articular cartilage and intervertebral discs. An experimental study in transgenic mice bearing a type IX collagen mutation. *Int Orthop* 1996;20:177-81.
- [118] Kluba T, Niemeyer T, Gaissmaier C, Grunder T. Human annulus fibrosus and nucleus pulposus cells of the intervertebral disc: effect of degeneration and culture system on cell phenotype. *Spine (Phila Pa 1976)* 2005;30:2743-8.
- [119] Kolluru PV, Lipner J, Liu W, Xia Y, Thomopoulos S, Genin GM, et al. Strong and tough mineralized PLGA nanofibers for tendon-to-bone scaffolds. *Acta Biomater* 2013;9:9442-50.
- [120] Korecki CL, Kuo CK, Tuan RS, Iatridis JC. Intervertebral disc cell response to dynamic compression is age and frequency dependent. *J Orthop Res* 2009;27:800-6.
- [121] Kotani Y, Abumi K, Shikunami Y, Takada T, Kadoya K, Shimamoto N, et al. Artificial intervertebral disc replacement using bioactive three-dimensional fabric: design, development, and preliminary animal study. *Spine (Phila Pa 1976)* 2002;27:929-35; discussion 35-6.
- [122] Lam SK, Xiao J, Ruan D, Ding Y, Lu WW, Luk KD. The effect of remodeling on the kinematics of the malpositioned disc allograft transplantation. *Spine (Phila Pa 1976)* 2012;37:E357-66.
- [123] Lao L, Wang Y, Zhu Y, Zhang Y, Gao C. Poly(lactide-co-glycolide)/hydroxyapatite nanofibrous scaffolds fabricated by electrospinning for bone tissue engineering. *J Mater Sci Mater Med* 2011;22:1873-84.

- [124] Ledet EH, Jeshuran W, Glennon JC, Shaffrey C, De Deyne P, Belden C, et al. Small intestinal submucosa for annular defect closure: long-term response in an in vivo sheep model. *Spine (Phila Pa 1976)* 2009;34:1457-63.
- [125] Lee CH, Shin HJ, Cho IH, Kang YM, Kim IA, Park KD, et al. Nanofiber alignment and direction of mechanical strain affect the ECM production of human ACL fibroblast. *Biomaterials* 2005;26:1261-70.
- [126] Leung VY, Aladin DM, Lv F, Tam V, Sun Y, Lau RY, et al. Mesenchymal stem cells reduce intervertebral disc fibrosis and facilitate repair. *Stem Cells* 2014.
- [127] Lewis G. Nucleus pulposus replacement and regeneration/repair technologies: present status and future prospects. *J Biomed Mater Res B Appl Biomater* 2012;100:1702-20.
- [128] Li WJ, Cooper JA, Jr., Mauck RL, Tuan RS. Fabrication and characterization of six electrospun poly(alpha-hydroxy ester)-based fibrous scaffolds for tissue engineering applications. *Acta Biomater* 2006;2:377-85.
- [129] Li WJ, Mauck RL, Cooper JA, Yuan X, Tuan RS. Engineering controllable anisotropy in electrospun biodegradable nanofibrous scaffolds for musculoskeletal tissue engineering. *J Biomech* 2007;40:1686-93.
- [130] Lotz JC. Animal models of intervertebral disc degeneration: lessons learned. *Spine (Phila Pa 1976)* 2004;29:2742-50.
- [131] Lotz JC, Colliou OK, Chin JR, Duncan NA, Liebenberg E. Compression-induced degeneration of the intervertebral disc: an in vivo mouse model and finite-element study. *Spine (Phila Pa 1976)* 1998;23:2493-506.

- [132] Lu HH, Cooper JA, Jr., Manuel S, Freeman JW, Attawia MA, Ko FK, et al. Anterior cruciate ligament regeneration using braided biodegradable scaffolds: in vitro optimization studies. *Biomaterials* 2005;26:4805-16.
- [133] Luk KD, Ruan DK, Lu DS, Fei ZQ. Fresh frozen intervertebral disc allografting in a bipedal animal model. *Spine (Phila Pa 1976)* 2003;28:864-9; discussion 70.
- [134] Maher SA, Rodeo SA, Doty SB, Brophy R, Potter H, Foo LF, et al. Evaluation of a porous polyurethane scaffold in a partial meniscal defect ovine model. *Arthroscopy* 2010;26:1510-9.
- [135] Maidhof R, Jacobsen T, Papatheodorou A, Chahine NO. Inflammation induces irreversible biophysical changes in isolated nucleus pulposus cells. *PLoS One* 2014;9:e99621.
- [136] Maier CF, Tan SG, Hariharan H, Potter HG. T2 quantitation of articular cartilage at 1.5 T. *J Magn Reson Imaging* 2003;17:358-64.
- [137] Mainil-Varlet P, Rieser F, Grogan S, Mueller W, Saager C, Jakob RP. Articular cartilage repair using a tissue-engineered cartilage-like implant: an animal study. *Osteoarthritis Cartilage* 2001;9 Suppl A:S6-15.
- [138] Makris EA, Responde DJ, Paschos NK, Hu JC, Athanasiou KA. Developing functional musculoskeletal tissues through hypoxia and lysyl oxidase-induced collagen cross-linking. *Proc Natl Acad Sci U S A* 2014;111:E4832-41.
- [139] Manly BFJ. *Multivariate statistical methods : a primer*. 3rd ed. Boca Raton, FL: Chapman & Hall/CRC Press; 2005.
- [140] Marchand F, Ahmed AM. Investigation of the laminate structure of lumbar disc annulus fibrosus. *Spine (Phila Pa 1976)* 1990;15:402-10.

- [141] Marcos-Campos I, Marolt D, Petridis P, Bhumiratana S, Schmidt D, Vunjak-Novakovic G. Bone scaffold architecture modulates the development of mineralized bone matrix by human embryonic stem cells. *Biomaterials* 2012;33:8329-42.
- [142] Marinelli NL, Haughton VM, Anderson PA. T2 relaxation times correlated with stage of lumbar intervertebral disk degeneration and patient age. *AJNR Am J Neuroradiol* 2010;31:1278-82.
- [143] Marinelli NL, Haughton VM, Munoz A, Anderson PA. T2 relaxation times of intervertebral disc tissue correlated with water content and proteoglycan content. *Spine (Phila Pa 1976)* 2009;34:520-4.
- [144] Martin BI, Mirza SK, Comstock BA, Gray DT, Kreuter W, Deyo RA. Reoperation rates following lumbar spine surgery and the influence of spinal fusion procedures. *Spine (Phila Pa 1976)* 2007;32:382-7.
- [145] Martin JT, Collins CM, Ikuta K, Mauck RL, Elliott DM, Zhang Y, et al. Population average T2 MRI maps reveal quantitative regional transformations in the degenerating rabbit intervertebral disc that vary by lumbar level. *J Orthop Res* 2015;33:140-8.
- [146] Martin JT, Gorth DJ, Beattie EE, Harfe BD, Smith LJ, Elliott DM. Needle puncture injury causes acute and long-term mechanical deficiency in a mouse model of intervertebral disc degeneration. *J Orthop Res* 2013;31:1276-82.
- [147] Martin JT, Gullbrand SE, Kim DH, Ikuta K, Pfeifer CG, Smith LJ, et al. In Vitro Growth Trajectory and In Vivo Implantation of a Cell-Based Disc-like Angle Ply Structure for Total Disc Arthroplasty. Manuscript submitted for publication.
- [148] Martin JT, Kim DH, Ikuta K, Pfeifer CG, Smith LJ, Elliott DM, et al. In Vitro Growth Trajectory and In Vivo Implantation of a Cell-Based Disc-like Angle Ply

Structure for Total Disc Replacement Transactions of the Summer Biomechanics, Bioengineering, and Biotransport Conference, Snowbird, UT 2015.

[149] Martin JT, Milby AH, Chiaro JA, Kim DH, Hebela NM, Smith LJ, et al.

Translation of an engineered nanofibrous disc-like angle-ply structure for intervertebral disc replacement in a small animal model. *Acta Biomater* 2014;10:2473-81.

[150] Martin JT, Milby AH, Ikuta K, Poudel S, Pfeifer CG, Elliott DM, et al. A

radiopaque electrospun scaffold for engineering fibrous musculoskeletal tissues: Scaffold characterization and in vivo applications. *Acta Biomater* 2015.

[151] Martin JT, Smith LJ, Gorth DJ, Adan A, Hebela NM, Elliott DM, et al.

Nanofibrous disc-like angle ply structures maintain disc height in the rat caudal spine.

Transactions of the Annual Meeting of the Orthopaedic Research Society 2013.

[152] Masuda K. Biological repair of the degenerated intervertebral disc by the injection of growth factors. *Eur Spine J* 2008;17 Suppl 4:441-51.

[153] Masuda K, Aota Y, Muehleman C, Imai Y, Okuma M, Thonar EJ, et al. A novel

rabbit model of mild, reproducible disc degeneration by an anulus needle puncture:

correlation between the degree of disc injury and radiological and histological appearances of disc degeneration. *Spine (Phila Pa 1976)* 2005;30:5-14.

[154] Mauck RL, Soltz MA, Wang CC, Wong DD, Chao PH, Valhmu WB, et al.

Functional tissue engineering of articular cartilage through dynamic loading of

chondrocyte-seeded agarose gels. *J Biomech Eng* 2000;122:252-60.

[155] Mauck RL, Yuan X, Tuan RS. Chondrogenic differentiation and functional

maturation of bovine mesenchymal stem cells in long-term agarose culture. *Osteoarthritis*

Cartilage 2006;14:179-89.

- [156] McGill SM, McDermott A, Fenwick CM. Comparison of different strongman events: trunk muscle activation and lumbar spine motion, load, and stiffness. *J Strength Cond Res* 2009;23:1148-61.
- [157] McMurray RJ, Gadegaard N, Tsimbouri PM, Burgess KV, McNamara LE, Tare R, et al. Nanoscale surfaces for the long-term maintenance of mesenchymal stem cell phenotype and multipotency. *Nat Mater* 2011;10:637-44.
- [158] Melrose J, Shu C, Young C, Ho R, Smith MM, Young AA, et al. Mechanical destabilization induced by controlled annular incision of the intervertebral disc dysregulates metalloproteinase expression and induces disc degeneration. *Spine (Phila Pa 1976)*;37:18-25.
- [159] Menzel EJ, Farr C. Hyaluronidase and its substrate hyaluronan: biochemistry, biological activities and therapeutic uses. *Cancer Lett* 1998;131:3-11.
- [160] Michalek AJ, Funabashi KL, Iatridis JC. Needle puncture injury of the rat intervertebral disc affects torsional and compressive biomechanics differently. *Eur Spine J* 2010.
- [161] Michalek AJ, Iatridis JC. Penetrating annulus fibrosus injuries affect dynamic compressive behaviors of the intervertebral disc via altered fluid flow: an analytical interpretation. *J Biomech Eng*;133:084502.
- [162] Miller JA, Schmatz C, Schultz AB. Lumbar disc degeneration: correlation with age, sex, and spine level in 600 autopsy specimens. *Spine (Phila Pa 1976)* 1988;13:173-8.
- [163] Mimura M, Panjabi MM, Oxland TR, Crisco JJ, Yamamoto I, Vasavada A. Disc degeneration affects the multidirectional flexibility of the lumbar spine. *Spine (Phila Pa 1976)* 1994;19:1371-80.

- [164] Miyamoto K, Masuda K, Kim JG, Inoue N, Akeda K, Andersson GB, et al. Intradiscal injections of osteogenic protein-1 restore the viscoelastic properties of degenerated intervertebral discs. *Spine J* 2006;6:692-703.
- [165] Mizuno H, Roy AK, Vacanti CA, Kojima K, Ueda M, Bonassar LJ. Tissue-engineered composites of annulus fibrosus and nucleus pulposus for intervertebral disc replacement. *Spine (Phila Pa 1976)* 2004;29:1290-7; discussion 7-8.
- [166] Mizuno H, Roy AK, Zaporozjan V, Vacanti CA, Ueda M, Bonassar LJ. Biomechanical and biochemical characterization of composite tissue-engineered intervertebral discs. *Biomaterials* 2006;27:362-70.
- [167] Moffat KL, Kwei AS, Spalazzi JP, Doty SB, Levine WN, Lu HH. Novel nanofiber-based scaffold for rotator cuff repair and augmentation. *Tissue Eng Part A* 2009;15:115-26.
- [168] Mohanraj B, Farran AJ, Mauck RL, Dodge GR. Time-dependent functional maturation of scaffold-free cartilage tissue analogs. *J Biomech* 2014;47:2137-42.
- [169] Mosher TJ, Collins CM, Smith HE, Moser LE, Sivarajah RT, Dardzinski BJ, et al. Effect of gender on in vivo cartilage magnetic resonance imaging T2 mapping. *J Magn Reson Imaging* 2004;19:323-8.
- [170] Mosher TJ, Liu Y, Yang QX, Yao J, Smith R, Dardzinski BJ, et al. Age dependency of cartilage magnetic resonance imaging T2 relaxation times in asymptomatic women. *Arthritis Rheum* 2004;50:2820-8.
- [171] Moss IL, Zhang Y, Shi P, Chee A, Piel MJ, An HS. Retroperitoneal approach to the intervertebral disc for the annular puncture model of intervertebral disc degeneration in the rabbit. *Spine J* 2013;13:229-34.

- [172] Mwale F, Masuda K, Pichika R, Epure LM, Yoshikawa T, Hemmad A, et al. The efficacy of Link N as a mediator of repair in a rabbit model of intervertebral disc degeneration. *Arthritis Res Ther* 2011;13:R120.
- [173] Natarajan RN, Williams JR, Andersson GB. Modeling changes in intervertebral disc mechanics with degeneration. *J Bone Joint Surg Am* 2006;88 Suppl 2:36-40.
- [174] Nathan AS, Baker BM, Nerurkar NL, Mauck RL. Mechano-topographic modulation of stem cell nuclear shape on nanofibrous scaffolds. *Acta Biomater* 2011;7:57-66.
- [175] Nerurkar NL, Baker BM, Sen S, Wible EE, Elliott DM, Mauck RL. Nanofibrous biologic laminates replicate the form and function of the annulus fibrosus. *Nat Mater* 2009;8:986-92.
- [176] Nerurkar NL, Elliott DM, Mauck RL. Mechanics of oriented electrospun nanofibrous scaffolds for annulus fibrosus tissue engineering. *J Orthop Res* 2007;25:1018-28.
- [177] Nerurkar NL, Mauck RL, Elliott DM. ISSLS prize winner: integrating theoretical and experimental methods for functional tissue engineering of the annulus fibrosus. *Spine (Phila Pa 1976)* 2008;33:2691-701.
- [178] Nerurkar NL, Mauck RL, Elliott DM. Modeling interlamellar interactions in angle-ply biologic laminates for annulus fibrosus tissue engineering. *Biomech Model Mechanobiol* 2011;10:973-84.
- [179] Nerurkar NL, Sen S, Huang AH, Elliott DM, Mauck RL. Engineered disc-like angle-ply structures for intervertebral disc replacement. *Spine (Phila Pa 1976)* 2010;35:867-73.

- [180] Nesti LJ, Li WJ, Shanti RM, Jiang YJ, Jackson W, Freedman BA, et al. Intervertebral disc tissue engineering using a novel hyaluronic acid-nanofibrous scaffold (HANFS) amalgam. *Tissue Eng Part A* 2008;14:1527-37.
- [181] Ng KW, O'Connor CJ, Kugler LE, Cook JL, Ateshian GA, Hung CT. Transient supplementation of anabolic growth factors rapidly stimulates matrix synthesis in engineered cartilage. *Ann Biomed Eng* 2011;39:2491-500.
- [182] Nimni ME. Collagen: structure, function, and metabolism in normal and fibrotic tissues. *Semin Arthritis Rheum* 1983;13:1-86.
- [183] Niu G, Yang J, Wang R, Dang S, Wu EX, Guo Y. MR imaging assessment of lumbar intervertebral disk degeneration and age-related changes: apparent diffusion coefficient versus T2 quantitation. *AJNR Am J Neuroradiol* 2011;32:1617-23.
- [184] Noshchenko A, Hoffecker L, Lindley EM, Burger EL, Cain CM, Patel VV. Perioperative and long-term clinical outcomes for bone morphogenetic protein versus iliac crest bone graft for lumbar fusion in degenerative disk disease: systematic review with meta-analysis. *J Spinal Disord Tech* 2014;27:117-35.
- [185] Nover AB, Lee SL, Georgescu MS, Howard DR, Saunders RA, Yu WT, et al. Porous titanium bases for osteochondral tissue engineering. *Acta Biomater* 2015.
- [186] O'Connell GD, Jacobs NT, Sen S, Vresilovic EJ, Elliott DM. Axial creep loading and unloaded recovery of the human intervertebral disc and the effect of degeneration. *J Mech Behav Biomed Mater*;4:933-42.
- [187] O'Connell GD, Jacobs, N.T., Sen, S., Vreslovic, E.J., Elliott, D.M. Axial Creep Loading and Unloaded Recovery of the Human Intervertebral Disc and the Effect of Degeneration. *J Biomech* 2011.

- [188] O'Connell GD, Vresilovic EJ, Elliott DM. Comparison of animals used in disc research to human lumbar disc geometry. *Spine (Phila Pa 1976)* 2007;32:328-33.
- [189] O'Connell GD, Vresilovic EJ, Elliott DM. Human intervertebral disc internal strain in compression: the effect of disc region, loading position, and degeneration. *J Orthop Res* 2011;29:547-55.
- [190] Oegema TR, Jr. Biochemistry of the intervertebral disc. *Clin Sports Med* 1993;12:419-39.
- [191] Osti OL, Vernon-Roberts B, Fraser RD. 1990 Volvo Award in experimental studies. Anulus tears and intervertebral disc degeneration. An experimental study using an animal model. *Spine (Phila Pa 1976)* 1990;15:762-7.
- [192] Palmer EI, Lotz JC. The compressive creep properties of normal and degenerated murine intervertebral discs. *J Orthop Res* 2004;22:164-9.
- [193] Parenteau N, Hardin-Young J, Shannon W, Cantini P, Russell A. Meeting the need for regenerative therapies I: target-based incidence and its relationship to U.S. spending, productivity, and innovation. *Tissue Eng Part B Rev* 2012;18:139-54.
- [194] Park SH, Gil ES, Cho H, Mandal BB, Tien LW, Min BH, et al. Intervertebral disk tissue engineering using biphasic silk composite scaffolds. *Tissue Eng Part A* 2012;18:447-58.
- [195] Pelttari K, Winter A, Steck E, Goetzke K, Hennig T, Ochs BG, et al. Premature induction of hypertrophy during in vitro chondrogenesis of human mesenchymal stem cells correlates with calcification and vascular invasion after ectopic transplantation in SCID mice. *Arthritis Rheum* 2006;54:3254-66.

- [196] Pfirrmann CW, Metzdorf A, Zanetti M, Hodler J, Boos N. Magnetic resonance classification of lumbar intervertebral disc degeneration. *Spine (Phila Pa 1976)* 2001;26:1873-8.
- [197] Pham QP, Sharma U, Mikos AG. Electrospun poly(epsilon-caprolactone) microfiber and multilayer nanofiber/microfiber scaffolds: characterization of scaffolds and measurement of cellular infiltration. *Biomacromolecules* 2006;7:2796-805.
- [198] Punt IM, Visser VM, van Rhijn LW, Kurtz SM, Antonis J, Schurink GW, et al. Complications and reoperations of the SB Charite lumbar disc prosthesis: experience in 75 patients. *Eur Spine J* 2008;17:36-43.
- [199] Qu F, Pintauro MP, Haughan JE, Henning EA, Esterhai JL, Schaer TP, et al. Repair of dense connective tissues via biomaterial-mediated matrix reprogramming of the wound interface. *Biomaterials* 2015;39:85-94.
- [200] Rajae SS, Bae HW, Kanim LE, Delamarter RB. Spinal fusion in the United States: analysis of trends from 1998 to 2008. *Spine (Phila Pa 1976)* 2012;37:67-76.
- [201] Rajae SS, Kanim LE, Bae HW. National trends in revision spinal fusion in the USA: patient characteristics and complications. *Bone Joint J* 2014;96-B:807-16.
- [202] Reza AT, Nicoll SB. Serum-free, chemically defined medium with TGF-beta(3) enhances functional properties of nucleus pulposus cell-laden carboxymethylcellulose hydrogel constructs. *Biotechnol Bioeng* 2010;105:384-95.
- [203] Risbud MV, Di Martino A, Guttapalli A, Seghatoleslami R, Denaro V, Vaccaro AR, et al. Toward an optimum system for intervertebral disc organ culture: TGF-beta 3 enhances nucleus pulposus and anulus fibrosus survival and function through modulation of TGF-beta-R expression and ERK signaling. *Spine (Phila Pa 1976)* 2006;31:884-90.

- [204] Risbud MV, Fertala J, Vresilovic EJ, Albert TJ, Shapiro IM. Nucleus pulposus cells upregulate PI3K/Akt and MEK/ERK signaling pathways under hypoxic conditions and resist apoptosis induced by serum withdrawal. *Spine (Phila Pa 1976)* 2005;30:882-9.
- [205] Rizza R, Liu X. Mechanics and validation of an in vivo device to apply torsional loading to caudal vertebrae. *J Biomech Eng* 2013;135:81003.
- [206] Roberts S, Evans H, Trivedi J, Menage J. Histology and pathology of the human intervertebral disc. *J Bone Joint Surg Am* 2006;88 Suppl 2:10-4.
- [207] Rousseau MA, Ulrich JA, Bass EC, Rodriguez AG, Liu JJ, Lotz JC. Stab incision for inducing intervertebral disc degeneration in the rat. *Spine (Phila Pa 1976)* 2007;32:17-24.
- [208] Ruan DK, Xin H, Zhang C, Wang C, Xu C, Li C, et al. Experimental intervertebral disc regeneration with tissue-engineered composite in a canine model. *Tissue Eng Part A* 2010;16:2381-9.
- [209] Sahlman J, Inkinen R, Hirvonen T, Lammi MJ, Lammi PE, Nieminen J, et al. Premature vertebral endplate ossification and mild disc degeneration in mice after inactivation of one allele belonging to the *Col2a1* gene for Type II collagen. *Spine (Phila Pa 1976)* 2001;26:2558-65.
- [210] Sakai D, Mochida J, Iwashina T, Hiyama A, Omi H, Imai M, et al. Regenerative effects of transplanting mesenchymal stem cells embedded in atelocollagen to the degenerated intervertebral disc. *Biomaterials* 2006;27:335-45.
- [211] Samavedi S, Olsen Horton C, Guelcher SA, Goldstein AS, Whittington AR. Fabrication of a model continuously graded co-electrospun mesh for regeneration of the ligament-bone interface. *Acta Biomater* 2011;7:4131-8.

- [212] Sarver JJ, Elliott DM. Altered disc mechanics in mice genetically engineered for reduced type I collagen. *Spine (Phila Pa 1976)* 2004;29:1094-8.
- [213] Showalter BL, Beckstein JC, Martin JT, Beattie EE, Espinoza Orias AA, Schaer TP, et al. Comparison of Animal Discs Used in Disc Research to Human Lumbar Disc: Torsion Mechanics and Collagen Content. *Spine (Phila Pa 1976)*.
- [214] Showalter BL, Malhotra NR, Vresilovic EJ, Elliott DM. Nucleotomy reduces the effects of cyclic compressive loading with unloaded recovery on human intervertebral discs. *J Biomech* 2014;47:2633-40.
- [215] Shriver MF, Lewis DJ, Kshetry VR, Rosenbaum BP, Benzel EC, Mroz TE. Pseudoarthrosis rates in anterior cervical discectomy and fusion: a meta-analysis. *Spine J* 2015.
- [216] Smit TH. The use of a quadruped as an in vivo model for the study of the spine - biomechanical considerations. *Eur Spine J* 2002;11:137-44.
- [217] Smit TH, van Tunen MS, van der Veen AJ, Kingma I, van Dieen JH. Quantifying intervertebral disc mechanics: a new definition of the neutral zone. *BMC Musculoskelet Disord*;12:38.
- [218] Smith HE, Anderson DG, Albert TJ, Vaccaro AR, Hilibrand AS, Zhang Y, et al. High Resolution T2 Mapping of the Intervertebral Disc: A Potential Biomarker. *Spine Week (ISSLS Section)*. Geneva, Switzerland 2008.
- [219] Smith HE, Collins CM, Oh S, Anderson DG, Zhang Y, Miller PA, et al. T2 Mapping as a Potential Biomarker in a Rabbit Model of Intervertebral Disk Damage and Degeneration. *Lumbar Spine Research Society*. Chicago, IL 2009.

- [220] Smith HE, Lee L, Collins CM, Oh S, Rihn JA, Anderson DG, et al. Feasibility and Initial Results of In Vivo MRI T2 Mapping in a Small Animal Model of Intervertebral Disc Injury: A Potential Imaging Biomarker. Cervical Spine Research Society. Salt Lake City, Utah 2009.
- [221] Smith HE, Mosher TJ, Dardzinski BJ, Collins BG, Collins CM, Yang QX, et al. Spatial variation in cartilage T2 of the knee. *J Magn Reson Imaging* 2001;14:50-5.
- [222] Smith LJ, Chiaro JA, Nerurkar NL, Cortes DH, Horava SD, Hebel NM, et al. Nucleus pulposus cells synthesize a functional extracellular matrix and respond to inflammatory cytokine challenge following long-term agarose culture. *Eur Cell Mater* 2011;22:291-301.
- [223] Smith LJ, Nerurkar NL, Choi KS, Harfe BD, Elliott DM. Degeneration and regeneration of the intervertebral disc: lessons from development. *Dis Model Mech* 2011;4:31-41.
- [224] Sobajima S, Kompel JF, Kim JS, Wallach CJ, Robertson DD, Vogt MT, et al. A slowly progressive and reproducible animal model of intervertebral disc degeneration characterized by MRI, X-ray, and histology. *Spine (Phila Pa 1976)* 2005;30:15-24.
- [225] Sobajima S, Shimer AL, Chadderdon RC, Kompel JF, Kim JS, Gilbertson LG, et al. Quantitative analysis of gene expression in a rabbit model of intervertebral disc degeneration by real-time polymerase chain reaction. *Spine J* 2005;5:14-23.
- [226] Stegemann H, Stalder K. Determination of hydroxyproline. *Clin Chim Acta* 1967;18:267-73.
- [227] Stokes IA. Surface strain on human intervertebral discs. *J Orthop Res* 1987;5:348-55.

- [228] Stolworthy DK, Bowden AE, Roeder BL, Robinson TF, Holland JG, Christensen SL, et al. MRI evaluation of spontaneous intervertebral disc degeneration in the alpaca cervical spine. *J Orthop Res* 2015.
- [229] Sun W, Zhang K, Zhao CQ, Ding W, Yuan JJ, Sun Q, et al. Quantitative T2 mapping to characterize the process of intervertebral disc degeneration in a rabbit model. *BMC Musculoskelet Disord* 2013;14:357.
- [230] Taylor BA, Okubadejo GO, Patel AA, Talcott MR, Imamura T, Hu N, et al. Evaluation of total disc arthroplasty: a canine model. *Am J Orthop (Belle Mead NJ)* 2008;37:E64-70.
- [231] Thompson JP, Pearce RH, Schechter MT, Adams ME, Tsang IK, Bishop PB. Preliminary evaluation of a scheme for grading the gross morphology of the human intervertebral disc. *Spine (Phila Pa 1976)* 1990;15:411-5.
- [232] Turner KG, Ahmed N, Santerre JP, Kandel RA. Modulation of annulus fibrosus cell alignment and function on oriented nanofibrous polyurethane scaffolds under tension. *Spine J* 2014;14:424-34.
- [233] Urban JP, Roberts S. Degeneration of the intervertebral disc. *Arthritis Res Ther* 2003;5:120-30.
- [234] Vadala G, Mozetic P, Rainer A, Centola M, Loppini M, Trombetta M, et al. Bioactive electrospun scaffold for annulus fibrosus repair and regeneration. *Eur Spine J* 2012;21 Suppl 1:S20-6.
- [235] van den Eerenbeemt KD, Ostelo RW, van Royen BJ, Peul WC, van Tulder MW. Total disc replacement surgery for symptomatic degenerative lumbar disc disease: a systematic review of the literature. *Eur Spine J* 2010;19:1262-80.

- [236] Venugopal J, Low S, Choon AT, Kumar AB, Ramakrishna S. Electrospun-modified nanofibrous scaffolds for the mineralization of osteoblast cells. *J Biomed Mater Res A* 2008;85:408-17.
- [237] Vinardell T, Sheehy EJ, Buckley CT, Kelly DJ. A comparison of the functionality and in vivo phenotypic stability of cartilaginous tissues engineered from different stem cell sources. *Tissue Eng Part A* 2012;18:1161-70.
- [238] Wade KR, Robertson PA, Broom ND. A fresh look at the nucleus-endplate region: new evidence for significant structural integration. *Eur Spine J*.
- [239] Walter BA, Korecki CL, Purmessur D, Roughley PJ, Michalek AJ, Iatridis JC. Complex loading affects intervertebral disc mechanics and biology. *Osteoarthritis Cartilage* 2011;19:1011-8.
- [240] Wang JY, Baer AE, Kraus VB, Setton LA. Intervertebral disc cells exhibit differences in gene expression in alginate and monolayer culture. *Spine (Phila Pa 1976)* 2001;26:1747-51; discussion 52.
- [241] Welsch GH, Trattnig S, Paternostro-Sluga T, Bohndorf K, Goed S, Stelzeneder D, et al. Parametric T2 and T2* mapping techniques to visualize intervertebral disc degeneration in patients with low back pain: initial results on the clinical use of 3.0 Tesla MRI. *Skeletal Radiol* 2011;40:543-51.
- [242] Wilke HJ, Neef P, Caimi M, Hoogland T, Claes LE. New in vivo measurements of pressures in the intervertebral disc in daily life. *Spine (Phila Pa 1976)* 1999;24:755-62.
- [243] Woods BI, Vo N, Sowa G, Kang JD. Gene therapy for intervertebral disk degeneration. *Orthop Clin North Am* 2011;42:563-74, ix.

- [244] Wuertz K, Godburn K, MacLean JJ, Barbir A, Donnelly JS, Roughley PJ, et al. In vivo remodeling of intervertebral discs in response to short- and long-term dynamic compression. *J Orthop Res* 2009;27:1235-42.
- [245] Xin H, Zhang C, Wang D, Shi Z, Gu T, Wang C, et al. Tissue-engineered allograft intervertebral disc transplantation for the treatment of degenerative disc disease: experimental study in a beagle model. *Tissue Eng Part A* 2013;19:143-51.
- [246] Xinzhi Zhang J-MC, Jeremiah T. Easley, Eileen Hackett, Stephen Doty, William M. Levine, X. Edward Guo, Helen H. Lu. In vivo Evaluation of a Biomimetic Biphasic Scaffold in Sheep. *Transaction of the Orthopaedic Research Society, 60th Annual Meeting* 2014.
- [247] Yang F, Leung VY, Luk KD, Chan D, Cheung KM. Injury-induced sequential transformation of notochordal nucleus pulposus to chondrogenic and fibrocartilaginous phenotype in the mouse. *J Pathol* 2009;218:113-21.
- [248] Yao H, Justiz MA, Flagler D, Gu WY. Effects of swelling pressure and hydraulic permeability on dynamic compressive behavior of lumbar annulus fibrosus. *Ann Biomed Eng* 2002;30:1234-41.
- [249] Yurube T, Nishida K, Suzuki T, Kaneyama S, Zhang Z, Kakutani K, et al. Matrix metalloproteinase (MMP)-3 gene up-regulation in a rat tail compression loading-induced disc degeneration model. *J Orthop Res* 2010;28:1026-32.
- [250] Zhang H, La Marca F, Hollister SJ, Goldstein SA, Lin CY. Developing consistently reproducible intervertebral disc degeneration at rat caudal spine by using needle puncture. *J Neurosurg Spine* 2009;10:522-30.

- [251] Zhang Y, Drapeau S, An HS, Markova D, Lenart BA, Anderson DG. Histological features of the degenerating intervertebral disc in a goat disc-injury model. *Spine (Phila Pa 1976)*;36:1519-27.
- [252] Zhang Y, Venugopal JR, El-Turki A, Ramakrishna S, Su B, Lim CT. Electrospun biomimetic nanocomposite nanofibers of hydroxyapatite/chitosan for bone tissue engineering. *Biomaterials* 2008;29:4314-22.
- [253] Zheng X, Baker H, Hancock WS, Fawaz F, McCaman M, Pungor E, Jr. Proteomic analysis for the assessment of different lots of fetal bovine serum as a raw material for cell culture. Part IV. Application of proteomics to the manufacture of biological drugs. *Biotechnol Prog* 2006;22:1294-300.
- [254] Zhuang Y, Huang B, Li CQ, Liu LT, Pan Y, Zheng WJ, et al. Construction of tissue-engineered composite intervertebral disc and preliminary morphological and biochemical evaluation. *Biochem Biophys Res Commun* 2011;407:327-32.
- [255] Zou J, Yang H, Miyazaki M, Morishita Y, Wei F, McGovern S, et al. Dynamic bulging of intervertebral discs in the degenerative lumbar spine. *Spine (Phila Pa 1976)* 2009;34:2545-50.